Spring 2010

Congenital LCMV virus: mechanism of brain disease in a rat model of congenital viral infection

Hannah Washington Klein de Licona
University of Iowa

CONGENITAL LCM VIRUS: MECHANISM OF BRAIN DISEASE IN A RAT MODEL OF CONGENITAL VIRAL INFECTION

by

Hannah Washington Klein de Licona

An Abstract

Of a thesis submitted in partial fulfillment
of the requirements for the Doctor of
Philosophy degree in Neuroscience
in the Graduate College of
The University of Iowa

May 2010

Thesis Supervisor: Professor Daniel J. Bonthius

ABSTRACT

Of a thesis on Lymphocytic choriomeningitis virus (LCMV) infection during pregnancy severely injures the human fetal brain. Neonatal rats inoculated with LCMV are an excellent model of congenital LCMV infection, as they develop neuropathology, including cerebellar injuries, similar to those seen in humans. The goal of this thesis was to determine what underlies brain injury and the differential immune response and to determine the role of T-cells in LCMV induced pathology. First, I examined whether cytokine and chemokine expression after LCMV infection was higher in the cerebellum and olfactory bulbs, which undergo destruction, compared to the hippocampus and septum, which undergo no acute destruction. Second, I used T-cell deficient and T-cell competent animals to evaluate the role of T-lymphocytes in LCMV-induced cerebellar and hippocampus pathology. Finally, I characterized the migration abnormality that develops in the cerebellum after LCMV infection. My results showed that cytokine and chemokine expression is higher in the cerebellum and olfactory bulb than in the hippocampus and septum. Using astrocyte cultures, I determined that astrocytes isolated from the cerebellum have a more robust cytokine response to infection compared to astrocytes from the hippocampus. Furthermore, inoculation of congenitally athymic (*rnu/rnu*) rats, which are deficient in T-lymphocytes, demonstrated that cerebellar hypoplasia is T-cell independent while cerebellar destruction and abnormal neuron migration is T-cell dependent. In the hippocampus, T-cells protect against loss of dentate granule cells. A study of the migration abnormality determined that LCMV infection disrupts radial glia fibers and extends proliferation of granule cells in a T-cell dependent manner. The findings reported here support a pivotal role of the immune system in regional brain pathology as well as in the disruption of migration.

Abstract Approved: _____
Thesis Supervisor

_____
Title and Department

_____
Date

CONGENITAL LCM VIRUS: MECHANISM OF BRAIN DISEASE IN A RAT MODEL OF CONGENITAL VIRAL INFECTION

by

Hannah Washington Klein de Licona

A thesis submitted in partial fulfillment
of the requirements for the Doctor of
Philosophy degree in Neuroscience
in the Graduate College of
The University of Iowa

May 2010

Thesis Supervisor: Professor Daniel J. Bonthius

Graduate College
The University of Iowa
Iowa City, Iowa

CERTIFICATE OF APPROVAL

_____

PH.D. THESIS

_____

This is to certify that the Ph.D. thesis of

Hannah Washington Klein de Licona

has been approved by the Examining Committee
for the thesis requirement for the Doctor of Philosophy
degree in Neuroscience at the May 2010 graduation.

Thesis Committee: _____
Daniel J. Bonthius, Thesis Supervisor

_____
Michael E. Dailey

_____
Charles Grose

_____
Robert A. Cornell

_____
Stanley Perlman

_____
Joshua Weiner

To my family and friends for their help and support during my research time and thesis document preparation. To my beloved husband, Humberto, and my little girls Gloria and Isabel who provided me with emotional and intellectual support during my thesis research and watched me tirelessly while I worked towards this degree. To my parents, David and Elizabeth, and my siblings, Zachariah, Rebekah, Nich, Valerie, Kevin, Caitlin, Thomas, and Emily, who tenderly cared for my children during the long days when my research occupied my mental and physical might. And lastly, to my fellow lab mates and advisors, Jo Mahoney, Glenda Rabe, Arya Ordoubadian, Shenglan Li, Bahri Karacay, and Daniel J Bonthius, who taught me many techniques, helped me with experiments, and aided me in my scientific and intellectual growth throughout my PhD years.

ACKNOWLEDGMENTS

First, I would like to acknowledge the Neuroscience Program and the NINDS F31 fellowship or funding my PhD training. I would like to acknowledge my thesis committee, Daniel J. Bonthius (chair), Joshua Weiner, Robert Cornell, Stanley Perlman, Charles Grose, and Michael Dailey, for their insight and intellectual support during my PhD training and thesis preparation. I would like to acknowledge Paul Riemann for his help with photography. I would like to acknowledge Einat Snir, Gary Hauser, and Kevin Knudson in the DNA core, who helped me with my RT-PCR planning and running of 384 well plates, and Justin Fishbaugh in the flow cytometry core, who taught me to do flow cytometry and helped me with my initial flow cytometry experiments. I would like to give special thanks to my dad, David, for helping me construct the behavioral open field, and beam walk apparatuses for my experiments and to Rachel Gold for helping me with thesis editing. Furthermore, I would like to acknowledge Michael Dailey, for generously providing me with aliquots of PCNA and lectin IB4, Josh Weiner, for teaching me immunofluorescence and providing me with aliquots of NeuN and Tuj-1 antibodies. Lastly, the monoclonal antibody, TAG-1, was developed by Yamamoto, M, and was obtained from the Developmental Studies Hybridoma Bank developed under the auspices of the NICHD and maintained by The University of Iowa, Department of Biology, Iowa City, IA 52242.

ABSTRACT

Lymphocytic choriomeningitis virus (LCMV) infection during pregnancy severely injures the human fetal brain. Neonatal rats inoculated with LCMV are an excellent model of congenital LCMV infection, as they develop neuropathology, including cerebellar injuries, similar to those seen in humans. The goal of this thesis was to determine what underlies brain injury and the differential immune response and to determine the role of T-cells in LCMV induced pathology. First, I examined whether cytokine and chemokine expression after LCMV infection was higher in the cerebellum and olfactory bulbs, which undergo destruction, compared to the hippocampus and septum, which undergo no acute destruction. Second, I used T-cell deficient and T-cell competent animals to evaluate the role of T-lymphocytes in LCMV-induced cerebellar and hippocampus pathology. Finally, I characterized the migration abnormality that develops in the cerebellum after LCMV infection. My results showed that cytokine and chemokine expression is higher in the cerebellum and olfactory bulb than in the hippocampus and septum. Using astrocyte cultures, I determined that astrocytes isolated from the cerebellum have a more robust cytokine response to infection compared to astrocytes from the hippocampus. Furthermore, inoculation of congenitally athymic (*rnu/rnu*) rats, which are deficient in T-lymphocytes, demonstrated that cerebellar hypoplasia is T-cell independent, while cerebellar destruction and abnormal neuronal migration are T-cell dependent. In the hippocampus, T-cells protect against loss of dentate granule cells. A study of the migration abnormality determined that LCMV infection disrupts radial glia fibers and extends proliferation of granule cells in a T-cell dependent manner. The findings reported here support a pivotal role of the immune system in regional brain pathology as well as in the disruption of migration.

.

TABLE OF CONTENTS

LIST OF TABLES

LIST OF FIGURES

LIST OF ABBREVIATIONS

LCMV - Lymphocytic choriomeningitis virus

BBB – Blood Brain Barrier

PD – Postnatal Day

NGF – Neural Growth factor

NK – Natural Killer

EGL- External Granule Layer

IGL- Internal Granule Layer

PC- Purkinje Cell Layer

ML- Molecular Layer

AD.T- Adoptive Transfer

TNF-α- Tumor Necrosis Factor α

IFN-γ- Interferon γ

IL-1β- Interleukin 1 β

IL-6- Interleukin 6

RANTES- regulated upon activation, normal T cell expressed and secreted

MCP-1- Monocyte chemotactic protein-1

IP-10- Interferon-inducible protein 10

VCAM-1- Vascular cell adhesion molecule-1

IHC- Immunohistochemistry

RPMI Medium – Roswell Park Memorial Institute medium

TUNEL- terminal deoxynucleotidyl transferase dUTP nick end labeling

CHAPTER 1: INTRODUCTION AND BACKGROUND

Congenital Lymphocytic Choriomeningitis Virus (LCMV) Infection

Congenital viral and protozoal infections are a serious source of neurological disorders in the pediatric population [1-2]. The most common congenital infections are classified under the acronym TORCH, which includes Toxoplasmosis, Rubella, Cytomegalovirus, and Herpes Simples virus. One important congenital infection that is not included in the TORCH group is LCMV [1, 3]. LCMV is a prominent human pathogen that can cause substantial damage to the fetal brain when the infection occurs during pregnancy.

A member of the arenavirus family, LCMV is a non-cytolytic virus carried by wild mice [4-7]. Mice infected prenatally with LCMV are essentially asymptomatic and shed the virus in large quantities for life [8]. Humans are infected with LCMV when they come into contact with feces, urine, or other secretions or aerosols from infected mice [9-11]. Human infection acquired postnatally manifests itself in a variety of ways. It is asymptomatic in up to one-third of cases, while a flu-like illness develops in most others [9, 12]. The symptoms are usually biphasic. First, infected humans develop a classic flu-like illness, including fever, chills, myalgias, and vomiting, followed by the second phase where central nervous system symptoms predominate and include photophobia, headache and nuchal rigidity. In the vast majority of postnatally acquired cases, the infection resolves without sequelae. Rarely, LCMV infection leads to a fatal disease.

Far more serious consequences typically occur when the infection occurs during pregnancy. LCMV infection during pregnancy can lead to spontaneous abortion or can result in severe neurological disability, such as cerebral palsy, epilepsy, and mental retardation [5, 9, 13-14]. These neurologic disabilities among offspring of maternally infected people reflect severe central nervous system damage to the fetus and include

chorioretinitis, encephalomalacia, microencephaly, cerebellar hypoplasia, hydrocephalus, and neuronal migration disturbances. The neuropathology observed in these infected fetuses virtually never occur in their mothers, thus reflecting the particular vulnerability of the fetal brain, compared to the mature brain.

While the fetus is generally much more vulnerable than the adult to LCMV, the virus can be life-threatening to adults when the infection occurs in immunocompromised patients. The severe consequences of LCMV infection in immunocompromised patients came to public attention after two separate cases of asymptomatic organ donors resulted in serious infection and death to the multiple organ recipients in each case [15-16]. In these patients, LCMV lead to a fatal hemorrhagic illness, which also commonly occurs after infections by other viruses in the arenavirus family [17]. A well known example is the hemorrhagic fever caused by Lassa virus, which accounts for over 300,000 infections and several thousand deaths per year in Africa [18-19].

LCMV was discovered by Armstrong and Lillie in 1933, when a woman became ill, first presenting with malaise, and later developing meningitis, followed by death [20]. It was initially assumed that the woman had died of a particularly severe case of St. Louis Encephalitis. To verify that the offending pathogen was the virus of St. Louis Encephalitis, Armstrong and Lillie isolated her cerebrospinal fluid and passaged it five times through monkeys, each of whom developed a disease similar to St. Louis encephalitis. On the sixth passage, they inoculated a monkey immune to St. Louis encephalitis, yet the same illness developed. This demonstrated that the pathogen was not the St. Louis encephalitis virus, and must, instead be a novel virus. They named the virus Lymphocytic Choriomeningitis Virus because of the strong lymphocytic infiltration seen in the choroid plexus and meninges in infected animals [20]. LCMV was subsequently isolated from many additional patients presenting with aseptic meningitis, thus, establishing LCMV as one of the leading causes of viral meningitis in humans [21].

LCMV is prevalent in the environment and is considered an emerging pathogen. A study in Baltimore demonstrated that 9% of house mice carry LCMV [22]. A much higher prevalence can occur in domestic clustering of mice. One case study in France found that 70% of mice captured from a single house, in which a known childhood case of LCMV also occurred, tested positive for LCMV [23]. Serologic testing has shown that approximately 5% of human adults have antibodies to the virus, demonstrating prior infection [22, 24]. Prevalence is higher in laboratory workers exposed to LCMV infected mice [25] .

The prevalence of LCMV infection during pregnancy is unknown. The first case of congenital LCMV was reported in England in 1955 [26]. Many more cases have subsequently been reported [11, 26-29]. The first cases in the US were reported in 1993 [30] [31]. Since then, there have been 77 additional American cases of congenital LCMV reported [32].

Most cases of diagnosed congenital LCMV have severe hydrocephalus, microcephaly, and chorioretinitis, and most of these children are severely neurologically disabled [11, 14, 26-29]. Whether congenital LCMV uniformly leads to such drastic consequences is unknown. Possibly, congenital LCMV infection is much more common than generally recognized, but has a spectrum of signs, the milder of which may go undiagnosed. The high prevalence of LCMV in the environment and of positive LCMV serologies in humans, combined with the increasing reports of childhood chorioretinitis, suggest that congenital LCMV is more prevalent than previously recognized and might be highly under-diagnosed [11, 28, 33-35].

The pathway of LCMV transmission to the developing fetus is transplacental [9, 26]. Virus crosses the placenta during maternal viremia and reaches the fetus. The neurotropism of LCMV directs it toward the developing central nervous system, where it targets mitotically active neurons [9, 36-37]. Microencephaly, periventricular

calcifications, gyral dysplasia, cerebellar hypoplasia, and focal cerebral destruction are common pathological consequences of congenital LCMV infection [5, 14, 29].

The mechanism by which LCMV damages the human fetal brain is unknown. LCMV differs from many other viruses in that it is non-cytolytic in most cell types, including neurons. Therefore, direct killing of neurons by virus, as occurs with the cytolytic herpes simplex virus [2], is not a likely mechanism of damage [37].

Over the last 70 years, LCMV research using mice has advanced scientific understanding of many fundamental concepts in virology and immunology, many of which have been applied to other viral pathogens and immune-mediated diseases [4, 38-40]. The mote noteworthy of this research was the identification of T-cell recognition of MHC molecules by Doherty and Zinkernagel, leading to their winning the 1996 Nobel-Prize [41-44]. Some of these fundamentals include mechanisms of immune tolerance to virus and the role that CD8 and CD4 cells play in viral clearance [40].

While the mouse model of LCMV infection has yielded invaluable information regarding immune mechanisms in general and immune-virus interactions in particular, the mouse model has been of limited value in elucidating the biology of congenital LCMV infection. Prenatal mice infected with LCMV develop immune tolerance to the virus, while adult mice develop fatal meningitis without brain parenchymal involvement [40]. Neither of these outcomes reflects the human condition of congenital LCMV infection. In contrast, the *neonatal rat* infected with LCMV is a superb model of human congenital LCMV infection [14]. Unlike the mouse, the neonatal rat inoculated with LCMV is vulnerable to widespread brain parenchymal infection. Furthermore, the neonatal rat inoculated with LCMV develops virtually all of the neuropathologic and behavioral changes observed in children with congenital LCMV infection [29, 37]. Thus, for the work of this thesis, I have utilized the neonatal rat model system of LCMV infection.

Initial Studies Using the Neonatal Rat Model

During development, the brains of all mammalian species pass through a period of rapid brain growth, referred to as the "brain growth spurt" [45]. During the brain growth spurt, the developing brain is particularly vulnerable to neuroteratogenic agents. While all mammalian species have a brain growth spurt, the timing of this event, relative to birth, varies among the species [45]. In humans, the brain growth spurt is a prenatal event and occurs during the third trimester. In contrast, in rats, the brain growth spurt is a postnatal event and occurs during the first two postnatal weeks [46]. Thus, in order to mimic human exposure to injurious agents during the third trimester, rats must be exposed during the early postnatal period. For this reason, the neonatal rat is commonly utilized as a model system for the study of human neuroteratogens, including viruses.

Monjan and coworkers first developed the rat model of congenital LCMV in the 1970's [47-49]. In this model system, LCMV is injected intracerebrally. They found that neonatal rats injected at PD 4 developed destructive lesions of the cerebellum, which resulted in severe ataxia. They also found that specific neuronal populations were consistently infected by the virus, while other neuronal populations were consistently spared. In addition, they found that the virus induced retinopathy, altered behavior, and disturbed neurotransmission [50]. Finally, they administered anti-lymphoid serum to infected rats and found that much of the pathology could be averted, thus suggesting that much of the virus-induced disease was immune-mediated [48]. Following this flurry of research activity in the 1970s, the rat model of LCMV infection was virtually unused and almost forgotten for several decades. Recently, however, interest in congenital LCMV infection has increased, and the neonatal rat model has re-emerged.

A Review of Recent Research in the Neonatal Model

LCMV research in our laboratory has focused on characterizing the patterns of infection and pathology induced by LCMV in the developing brain. Our work has shown

that LCMV utilizes specific cell types to sequentially spread throughout the brain and that the virus infects specific neuronal populations, within specific brain regions, while completely sparing others [36]. Our laboratory has further shown that LCMV induces region-specific forms of neuropathology [36]. In addition, our laboratory has shown that patterns of infection and pathology depend strongly on the age of the animal at the time of infection [37]. Furthermore, our laboratory has shown that virtually all of the various forms of pathology evident in children with congenital LCMV infection can be replicated in the rat model [14, 29, 37]. These findings will be reviewed briefly here.

Pattern of infection, pathology and T-cell infiltration

Our initial work on LCMV elucidated the pathway that LCMV utilizes in infecting different brain regions, as well as the time frames of infection and pathology [36]. Following intracranial inoculation on PD4, astrocytes and Bergmann glia are the first cells infected with LCMV. These glial cells are also the site in which the virus replicates to high titers and are the conduit through which the virus spreads throughout the brain parenchyma, by sequentially moving from one astrocyte to the next. Thus, glial cells play a central role in LCMV infection of the developing brain. After infecting glial cells, the virus then spreads into neurons. However, not all neurons are susceptible to infection. Neurons are infectable in only four specific brain regions. These susceptible regions are the cerebellum, olfactory bulb, hippocampus, and periventricular region. After viral titers reach a peak, LCMV is then cleared from glial cells, but persists in neurons. At approximately the same time that viral clearance begins, neuropathologic changes occur, as well. However, the nature, severity, and timing of the pathology, as well as the infiltration of T-lymphocytes, differ among brain regions in a highly stereotyped fashion.

Why neuronal infection with LCMV is restricted to the four aforementioned brain regions is unknown, but several possibilities exist. These four regions are the most

developmentally immature regions of the brain and are precisely the same four brain regions where neurogenesis is still occurring in the postnatal rat [46, 51-56]. Thus, LCMV may have a tropism for neurons that express mitotic machinery, allowing LCMV to hijack the replication machinery to replicate itself. An alternative explanation is that the purported LCMV receptor, alpha-dystroglycan, may be expressed at higher levels on the surfaces of some neuronal types than on others and that this inhomogeneous expression determines LCMV susceptibility [57].

Despite the fact that the cerebellum, olfactory bulb, hippocampus, and periventricular region are simultaneously infected with LCMV and have similarly high viral titers, the severity and nature of neuropathology, including the degree of T-cell infiltration, differ strongly among the brain regions (Table 1) [36-37].

- In the cerebellum, there is an acute and permanent destruction of the dorsal lobules, accompanied by a massive infiltration of T-lymphocytes. The ventral lobules are relatively spared from a destructive process and have far fewer infiltrating lymphocytes. However, in the ventral lobules, there is a neuronal migration disturbance involving the granule neurons. A global hypoplasia occurs in the dorsal lobules. The term hypoplasia refers to a smaller structure, while the cytoarchitecture is unchanged.
- In the olfactory bulb, there is a temporary hypoplasia, associated with a robust infiltration of lymphocytes. Unlike the cerebellum, which remains permanently small, the olfactory bulb hypoplasia is reversible and fully recovers by PD120.
- In the hippocampus, there is initially no cell loss and only a paucity of infiltrating lymphocytes, despite a heavy viral load within the dentate gyrus. However, several months post-infection, there is a dramatic loss of granule cells specifically from the dentate gyrus.

- In the periventricular region, there is neither an acute- nor a late-onset neuronal loss, nor an evident lymphocytic infiltration, despite a heavy viral load.

Thus, LCMV infects four specific brain regions by spreading from glia cells to neurons and then induces different pathological changes in each region. The mechanism underlying the different pathologies in different brain regions is unknown and is one focus of this thesis.

Critical role of host age in LCMV induced disease

The next area of recent research aimed to determine why a relatively wide range in human pathology is seen after congenital infection with LCMV [29, 37]. Our laboratory hypothesized that the differences in outcomes among infected human fetuses is due to differences in the gestational timing of infection. To determine if developmental age at the time of the infection could explain the differences in outcome, rats were injected at a variety of postnatal ages. It was found that the cellular targets of infection, viral titers in the brain, and the nature and severity of pathology all depended strongly on the age at which an animal was infected. For example, infection at PD 1 results in a widespread infection of neurons and glia in the cerebral cortex, whereas infection just three days later results in infection of astrocytes, but no infection of cerebral cortex neurons. Furthermore, infection at PD21 results in no infection of any cell type in the cerebral cortex. Therefore, cellular targets in the cerebral cortex change dramatically with respect to age of infection [37].

Pathology also changes dramatically depending on age of infection [37]. For example, infection at PD1 leads to hypoplasia in the cerebellum with an otherwise normal cytoarchitecture. However, infection at PD4 and PD6 leads to cerebellar destruction, complete disorganization of cerebellar cytoarchitecture, and cerebellar hypoplasia.

Thus, the effects of LCMV infection greatly change depending on host age at the time of infection. A possible mechanism accounting for such findings is that viral targets change as the different cell populations mature, which could affect expression of the receptor for LCMV, as well as the ability of the virus to replicate in the cell [14, 37]. Alternatively, the changes in pathology with age may reflect differences in the strength of the immune response [14, 37]. In all likelihood, the age-related changes in outcome reflect both changes in infectability and changes in the immune response. The brain becomes less infectable with increasing age, as fewer cell populations are mitotically active, but immune-mediated damage from the infection increases with age, as the immune response matures. Regardless of the mechanism, age at the time of infection is critically important in determining outcome from LCMV infection. Virtually all of the diverse pathology observed among children with congenital LCMV infection can be replicated in the rat model by infecting rats at different ages. For the work of this thesis, rats were infected on PD4, because infection at this age leads to cerebellar destructive lesions, neuronal migration disturbances, hypoplasia, and lymphocytic infiltration, along with delayed onset neuronal dropout from the dentate gyrus – all of which are clinically important components of the human condition [37].

Key Areas of Research for this Thesis

Despite the past 40 years of research into congenital LCMV, the biology behind the disease is just beginning to be understood and much is left to be discovered. Why there is a more robust lymphocytic infiltration in some brain regions than in others is one key question. What role T-cells play in viral clearance and in neuronal loss is another. How LCMV infection leads to abnormal neuron migration is a third key question. These are the questions on which this thesis work will focus.

Key question I: What underlies a stronger lymphocytic infiltration in the olfactory bulb and cerebellum compared to hippocampus and septum?

Our first hypothesis is that the cerebellum and olfactory bulbs have a higher cytokine/chemokine response to LCMV and, therefore, a stronger lymphocyte recruitment and subsequent pathology than do the hippocampus and septum. To begin exploring this hypothesis an understanding of the immune response to viral infection is needed and will be reviewed here.

Background on the immune response to viral infection

Most research on viral brain infections has been conducted with cytolytic viruses, such as herpes and parvovirus infection. However, in general, activation of parenchymal cells and some properties of the immune response are similar in cytolytic and non-cytolytic infections [58]. The primary difference is that, because non-cytolytic viruses do not kill infected cells through lysis, viral clearance relies on lysis by immune cells or activation of antiviral mechanisms within the infected cell [59]. Under normal circumstances, the brain is an immunoprivileged organ, partially controlled by the tight junctions around blood vessels making up the blood-brain-barrior (BBB) [58]. Furthermore, it is maintained in an immunologically suppressed state by expression of the cytokine TGF-β, and the growth factor NGF, thereby protecting it from detrimental effects of the immune system [60]. When a virus infects the brain, the immunosuppressive milieu is overcome in order to protect it from the infecting pathogen. Resident natural killer (NK) cells, astrocytes, and microglia secrete cytokines, such as TNF-α and IFN-γ, which are immune warning signals that alert the immune system to the infection and overcome the immune silence [58]. Microglia are extremely sensitive to changes in the brain parenchyma and likely contribute to the initial detection of and response to infection [61-64]. Local production of cytokines during the early non-

lymphocyte mediated, also known as “innate”, immune response leads to upregulation of MHC molecules on CNS cells and endothelial cells [65-66]. Cytokines also lead to upregulation of adhesion molecules on endothelial cells of the blood brain barrier, allowing transmigration and infiltration of activated T lymphocytes [58].

Cytokines are a group of low-molecular weight proteins. They are produced by infiltrating inflammatory cells, as well as by astrocytes and microglia [64, 67-69]. They not only help coordinate the immune response, but also contribute directly to the pathology associated with many viral infections. Cytokines can induce neuronal loss, influence inflammatory cells, and induce apoptosis [67, 70-75]. Chemokines are a family of chemoattractant cytokines that are important in leukocyte adhesion to the endothelium and leukocyte migration into tissues during inflammation.

T-cell recruitment is induced by cytokine and chemokine expression in the brain. Cytokine signals from within the brain can upregulate endothelial molecules that promote lymphocytic attachment to endothelium and transmigration [76] [58, 77]. Examples are seen in retrovirus, FIV or SIV, infection of the brain, which leads to microglial expression of IL-1β and TNF-α [78]. Both of these cytokines increase expression of cell adhesion molecules, including VCAM-1, which facilitates T-lymphocyte attachment and infiltration of CD8 T cells and CD4 T cells [79] [80]. Endothelial vascular cells may increase expression of antigen presenting molecules and, through this mechanism, recruit antigen specific CD8 T-cells [58]. Further lymphocyte infiltration is facilitated when virus primed CD8 cells recognize MHC I molecules on infected endothelial cells, leading to lysis of endothelial cells and a subsequent break down of the blood brain barrier [76, 81].

Before T-cells can infiltrate the brain and respond to an infection, they must mature and become primed against the virus [58]. T-cell maturation occurs in the thymus, and, in the case of intracerebral infection, priming and activation occurs in the cervical lymph node [58]. Studies of intracranial injection of radioactive antigen have

revealed that antigen can reach the cervical lymph node rapidly and that a T-cell response can occur within days of injection [82]. In the case of LCMV, when the virus is injected intracranially, up to 90% of the virus reaches the blood systemically, and an immune response begins 3 -5 days later [83]. Following T-cell priming, activated T-cells enter circulation and traffic to the CNS.

For activated T-cells to recognize virus antigen, MHC I and MHC II molecules must be present. MHC I molecules are expressed by nearly every cell in the body and are recognized by CD8 cells. However, neurons and astrocytes are an exception. They normally do not express MHC I molecules, but in some rare situations, such as infection (and/or inflammation), some neurons can be induced to express MHC I molecules [40, 58, 84-87]. MHC II molecules are expressed by antigen presenting cells, such as inflammatory macrophages/monocytes, some T-cell subsets, and B-lymphocytes and are recognized by CD4 cells. Brain cells that can be induced to express MHC II molecule include endothelial cells, pericytes, astrocytes, and microglia [58]. IFN-γ helps increase the expression of MHC antigens on resident CNS cells, including microglia [88]. In viral infections, T-cells are principally responsible for expression of IFN-γ. In fact, in the course of viral-induced damage in the CNS, MHC II expression by microglia follows the infiltration of CD4-T cells, and the disappearance of MHC II proceeds the disappearance of CD4-T cells [58].

Both CD8 and CD4 T-cells can play important roles in the immune response to viral brain infections. However, studies from LCMV infections in the adult mouse have demonstrated that LCMV-induced meningitis is entirely CD8 dependent [76, 89-92]. Adoptive transfer experiments have shown that CD4 T-cells, B-cells and NK-cells are not essential for the development of meningitis [93-94] [95]. CD4 cells, however, do play a role in LCMV induced wasting disease [96].

In mice infected with LCMV, cytokines and chemokines orchestrate the early CD8 recruitment and initiate the immune response to LCMV infection [97-99]. In

LCMV meningitis, cytokines and chemokines are expressed highly [97, 99-101]. These include the cytokines, IFN-γ and TNF-α as well as the chemokines, RANTES (CCL5), IP-10 (CXCL10) and MCP-1 (CCL2). The chemokines are expressed before CD8 T-cells infiltrate the meninges at postinfection day 3 [97-98]. However, these cytokines reach much higher expression levels at postinfection day 6, after CD8 T-cells begin to infiltrate [97]. Therefore, cytokine and chemokine expression is present very early in the infection, and later amplified after CD8 cells infiltrate the brain, suggesting an important role of chemokines for initial CD8 recruitment.

The above description of the immune response in cases of viral infection highlights the complexity involved in lymphocyte recruitment and activation. The mechanism of T-cell infiltration and trafficking into the brain is not entirely known, but the secretion of cytokines and chemokines is a vital early step in lymphocyte recruitment.

Astrocytes are a major source of cytokines and chemokines and are a principal target of LCMV in the developing brain. Furthermore, astrocytes are not homogeneous throughout the brain, as will be discussed later. Thus, regional differences across the brain in the immune response to LCMV may be due to regional differences in astrocytes. In particular, we hypothesize that LCMV induces regionally different patterns of cytokine and chemokine production from astrocytes. This hypothesis will be discussed and tested in the first group of experiments in this thesis.

Key Question 2: What is the role of the immune system versus the virus in producing neuropathology?

One key question in congenital LCMV infection is what role the immune system plays in neuropathology. This is a very important area of research because the immune response is a common factor in all congenital infections. Furthermore, the immune response can be pharmacologically manipulated. Thus, to the extent that brain injury is

immune-mediated, it may be possible to ameliorate the damage by suppressing the immune response.

Early evidence for the role of the immune system in LCMV induced pathology came from work by Monjan over 30 years ago. First, immune cell infiltration was correlated with cerebellar destruction [47, 49]. Second, suppression of the immune system with anti-lymphoid serum prevented the destruction [48]. Monjan and coworkers concluded that LCMV-induced pathology in the developing rat brain is virtually entirely immune-mediated.

Later research from our laboratory and from others [102], however, has suggested that the neuropathology in LCMV infection might not be entirely immune-mediated. Pearce and co-workers (1999) found that the loss of granule cells from the dentate gyrus occurs in the virtual absence of any infiltrating lymphocytes. Our laboratory has confirmed this observation and has further found that the cerebellar hypoplasia and olfactory hypoplasia that follows LCMV infection on PD1 occurs in the virtual absence of infiltrating lymphocytes. These results suggest that some forms of pathology may be virus-mediated, rather than immune-mediated. The second goal of this thesis work was to determine which aspects of LCMV-induced pathology in the cerebellum and hippocampus depend upon the infiltration of T-lymphocytes and which do not.

Key Question 3: What mechanism underlies the development of abnormal neuronal migration in the cerebellum of LCMV infected rats?

Previously, we showed that LCMV infection in the neonatal rat leads to a severe destructive pathology in the dorsal cerebellar lobules while sparing ventral lobules [36]. However, the "spared" lobules are not free of pathology. H & E and Nissl stains showed that the ventral lobules and non-destroyed areas of the dorsal regions have a severe neuronal migration disorder. To determine what pathological processes might lead to

abnormal migration, we looked for alterations in structural components needed for normal granule cell migration and looked for alteration in the differentiation and proliferation of granule cells.

Cerebellar granule cells originate from neuronal precursors in the rostral rhombic lip [103]. Cerebellar granule precursor cells undergo their first wave of proliferation at embryonic day 13 in the mouse. After embryonic day 17, they migrate to form the external granular layer (EGL), where they undergo a massive proliferation. In the mouse, this proliferative phase peaks between PD5-8 and ends around PD15, and in the rat it peaks between PD8-12 and stops at around PD18 [104-107]. During and after this proliferative phase, a very tightly regulated developmental expression of molecules occurs. For migration to proceed normally, granule cells have an intrinsic developmental clock [108-109], which governs granule cell morphologic changes and allows for their inward migration. Furthermore, granule cell proliferation and migration are guided by external cues. Two of these external cues are sonic hedge hog (SHH), which is produced by Purkinje cells and promotes granule cell proliferation [110], and CXCL12, which is expressed by the meninges and keeps granule cells inside the proliferative zone during proliferation [111-113]. As granule cells leave the proliferative state, they become resistant to SHH and move into the inner layers of the external granule cell layer (EGL), where they differentiate, extend axons, and begin to migrate inward [103, 114]. During their migration through the molecular layer, granule cells become elongated and send out a leading process, which juxtaposes with radial glia fibers, called “Bergmann glia” [114-117]. The migrating granule cells use these Bergmann glia fibers as a scaffold to guide their migration inwards. All of these chemical and morphological components must be in place for granule cell migration to occur normally.

Bergmann glia are an early target of LCMV in the developing cerebellum. Within several days of inoculation, the Bergmann glia fibers contain large quantities of LCMV antigen. Since Bergmann glia play a key role in granule cell migration, LCMV-induced

migration disorder may be due to virus-induced corruption of the structure or function of Bergmann glia.

Under normal circumstances, Bergmann glia are attached to the basal lamina. Disruption in the basal lamina has been linked to ectopic granule cell formation [118-120]. In animals with abnormalities in their basal lamina, Bergmann glia become irregular, and granule cells exit the cell cycle, where they mature ectopically. Therefore, when the basal lamina is disrupted, granule cells form ectopias. Thus, LCMV infection may alter neuronal migration by disrupting the basal lamina, to which Bergmann glia attach. This possibility is further strengthened by the fact that the basal lamina juxtaposes the meninges, which are heavily infected by LCMV. Infiltration of the meninges by immune cells could injure the basal lamina, disrupting Bergmann glia morphology and hence interfere with normal granule cell migration.

A third possibility is that LCMV might abnormally prolong granule cell proliferation in the EGL, thus postponing granule cell inward migration. This possible mechanism is supported by studies on damage and inflammation in the central nervous system, which have shown that a reparative process occurs subsequent to damage, resulting in proliferation of neuroprogenitors and subsequent ectopias [121-124]. For example, x-irradiation, gamma-irradiation, and cisplatin treatment in the cerebellum temporarily depletes granule cells in the EGL, followed by regeneration and abnormal thickening of the EGL, and subsequently by ectopic granule cell formation [121-124].

A fourth possibility is that the inflammatory milieu may alter the expression of genes involved in neuronal proliferation and migration. Recently, many overlaps have been discovered between signaling molecules used by the immune system in fighting off diseases and signaling molecules used by the developing brain in normal patterning and development [97, 125-127]. In fact, both systems use cytokines to traffic migrating cells [126]. In the case of the immune system, cytokines are used to traffic immune cells to sites of infection and inflammation, while in the brain, cytokines are used to regulate

neuronal migration and proliferation during normal development and after stroke [128-129]. The final goal of this thesis is to determine the mechanism by which LCMV disturbs neuronal migration in the developing cerebellum.

Summary

Congenital LCMV infection has devastating results on the developing fetus, yet little is known regarding disease pathogenesis. Three key unknowns are addressed in this work. First, I will investigate the mechanism underlying regional differences in pathology by exploring regional differences in cytokine/chemokine responses and by comparing the responses of astrocytes derived from various brain regions. Second, I will determine what forms of cerebellar pathology are T-cell-induced and which are T-cell independent. Third, I will explore the mechanisms underlying the granule cell migration disorder in the LCMV-infected cerebellum.

The implications of the results from this research are far reaching. Understanding the mechanisms of brain injury in congenital infection and the role of the immune system in development may provide targets for intervention. In addition, because signals used by the immune system are also used by the nervous system to pattern brain development, discovering a link between the immune response to a brain infection and its simultaneous effects on development may reveal a common mechanism underlying developmental pathology in many additional brain infections. Furthermore, virtually all previous work examining the role of immune mediators in brain development has utilized transgenic models. Never before has altered expression of immune molecules in infection been directly tied to abnormal neuronal migration. This work may provide novel evidence that a viral infection may disrupt neuronal migration by increasing the expression of particular cytokines that govern normal neuronal migration.

CHAPTER 2: REGIONAL DIFFERENCES IN ASTROCYTE-DERIVED CYTOKINE/CHEMOKINE EXPRESSION CONTRIBUTES TO REGIONAL DIFFERENCES IN LYMPHOCYTE INFILTRATION AND PATHOLOGY IN LCMV INFECTION

Introduction

In the neonatal rat model of congenital LCMV infection, different forms and severity of pathology occur in different brain regions infected by the virus [36-37]. LCMV has a tropism for neurons that are mitotically active. Therefore, brain regions susceptible to infection are those undergoing neurogenesis [46, 51-56]. Infection of the neonatal rat at PD 4 leads to high viral titers in four brain regions [36]. These are the cerebellum, hippocampus, olfactory bulb and septum. Although all four regions have high viral titers, very different pathologic changes result in each region. Pathology ranges from an acute destruction and hypoplasia of the cerebellum to milder cell loss in the olfactory bulb, to no pathology at all in the septum. The mechanism underlying such different outcomes is unknown and is clinically important because understanding the mechanism could help to elucidate the regional differences in pathology observed in cases of human congenital LCMV.

Previous studies point strongly to the immune system as the mechanism underlying the destructive pathology in the cerebellum and olfactory bulb of neonatally infected rats [36-37]. Immunohistochemical methods have demonstrated the presence of CD8 and CD4 T-cells in the olfactory bulb and cerebellum and their absence in the hippocampus and septum [36]. Further evidence for the role of T-cells in the destructive pathology of LCMV is the protection provided by anti-lymphoid serum [48] and the absence of destructive lesions in T-cell deficient rats (chapter 3 of this thesis). From these studies, a T-cell mediated destruction is evident. However, the factors leading to a stronger T cell response in the cerebellum and olfactory bulb than in the hippocampus

and septum are unknown. The differences in pathology are not due to differences in viral load, since viral titers are similar in all four brain regions [36].

One possibility is that a different cytokine and chemokine response occurs in the cerebellum and olfactory bulb, compared to the hippocampus and septum. Cytokines and chemokines are expressed in viral brain infections and can have direct pathologic effects [68, 74, 130]. Indeed, injection of IL1-β, IL-lα or TNF-α into the cerebral spinal fluid and brain induces inflammation and neurotoxicity [131-135]. The first goal of this study was to determine if there are regional differences among the cerebellum, olfactory bulb, hippocampus and septum in the expression of cytokines and chemokines during LCMV infection.

Immunopathologic processes are often marked by the presence of lymphocytes within the injured tissue. Recruitment of lymphocytes to tissues depends on cytokine expression [58]. In addition, lymphocytes are an important source of cytokines [101]. Previous studies have used immunohistochemical methods to demonstrate the presence of CD8+ and CD4+ lymphocytic infiltration following LCMV infection [36]. However, more sensitive and quantitative techniques to measure lymphocytic infiltration have not been used. Quantifying lymphocytic infiltration is critical for determining the potential role that regional chemokines play in recruiting lymphocytes. Therefore, the second goal of this study was to quantify regional infiltration of lymphocytes into infected brain regions.

To understand how different regions, equally infected by LCMV, may produce different cytokine and chemokine responses, we turn to their sources in the brain. Cytokines and chemokines are produced by astrocytes, microglia/macrophages and infiltrating lymphocytes [58, 62-63, 67, 136-137]. Astrocytes are the principal site of LCMV entry, propagation, and spread throughout the developing brain [36]. Furthermore, in inflammatory and infectious conditions, astrocytes can express cytokines and chemokines. Astrocytes are not uniform across the brain. Regional differences exist

in the physiology and properties of astrocytes, such as glutamate receptor and ion channel expression [138-139]. Astrocytic response to toxins, uptake of glutamate, and second messenger responses after local stimuli differ among brain regions [138, 140-142]. Therefore, astrocytic secretion of cytokines and chemokines in response to LCMV infection may also differ among brain regions and play a critical role in regional differences in LCMV-induced pathology. The third goal of this study was to determine if astrocytes express cytokines and chemokines and if astrocytes derived from different regions have different cytokine expression profiles in response to LCMV infection.

The expression of four specific cytokines, TNF-α, INF-γ, IL-6 and IL-1β, were evaluated. These particular cytokines were chosen because they frequently play a role in inflammatory diseases and antiviral responses. Furthermore, TNF-α, IL-1β and IL-6, are toxic to neurons and may play important roles in the tissue injury accompanying LCMV infection [130]. Chemokines that are chemotactic for T cells were also analyzed; these include RANTES/CCL2, IP-10/CXCL10, and MCP-2/CCL5 [97-99]. CX3CL1/fractalkine, a neuroprotective chemokine, was also included in the analysis [70, 136, 143-145].

To investigate which cytokine/chemokine responses depended upon the presence of T-cells, we compared cytokine expressions in infected Lewis and RNU/+ rats, both of which are T-cell competent, to RNU/RNU athymic rats, which lack a thymus and are consequently T-cell deficient [146-147]. This is an important addition to this study because infiltrating T-cells influence and magnify the cytokine/chemokine response and exacerbate cytokine expression in endogenous cells. Comparing cytokine expression profiles in animals possessing and lacking T-cells provides a better picture of which cytokines are likely produced in resident brain cells, as opposed to infiltrating lymphocytes, and might, therefore, underlie the regional differences in lymphocyte recruitment in response to the virus.

Materials and Methods

Animals

For the first set of cytokine/chemokine gene analysis, Lewis rats alone were used. In the second set of cytokine/chemokine gene expression studies, Lewis, RNU/+, and RNU/RNU (congenitally athymic) animals were used. Pregnant Lewis and RNU/+ rats on a hooded background were obtained from Harlan Sprague-Dawley (Indianapolis, IN)[146-147]. The Lewis rat dams were bred with Lewis males, while the RNU/+ rats were bred with RNU/RNU males. Thus, the litters of the Lewis dams were all of the Lewis genotype, while the litters of the RNU/+ dams were approximately 50% RNU/+ and 50% RNU/RNU. As the Lewis rats and athymic rats (RNU/RNU) are of different genetic backgrounds, we used the heterozygote siblings (RNU/+) of the athymic rats as a second comparison group. The rats were maintained in viral containment quarters at the University of Iowa Animal Care Facility. The pregnant rats were observed several times per day to establish time of birth of the litters. The day of birth was defined as postnatal day zero (PD 0). Prior to performing experiments, approval for all experiments was obtained from the University of Iowa Animal Care and Use Committee.

Virus

The neurotropic Armstrong-4 strain of LCMV was used for all inoculations. The virus stock was prepared in BHK-21 cells and harvested at 48 hours after infecting the cells. The virus was stored in 1 ml aliquots at -80°C. The stock had a titer of 2×10^8 plaque forming units (PFU) per ml.

Infections

On postnatal day 4 (PD 4), neonatal rat pups received injections at a depth of approximately 3 mm into the right frontal cortex with either LCMV or Dulbecco's modified Eagle's medium (DMEM), as a control. Injections were performed with a

Hamilton syringe with a needle depth guard. The animals received 0 PFU (control) or 1000 PFU of LCMV in a volume of 5µl of DMEM.

Cytokine and chemokine expression levels

Two separate experiments and groups of animals were used to determine the time course of LCMV-induced changes in selected cytokine and chemokine gene expression levels. In the first group of experiments, only Lewis rats were used to look at cytokine expression in different brain regions. The Lewis rats were sacrificed on PD 8, 10, 12, 14, 18, 25, and 34. In the second experiment, Lewis, heterozygote (RNU/+) and athymic (RNU/RNU) rats were used. Rats of all genotypes received intracerebral injections of 0 or 1000 PFU of LCMV on PD4. The Lewis rats were sacrificed on PD 8, 10, 14, 18, and 25. Infected and uninfected RNU/+ and RNU/RNU rats were sacrificed on this same set of postnatal ages, except that uninfected RNU/+ and RNU/RNU rats were not included on PD 8. For cytokine and chemokine analysis, baseline values were extrapolated for PD8 RNU/RNU and RNU/+ controls, based on the values at the other sampled time points. For each treatment, time point, and genotype, 3-5 rat pups were included.

On the day of sacrifice, the animals were euthanized with pentobarbital, and the brains were harvested. Tissue samples were obtained from the dorsal and ventral cerebellum, olfactory bulb, hippocampus, and septum, and immediately frozen on powdered dry ice. Samples were stored frozen at -80°C.

Real-time PCR

mRNA was isolated using Trizol reagent (Invitrogen, Carlsbad, CA), according to the manufacturer's protocol. Total RNA (2 µg) was reverse-transcribed using SuperscriptTM II (Invitrogen). The resultant cDNA was suspended to 300 µl with endonuclease-free water. 2.5 microliters of this cDNA was used as a template per reaction for the TaqMan assay of both the mRNA of interest and the internal control ribosomal RNA. TaqMan primer and probe sets for template and ribosomal RNA were

purchased from Applied Biosystems Inc. (Foster City, CA). Probes for the target genes [Interferon-gamma (IFN-γ), tumor necrosis factor-alpha (TNF-α), interleukin 6, interleukin 1β, CCL2/monocyte chemotactic protein-1 (MCP-1), CCL5/RANTES, CXCL10/IP-10, and CX3CL1/fractalkine, were labeled with the reporter dye, and the rRNA probe was labeled with the reporter fluorescein dye to allow analysis of the target gene and the rRNA in the same well. Serial dilutions of 596-bp cloned cDNA from ribosomal RNA (5 to 5000 pg) were used to construct a standard curve of cDNA amount versus threshold cycle (Ct). The results were expressed as relative amounts of mRNA per 12.5 pg of rRNA.

Isolation of lymphocytes from brain regions

Animals were anesthetized and brain samples (dorsal and ventral cerebellum, olfactory bulb, hippocampus, and septum) were removed and placed into digestion buffer (HBSS with calcium and MG + 1mg/ml collagenase D and 100ug/ml DNASE + 25mM Hepes + 2% FBS). Brain tissue was separated into smaller pieces using two 25G needles tips and then homogenized with a P1000 pipette. Homogenized brain was then incubated in 15ml corning tube for 30min at 37˚C mixing every 2-3 minutes. 0.5 M EDTA was added to a final volume of 5mM and homogenate was incubated an additional 5 min. The tube was then transferred to ice to stop the digestion. Homogenates were then passed through a 70um cell strainer, followed by centrifugation at 1300rpm for 8 min. Supernatant was discarded, pellet was resuspended in 30% Percoll gradient mixed with RP10 media (RPMI 16-40, Pen/Strep, L-glutamine, 10% Fetal Calf Serum) and then centrifuged for 30 minutes at 1300 rpm and 4˚C. Percoll was removed and lymphocytes were washed 2x with 2% RP10 wash media (1:4 RP10 media: RPMI 16-40).

Splenocyte isolation

Spleens were removed from animals after anesthetizing with Nembutal followed by cervical dislocation. Spleens were placed in FACs buffer (PBS + 5% serum) and

homogenized using the rough ends of frosted slides. Homogenate was then passed through a 30um strainer. Cells were centrifuged at 1700 rpm, red blood cells were lysed using AKT lysis buffer, followed by centrifugation. The pellet was then washed once with FACs buffer, followed by PBS. Cells were resuspended in PBS, passed through a 70 um nylon mesh and counted. Cells were then centrifuged and resuspended at a concentration of 30 x10^6 / ml and used for flow cytometry.

Quantification of lymphocytes by brain region using flow cytometry

Spleens and brains were collected from PD 10, 14 and 18 animals who had previously been infected with LCMV at PD4. Three animals were used for each individual experimental replication at each time point, and the experiment was repeated three times for each time point, for a total of n=9 animals per time point, with 3 pooled for each experiment. Dorsal and ventral cerebellum, olfactory bulbs, septum and hippocampus were dissected from each brain and pooled for the three animals. The pooled brain samples were weighed. Lymphocytes were then isolated. The entire final isolate was diluted in 500ul of PBS, and 30ul of 0.3nm diameter FITC beads (internal control for quantification), diluted to a concentration of 4.22 x 10^6/ml, were added to each tube. The number of events for each cell population and number of beads were obtained from flow cytometry. The data was then normalized to the number of beads collected by the flow cytometer. The total number of lymphocytes was calculated for each sample. The total number of lymphocytes was then divided by regional brain weight to attain the number of lymphocytes per gram of tissue. To control for variation between experimental runs which naturally occurred due to subtle differences in flow cytometer setting at each run, each experimental result was calculated as relative to the septum, allowing for comparison across multiple repeats. To calculate relative values of lymphocytes per brain region for each individual experiment, total lymphocytes for

dorsal cerebellum, ventral cerebellum, olfactory bulb and hippocampus were divided by the total lymphocytes isolated in the septum, thus yielding a final number, representing the fold increase of lymphocytes in each region over the amount in the septum. These values were then averaged for three different repeats.

Flow Cytometry

Cells were labeled following typical flow cytometry protocols. Briefly, splenocytes or lymphocytes were placed in a 2ml tube at a concentration of 0.5-5 x10^6 /ml in a volume of 500ul of PBS. Cells were centrifuged, supernatant was removed, and the cells were incubated with biotinylated anti-rat CD161 (1:200, Biolegand San Diego CA) and Alexa fluor 647 anti-rat CD45RA (1:400 Biolegend San Diego CA). The cells were then washed 2x and incubated with streptavidin-PercP (1:50, Biolegand San Diego, CA), APC/Cy7 anti-rat CD4 (1:200 Biolegend San Diego CA), PE anti-rat CD8a (1:800 eBioscience), FITC anti-rat CD3 (1:200 ebioscience), PE/Cy7 anti-rat CD45 (1:400 Biolegend, San Diego). The cells were then washed 2x with PBS and fixed with 2% paraformaldehyde. Hoechst was added to gate for nucleated cells. All centrifugation steps were carried out for 8 min at 4 ℃ and 350g. Optimal antibody dilutions were chosen based on titration labeling of control splenocytes.

Forward and side scatter were adjusted accordingly for lymphocyte signal. Compensation controls were used in each experiment for each antibody. Once the flow cytometry was complete, all samples were gated for CD45 to analyze only blood-derived cells.

Astrocyte Cultures

Astrocyte cultures were produced from the cerebellum and hippocampus of 5-8 PD2 uninfected Lewis rat pups. Animals were decapitated, and the cerebella and hippocampi were dissected using surgical magnifying glasses (4x). Each dissected region was rolled on a filter paper to remove meninges and was placed in HBSS. Once all

regions were collected from a litter of pups (5-8 pups per isolation) tissue was then placed in a digestion media (for 25ml HBSS, 0.5ml 2.5% Trypsin, 0.5ml 4x pancreatin, 50ul 1.5M MgSO4, 100ul of 20mg/ml DNASE I) at 37 ℃ for 15-20min, shaking every 2-3 minutes. Tissues were then centrifuged for 1 min at 1500rpm. Supernatant was removed, and tissues were resuspended in 1ml of triturating media (10ml DMEM, 40ul DNASE 20mg/ml, 20ul 1.5M MgSO4). Tissue was then triturated 15x using flamed Pasteur pipettes, followed by 21 gauge and 23 gauge needles on a 1cc syringe. After trituration, tissues were washed with astrocyte media (DMEM/F12, 10% FBS, 2% dextrose, Primocen) and spun for 10 min at 150g and 4 ℃. The pellet was then resuspended in astrocyte media and plated into Corning T75 flasks, which had previously been treated overnight with poly-d-lysine. Astrocytes were then fed every 2-3 days and grown for 3-4 weeks, including 3 subculture passages before using. To purify cultures, astrocytes cultures were shaken to remove microglia on two different occasions at 180rpm for 45min. Astrocyte purity was assessed using immunohistochemistry and was found to be greater than 99.5% GFAP-positive and less than 0.005% microglia IB4-positive (isolectin B_4 conjugated to Alexa Fluor-488, or -647 (Molecular Probes))[148] for both hippocampal and cerebellar cultures.

For the cytokine/chemokine gene analysis, cerebellar and hippocampal astrocytes were cultured in 24 well plates at a concentration of 1 x 10^5 cells/well. 18-24 hours after plating, the cells were infected with 1x10^5 pfu of virus/well suspended in astrocyte media (1pfu/astrocyte initially plated). At the same time, new media was replaced on the uninfected control wells. Supernatant was removed, and cells were placed in Trizol at 12, 24 and 48 hours postinfection. mRNA was isolated, and RT-PCR performed, as described above. A total of 3 wells were collected for each group, and the experiment was repeated 2 times for a total of 6 wells per group.

Cell culture immunohistochemistry

Cell culture Immunohistochemistry was performed to asses for astrocyte purity and percentage of astrocytes infected by LCMV virus. To do this, cells were plated at a density of 10 x 10^3 astrocytes per well in four-well polystyrene, poly-d-lysine coated, chamber slides. Experimental cells were infected with LCMV 18 hours after plating using 1pfu/cell. At the time of infection, media was changed on non-infected wells. 48 hours after infection, cells were fixed with 4% paraformaldehyde. After fixation, ice cold methanol was placed on the cells for 10min. The cells were washed with PBS 3x. They were then blocked in 1.5% goat serum for 45 min, and incubated overnight with rabbit anti-GFAP and guinea pig anti-LCMV. The cells were then washed 3x with PBS and incubated with Alexa fluor 567 goat anti-guinea pig and alexa-fluor-488 goat-anti rabbit. Microglia were labeled using isolectin B_4 (IB_4, 5 μg/ml; [148] conjugated to Alexa Fluor-488, or -647 (Molecular Probes). Slides were examined and photographed using an Olympus BX-51 Light Microscope.

Statistical Analyses

Regional cytokine analysis

Gene expression levels by brain region (real time PCR results) for each cytokine and chemokine were analyzed separately by three-way ANOVA with brain region, infection status (infected or not infected) and time point (8, 10, 12, 14, 18, 25, and 34 days postnatal) as the three factors in the analysis.

Analysis of quantity of lymphocytes isolated from different brain regions

Quantity of CD8+, CD4+ and CD161+ lymphocytes isolated from each brain region were analyzed by three-way ANOVA with cell-type, brain region, and time point of isolation (10, 14, and 18 days) as the three factors in the analysis.

Analysis of the percentage of lymphocytes that were CD8+, CD4+, or CD161+

Percentage of CD8+, CD4+ and CD161+ lymphocytes isolated from each brain region and from the spleen (flow cytometry) were each analyzed using a three-way ANOVA with cell-type, tissue region, and time point of isolation (10, 14, and18 days) as the three factors in the analysis.

Astrocyte gene expression

Astrocyte gene expression (real time PCR results) for each cytokine and chemokine were analyzed separately by three-way ANOVA with brain region, infection status (infected or not infected) and time point (12, 24, and 48hr) as the three factors in the analysis.

Cerebellum gene expression levels by genotype

Gene expression levels by genotype (real time PCR results) for each cytokine and chemokine were analyzed separately by three-way ANOVA with genotype, infection status (infected or not infected) and time point (8, 10, 14, 18, and 25 days) as the three factors in the analysis.

For all analyses, post hoc pairwise comparisons were conducted with Bonferroni adjustments for multiple comparisons, and Fisher's LSD test. Unless otherwise stated in the Figure legend, p values were reported for the Bonferroni post-hoc results. A p-value of < 0.05 was considered statistically significant. All statistics were conducted using the SPSS statistical software package.

Results

To determine if cytokine expression differed among brain regions in LCMV infected animals, real-time PCR was used to measure cytokine mRNA levels. Three groups of Lewis rats were used: a group infected with LCMV on PD4, a sham injected

control group, and a suckle control group. Samples were taken from five infected brain regions: the dorsal cerebellum, ventral cerebellum, olfactory bulb, hippocampus, and septum. The dorsal cerebellum was collected separately from the ventral cerebellum because previous studies showed a greater destructive pathology in the dorsal cerebellum, compared to the ventral cerebellum. To analyze the full cytokine and chemokine response throughout the acute phase of disease, samples were collected at seven time points: postnatal days 8, 10, 12, 14, 18, 25, and 34. These time points were chosen based on the known time courses of viral infection and pathology development.

Peak Cytokine and Chemokine expression was higher in the cerebellum and olfactory bulb than in the hippocampus and septum

Figure 1 shows that cytokine mRNA expression was higher in the cerebellum and olfactory bulb than in the hippocampus and septum for all four cytokines examined. The most salient differences among regions were in the peak expression, while the most salient differences among cytokines were in the timing of peak expression. For all four cytokines, expression was higher in cerebellum and olfactory bulb than in hippocampus and septum. IL-6 peaked earliest and recovered the most quickly of all cytokines (Figure 1d). Its peak occurred at PD8 in the olfactory bulb, and at PD10 in all other regions. The highest IL-6 expression was in the dorsal cerebellum. IL-6 levels did increase up to 40 fold above normal in the septum and hippocampus, but this effect was dwarfed by the 250 fold increase in the cerebellum. The next cytokines to peak were TNF-α and IL-1b (Figure 1 B and C), which first occurred in the dorsal cerebellum, followed by the ventral cerebellum at PD 12 and 14. TNF-α expression was highest in the olfactory bulb, but was also very high in the cerebellum and septum. TNF-α declined most quickly in the hippocampus and septum, returning to near baseline by PD25. In contrast, in the cerebellum and olfactory bulb, TNF-α remained high as far out as PD34. IL-1β reached

its highest expression in the dorsal and ventral cerebella, compared to a lower expression in the hippocampus and septum. Il-1β values peaked earlier in the cerebellum than in the olfactory bulb, hippocampus, or septum. The high IL-1β levels were sustained longer in the cerebellum and olfactory bulbs than in the hippocampus or septum. INF-γ was the last of the four cytokines to peak, and the peaks were highest in the olfactory bulbs and the dorsal and ventral cerebellum (Figure 1A). The first IFN-γ peak occurred in the dorsal and ventral cerebellum as well as the septum at PD12, followed by hippocampus and olfactory bulb at PD14. IFN-γ remained elevated in the cerebellum and the olfactory bulb as late as PD34, compared to lower expression in the hippocampus and the septum.

In summary, in response to LCMV infection, all cytokines examined were significantly elevated above uninfected control levels in all brain regions. However, strong regional differences emerged, with the cerebellum and olfactory bulbs expressing substantially higher and longer sustained cytokine levels than the hippocampus and septum. Findings are summarized in Table 2.

Chemokine results by brain region

Similar to the cytokines, the chemokines CCL5, CCL2 and CXCL10 were all expressed at higher levels in the olfactory bulb and cerebellum than in the hippocampus and septum (Figure 2). CCL2 and CXCL10 peaked first, at PD10 in the cerebellum and later in the other regions (Figure 2 A and C). CCL5 peaked between PD12 and PD14 in all regions (Figure 2 B). Sustained expression past PD18 of CXCL10 and CCL5 levels remained much higher in the olfactory bulb and cerebellum than in the hippocampus and septum. Sustained CCL2 expression past PD18 was not as prominent as that of CXCL10 and CCL5. Regional differences emerged for all chemokines, with the cerebellum and olfactory bulb expressing significantly higher levels than hippocampus and septum.

The pattern of CX3CL1/fractalkine expression was different from the pattern of the other cytokines and chemokines (Figure 2 D). LCMV infection led to upregulation of

CX3CL1 expression in the cerebellum, but downregulation in the olfactory bulb and hippocampuses at some of the time points. Interestingly, a drastic difference in baseline CX3CL1 expression is evident between forebrain regions and the cerebellum. CX3CL1 expression at a baseline level is more than 1000 fold higher in forebrain regions than in cerebellum.

Total Lymphocytic infiltration differed among brain regions but cell type proportions were similar

Quantification of lymphocytes in the infected brain regions

To determine if lymphocyte infiltration is correlated with cytokine and chemokine levels, lymphocytes were isolated and quantified in the same five brain regions in which cytokine and chemokine levels were measured. Brains were removed from three animals at PD10, PD14, and PD18, and the dorsal and ventral cerebella, olfactory bulbs, and hippocampus were pooled and weighed. Lymphocytes were isolated from pooled samples, and the entire isolate was quantified. Splenocytes were simultaneously pooled and isolated at each time point to determine if there was a difference in the proportion of cells recruited in each brain region, compared to in the spleen. The experiment was repeated three times for each time point. These time points were chosen because they represent the time at which immune infiltration is first seen at PD10, through the peak times at PD14 and 18.

Additionally, to identify the subclasses of lymphocytes present at different time points, antibodies against CD3 (a pan T-cell marker), CD4 (a marker for Th1 cells), CD8 (a marker for cytotoxic T-cells), CD161 (a marker for NK cells) (homologue to the mouse and human NKPR) [149], and CD45RA (a pan-B cell marker), were used to label the cells [150-151]. Because developing neurons express many of these markers, anti-CD45 was used to gate for blood derived cells only [151-152]. A representative result of the flow cytometry experiment from the dorsal cerebellum is shown in Figure 3.

Figure 4 shows that lymphocyte infiltration at each time point (PD10, PD14, and PD18) was higher in the cerebellum than in the olfactory bulb, hippocampus and septum. At PD10, the dorsal cerebellum had as much as a 50 fold greater amount of CD4 and CD8 cells and a 30 fold greater amount of CD161+ cells than all other regions. At PD14, the dorsal and ventral cerebellum were similar in their quantities of CD4, CD8 and CD161, reaching as much as 3 fold higher than in olfactory bulb and septum and as much as 6 fold higher than in the hippocampus. At PD18, the dorsal and ventral cerebellum had proportionally similar quantities of CD4 and CD8 cells, which were 20 fold greater than septum, 5 fold greater than hippocampus, and 3 fold greater than olfactory bulb. Notably, at PD18, the quantity of CD161+ cells was significantly higher in the dorsal cerebellum than in the extra-cerebellar regions, reaching 50 times greater in the dorsal cerebellum than in the septum. In summary, the dorsal and ventral cerebella had a substantially greater lymphocyte recruitment than did the hippocampus and septum. These patterns of regional differences in lymphocyte recruitment parallel the patterns of cytokine and chemokine upregulation. Thus, the results are consistent with the notion that regional differences in cytokine/chemokine responses underlie the regional differences in lymphocytic infiltration.

Changes in the proportion of lymphocyte subclasses over time course of disease

Flow cytometry provides a means of measuring the percentage of cells that express specific cell surface markers. In the case of lymphocytes, flow cytometry can be used to quantify lymphocytic subclasses. Figure 5 shows the percentage of each lymphocyte population in spleen and in each brain region at PD10, 14 and 18. The results demonstrate that there was no significant difference between percentages of CD4, CD8, CD161 cells by brain region. However, with the passage of time, there was a substantial change in the percentage of each cell type. In particular, at the earliest time

point (PD10), the lymphocyte infiltration was predominantly CD161+ cells, with approximately 25% CD8+ cells, and only a very low percentage (less than 10%) CD4+ cells. By four days later (PD14), the proportions had changed substantially, as CD8+ cells became predominant. The percentage of cells that were CD4+ also rose, while the percent that were CD161+ plummeted to less than 10%. Between PD14 and PD18, the proportions continued to change, as the percentage that were CD8+ fell slightly, while the percentage that were CD4+ continued to rise. The percentages were significantly different at each time point. In addition, at each time point, the composition of lymphocytic subclasses in the brain regions differed from those of the spleen, implying a tissue specific homing of T-cells from the systemic circulation.

Astrocytes from the cerebellum had a stronger cytokine/ chemokine response to infection than did astrocytes from the hippocampus

To determine if LCMV infection induces astrocytes to express cytokines and chemokines, we isolated astrocytes from the hippocampus and cerebellum and infected them with LCMV. We chose the cerebellum and hippocampus for astrocyte cultures, (a) because these two brain regions exhibit very different patterns of LCMV-induced pathology (acute destruction in the cerebellum versus delayed onset cell loss from the hippocampus) [36-37], (b) because these regions have different patterns of cytokine and chemokine expression in vivo (Figure 1 and Figure 2), and (c) because astrocyte cultures can be readily established from them.

Cultures were first assessed for astrocyte purity using immunohistochemistry for GFAP to label astrocytes and isolectin B4 to label microglia. DAPI was used to identify all cells bodies. Hippocampus and cerebellum cultures were greater than 99.5% GFAP-positive and less than .005% isolectin B4-positive, thus indicating that the cultures were virtually purely astrocytic.

Cultures were then infected with a range of LCMV virus concentrations (0.1 pfu-4 pfu per cell) and were labeled immunohistochemically for GFAP and LCMV to determine the optimal concentration of LCM virus for infection. Both the cerebellar and hippocampal astrocyte cultures were infected uniformly at each of these concentrations, resulting in greater than 95% of cells infected. No cytotoxicity was evident at any LCMV concentration (n=1 for each concentration).

Figure 6 shows immunofluorescence of control and infected astrocytes from the hippocampus and cerebellum labeled with anti-GFAP and anti-LCMV antibodies. GFAP labeling revealed a uniform astrocyte cell population in cultures from both brain regions (top two rows, green), which remained equally uniform in GFAP labeling after LCMV infection (bottom two rows, green). Anti-LCMV labeling was uniform in both cerebellum and hippocampus cultures and no immunolabeling for LCMV antigen was seen in the noninfected wells (second column, red). Triple labeling with isolectin B4 was also performed, and no positive cells were found (data not shown). Quantification of LCMV positive cells 48 hours postinfection showed that greater than 99% of cerebellar astrocytes (n=4) and hippocampal astrocytes (n=2) were infected with LCMV. The percentage of cerebellar versus hippocampal astrocytes infected with LCMV were not significantly different from each other.

Cytokine expression was evaluated using real-time PCR from RNA isolated from the astrocyte cultures at 12, 24 and 48 hr post infection (Figure 7). Three of the four cytokines, TNF-α, IL-1β and IL-6, were increased by LCMV infection and in a region-specific manner. In particular, LCMV infection substantially increased the expression of TNF-α, IL-1β and IL-6 in astrocytes derived from the cerebellum, but not in astrocytes derived from the hippocampus. Furthermore, the extent to which LCMV increased expression of these cytokines in cerebellum-derived astrocyte cultures increased with time post-infection. By 48 hours post-infection, LCMV increased TNF-α, IL-1β and IL-6 expression by 7-fold, 3-fold, and 6-fold, respectively.

In contrast to the other cytokines, IFN-γ expression was not affected by LCMV infection in astrocyte cultures from either brain region with the exception of a small decrease at the 48hr time point in the hippocampal cultures only (Figure 7 A). IFN-γ also differed from the other cytokines in its relative baseline expression. At baseline (uninfected state), TNF-α, IL-1β and IL-6 were all expressed at higher levels in cerebellum-derived astrocyte cultures than in the hippocampus-derived cultures. In contrast, at baseline, IFN-γ expression was higher in the hippocampus-derived cultures than in those from the cerebellum. Overall, IFN-γ expression was extremely low in these astrocyte cultures, which is expected since IFN-γ is expressed almost exclusively by T-cells and microglia. However, the low expression levels reported here is consistent with research showing low IFN-γ expression in astrocyte cultures and immunohistochemical research labeling astrocytes as a source of IFN-γ production in vivo [153-155]. Thus, LCMV can induce astrocytes to express cytokines, and this effect is region-specific.

Figure 8 shows that chemokine expression, like cytokine expression, could similarly be induced by LCMV in a region-specific manner. For all of the chemokines examined (CCL2, CCL5, CXCL10, and CX3CL1), LCMV infection substantially increased their expression in astrocytes derived from the cerebellum, but not in those derived from the hippocampus. This was most dramatically evident in the expression of CXCL10, which LCMV increased 34-fold in cerebellum-derived cultures, while having virtually no effect in hippocampus-derived cultures.

T-cell independent cytokine/ chemokine expression is demonstrated in infection of RNU/RNU rats

To determine which cytokines and chemokines are expressed independently of T-cells, and, therefore, to determine which ones may be either coordinating the recruitment of lymphocytes or participating in T-cell-independent pathology, we infected Rowett Nude rats (RNU/RNU), which are deficient in thymus derived T-cells [146-147], and

compared their cytokine and chemokine expression to their T-cell competent heterozygote littermates (RNU/+) and to Lewis animals. RNA was isolated from the cerebella of these animals because, as seen in Figure 1 and 2 the cerebellum is the region with the greatest pathology and the strongest cytokine/chemokine response.

Figure 9 shows the cytokine expression in the cerebella of T-cell competent versus athymic (nude) rats. LCMV infection did not affect IFN-γ expression at PD8 for any genotype. However, from PD10 onwards, LCMV substantially increased IFN-γ expression in both of the immunocompetent genotypes (Lewis and RNU/+). At its peak, IFN-γ increased nearly 3000 fold over uninfected controls in the Lewis and RNU/+ animals, before falling toward baseline. In stark contrast, in the athymic animals (RNU/RNU), LCMV infection had no effect on IFN-γ expression at any time point. For the RNU/RNU animals, IFN-γ expression remained low and virtually unchanged throughout the time course. Thus, the LCMV-induced increase in IFN-γ expression was clearly T-cell-dependent.

Very different patterns were seen for the three other cytokines (TNF-α, IL-1β, and IL-6). On PD8, LCMV infection moderately, but significantly, increased the expression of TNF-α, IL-1β, and IL-6 in rats of all three genotypes. Furthermore, the extent to which LCMV increased the expression of these three cytokines on PD8 was similar for all three genotypes. However, after PD8, the genotypes diverged in their responses to LCMV infection. In particular, for the immunocompetent rats (Lewis and RNU/+), levels of TNF-α, IL-1β, and IL-6 continued to rise toward higher peaks, eventually reaching levels hundreds fold greater than baseline, before falling toward control levels. In contrast, in the athymic rats (RNU/RNU), TNF-α, IL-1β, and IL-6 rose no further after PD8 and rapidly plummeted toward baseline. Thus, the initial rise in TNF-α, IL-1β, and IL-6 was T-cell-independent, but its continued rise and sustained expression above baseline after PD8 were T-cell-dependent.

A similar pattern of T-cell-dependent and T-cell-independent responses were observed for the chemokines (Figure 10). LCMV infection induced a significant rise in the expression of CCL2, CCL5, and CXCL10 on PD8 in both immunocompetent and athymic animals. However, after PD8, these chemokines continued to rise to higher peaks in the immunocompetent rats, while they fell to baseline in the athymic rats. This same basic pattern was also true for CX3CL1, except that, on PD8, LCMV infection significantly increased expression only in the athymic rats. As was true of the other chemokines, after PD8, CX3CL1 expression continued to be induced by LCMV in immunocompetent rats, but not in athymic rats. Thus, the initial rise in chemokine expression occurred independently of T-cells, while their continued rise toward peak values and their sustained expression depended on the presence of T-cells.

Discussion

Regional differences in cytokine and chemokine expression anticipate and reflect regional differences in lymphocytic infiltration and tissue destruction

As a consequence of LCMV infection, the cerebellum and olfactory bulb attract greater numbers of lymphocytes and undergo substantially more severe destruction than do the septum and hippocampus. This unequal pathology among brain regions is not due to differences in infectivity, since viral titers are essentially equivalent among the regions. Instead, the differences in pathology must be due to local differences in response to the infection or to regionally different interactions with the immune system.

The expression of cytokines is tightly associated with homing of lymphocytes to areas of inflammation [98, 130]. Furthermore, as will be seen in chapter 3, much of the tissue damage induced by LCMV infection, especially in the cerebellum, is immune-mediated, and, in particular, lymphocyte-mediated. Thus, it is likely that the regional differences in destruction are due to regional differences in the attraction of lymphocytes,

which, in turn, are likely due to regional differences in the production of the cytokines and chemokines that govern lymphocytic infiltration.

The results of the present studies strongly support these notions. The cerebellum and olfactory bulb produced much greater and longer-sustained expression of cytokines and chemokines than did the hippocampus and septum. Furthermore, these same brain regions that produced large quantities of cytokines and chemokines were precisely the same as those in which lymphocytic infiltration was greatest, and, as has been shown previously, are precisely the same regions in which tissue destruction is greatest. Thus, regional differences in cytokine and chemokine production may underlie the regional differences in pathology. These findings have strong clinical implications, since regional differences are observed, not only in the rat model, but also in human cases of congenital LCMV infection.

Another possible contributor underlying the stronger lymphocytic infiltration and subsequent destruction in the cerebellum versus the forebrain regions may be differences in the immunosuppressive environment of the two regions. Under normal conditions, the brain has immunosuppressive elements that protect it from immune-mediated injury. This is accomplished through the BBB and the expression of TGF-β, NGF, and other immune modulators [58]. Regional differences in LCMV-induced destruction and lymphocyte recruitment may reflect regional differences in immunosuppressive properties. One of these immunosuppressive components are resident microglia, which can either be neuroprotective or neurotoxic [70, 143-145]. One chemokine that has been shown to recruit neuroprotective microglia and to attenuate TNF-α neurotoxicity is CX3CL1 [136, 143-144, 156]. CX3CL1 is expressed by monocytes, dendritic cells, subsets of T cells and natural killer cells, and by microglia [157]. However, microglia are the only cells in the brain that express the receptor for CX3CL1 [144]. In our analysis of CX3CL1 gene expression, we found that the cerebellum expresses a very small fraction of CX3CL1, when compared to the other brain regions. Because CX3CL1 is important

for the recruitment of neuroprotective microglia, the cerebellum may have fewer neuroprotective microglia, and, therefore, may be more susceptible to the damage of an inflammatory LCMV infection.

Regional differences in the time course of cytokine and chemokine expression reflect differences in lymphocytic infiltration.

Cytokines and chemokines are important for the recruitment of lymphocytes. Therefore, brain regions with elevated expression of lymphotactic cytokines, such as the chemokines CCL5, CXCL10, and CCL2, would be expected to have higher amounts of lymphocytes than regions with lower expression of the same cytokines. This should also be true in terms of the timing of infiltration. Brain regions that express high levels of lymphotactic cytokines at early time points should have an earlier lymphocytic infiltration than regions in which expression of these cytokines is delayed. Our results support both of these assumptions.

Pro-inflammatory cytokines and chemokines were highest in the dorsal cerebellum and were lowest in the hippocampus and septum. Likewise, lymphocytic infiltration was greatest in the dorsal cerebellum and least in the hippocampus and septum. Thus, the degree of lymphocytic infiltration among regions was correlated with the magnitude of the cytokine/chemokine response. These findings are summarized briefly in Table 2.

The data also support the notion that the timing of the cytokine response is important. The olfactory bulb had very high peak cytokine levels, sometimes even surpassing those of the cerebellum. However, the lymphocytic infiltration was not as great in the olfactory bulb as in the cerebellum. This may be a function of timing at which peak cytokine/chemokine levels occurred versus the timing at which lymphocyte infiltration was the most robust by brain region. Of important note is that peak

expression of most cytokines and chemokines occurs between PD10-12 in the cerebellum and PD14-18 in the olfactory bulb. Therefore, peak cytokine level occurs several days earlier in the cerebellum compared to the olfactory bulbs. This indicates that lymphocytes begin infiltrating the cerebellum earlier than in the olfactory bulbs. The cytokine levels persist at high levels in the cerebellum and therefore lymphocyte recruitment is sustained in this brain area, likely resulting in significant accumulation of lymphocytes over the two to four day period prior to peak levels in the olfactory bulb. Thus, by the time cytokine levels peak in the olfactory bulb, the cerebellum has already had several days of high cytokine expression. It is perhaps this temporally advanced expression of peak cytokine levels that underlies the greater lymphocytic infiltration/accumulation in the cerebellum compared to the olfactory bulb.

Infected astrocyte cultures provide evidence for a stronger astrocyte driven cytokine response in the cerebellum versus the hippocampus

The fact that different brain regions consistently undergo different forms and severity of pathology in response to LCMV infection strongly suggests that local factors among brain regions respond differently to the virus. A particularly noteworthy example is the difference between the cerebellum and hippocampus. As a result of LCMV infection, the cerebellum undergoes an acute destructive process that nearly obliterates the entire cerebellum. In stark contrast, the hippocampus undergoes little or no acute pathologic change. What can account for this marked difference in pathology between two brain regions simultaneously infected with a single viral species within the same animal?

Astrocytes are known to play a key role in LCMV infection of the developing brain. They are the first parenchymal cell type infected, the principal site of LCMV replication, and the major vehicle by which LCMV sequentially spreads across the brain.

Astrocytes are also an intrinsic source of cytokines and chemokines during infectious and inflammatory processes. Furthermore, astrocytes are not uniform throughout the brain [138-142]. Regional differences exist in the physiology of astrocytes. Therefore, we tested the hypothesis that the regional differences in LCMV-induced pathology might be due to regional differences in astrocyte response to LCMV infection.

We found that astrocytes derived from different brain regions respond differently to LCMV infection. In particular, we found that LCMV infection induces a robust expression of cytokines and chemokines in astrocytes derived from cerebellum, but not in those derived from hippocampus. Thus, the cerebellum, which is subject to an overwhelming lymphocytic infiltration and tissue destruction in response to LCMV infection in vivo is the same brain region whose astrocytes express large quantities of cytokines and chemokines in response to LCMV infection in vitro. Likewise, the hippocampus, which is subject to little lymphocytic infiltration and virtually no tissue destruction in response to LCMV infection in vivo is the same brain region whose astrocytes express virtually no cytokines or chemokines in response to LCMV infection in vitro. These results suggest that astrocytes may play a central role, not only in LCMV infection, but also in the disease pathogenesis.

Table 1 Table of brain regions infected and pathology

Brain Region	Peak Virus Titter	Cell Population Infected in Parenchyma	LCMV-Induced Pathology	Lymphocyte infiltration (by IHC)
Olfactory bulb	>10^9	Astrocytes, Mitral Cells, Granule Cells	acute hypoplasia that recovers by 4 months of age, no destruction	mild
Cerebellum	5x10^8	Astrocytes, Bergmann Glia, Purkinje Cells, Granule cells	global hypoplasia, destruction of dorsal lobules, disturbed granule cell migration	robust (dorsal), moderate (ventral)
Hippocampus	10^8	Astrocytes, Dentate Granule Cells	no acute pathology, delayed onset loss of dentate granule cells	undetectable
Septum	Not assayed	Astrocytes, Neurons	no pathology	undetectable

Figure 1 Cytokine expression by brain region: 1a. **IFN-γ** PD8: No significant differences. PD10: OLF, D and V CB are different from sham and suckle control (P<.01, P<.002). PD12 all regions are different from control values (P<.005). PD14: all regions are different from sham and suckle control values (P<.005). PD18: Olf, D CB and V CB are different from sham and suckle control values (P<.005), Olf is higher than Sep and Hip infected (P<.01). PD25 Olf, D CB and V CB are different from sham and suckle control (P<.01, P<.001, P<.05), DCB infected is higher than Hip infected (P<.05). PD35: D CB, V CB and Olf are greater than control (P<.001, P<.001, P<.005), and infected D CB and V CB are different from Hip (P<.05) 1b.**TNF-α** PD8: No significant difference between groups. PD10: Olf, D CB and VCB are different from control values (P<.01, P<.002). PD12 Olf, D CB and V CB, Hip, and Sep were different from controls (P<.005, P<.001, P<.001, P<.05, P<.001). PD14: Olf, D CB and V CB were different from control values (P< .001, P<.01, P<.05). PD18: Olf, D CB and V CB were different from control values (P<.001, P<.005, P<.005) and Olf was different from Sept infected (P<.05). PD25: Olf, D CB and V CB were different from control values (P<.01, P<.02, P<.05) DCB and Olf were different from Hip and Sep (P<.001, P<.01). PD35: Olf, D CB and V CB were different from control values (P<.05, P<.002, P<.001). D CB and V CB is different from Hip and Sep (P<.01, P<.01) Olf is different from Hip infected (P<.05). 1c. **IL1-β** PD8: no significant differences between groups. PD10: D CB and V CB, Hip and Sep are different from control values (P<.001, P<.001, P<.05, P<.03) and DCB is different from V CB, Olf, Hip and Sept (P<.01, P<.001, P<.001, P<.001). PD12: D CB, V CB, Hip and Sep are different from control (P<.001, P<.005, P<.005, P<.02) and D CB is different from Hip (P<.05). PD14 Olf, D CB and V CB, and Sep are different from control (P<.001, P<.004, P<.03, P<.005). PD18: All regions differ from control values (P<.05, P<.001, P<.001, P<.05, P<.005) and V CB is different from Olf (P<.05), Olf is different from hip and sept (P<.01, P<.006). PD25: All regions are different from control values (P<.001, P<.001, P<.001, P<.002, P<.002) and D CB is different from Hip and Sep (P<.01). Olf is different from Hip and Sep (P<.02). PD35: Olf, D CB and V CB are different from control values (P<.001) and Olf, DCB and V CB are different from Hip and Sep (P<.01, P<.001, P<.01). 1d.**IL-6** PD8: Olf is different from control and all other regions (P<.01). PD10 D CB, Hip and Sep are different from control values (P<.001, P<.05, P<.005) and DCB is different from Olf, Hip and Sep (P<.01). PD12: Olf, DCB, V CB, Hip is different from control (P<05, P<.05, P<.05, P<.001). PD14: All regions were different from control (P<.05, P<.05, P< .002, P<.001). PD18: Olf is different from suckle (P<.026) but not sham (P<.06). PD25: No significant differences. PD34: No significant differences. * All regions are significant compared to control, @ D B is significant over control, # VCB significant over control, & Olf is significant over control, ^ Sep is significant over control, + Hip is significant over its control, ** Some infected regions differ from other infected regions. n=3 or greater / time point / group

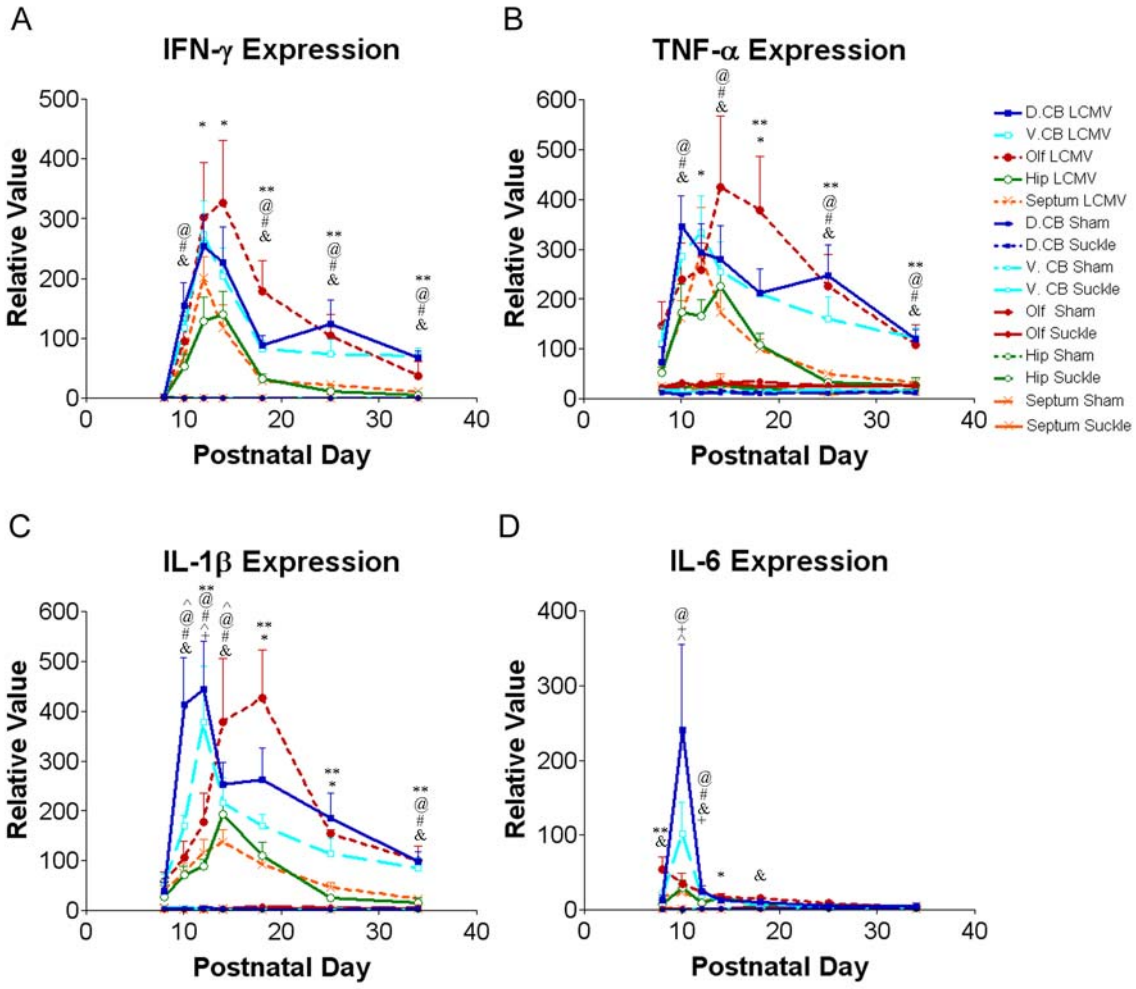
A
IFN-γ Expression
Relative Value
Postnatal Day
B
TNF-α Expression
Relative Value
Postnatal Day
D.CB LCMV
V.CB LCMV
Olf LCMV
Hip LCMV
Septum LCMV
D.CB Sham
D.CB Suckle
V. CB Sham
V. CB Suckle
Olf Sham
Olf Suckle
Hip Sham
Hip Suckle
Septum Sham
Septum Suckle
C
IL-1β Expression
Relative Value
Postnatal Day
D
IL-6 Expression
Relative Value
Postnatal Day

Figure 2 Chemokine expression by brain region: 2a. **CCL2** PD8: Olf is different from control (P<.005). PD10: D CB and V CB are different from control values (P=.05, P<.05,) and D CB is different from Olf, Hip and Sep (P<.01). PD12: D CB, V CB, Olf and Sep are different from control (P<.05, P<.05, P<.05, P<.025). PD14: Olf, D CB, V CB, Hip, Sep are all different from control values (P<.01, P<.001, P<.01, P<.05, P<.05) and both D CB and V CB are different from Hip and Sep (P<.05). PD18: All regions were different from controls values (P<.05, P<.05, P<.01, P<.02, P<.001) and Olf was different from all other regions (P<.001). PD25: Olf, D CB, Hip and Sep were different from control (P<.02, P<.05, P<.03, P<.001) and D CB is different from Hip (P<.05). PD34: D CB and V CB were different from control values (P<.02, P<.002). 2b.**CCL5** PD8: All regions are significantly different from their control, but not from each other (P<.001, P<.02, P<.025, P<.001, P<.05). PD 10: All are significant from control values (P<.05, P<.05, P<.025, P<.01) and the D CB is different from Olf, Hip and Sep (P<.005, P<.005, P<.001). PD12: Olf, D CB, V CB, and Sep are different from control values but not from each other (P<.05, P<.005, P<.02, P<.025). PD14: Hip and Sep were different from control values (P<.01, P<.05) and OLF, D CB, and V CB only reached a significance of P<.056, P<.068, P<.066. PD18: All are significant from control values (P<.001, P<.005, P<.007, P<.02, P<.001) and Olf is different from the Hip and Sep (P<.005). PD25: All are significant from control values (P<.03, P<.007, P<.001, P<.005, P<.001). PD35: D CB and V CB differ from control value (P<.001, P<.005) and Olf differs from the sham control (P<.05) and V CB differs from Olf, Hip and Sep (P<.05, P<.005, P<.01). 2c. **CXCL10** PD8: D CB, V CB, Hip and Septum were different from control values (P<.05, P<.02, P<.02, P<.03) and Olf was different from suckle but not sham (P<.05 vs. P<.09). PD10: Olf, D CB, and V CB were different from control values (P<.001, P<.001, P<.005). PD12: DCB, V CB, Hip and Sep were significantly higher than control values (P<.002, P<.005, P<.004, P<.02). PD14: Olf, D CB, V CB, Hip and Sep were all significantly different from controls (P<.02, P<.005, <.02, P<.02, P<.005) and Olf was different from all other regions (P<.05). PD18: D CB, V CB, Hip and Sep were different from control values (P<.05, P<.05, P< .01, P<.01) Olf was different from suckle control at P<.05 but did not reach significance for the sham control P.067. PD 24: Olf, D CB and V CB were different from control values (P<.001, P<.001, P<.001) and D CB and V CB were different from Hip and Sep (P<.001, P<.01). PD 35: D CB and V CB differed from control values (P<.001, P<.005) and D CB and V CB were different from Hip and Sep (P<.001, P<.02). 2d. CX3CL1 For all time points, D CB and V CB differed from all other regions independent of treatment (P<.02 at PD8 and P<.001 for points between PD10-PD25, and P<.02 or less at PD35). PD12: Hip infected differed from Hip suckle control (P<.01). PD14: No significant differences seen between infected and control groups. PD18: Olf was different from sham and suckle control (P<.03) and Hip was different from Hip suckle control (P<.001). PD24: Hip was different from Hip suckle control (P<.001). PD35: No significant differences between control and infected. n=3 or greater / time point / group

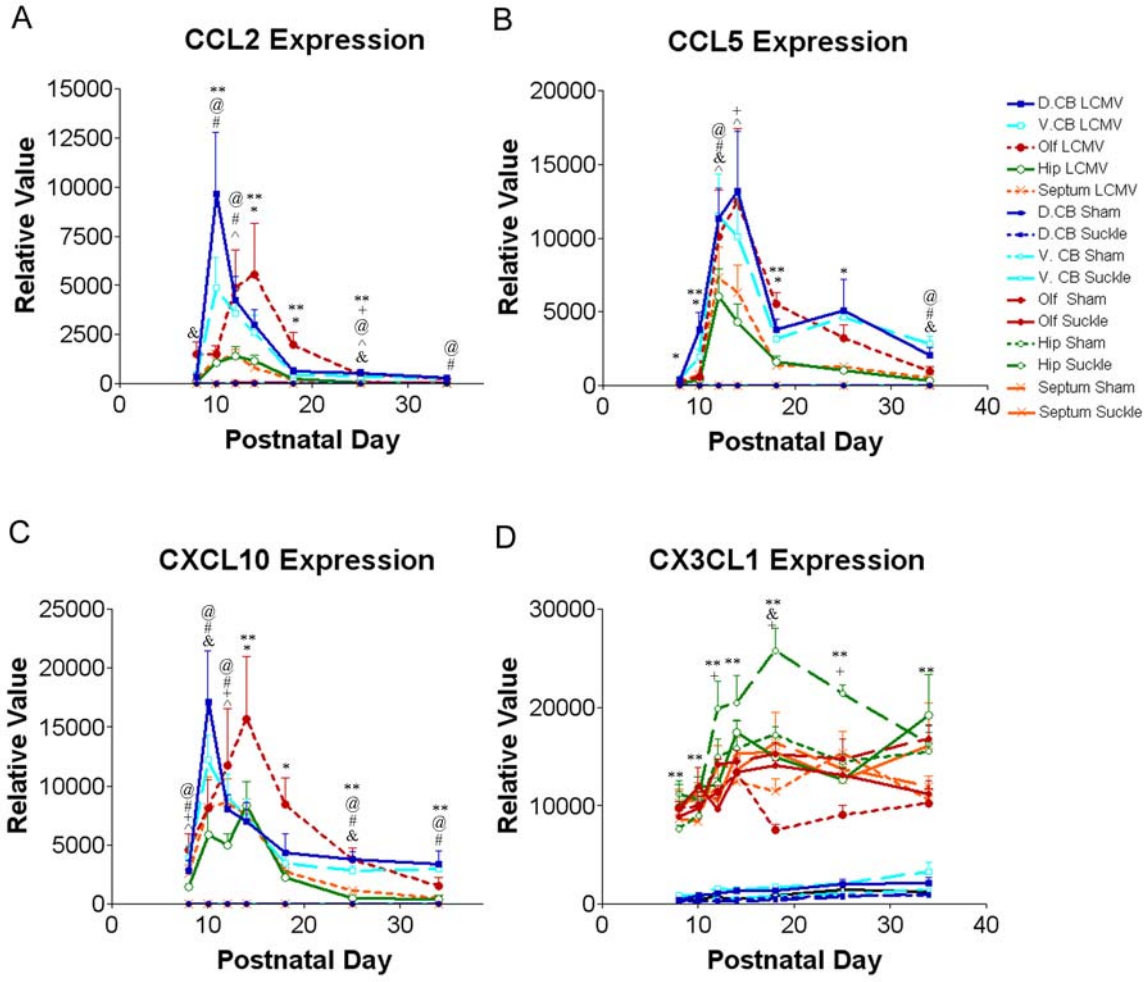
A
CCL2 Expression
Relative Value
Postnatal Day
B
CCL5 Expression
Relative Value
Postnatal Day
D.CB LCMV
V.CB LCMV
Olf LCMV
Hip LCMV
Septum LCMV
D.CB Sham
D.CB Suckle
V. CB Sham
V. CB Suckle
Olf Sham
Olf Suckle
Hip Sham
Hip Suckle
Septum Sham
Septum Suckle
C
CXCL10 Expression
Relative Value
Postnatal Day
D
CX3CL1 Expression
Relative Value
Postnatal Day

Figure 3 Representative flow cytometry output showing the result from the D CB regions. In the top panels, CD3 is graphed along the horizontal axis and CD8 and CD4 along the vertical axis. In the bottom left panel, CD3 is graphed along the horizontal and CD161 along the vertical axis. In the bottom right panel, CD45 is graphed along the horizontal axis and CD45RA along the vertical axis. CD3CD8+ cells are circled in the top left panel and are indicated by the purple color in all four panels. In the top right panel, CD3CD4+ cells are circled and are indicated by the color orange in all panels. In the bottom left panel, CD3CD161+ cells are circled and are indicated by the color blue. In the bottom right panel, CD45RA+ cells are circled and are indicated by the color yellow. n=3 animals per replicate, repeated 3 times

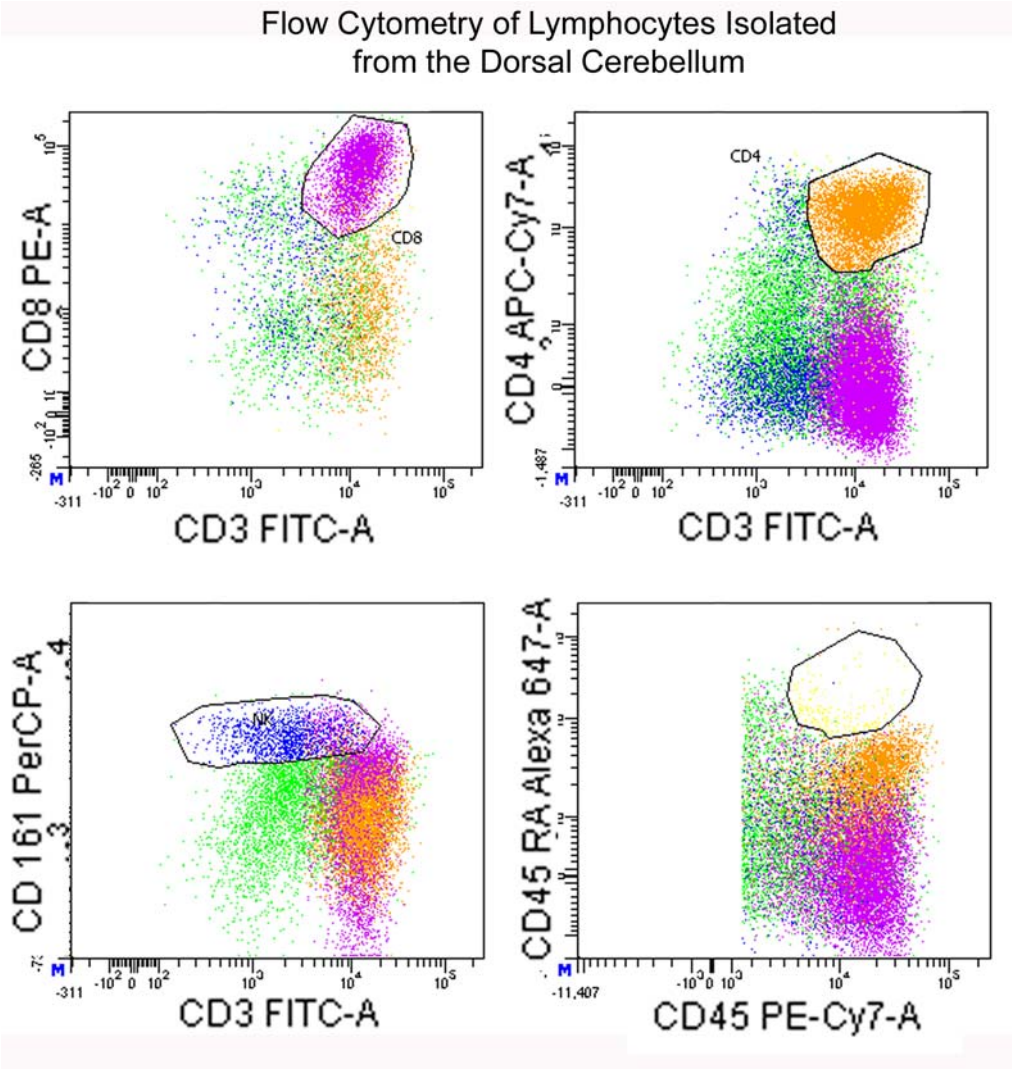

Figure 4 Quantity of infiltrating lymphocytes isolated from each brain region measured by flow cytometry. Values are expressed as fold lymphocytes in each region divided by lymphocytes isolated from the septum from one group of brains, averaged over three different experiments per time point. The cerebellum regions had significantly greater lymphocyte infiltration than the hippocampus region for each cell type analyze. The following results were found: At PD10, the quantity of CD8+ (a) CD4+ (b) CD161+CD3- (c) was as much as 50 fold higher in the D CB than in the other regions. This reached a significance for D CB over the Hip ($P<.05$). At PD14, there was 4.5 fold higher number of lymphocytes in the D CB and V CB than in the Hip for CD8 and CD4 cells ($P<.05$), CD161 was significantly different for the D CB compared to the hippocampus ($P<.05$) but was not significant for the V CB. At PD18, D CB and V CB had as much as a 20 fold greater quantity of CD8+ and CD4+ cells than the septum, 5 fold higher than the hippocampus, and 2.5 fold higher than the Olf ($P<.05$,). The quantity of CD161+ cells at PD18 was highest in the D CB and differed significantly from Olf, Hip and septum. This value was as much as 25 times higher than in the septum and 10 times higher than in the hippocampus ($P<.05$). * Spleen is different from at least one brain region * indicates significant difference in cell population between time points. Statistical differences were found using a Univariate analysis followed by LSD post hoc analysis. n=3

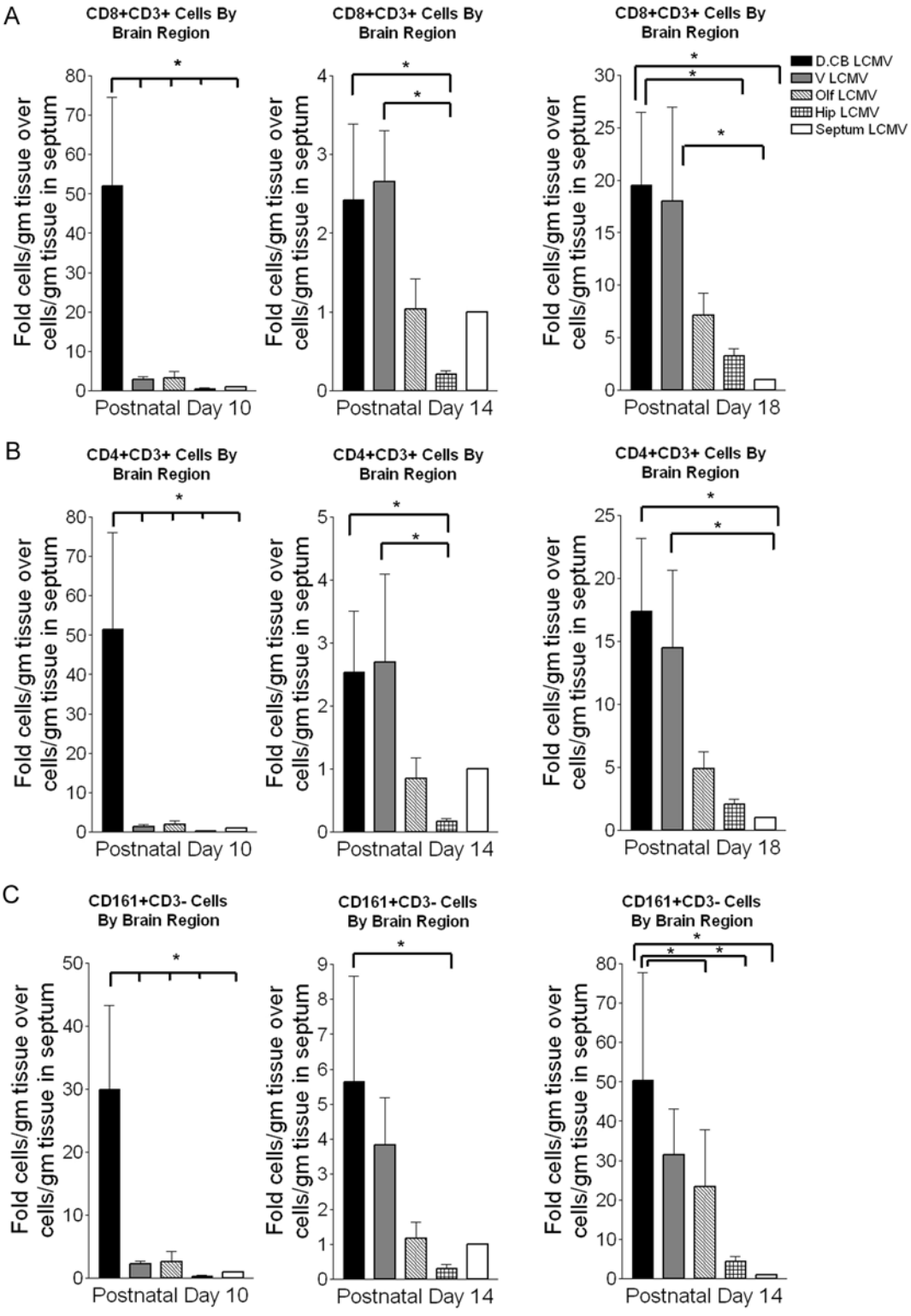
A
CD8+CD3+ Cells By Brain Region
Fold cells/gm tissue over cells/gm tissue in septum
Postnatal Day 10
Postnatal Day 14
Postnatal Day 18
D.CB LCMV
V LCMV
Olf LCMV
Hip LCMV
Septum LCMV
B
CD4+CD3+ Cells By Brain Region
C
CD161+CD3- Cells By Brain Region

Figure 5 Proportion of each lymphocyte population: The proportion of lymphocytes by population was not different between brain regions but did differ from the spleen indicating a brain specific recruitment of lymphocytes from the blood stream. Proportion of cells by region: The percentage of each population did change over time. At PD10, the percent of CD4+ (b) cells in all the brain regions was significantly different from the percent in the spleen ($P<.005$) and the proportion of CD161+CD3- cells in the DCB, VCB and Sep were different from the spleen ($P<.05$). CD8 had no significant difference in cell population between the brain regions or the spleen. At PD14, the spleen had a significantly smaller proportion of CD8 (a) and larger proportion of CD4 (b) cells compared to all brain regions ($P<.001$, $P<.0001$). There was no difference in proportion of CD161+CD3- cells at PD14. At PD18 the spleen had a significantly smaller proportion of CD8 (a) cells compared to all brain regions ($P<.01$). There was no significant difference in proportion of CD4+ or CD161+CD3- cells at PD18. Cell subtype percentage over time: The percent of CD8+, CD4+ and CD161+CD3- lymphocytes in the brain changed over the course of the infection. Of the total CD45 population, CD8+ cells accounted for 27 % at PD10, 71 % at PD14 and 51% at PD18. The change in percentage was significant between each time point ($P<.001$). Of the total lymphocyte population, CD4+ cells accounted for 3% at PD10, 9 % at PD14 and 14% at PD18. The change in percentage was significant between each time point ($P<.001$). Of the total CD45 population, CD161+CD3- cells accounted for 34% at PD10, 8 % at PD14 and 8% at PD18. The change in percentage between PD10 and PD14 was significant ($P<.001$), and there was no change in CD161+CD3- cell proportion from PD14 to PD18. n=3

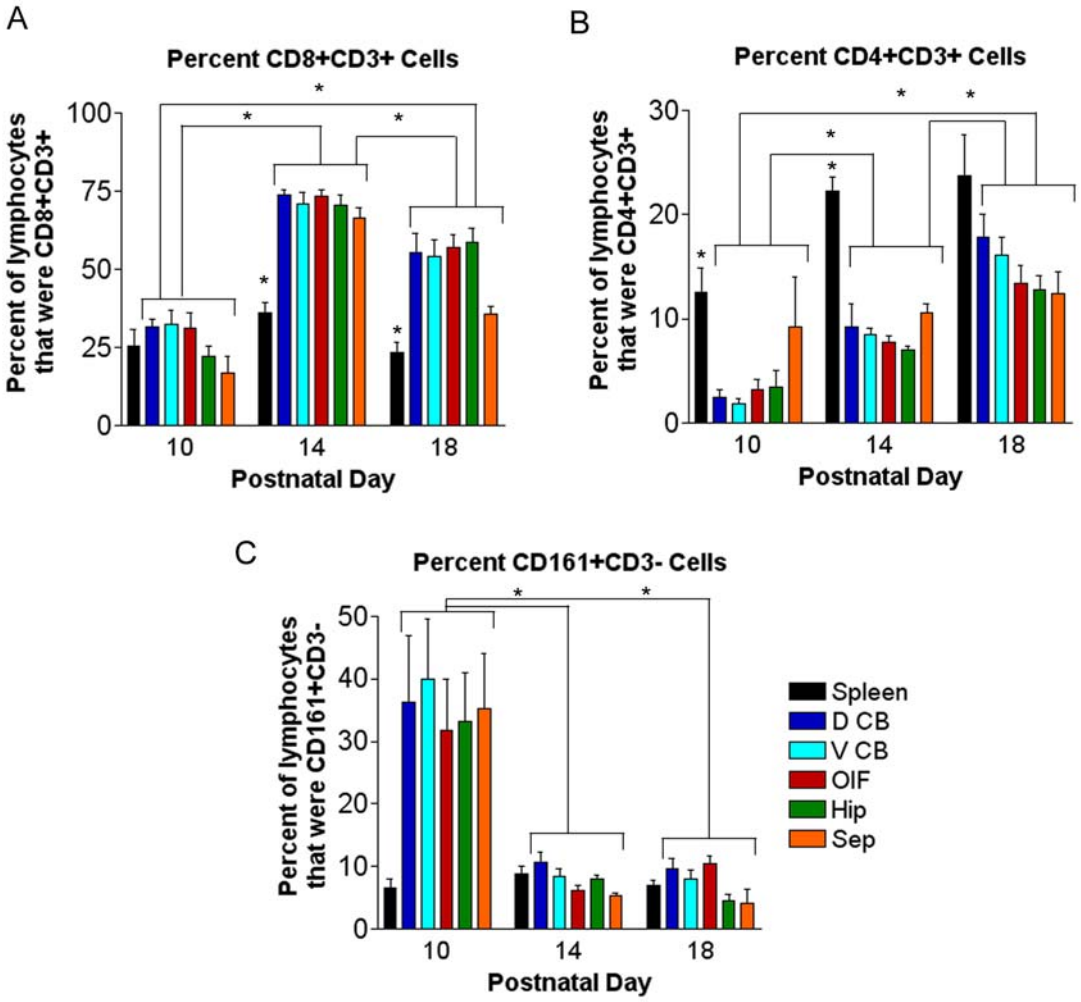
A
Percent CD8+CD3+ Cells
Percent of lymphocytes that were CD8+CD3+
100
75
50
25
0
10
14
18
Postnatal Day
B
Percent CD4+CD3+ Cells
Percent of lymphocytes that were CD4+CD3+
30
20
10
0
10
14
18
Postnatal Day
C
Percent CD161+CD3- Cells
Percent of lymphocytes that were CD161+CD3-
50
40
30
20
10
0
10
14
18
Postnatal Day
Spleen
D CB
V CB
OIF
Hip
Sep

Figure 6 Astrocyte cultures from the hippocampus and cerebellum. Astrocyte cultures were isolated from PD2 pups, and were established 3 weeks later, then infected 18 hours later after being plated. Forty-eight hours after infection, infected and control astrocytes were labeled with anti-GFAP and anti-LCMV to asses for purity and quantify infection with virus. More than 99% of cells labeled positive for anti-GFAP for both the hippocampus and cerebellum astrocytes in both the control and infected conditions. More than 95% of cells labeled with anti-LCMV in both the hippocampus and cerebellum astrocytes cultures. No anti-LCMV labeling was seen in hippocampus and cerebellum non-infected cultures. Magnification bar is equal to 100um. n=3 for cerebellar cultures and n=2 for hippocampus cultures

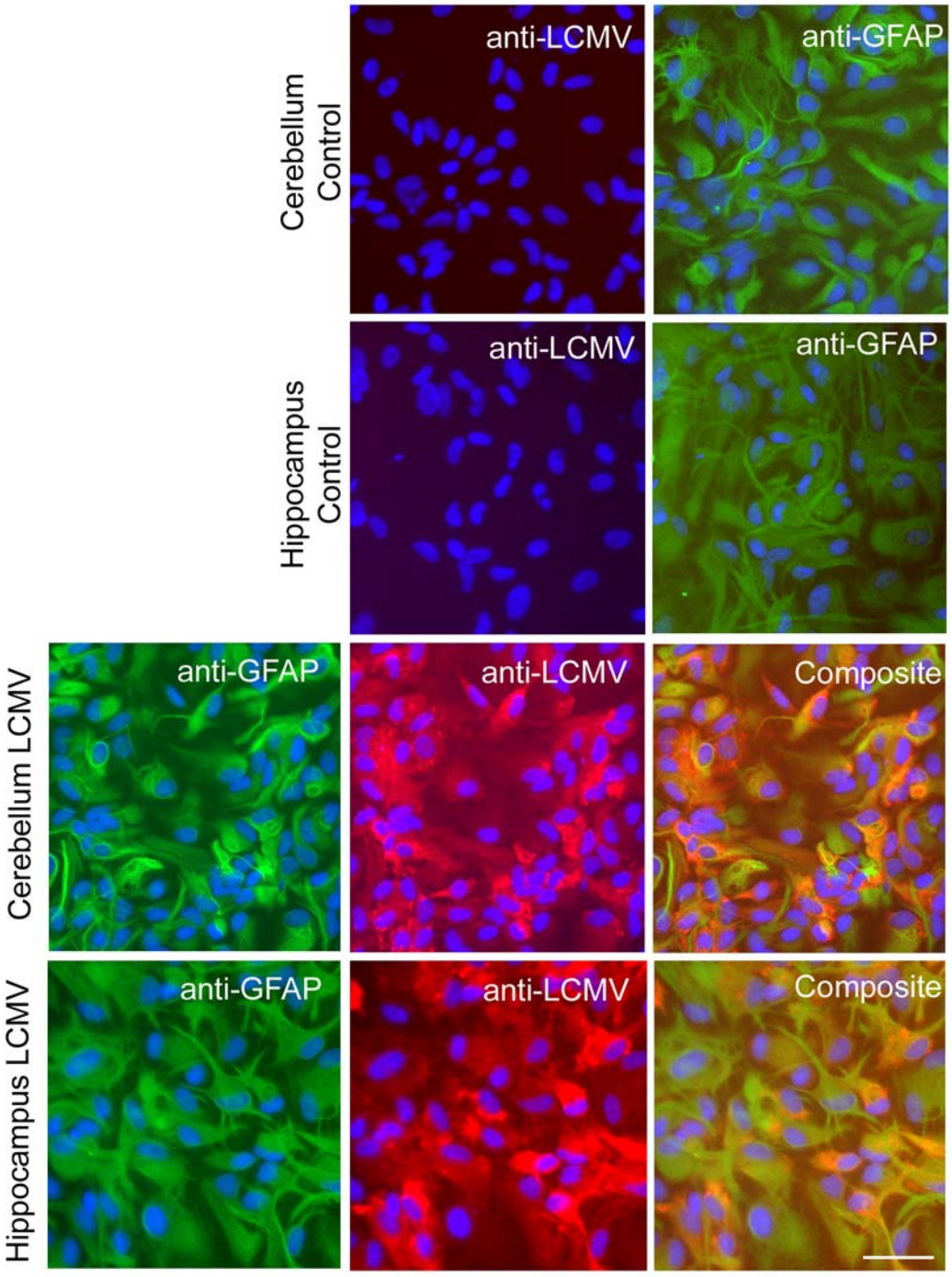
Cerebellum Control
anti-LCMV
anti-GFAP
Hippocampus Control
anti-LCMV
anti-GFAP
Cerebellum LCMV
anti-GFAP
anti-LCMV
Composite
Hippocampus LCMV
anti-GFAP
anti-LCMV
Composite

Figure 7 Cytokine expression in infected astrocyte cultures from the hippocampus and cerebellum: a. **IFN-γ** expression was elevated in infected hippocampus astrocytes but not cerebellum infected astrocytes. In addition, the hippocampus consistently expressed higher levels of IFN-γ than the CB both at a baseline level and in infected conditions. At 12hr postinfection (PI), there were no significant differences. At 24 hr PI, the Hip infected was significantly higher than CB infected (P<.0001) but no differences were seen between infected and control values. At 48 hr PI, Hip infected was significantly higher than control infected (P<.02) and Hip infected and control were significantly higher than CB infected and control (P<.02). b. **TNF-α** expression was elevated in infected cerebellum astrocytes but not in hippocampus astrocytes. At 12hr PI, CB infected was significantly higher than Hip infected and Hip control expression (P<.004) but not significantly higher than CB control. At 24hr PI, CB infected was significantly higher than CB control, Hip infected and Hip control (P<.005, P<.0001). At 48hr PI, CB infected was higher than CB control, Hip infected and Hip control (P<.05). c. **IL1β** expression was elevated in the infected cerebellum astrocytes but not in the hippocampus astrocytes. This reached significance at 48hr PI only at which time, CB infected was higher than the CB control, Hip infected and Hip control (P<.03, P<.001, P<.001). d. **IL-6** expression was elevated in infected cerebellum astrocytes but not in hippocampus astrocytes. At 12hr PI, CB infected was higher than CB control, Hip infected, and Hip control (P<.001, P<.0001, P<.0001). At 24hr PI, CB infected was higher than CB control but only reached a significance of P<.062. CB infected was also higher than Hip infected and Hip control (P<.004, P<.003). At 48hr PI, CB infected was higher than CB control, Hip infected and Hip control (P<.012, P<.002, P<.005). @ CB infected is significantly different from CB control, # Hip infected is significantly different from Hip control, * There is a significant difference between Hip and CB expression for the gene. n=3 wells /group repeated 2 times. RT-PCR data was collected in duplicates

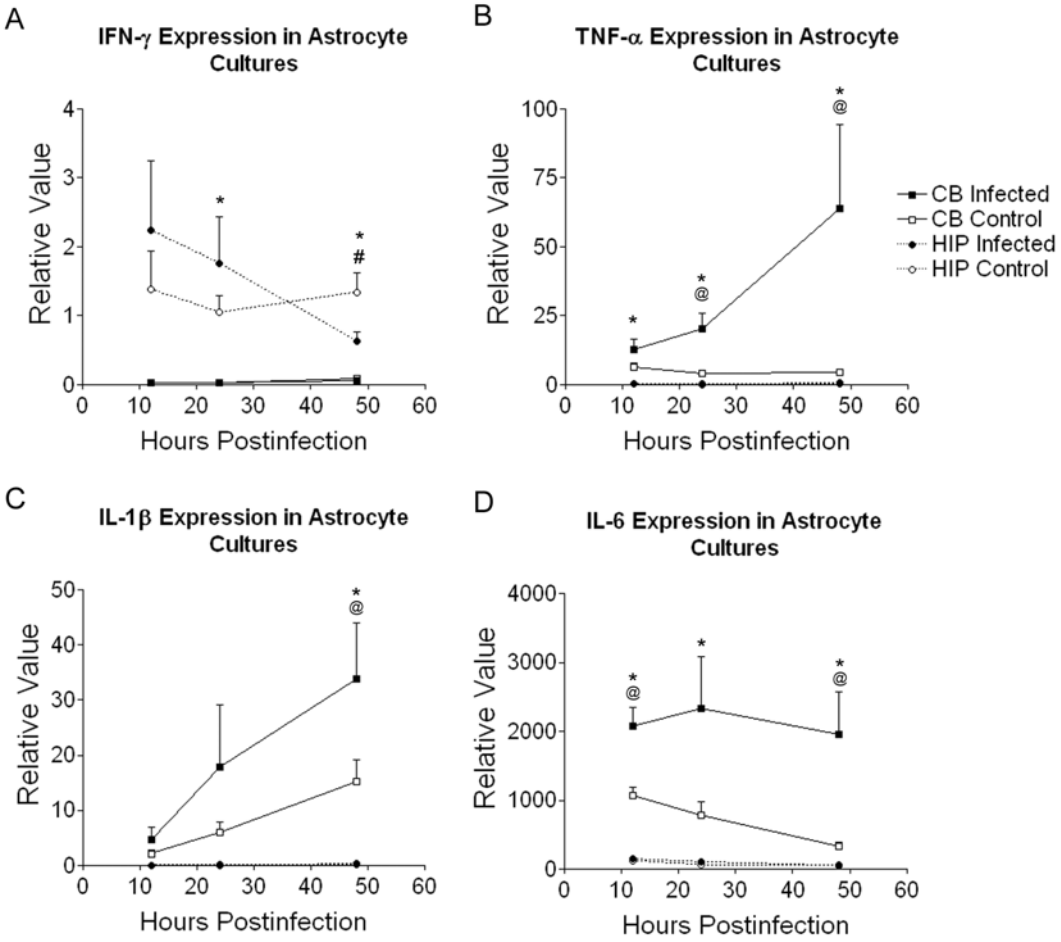
A
IFN-γ Expression in Astrocyte Cultures
Relative Value
Hours Postinfection
B
TNF-α Expression in Astrocyte Cultures
Relative Value
Hours Postinfection
CB Infected
CB Control
HIP Infected
HIP Control
C
IL-1β Expression in Astrocyte Cultures
Relative Value
Hours Postinfection
D
IL-6 Expression in Astrocyte Cultures
Relative Value
Hours Postinfection

Figure 8 Chemokine expression in infected astrocyte cultures from the hippocampus and cerebellum: a. **CCL2** expression was elevated in infected cerebellum astrocytes but not in hippocampus astrocytes. At 12hr PI, CB infected was higher than Hip infected and control (P<.003), and although it was higher than CB control it did not reach significance. At 24hr PI, CB infected was higher than Hip infected and control (P<.05), and although it was higher than CB control it did not reach significance. At 48hr PI, CB infected was significantly higher than CB control, Hip infected and Hip control (P<.04, P<.009, P<.015). b. **CCL5** expression was elevated in infected cerebellum astrocytes but not in hippocampus astrocytes. At 12hr PI, CB infected was higher than Hip infected and control (P<.03), and although it was higher than CB control it did not reach significance. At 24hr PI, CB infected was higher than CB control but did not reach significance. At 48hr PI, CB infected was significantly higher than CB control, Hip infected and Hip control (P<.05, P<.03, P<.05). c. **CXCL10** expression was elevated in infected cerebellum astrocytes but not in hippocampus astrocytes. At 12hr PI, CB infected was higher than Hip infected and control (P<.03), and although it was higher than CB control it did not reach significance. At 24hr PI, CB infected was significantly higher than CB control, Hip infected and Hip control (P<.04, P<.02, P<.02). At 48hr PI, CB infected was significantly higher than CB control, Hip infected and Hip control (P<.02, P<.02, P<.03). d. **CX3CL1** expression was elevated in infected cerebellum astrocytes but not in hippocampus astrocytes. At 12hr PI, CB infected was higher than Hip infected and control (P<.009, P<.009), and although it was higher than CB control it did not reach significance. At 24hr PI, CB infected was higher than control values but did not reach significance. At 48hr PI, CB infected was higher than Hip infected and control (P<.005, P<.008), and although it was higher than CB control it did not reach significance. n=3 wells /group repeated 2 times. RT-PCR data was collected in duplicates

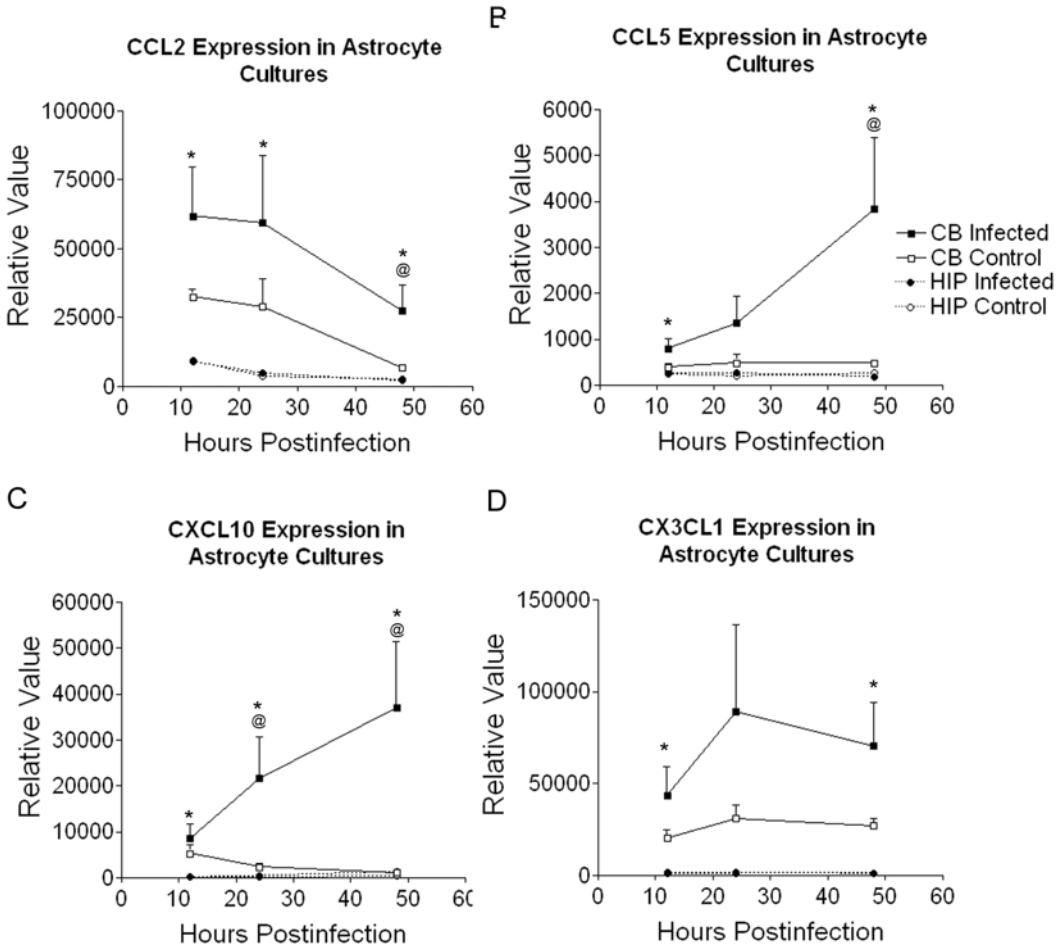
B
CCL2 Expression in Astrocyte Cultures
Relative Value
Hours Postinfection
CCL5 Expression in Astrocyte Cultures
CB Infected
CB Control
HIP Infected
HIP Control
C
CXCL10 Expression in Astrocyte Cultures
D
CX3CL1 Expression in Astrocyte Cultures

Figure 9 Cytokine expression in Lewis, RNU/+ and RNU/RNU cerebellum. Bar graphs are shown here, in comparison to line graphs shown in Figure 1 and 2 because these graphs are within the same brain regions (cerebellum) but different genotypes. Genotypes can be compared more easily using a bar graph. a. **IFN-γ** PD8: No significant differences. PD10: Lewis and RNU/+ infected were different from control (P<.001, P< .02). PD 14: Lewis and RNU/+ infected was significantly different from control (P<.001, P<.05). PD18: Lewis infected reached significance with the LSD post hoc (P<.05) and RNU/+ infected was significant above control (P<.02). RNU/+ infected was different from RNU/RNU infected. PD25: Lewis was significantly different from control (P<.001). b. **TNF-α** PD8: RNU/RNU infected was significantly higher then RNU/RNU control (P<.02). RNU/+ infected was higher than control (P<.005, LSD). PD10: Lewis and RNU/+ infected were significantly higher than control values (P<.0001, P<.001) and RNU/RNU was significantly higher than control values (P<.05, LSD). PD14: Lewis and RNU/+ infected were significantly higher than control values (P<.0001, P<.03) RNU+ infected was different from RNU/RNU infected (P<.05). PD18: Lewis and RNU/+ infected were significantly higher than control values (P<.0001, P<.0001) and RNU/+ infected was higher than RNU/RNU (P<.001). PD 25: Lewis and RNU/+ infected were significantly higher than control values (P<.0001, P<.002). c. **IL-1β** PD8: Lewis, RNU/+ and RNU/RNU infected were significantly higher than control (P<.05). PD10: Lewis and RNU/+ infected were higher than control values (P<.001, P<.005) and RNU/+ infected was higher than RNU/RNU infected (P<.02). PD14: Lewis infected was significantly higher than Lewis control (P<.001). PD18: Lewis and RNU/+ infected were higher than controls (P<.001, P<.001) and RNU/+ infected was significantly higher than RNU/RNU infected (P<.001). PD25: Lewis infected was higher than control (P<.001). d. **IL-6** PD8: Lewis infected is different from Lewis control (P<.001) and RNU/+ and RNU/RNU were significantly higher then control (P<.05 and P<.02, LSD). PD10: Lewis infected is higher than Lewis control (P<.03). PD14: Lewis was significantly different from control (P<.0001) and RNU/+ infected was nearly significant from control (P<.075). PD18: Lewis and RNU/+ infected were higher than control (P<.0001, .002) and RNU/+ was different from RNU/RNU infected (P<.03). PD25: No significant differences were found. * Lewis infected is significantly different from Lewis control at leas P<.05, @ RNU/+ is significantly different from RNU/+ control, # RNU/RNU is significantly different from RNU/RNU control, @# RNU/RNU+ is different from RNU/RNU infected. n=3 for each group at each time point

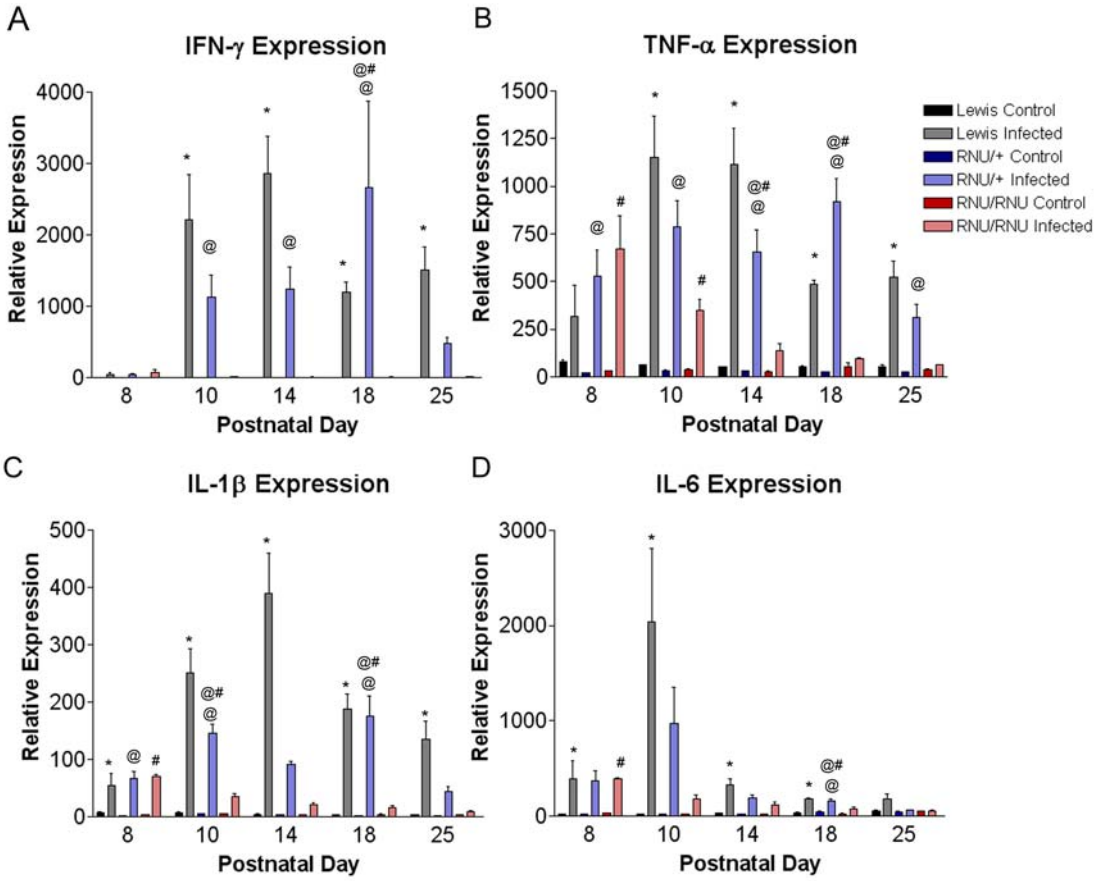
A
IFN-γ Expression
Relative Expression
Postnatal Day
B
TNF-α Expression
Relative Expression
Postnatal Day
Lewis Control
Lewis Infected
RNU/+ Control
RNU/+ Infected
RNU/RNU Control
RNU/RNU Infected
C
IL-1β Expression
Relative Expression
Postnatal Day
D
IL-6 Expression
Relative Expression
Postnatal Day

Figure 10 Chemokine expression in Lewis, RNU/+ and RNU/RNU cerebellum: a. **CCL2**. PD8: RNU/+ and RNU/RNU infected were significant from control (P<.025, P<.001), Lewis infected was also significantly higher than control (P<.03 LSD). PD10: Lewis infected was significantly higher than control (P<001). PD14: Lewis infected was significantly higher than control (P<.0001). PD18: Lewis and RNU/+ infected were significantly higher than control (P< .01, P<.01, P<.0001) and RNU/+ infected was significantly different from RNU/RNU infected (P<.001). PD25: Lewis infected was significantly higher then control (P<.001). b. **CCL5.** PD8: RNU/+ and RNU/RNU infected were significantly different from controls (P<.003, .P<.009). PD10: Lewis and RNU/+ infected were significantly higher than control (p<.0001, p<.0001) and RNU/+ infected was significantly higher than RNU/RNU infected (P<.001). PD14: Lewis and RNU/+ were significantly higher than control (p<.0001, P<.05). PD18: Lewis and RNU/+ infected were significantly higher than control (p<.007, p<.008) and RNU/+ infected was significantly higher than RNU/RNU infected (P<.008). PD25: Lewis was significantly higher than control (p<.001). c. **CXCL10.** PD8: RNU/+ and RNU/RNU infected were significantly higher than controls (P>.005, P<.02). PD10: Lewis and RNU/+ infected were higher than controls (P<.0001, P<.004) and RNU/+ was higher than RNU/RNU infected (P<.004). PD14: Lewis and RNU/+ infected were higher than controls (P<.0001, P<.0001) and RNU/+ was higher than RNU/RNU infected (P<.001). PD18: Lewis and RNU/+ infected were higher than controls (P<.0001, P<.0001) and RNU/+ was higher than RNU/RNU infected (P<.0001). PD25: Lewis and RNU/+ infected were higher than controls (P<.0001, P<.05) and RNU/+ was higher than RNU/RNU infected (P<.05). d. **CX3CL1** PD8: RNU/RNU was significantly higher than control (P<.05). PD10: RNU/+ infected was significantly higher than control (P<.05) PD14: There were no significant differences between groups. PD18: Lewis and RNU/+ were higher than control (P<.05, P<.02) and RNU/+ infected was higher than RNU/RNU infected (P<.02). PD25: Lewis infected is significantly higher than control (P<.05). n=3 for each group at each time point

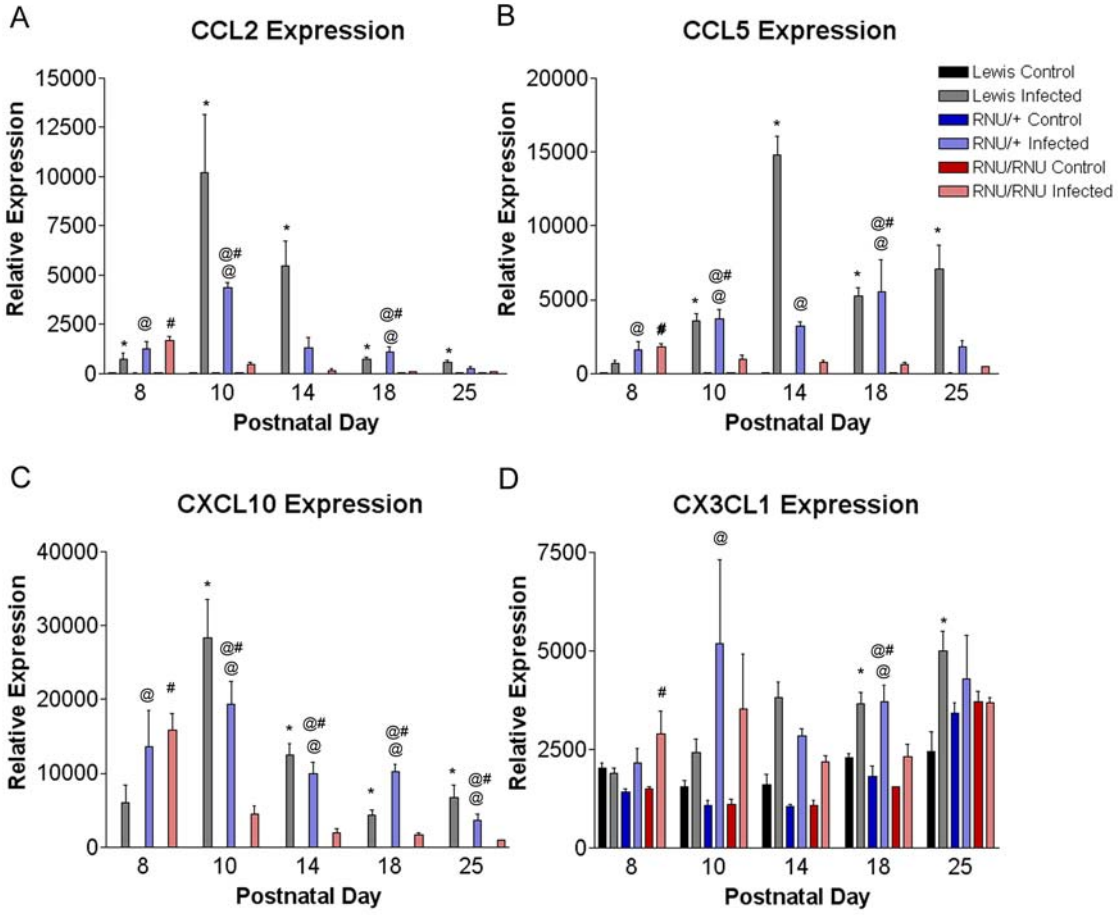
A
CCL2 Expression
Relative Expression
15000
12500
10000
7500
5000
2500
0
8
10
14
18
25
Postnatal Day
B
CCL5 Expression
Relative Expression
20000
15000
10000
5000
0
Postnatal Day
Lewis Control
Lewis Infected
RNU/+ Control
RNU/+ Infected
RNU/RNU Control
RNU/RNU Infected
C
CXCL10 Expression
Relative Expression
40000
30000
20000
10000
0
Postnatal Day
D
CX3CL1 Expression
Relative Expression
7500
5000
2500
0
Postnatal Day

Table 2 Summary of results by brain region for cytokine, chemokine, lymphocyte infiltration and astrocyte cultures.

Brain Region	Cytokines and chemokines with high peaks by region	Lymphocyte infiltration (relative to septum)	Chemokine and Cytokine Expression in Astrocyte Cultures
Olfactory bulb	Cytokines: IFN-γ, TNF-α, IL-1β. Chemokines: CCL5, CXCL10	Not higher than other regions	
Cerebellum	Cytokines: IL-6, IFN-γ, TNF-α IL-1β. Chemokines: CCL2, CCL5, CXCL10	PD10: As much as 50 fold above septum and hippocampus PD14: As much as 4.5 fold above hippocampus. PD18: as much as 20 fold higher than septum and 4 fold higher than hippocampus	Elevation in Cytokines: TNF-α, IL-1β and IL-6. Elevation in Chemokines: CCL2, CCL5, CXCL10, CX3CL1
Hippocampus	All cytokines and chemokines were below levels of cerebellum and olfactory bulb	Not higher than other regions	IFN-γ decrease in infected cultures, otherwise no change for cytokines or chemokines after infection
Septum	All cytokines and chemokines were below levels of cerebellum and olfactory bulb	Not higher than other regions	

CHAPTER 3: CEREBELLAR PATHOLOGY IN A RAT MODEL OF CONGENITAL LCM VIRUS INFECTION IS IMMUNE-MEDIATED AND VIRUS-MEDIATED

Introduction

The neonatal rat cerebellum is a particularly useful brain region in which to study the effects of LCMV on the developing brain [14]. Following intracranial inoculation, LCMV replicates to high titers within the cerebellum [36], where the viral infection induces hypoplasia, focal destructive lesions, and neuronal migration disturbances [14, 36-37, 47-49], all of which are also observed in humans with congenital LCMV infection [1, 29] (16, 65).

The principal goal of this study was to evaluate the role of T-lymphocytes in the cerebellar neuropathology found in neonatal rat LCMV infections. In prior studies, we [14, 36-37] and others [47-49, 158-159] have used the Lewis rat as the model system for congenital LCMV infections. In this study, we compared the immunocompetent Lewis rats, which possess a normally functioning immune system, to congenitally athymic (nude) rats, which are immunocompromised and specifically deficient in thymus-derived T-lymphocytes [146-147].

Cytokines are a group of proteins that play key roles in regulating the humoral and cellular antiviral immune responses. Produced by infiltrating inflammatory cells, as well as by astrocytes and microglia [67, 70, 160], cytokines not only help to coordinate immune responses, but can also exert antiviral effects and neurotoxic effects, thus directly contributing to viral clearance and to neuropathologic changes [74, 130].

In adult mice, LCMV infection upregulates the cytokines TNF-α and IFN-γ in spatiotemporal patterns that correlate with viral infection and neuropathology[100] [101]. The role of cytokines in human congenital infection and in the neonatal rat model is unknown. A second goal of this study was to determine whether neonatal rats express

cytokines when infected with LCMV, and whether the patterns of cytokine expression depend upon the presence of T-lymphocytes.

Materials and Methods

Animals

The nude mutation (RNU) is a homozygous recessive mutation [146-147]. The homozygous (RNU/RNU) state in rats is characterized by hairlessness and congenital aplasia of the thymus. This athymic state results in a severely deficient cell-mediated branch of the immune system. Non-thymus-dependent immune reactivity, such as cytotoxicity by natural killer cells and antibody production to T-cell-independent antigens is of a similar or slightly higher magnitude than in euthymic rats. Heterozygote rats (RNU/+) generate a normal complement of functional T-cells, are fully immunocompetent, and are virtually indistinguishable from homozygous wild type rats [147].

Pregnant Lewis rats and RNU/+ rats on a hooded background were obtained from Harlan Sprague-Dawley (Indianapolis, IN). The Lewis rat dams were bred with Lewis males, while the RNU/+ rats were bred with RNU/RNU males. Thus, the litters of the Lewis dams were all of the Lewis genotype, while the litters of the RNU/+ dams were approximately 50% RNU/+ and 50% RNU/RNU. As the Lewis rats and athymic rats (RNU/RNU) are of different genetic backgrounds, we used the heterozygote siblings (RNU/+) of the athymic rats as a second comparison group. The rats were maintained in viral containment quarters at the University of Iowa Animal Care Facility. The pregnant rats were observed several times per day to establish time of birth of the litters. The day of birth was defined as postnatal day zero (PD 0). Prior to performing experiments, approval for all experiments was obtained from the University of Iowa Animal Care and Use Committee.

Virus

The neurotropic Armstrong-4 strain of LCMV was used for all inoculations [36]. The virus stock was prepared in BHK-21 cells and harvested at 48 hours after infecting the cells. The virus was stored in 1 ml aliquots at -80°C. The stock had a titer of 2×10^8 plaque forming units (PFU) per ml.

Infections

On postnatal day 4, neonatal rat pups received injections at a depth of approximately 3 mm into the right frontal cortex with either LCMV or Dulbecco's modified Eagle's medium (DMEM), as a control. Injections were performed with a Hamilton syringe with a needle depth guard. The animals received 0 PFU (control) or 1000 PFU of LCMV in a volume of 5µl of DMEM.

Histology and Immunohistochemistry.

For evaluation of neuropathology, cellular targets of LCMV, and presence of T-lymphocytes, rats were sacrificed at a series of ages following infection. For each treatment group (Lewis, RNU/+, and RNU/RNU; infected and uninfected), 3 - 4 rats were sacrificed at postnatal days (PD) 14, 25, 40, 60, and 90. The rats were perfused via the left cardiac ventricle with 0.9% saline, followed by 4% paraformaldehyde in 0.1 M sodium phosphate buffer. The brains were removed and stored in 4% paraformaldehyde fixative.

The cerebella were then separated from the brainstems. However, in some of the infected animals, the cerebellum was so small that it was left attached to the brain stem to facilitate orientation of the tissue. The cerebellar vermis was isolated, dehydrated through a graded series of alcohol, embedded in paraffin, and cut on a rotary microtome in the sagittal plane into 5 µm-thick sections. The sections were mounted onto glass slides and stained with hematoxylin and eosin for assessment of neuropathology.

For immunohistochemistry, the sections were de-paraffinized and re-hydrated through graded ethanol solutions. Antigen retrieval was performed in a citrate buffer steam bath for 20 minutes. Endogenous peroxidases were blocked by incubation with 3% hydrogen peroxide for 30 minutes. For LCMV viral antigen immunostaining, the sections were incubated with a goat serum blocking solution for 60 minutes. The sections were then incubated with guinea pig polyclonal anti-LCMV antibody (3) (diluted 1:1000) overnight at 4°C in a humidified chamber. Detection was performed using a biotinylated goat anti-guinea pig secondary antibody (Jackson ImmunoResearch, West Grove, PA). The reaction was completed with the ABC Elite (Vector Laboratories, Burlingame, CA) and diaminobenzidine (DAB) substrate.

The technique for CD8 antigen staining was identical to that used for LCMV staining, except that the blocking solution was horse serum, and the primary antibody was mouse anti-rat CD8a antigen (Pharmingen) with a secondary antibody of horse anti-mouse IgG (Vector Laboratories).

Virus Quantification

A separate group of animals was used to quantify viral load within, and viral clearance from, the cerebellum. Animals (Lewis, RNU/+, and RNU/RNU) received intracerebral injections of 1000 PFU of LCMV in a volume of 5 µl of DMEM, as described above. At a series of time points, the rats were sacrificed for viral titer determination. Three or four animals per group and per time point were sacrificed at PD 8, 10, 14, 18, 21, 25, and 30. The animals were euthanized with pentobarbital, and the brains were harvested. Tissue samples were taken from the cerebellum and immediately frozen on powdered dry ice. Samples were stored frozen at -80°C. To determine the viral titer, the tissue sample was weighed and homogenized in plaquing media, as described previously [161]. Viral concentration was determined by plaque assay on Vero cell monolayers [159]. Viral titers were recorded as viral quantity per gram of tissue.

Cytokine, chemokine, and chemokine receptor expression levels

A third group of animals was used to determine the time course of LCMV-induced changes in selected cytokine, chemokine and chemokine receptor gene expression levels. Lewis, heterozygote (RNU/+) and athymic (RNU/RNU) rats received intracerebral injections of 0 or 1000 PFU of LCMV on PD4. The Lewis rats were sacrificed on PD 8, 10, 12, 14, 18, 21, 25, 30, and 34. Infected and uninfected RNU/+ and RNU/RNU rats were sacrificed on this same set of postnatal ages, except that uninfected RNU/+ and RNU/RNU rats were not included on PD 8, 12, 21 and 30. For each treatment, time point, and genotype, 3-5 rat pups were included.

On the day of sacrifice, the animals were euthanized with pentobarbital, and the brains were harvested. Tissue samples were taken from the cerebellum and immediately frozen on powdered dry ice. Samples were stored frozen at -80°C.

mRNA was isolated using Trizol reagent (Invitrogen, Carlsbad, CA), according to the manufacturer's protocol. Total RNA (2 μg) was reverse-transcribed using SuperscriptTM II (Invitrogen). The resultant cDNA was suspended to 300 μl with endonuclease-free water. 2.5 microliters of this cDNA was used as a template per reaction for the TaqMan assay of both the mRNA of interest and the internal control ribosomal RNA. TaqMan primer and probe sets for template and ribosomal RNA were purchased from Applied Biosystems Inc. (Foster City, CA). Probes for the target genes [Interferon-gamma (IFN-γ), tumor necrosis factor-alpha (TNF-α), stromal derived factor-1(sdf-1) and the sdf-1 receptor (CXCR4)] were labeled with the reporter dye, and the rRNA probe was labeled with the reporter fluorescein dye to allow analysis of the target gene and the rRNA in the same well. Serial dilutions of 596-bp cloned cDNA from ribosomal RNA (5 to 5000 pg) were used to construct a standard curve of cDNA amount versus threshold cycle (Ct). The results were expressed as relative amounts of mRNA per 12.5 pg of rRNA.

Statistical Analyses

The viral titer data was normalized through a logarithmic transformation, log (value+1). The constant (+1) was added, as the virus titer was zero in multiple samples, and the log cannot be determined for a value of zero. As most of the virus titers ranged in value from 10^3 to 10^9, the addition of the constant (+1) altered the values only trivially. The viral titer data was evaluated by two-way analysis of variance (ANOVA) with genotype (Lewis, RNU/+, and RNU/RNU) and time point (8, 10, 14, 18, 21, 25, and 30 days postnatal) as the two factors in the analysis.

Gene expression levels (real time PCR results) for IFN- γ, TNF-α , sdf-1 and CXCR4 were each analyzed separately by three-way ANOVA with genotype, infection status (infected or not infected) and time point (8, 10, 12, 14, 18, 21, 25, 30, and 34 days postnatal) as the three factors in the analysis.

To better assess the differential effects among the genotypes of LCMV infection on sdf-1 and CXCR4, expression levels in the infected animals were divided by mean expression levels in uninfected animals of the same genotype and age. These relative levels (fold changes) of expression were then analyzed by two-way ANOVA, with genotype and time point (10, 14, 18, and 25 days postnatal) as the two factors in the analysis.

For all analyses, post hoc pairwise comparisons were conducted with Bonferroni adjustments for multiple comparisons. A p-value of < 0.05 was considered statistically significant. All statistics were conducted using the SPSS statistical software package.

Results

LCMV infection induced ataxia and hind limb hypotonia in immunocompetent rats, but not in athymic rats.

All animals infected with LCMV were inoculated with the virus on PD 4. The animals of all groups remained well groomed and active. However, between 8 and 15

days postinoculation, the infected Lewis and heterozygote (RNU/+) rats developed marked ataxia and hind limb hypotonia. Some of these animals were unable to right themselves when turned onto their backs. In contrast, the athymic rats (RNU/RNU) never developed hind limb hypotonia or ataxia. However, they did develop jitteriness, consisting of tremulousness and subjectively increased responsiveness to tactile stimulation, during this same time period.

LCMV heavily infected the cerebellum, from which viral clearance was delayed in rats lacking T-lymphocytes.

After inoculation with LCMV on PD 4, animals were sacrificed at a series of ages to determine peak viral titers and rate of viral clearance. In all groups, viral titers rose to high levels (~10^9 PFU per gram of tissue) around PD 10 (Figure 11). There were no statistically significant differences in peak viral concentrations among the three groups. After PD 14, the titers declined in all groups, reflecting viral clearance. However, viral titers fell more slowly in the RNU/RNU rats than in the other two groups. As a result, by PD 21, the athymic rats had significantly higher viral titers than either the Lewis rats or the RNU/+ rats. Though the titers continued to decline in all groups, the athymic rats had significantly higher viral titers at all time points from PD21 through PD 30. Thus, absence of T-lymphocytes delayed LCMV clearance from the cerebellum.

The cellular targets of infection were identical in rats with and without T-lymphocytes, but absence of T-lymphocytes impaired viral clearance from astrocytes.

On PD 14, a time at or near peak viral titers, the cerebella of the animals were evaluated for the cellular pattern of LCMV infection (Figure 12). Immunohistochemical staining for LCMV demonstrated that the cellular targets of infection were identical for animals of all three genotypes (Lewis, RNU/+, and RNU/RNU). LCMV antigen was widespread throughout the cerebellum of all infected animals and was located in virtually

all neurons, including Purkinje cells and granule cells, as well as in astrocytes. In fact, at the peak of infection, LCMV antigen appeared in virtually all of the cellular elements of the cerebellum of all three genotypes. Thus, the cellular targets of infection within the cerebellum were independent of T-lymphocytes.

In contrast, at later time points, when viral titers were falling, the cellular patterns of infection differed among the genotypes. In particular, after PD14, LCMV antigen was restricted to neurons and was no longer present within the astrocytes of the Lewis or RNU/+ rats, but remained within neurons and astrocytes of the RNU/RNU rats. Thus, viral clearance from astrocytes required T-lymphocytes.

Following inoculation with LCMV, T-cells infiltrated the cerebella of Lewis and RNU/+ rats, but not RNU/RNU rats.

Inoculation of Lewis and RNU/+ rats with LCMV led to a robust infiltration of CD8+ T-lymphocytes into the cerebellum (Figure 13). This lymphocytic infiltration was evident in the meninges and cerebellar parenchyma, was most marked at PD 14, and became less pronounced by PD25. In contrast, inoculation of RNU/RNU rats with LCMV led to no infiltration of CD8+ lymphocytes at any time point. Also, inoculation with DMEM alone led to no CD8+ lymphocytic infiltration in any of the rat genotypes. Thus, LCMV induced a CD8+ lymphocytic infiltration in rats possessing an intact immune system, but not in congenitally athymic rats.

Following inoculation with LCMV, increased expression of cytokines within the cerebellum was T-cell dependent.

As shown in Figure 14, LCMV infection led to marked changes in the expression of IFN-γ within the cerebellum. However, the magnitude of these changes depended strongly on time following inoculation and on the genotype of the animal. Following inoculation on PD 4, IFN-γ mRNA levels remained at low baseline levels for animals of all three genotypes at PD 8. By PD10, however, IFN-γ mRNA levels rose substantially

and continued to raise for several days thereafter to levels several thousand fold greater than the uninfected control levels. However, this LCMV-induced rise in IFN-γ expression occurred only in the genotypes possessing thymus-derived T-cells (Lewis and RNU/+). In contrast, in the athymic rats (RNU/RNU), IFN-γ mRNA levels remained low and virtually unchanged throughout this time period. After reaching peaks of approximately 4000 fold greater than baseline between PD 12 and PD 18, IFN-γ mRNA levels in the Lewis and RNU/+ rats remained elevated, but fell toward control levels by PD 30. In contrast, in the RNU/RNU rats, IFN-γ mRNA levels remained low and virtually unchanged from baseline throughout the entire time course. Thus, LCMV infection induced a monophasic rise and fall in the expression of IFN-γ mRNA, and this increased gene expression depended strongly on the presence of thymus-derived T-cells.

For TNF-α, LCMV similarly induced time-dependent and T-cell-dependent changes in expression levels. However, in the athymic rats, LCMV infection affected TNF-α somewhat differently than it did IFN-γ. In particular, following inoculation on PD 4, TNF-α levels rose substantially above baseline in rats of all three genotypes by PD 8. Thus, unlike the case of IFN-γ, the initial rise in TNF-α level did not depend on the presence of T-cells. However, following PD 8, the patterns of TNF-α expression diverged markedly between rats possessing thymus-derived T-cells and those lacking them. In particular, in the Lewis and RNU/+ rats, TNF-α levels continued to rise after PD 8 and reached high peaks between PD 10 and PD 18, before falling toward baseline. In contrast, in the athymic (RNU/RNU) rats, TNF-α level plummeted toward baseline immediately after PD 8. By PD 14, when TNF-α levels remained substantially elevated and near peak levels in the Lewis and RNU/+ rats, the levels were no longer significantly different from baseline in the RNU/RNU rats. Thus, in LCMV infection, the expression patterns of TNF-α depended strongly on rat genotype and, in particular, on the presence of thymus-derived T-cells.

LCMV induced encephalomalacia and disturbed neuronal migration only in the presence of T-lymphocytes.

For rats of all three genotypes (Lewis, RNU/+, and RNU/RNU), LCMV infection induced cerebellar pathology that was evident grossly (Figure 15) and microscopically (Figure 16). However, the nature and severity of this pathology differed among the genotypes. In particular, the presence of certain types of neuropathologic changes depended on whether the rats possessed T-lymphocytes (Lewis and RNU/+) or lacked them (RNU/RNU).

For rats of all three genotypes, LCMV infection reduced the size of the cerebellum, evident on gross inspection (Figure 15). However, this size reduction was distinctly more severe in the Lewis and RNU/+ rats than in the RNU/RNU rats. In addition, gross inspection revealed that the Lewis and RNU/+ rats possessed a type of neuropathologic change, contributing to the size reduction, which the RNU/RNU animals lacked. In particular, regions of encephalomalacia (softening or destruction within the brain), reflecting destructive lesions of the cerebellar hemispheres, were present only in the Lewis and RNU/+ rats, and were distinctly absent from the RNU/RNU rats (Figure 15).

Microscopic inspection confirmed and extended these findings. As shown in Figure 16, LCMV infection reduced the cross-sectional area of the cerebellar vermis in all three genotypes of rats. However, in the Lewis and RNU/+ rats, LCMV infection produced porencephalic cysts within the dorsal cerebellar lobules (porencephalic means a cyst or fluid filled region enclosed within the brain matter). These cystic structures reflected regional tissue destruction and were uniformly absent in the RNU/RNU rats. Thus, destructive lesions of the cerebellum were present in rats possessing T-lymphocytes and were absent in rats lacking them, demonstrating that T-lymphocytes are necessary for the destructive lesions induced by LCMV infection.

As shown in Figure 17, higher power microscopy revealed an additional neuropathologic change following LCMV infection. This neuropathologic change was neuronal migration disturbance. The normal cytoarchitecture of the cerebellar cortex consists of three layers. The outer layer is the molecular layer; the middle layer is the Purkinje cell layer, and the inner layer is the granule cell layer. This trilaminar structure of the cerebellar cortex is demonstrated in the uninfected control animal (Figure 17A). In the course of normal development, granule neurons migrate from the external granule cell layer through the molecular and Purkinje cell layers to reach their mature location in the internal granule cell layer [162] . In the Lewis and RNU/+ rats infected with LCMV, groups of granule neurons remained clustered and ectopically located within the molecular layer (Figure 17C and E), thus reflecting disturbed neuronal migration. In contrast, RNU/RNU rats infected with LCMV never had any ectopically located or clustered neurons. Thus, the neuronal migration disturbance induced by LCMV infection was immune-mediated and depended on the presence of T-lymphocytes.

LCMV-induced cerebellar hypoplasia did not require the presence of T-lymphocytes.

Figure 15 and 16 demonstrate that LCMV substantially reduced the size of the cerebellum in rats of all three genotypes (Lewis, RNU/+, and RNU/RNU). While infected RNU/RNU rats lacked the encephalomalacia and neuronal migration disturbances evident in rats of the other genotypes, the size of the cerebellum was substantially reduced by the viral infection. Yet, as shown in Figure 15 and 16, despite the overall reduction in size of the cerebellum, the cytoarchitectural arrangement of the cerebellum was preserved. Thus, LCMV infection of the RNU/RNU rats induced a true cerebellar hypoplasia. Therefore, unlike the destructive lesions and neuronal migration disturbances that depended upon the presence of T-lymphocytes, cerebellar hypoplasia following LCMV infection was not T-cell-mediated.

Only in T-cell competent animals did LCMV alter the expression of a chemokine/receptor pair involved in normal neuronal migration.

As noted above, LCMV infection induced a neuronal migration disturbance, but only in animals in which the virus likewise induced a T-cell infiltration. This prompted the question whether LCMV infection interacts with the immune system to alter the expression of a molecule that governs both the immune response and neuronal migration guidance. Stromal derived factor-1 (sdf-1), also known as CXCL12, is a chemokine important for lymphopoiesis and for normal neuronal migration [128, 163], especially for granule cell migration in the cerebellum [111, 113, 164-165] . In the brain, sdf-1 is expressed by the meninges, and can be induced to be expressed in astrocytes [111, 166-167]. Its receptor, CXCR4, is expressed in the cerebellar meninges and on granule cells in the external granule cell layer [111, 168] . Under normal conditions, sdf-1 maintains neuroprogenitors in their proliferative state. Developmentally-regulated decreasing levels of sdf-1 prompt granule cells to migrate toward the internal granule cell layer. Sdf-1 (CXCL12) and CXCR4 knockout animals have severe granule cell migration disorders in the cerebellum [169-170].

We sought to determine if LCMV infection alters sdf-1 and CXCR4 expression in a T-cell-dependent fashion. From the same cerebellar tissue samples in which IFN-γ and TNF-α gene expression were measured in the time-course studies described above, sdf-1 and CXCR4 mRNA levels were measured by real-time PCR.

As shown in Figure 18a, from PD 8 through PD 14, sdf-1 mRNA levels progressively declined in uninfected animals of all three genotypes, reflecting the normal developmental downregulation of the sdf-1gene with increasing age. LCMV infection during this early post-inoculation period had no effect on sdf-1 mRNA expression. After PD14, sdf-1 mRNA levels continued to decline slightly, then plateaued at low levels in the uninfected animals of all three genotypes. In contrast, in the infected Lewis and

RNU/+ rats, sdf-1 mRNA levels abruptly rose on PD 18 and remained abnormally elevated through PD 30. However, in the RNU/RNU rats, sdf-1 expression did not rise on PD 18 and remained lower than in Lewis and RNU/+ rats at all points thereafter. The differential effect of LCMV on sdf-1 expression in the three genotypes can best be appreciated when expression levels in infected animals are plotted relative to uninfected controls. As shown in Figure 8b, after PD 14, LCMV infection increased sdf-1 mRNA levels 2-3 fold in Lewis and RNU/+ rats, but had no significant effect in the RNU/RNU rats.

The same general patterns observed for sdf-1 also emerged for its receptor, CXCR4 (Figure 18 c and d). mRNA levels for CXCR4 fell progressively over PD 8-14, during which time LCMV had no significant effect. However, by PD18, LCMV infection significantly increased expression of CXCR4 in the Lewis and RNU/+ rats, but not in the RNU/RNU rats. On PD 18 and 25, LCMV infection increased CXCR4 levels 3-4 fold over uninfected control levels, but only in the Lewis and RNU/+ rats. In contrast, in the RNU/RNU rats, LCMV infection had no significant effect on CXCR4 mRNA levels at any time point. Thus, LCMV altered the expression of a chemokine/receptor pair involved in neuronal migration and lymphopoiesis. Furthermore, this altered expression occurred only in rat genotypes in which LCMV induced lymphocytic infiltration and neuronal migration defects. In addition, the altered expression occurred at stages of infection corresponding to lymphocytic infiltration and at stages of development corresponding to neuronal migration. These results suggest that the neuronal migration disturbance in LCMV infection is due, at least in part, to abnormal chemokine patterns, expressed by astrocytes or infiltrating lymphocytes.

Discussion

LCMV infection during pregnancy can severely and permanently damage the human fetal brain [1, 29-31], but little is known regarding the mechanisms of this injury.

This study utilized wild type Lewis rats, congenitally athymic nude rats *(*RNU/RNU) and their heterozygote littermate controls (RNU/+*)* to examine the role of T-lymphocytes in LCMV-induced neuropathology of the developing cerebellum. Infection of these various rat strains led to neuropathologic changes commonly observed in humans with congenital LCMV infection, suggesting that these strains will be valuable new animal models of the human infection. In addition, these experiments revealed five novel findings regarding the pathogenesis of congenital LCMV infection. First, absence of T-lymphocytes impairs the clearance of LCMV from the cerebellum, and particularly from astrocytes. Second, LCMV infection of the developing brain induces the formation of porencephalic cysts and T-lymphocytes are necessary for the generation of these destructive lesions. Third, LCMV infection of the developing brain markedly alters the expression of cytokines, the patterns of which depend upon the presence or absence of T-lymphocytes. Fourth, LCMV infection alters the expression of molecules that guide neuronal migration and leads to permanent granule cell ectopias in a T-cell-dependent manner. Finally, LCMV infection permanently reduces the size of the cerebellum, and this hypoplasia occurs even in the absence of T-lymphocytes. Taken together, the results strongly suggest that the focal destructive lesions and the neuronal migration disorder induced by LCMV infection are immune-mediated, while the cerebellar hypoplasia is virus-mediated.

In the absence of T-lymphocytes, clearance of LCMV is delayed.

T-lymphocytes play key roles in the clearance of LCMV from mice, which serve as the reservoir for the virus in nature [4, 171] . However, in neonatal rats, which serve as a model system of human congenital infection, the role of T-lymphocytes in controlling LCMV infection was unknown. We found that peak viral titers and cellular targets of infection within the cerebellar parenchyma were equivalent in athymic rats (RNU/RNU) and in rats possessing an intact immune system (Lewis and RNU/+). This

finding demonstrates that, at least in naïve developing animals, the capacity to produce T-lymphocytes does not influence the initial cellular targets of infection or the maximum viral titers of LCMV within brain parenchyma.

In contrast, clearance of LCMV was substantially affected by the presence of T-lymphocytes. Lewis rats and RNU/+ rats, of which possess functional thymus glands and produce normal numbers of T-lymphocytes, clear LCMV substantially faster than athymic nude rats, which lack T-lymphocytes. Furthermore, absence of T-lymphocytes especially impairs the clearance of LCMV from astrocytes. We have shown previously that astrocytes play critical roles in LCMV infection of the developing brain [36]. In particular, astrocytes are the portal through which LCMV enters the developing brain, the conduit through which the virus sequentially migrates through the brain, and the principal site of virus replication. Astrocytes can help defend the central nervous system against infectious agents by producing and responding to immune mediators, including cytokines and chemokines [172] [137]. However, the results of this study demonstrated that astrocytes do not have the intrinsic ability to self-clear LCMV and, instead, must depend upon the antiviral activity of T-lymphocytes.

In the human fetus, the presence and function of T-lymphocytes changes with development. T-lymphocytes first appear in the late first trimester [173], can proliferate in the early second trimester [174], and are functionally mature by the middle of the second trimester [175]. As a result of this staged progression of lymphocytic maturation, rates of viral clearance and strength of lymphocytic responses likely vary among fetuses infected with LCMV at different gestational ages. These maturational differences in fetal immune response likely contribute to the variability in brain injury observed among children with congenital LCMV infections [29].

In the absence of T-lymphocytes, destruction of the cerebellum is prevented.

The human fetus infected with LCMV often develops focal areas of brain parenchyma destruction which are demonstrated in neuroimaging studies as porencephalic cysts within the cerebral hemispheres and in the periventricular region [29]. These destructive lesions contribute substantially to the neurological deficits of congenital LCMV infection, as they underlie motor and cognitive deficits and play critical roles in the pathogenesis of hydrocephalus [29, 31, 176].

The present study revealed that Lewis and RNU/+ rats infected with LCMV developed destructive lesions in their cerebella, while infected athymic (RNU/RNU) rats did not. The differences in pathology among these rat strains cannot be attributed to differences in viral burden, as peak viral titers and cellular targets of infection were virtually identical in all three groups. Instead, the differences in pathologic outcome must be due to differences in the immune response. In particular, LCMV infection triggers a massive T-lymphocyte infiltration in Lewis and RNU/+ rats, but not in athymic rats. Thus, it is likely that the destructive lesions in LCMV infection are T-cell-mediated and develop during viral clearance.

Our results agree with prior studies suggesting that the destructive lesions accompanying LCMV infection are immune-mediated [48, 158]. We have shown previously that the timing and spatial pattern of cerebellar injury parallel the infiltration of CD8+ T-lymphocytes [36]. In addition, Monjan and colleagues [48] found that LCMV-induced cerebellar destruction could be prevented by administering anti-lymphoid serum at the time of infection. The present study extended the previous findings by demonstrating that the focal destructive lesions of LCMV infection do not occur when thymus-derived T-lymphocytes are congenitally absent.

LCMV in the developing brain alters the expression of cytokines in patterns that depend upon the presence or absence of T-lymphocytes.

We found that LCMV infection of the neonatal rat dramatically increases IFN-γ expression, but only in rats with thymus-derived T-lymphocytes. This finding suggests that T-lymphocytes are either the source of IFN-γ or provide an indispensable signal to other cell types, such as microglia and NK cells, for production of that cytokine in LCMV infection [177]. While IFN-γ did not rise in rats lacking T-lymphocytes (RNU/RNU), TNF-α initially did rise in these congenitally athymic rats to levels equivalent to or even higher than their euthymic counterparts (Lewis and RNU/+). However, in the athymic rats, this initial rise in TNF-α was not sustained, while in euthymic rats, TNF-α rose to even greater levels before falling. The initial rise in TNF-α expression in the RNU/RNU rats was likely a response by NK cells, astrocytes and microglia, all of which can produce TNF-α and are present in normal numbers in RNU/RNU rats [130, 178]. As has been shown for other cytokines, the initial rise in TNF-α was likely due to resident cells, while the sustained expression depended upon a lymphocyte infiltration [101].

IFN-γ and TNF-α can each kill neurons [71, 160], and both reached high levels only in the infected strains of rats in which massive neuronal death occurred (Lewis and RNU/- rats). While neuronal death and the subsequent porencephalic cysts in these strains were likely due primarily to the direct actions of cytotoxic T-lymphocytes, elevated levels of IFN-γ and TNF-α may also have contributed to the tissue destruction that accompanied LCMV infection.

LCMV infection disrupts neuronal migration, but only in the presence of T-lymphocytes.

The neuropathology of congenital LCMV infection in humans often includes pachygyria, deficits in cortical sulci, and other abnormal gyral formations [179]. These pathologic findings reflect abnormal neuronal migration within the developing cerebral cortex and contribute to the mental retardation, epileptic seizures, and motor disturbances that accompany congenital LCMV infection in humans. The pathogenesis of abnormal neuronal migration in the context of LCMV infection is unknown.

The results of the present study demonstrated that, in LCMV infection, clusters of cerebellar granule neurons remain permanently ectopically located within the cerebellar molecular layer. However, this disturbance of neuronal migration occurred only in Lewis and RNU/+ rats and was distinctly absent in the congenitally athymic (RNU/RNU) rats. Thus, as was true of the destructive lesions, neuronal migration disturbances in LCMV infection are immune-mediated and involve the actions of T-lymphocytes.

How T-lymphocytes lead to altered neuronal migration in LCMV infection is unknown, but two strong possibilities exist. First, cytotoxic T-lymphocytes may target Bergmann glia cells. Bergmann glia are a form of radial glial cell that serve as the scaffolding along which granule cells migrate to reach the internal granule cell layer [180]. We have shown previously that LCMV infects the Bergmann glia cells [181]. (This infection of Bergmann glia can be demonstrated only at earlier time points than those examined in the present study, because infection of neurons obscures the Bergmann glia [36].) Disturbances of Bergmann glia can disrupt cerebellar neuronal migration [182-184]. Cytotoxic T-lymphocytes may target and damage Bergmann glia, thus altering the structural system that guides migrating granule cells.

A second possibility is that T-lymphocytes disrupt neuronal migration by altering the chemical signals that guide neuronal movements. The migration of neurons is partly controlled by gradients of chemicals, including cytokines and chemokines [170, 185-

186]. T-lymphocytes secrete large quantities of cytokines and chemokines and, thus, could disrupt the extracellular chemical milieu guiding the movements of migrating granule neurons.

We found that LCMV infection substantially increases the expression of a particular chemokine, stromal derived factor-1, and its receptor, CXCR4. Furthermore, these altered expression levels occur at the very time that granule cells are migrating within the cerebellum. Sdf-1 and its receptor are necessary for cerebellar granule cell migration [111-113, 126, 165, 168]. Normally secreted by the meninges, sdf-1 exerts a chemoattractant effect on granule cells in the external granule cell layer [111, 113]. Immature granule cells express CXCR4 on their surfaces and downregulate its expression as they migrate toward the internal granule cell layer [111].

Because sdf-1 expression levels rose only in rat strains possessing T-lymphocytes, and because it is established that cytokines such as Il-1β and TNF-α can stimulate CXCL12 expression on astrocytes and brain endothelial cells[167, 187-188] , **it** is likely that infiltrating T-lymphocytes upregulate sdf-1 through their secretion of cytokines and chemokines . Possibly, the increased expression of sdf-1 on astrocytes promote the movement of granule cells away from the meninges, leaving them to mature in ectopic locations.

LCMV infection does not require T-lymphocytes to induce cerebellar hypoplasia.

Cerebellar hypoplasia, in which the cerebellum is abnormally small, but histologically intact, can occur in isolation or along with other neuropathology in humans with congenital LCMV infection [179]. While the mechanism underlying LCMV-induced cerebellar hypoplasia is unknown, this study reveals that it occurs in the *absence* of T-lymphocytes. In this regard, cerebellar hypoplasia is markedly different from the

destructive lesions and the neuronal migration disturbances, both of which require T-lymphocytes, while cerebellar hypoplasia does not.

Although T-lymphocytes are not necessary for the process, LCMV-induced cerebellar hypoplasia may still be due to immune mechanisms. The athymic rat is deficient in T-cells, but their non-thymus-dependent immunity remains intact [189]. The cytotoxicity of natural killer cells and macrophages may even be more robust than in euthymic animals, suggesting a compensatory mechanism for the lack of T-lymphocyte activity [189]. Our results confirmed this notion by demonstrating an initial rise in TNF-α expression following LCMV inoculation, thus indicating that there is at least a mild early immune response to the virus in athymic animals. Whether this response is sufficient or prolonged enough to affect cerebellar growth is unknown. Thus, the cerebellar hypoplasia may be immune-mediated and utilize immune mechanisms that are T-lymphocyte independent.

Alternatively, the LCMV-induced cerebellar hypoplasia might not involve immune mechanisms at all, but may instead be virus-mediated. In the developing brain, LCMV preferentially infects mitotically active neuronal precursors [47]. Thus, the dentate gyrus, cerebellum, and olfactory bulb, all of which contain mitotically active granule cell populations, are highly vulnerable to LCMV infection in the neonatal rat [14]. When LCMV infection occurs in Lewis rats on PD 1, the immune system is immature, tolerant to LCMV and little or no immune response is produced [37]. Yet, in these immature rats, LCMV induces hypoplasia specifically of the dentate gyrus, olfactory bulb and cerebellum [37]. In each of these brain regions, the hypoplasia is due to deficits in the number of granule cells. This suggests that the LCMV-induced hypoplasia of these brain regions is due to a virus-mediated interference with granule cell production. Furthermore, in the olfactory bulb, the initial hypoplasia resolves over time [37]. As the virus is cleared from the olfactory bulb, normal granule cell numbers are restored. In contrast, in the cerebellum, the hypoplasia is permanent. This difference in

outcome between the olfactory bulb and cerebellum likely reflects the fact that the olfactory bulb has an ongoing source of replacement granule cells in adulthood, while the cerebellum does not.

In humans, it is believed that a variety of viral infections during pregnancy can induce cerebellar hypoplasia in the offspring [190]. Yet, until now, no animal model existed to study this phenomenon. The congenitally athymic rat infected with LCMV may be an excellent new model system to uncover the mechanisms of virus-induced cerebellar hypoplasia in humans.

Figure 11 Absence of T-lymphocytes impaired clearance of LCMV. Plotted here are viral titers per gram of cerebellar tissue following intracerebral inoculation on PD4. Viral titers peaked at PD 10 and reached similar maximal values for all groups. After PD 14, the viral titers began to decline in all groups. However, viral titers declined more slowly for athymic (RNU/RNU) rats than for their immunocompetent littermates (RNU/+) or for Lewis rats. By PD 21, the athymic rats had significantly higher viral titers than the other groups. These differences persisted. Thus, viral clearance was delayed in the athymic rats. * Significantly higher viral titers in RNU/RNU rats than in RNU/+ rats ($p<0.01$). ** Significantly higher viral titers in RNU/RNU rats than in Lewis or RNU/+ rats ($p<0.01$). n=3 per group per time point

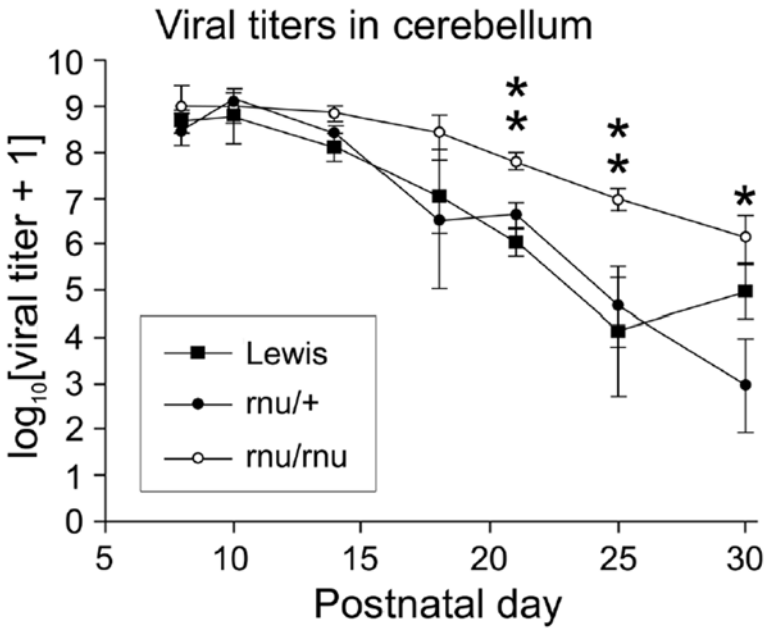

Figure 12 The cellular targets of infection were identical in rats with and without T-lymphocytes, but absence of T-lymphocytes impaired viral clearance from astrocytes. Shown here are 5 μm-thick sections of cerebella on PD 14 (A-F) and PD 40 (G-L) immunohistochemically stained for LCMV. At PD 14, the cellular targets of LCMV infection were the same for all groups. In the cortex (A-C), Purkinje cells (black arrows) and granule cells (black arrowheads) were infected in all 3 groups, while in the white matter (D-F), astrocytes (white arrows) were infected. Previous studies have confirmed that the cells labeled with white arrows are astrocytes, by demonstrating that they are GFAP-positive (13). By PD 40, the cell types still infected with LCMV depended on genotype. In the cortex (G-I), Purkinje cells and granule cells remained infected in all three genotypes. However, in the white matter (J-L), astrocytes were no longer infected in the Lewis and RNU/+ rats, but remained infected in the RNU/RNU rats. Thus, clearance of LCMV from astrocytes was impaired in the rats lacking T-lymphocytes. Magnification bar = 100 μm. n=3 per group per time point. WM=white matter

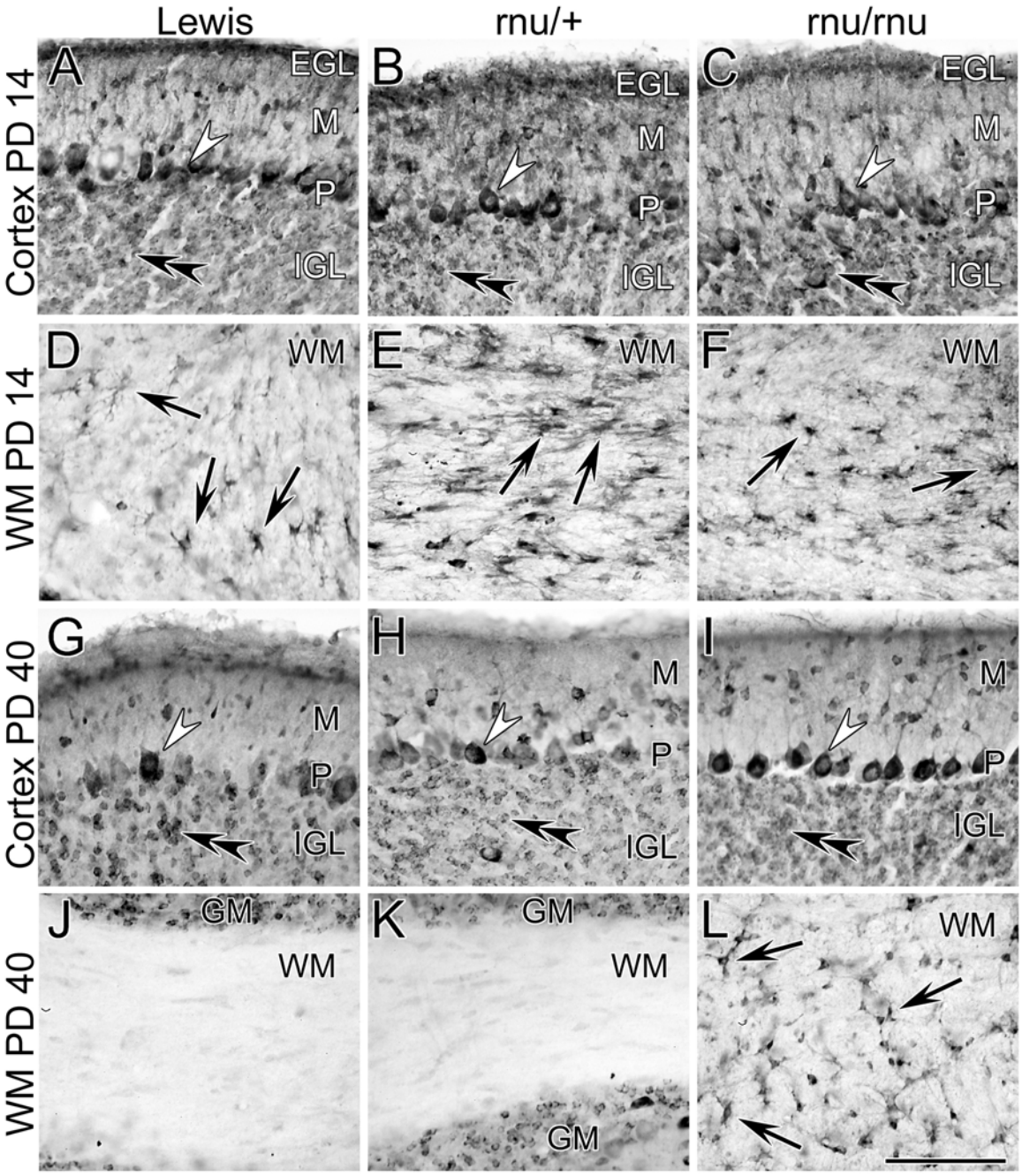
Lewis
rnu/+
rnu/rnu
Cortex PD 14
WM PD 14
Cortex PD 40
WM PD 40
A
B
C
D
E
F
G
H
I
J
K
L
EGL
M
P
IGL
WM
GM

Figure 13 LCMV infection triggered a robust lymphocytic infiltration of the cerebellum in rats possessing an intact immune system, but not in athymic rats. Shown here are 5 μm-thick sections of cerebellum immunohistochemically stained for CD8+ antigen X days following intracerebral inoculation with LCMV. Both the Lewis (A) and heterozygote (RNU/+) rats (B) developed an infiltration of CD8+ T-cells within the meninges (arrows) and cerebellar parenchyma (arrowheads). In contrast, the athymic rats (C) had no CD8+ T-cell infiltration of the meninges or cerebellar parenchyma. Magnification bar = 100 μm. n=3 per group per time point

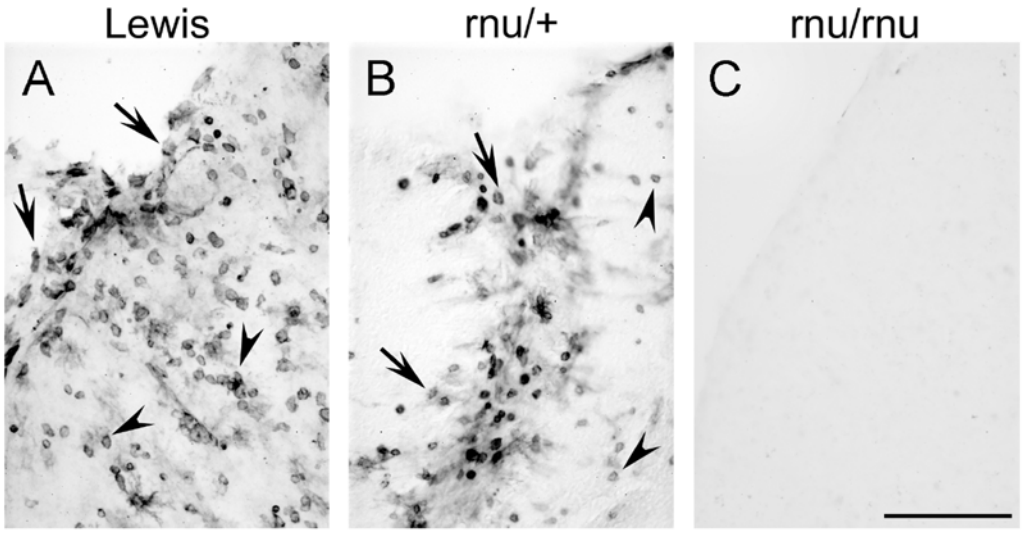

Figure 14 Increased expression levels of the cytokines IFN-γ and TNF-α were T-cell-dependent. Cytokine mRNA levels were measured by real-time PCR using primers and probes for IFN-γ and TNF-α. A) Following inoculation with LCMV on PD 4, IFN-γ levels remained low for all genotypes on PD 8. However, by PD 10, IFN-γ levels had risen substantially in the Lewis and RNU/+ rats. IFN-γ levels continued to rise to high peaks in rats of these two genotypes before falling toward control (uninfected) levels. In contrast, in the RNU/RNU rats infected with LCMV, IFN-γ expression remained low and unchanged throughout the time course. IFN-γ values for the uninfected rats of all three genotypes were close to zero and are not shown due to graphical overlap with RNU/RNU values. B) In all three rat genotypes, LCMV infection on PD 4 increased the expression of TNF-α on PD 8. However, following PD 8, TNF-α levels among the three genotypes diverged. In the T-cell competent Lewis and RNU/+ rats, TNF-α levels continued to rise to high peaks and remained elevated for multiple days before falling toward baseline levels. In contrast, in the T-cell deficient RNU/RNU rats, TNF-α did not rise further after PD 8 and, instead, declined rapidly toward baseline. In the uninfected rats of all three genotypes, TNF- α levels remained low and unchanged throughout the time course. * Significantly greater in the Lewis and RNU/+ rats than in RNU/RNU rats, $p<0.05$. n=3 per group per time point

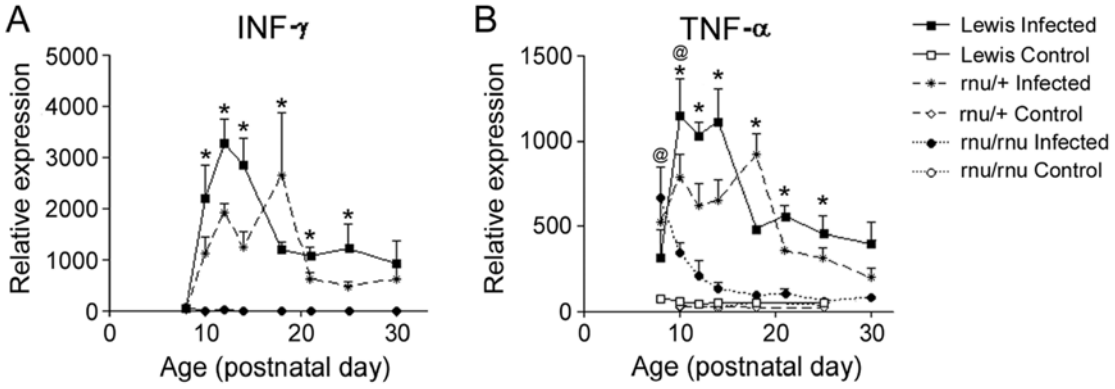

Figure 15 LCMV induced regions of encephalomalacia within the cerebella of immunocompetent rats, but not in athymic rats. Shown here are gross specimens at PD 90, photographed from the superior-dorsal aspect. The uninfected control animals are in the top row, while their infected counterparts are in the bottom row. In both the Lewis and heterozygote (RNU/+) rats, LCMV infection reduced the overall size of the cerebellum and induced focal destructive lesions (arrows). In contrast, in the athymic (RNU/RNU) rat, LCMV infection induced no focal destructive lesions, but did reduce the size of the cerebellum. The extent to which LCMV reduced cerebellar size was substantially less in the athymic rats than in the immunocompetent rats.

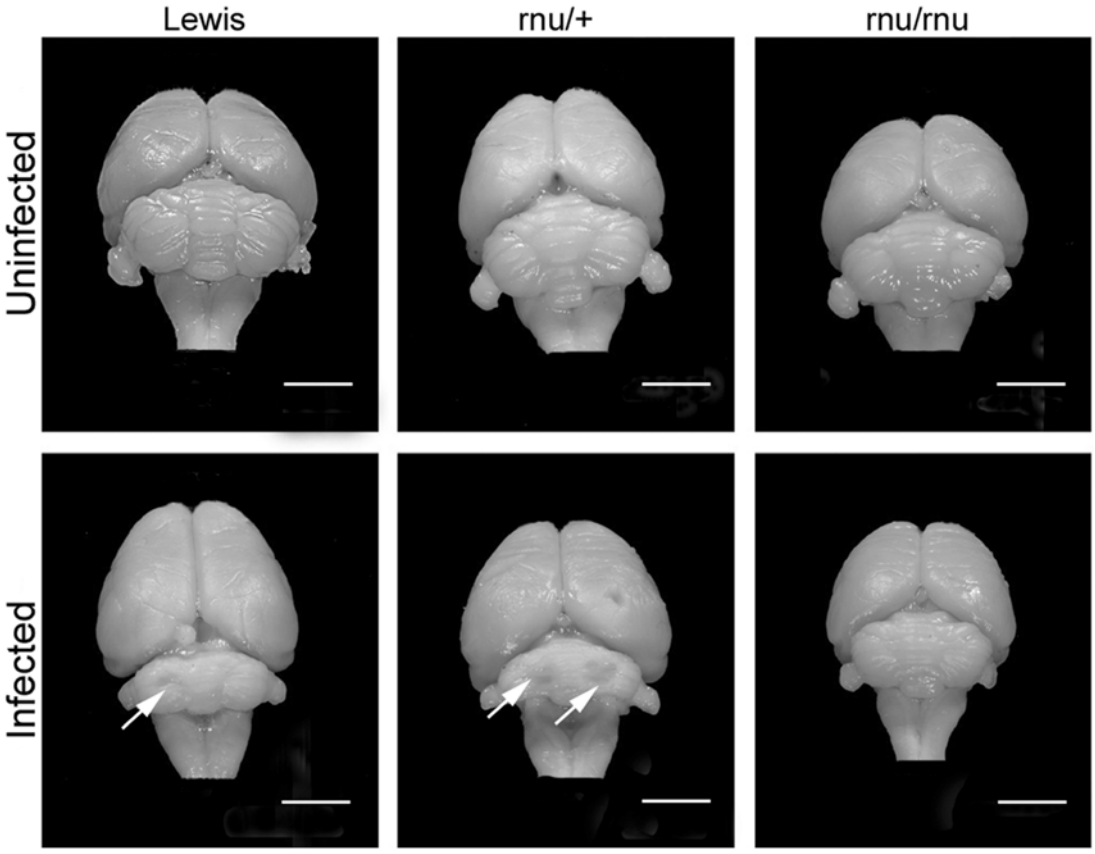

Figure 16 LCMV infection induced porencephalic cysts in rats with T-lymphocytes and pure cerebellar hypoplasia in rats without T-lymphocytes. Shown here are midsagittal 5 µm-thick sections through the cerebellar vermis of control and LCMV-infected rats at PD 90. All sections are stained with hematoxylin and eosin. The uninfected controls are in the top row, while the corresponding LCMV-infected animals are in the bottom row. Porencephalic cysts (arrows), reflective of focal tissue destruction, occurred only following infection of the Lewis and RNU/+ animals. An obliterated lobule (asterisk) in the Lewis rat likewise reflects focal tissue destruction. In sharp contrast, the infected RNU/RNU rats had no such destructive lesions, but did have an abnormally small cross-sectional area, reflecting cerebellar hypoplasia. Magnification bars represent 1mm. n=3

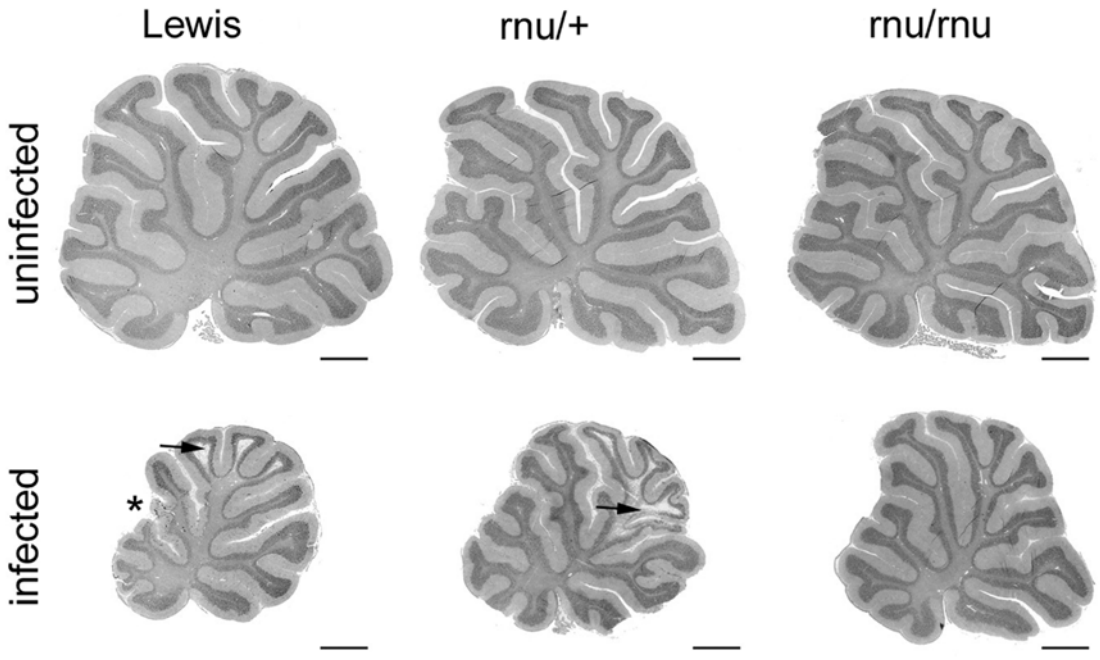

Figure 17 LCMV infection induced a neuronal migration disturbance in rats with an intact immune system, but not in congenitally athymic rats. Shown here are 5 μm-thick midsagittal sections through the cerebellar vermis of PD 90 rats, stained with hematoxylin and eosin. The section from an uninfected Lewis rat (A) demonstrates the normal trilaminar appearance of the cerebellar cortex, which consists of a molecular layer (M), a Purkinje cell layer (P), and a granule cell layer (G). In the LCMV-infected Lewis and RNU/+ rats (B and D), asterisks (*) denote porencephalic cysts, reflecting focal tissue destruction. In the LCMV-infected Lewis and RNU/+ rats (C and E), clusters of granule cells (arrows) are ectopically located within the molecular layer, reflecting a neuronal migration disturbance. In contrast, the LCMV-infected RNU/RNU rat (F) has a normal trilaminar appearance of the cerebellar cortex, with no porencephalic cysts or ectopically located granule cells. Magnification bars = 50 μm. n=3

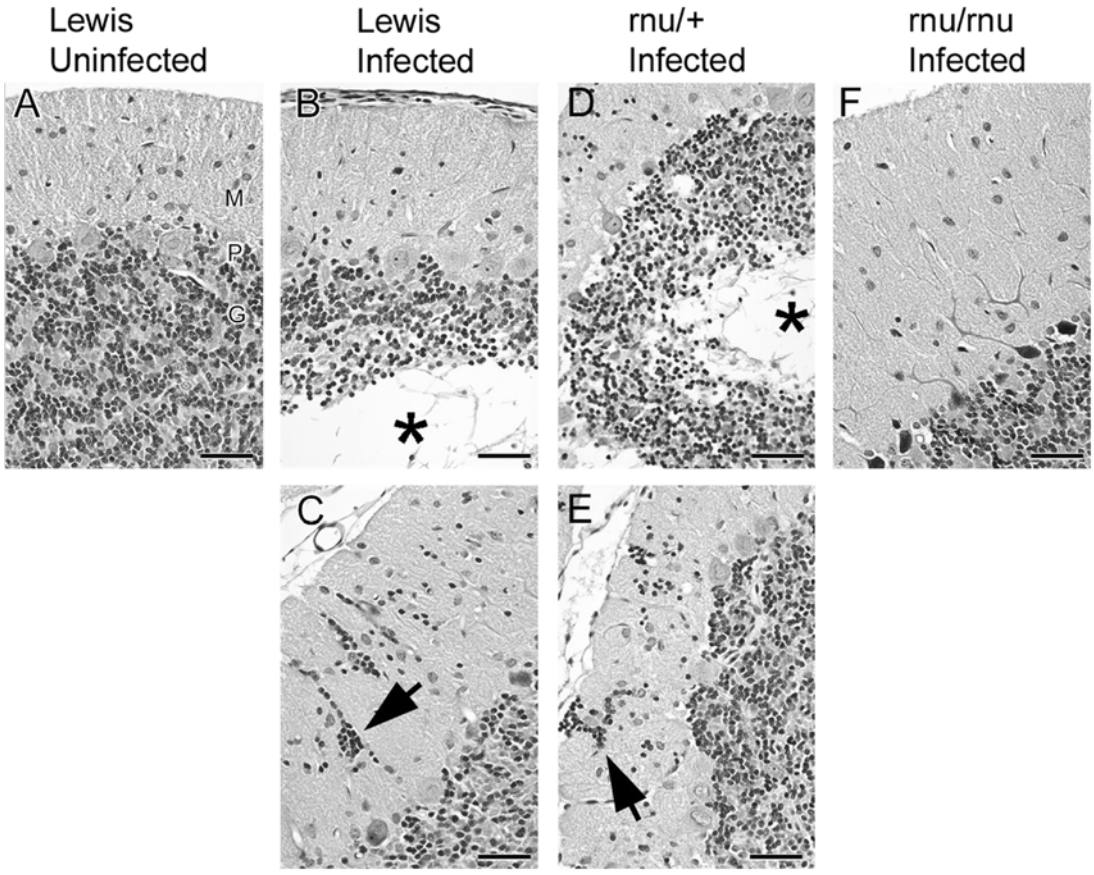

Figure 18 Only in rats with T-lymphocytes, LCMV infection altered expression of a chemokine/receptor pair that governs neuronal migration. Sdf-1 is a peptide with dual functions. It guides granule cell migration in the developing cerebellum and functions as a chemokine in the immune system. mRNA levels for sdf-1 and its receptor, CXCR4 were measured by real-time PCR. A) From PD 8 – PD 14, sdf-1 levels declined in the uninfected animals of all strains, reflecting developmental downregulation of this molecule. Over these initial time points, LCMV had no effect on sdf-1 expression. However, on PD 18, sdf-1 levels rose in the infected Lewis and RNU/+ rats, but continued to decline in the infected RNU/RNU rats and in the uninfected rats of all three strains. In the infected immunocompetent rats (Lewis and RNU/+) sdf-1 levels remained higher than in their uninfected counterparts and higher that infected athymic (RNU/RNU) rats. B) Because baseline sdf-1 levels change with time and differ among strains, the effect of LCMV on sdf-1 can best be appreciated by plotting expression levels in infected rats, relative to levels in uninfected rats of the same age and genotype. LCMV infection had no effect on sdf-1 levels at the early time points (PD 10 and 14). However, on PD 18, LCMV substantially increased sdf-1 levels in the Lewis and RNU/+ rats, but not in the athymic (RNU/RNU) rats. C) CXCR4 mRNA levels fell progressively across time and equally among groups until PD 18, when the patterns among groups diverged. At PD 18 and at later times, CXCR4 was expressed at higher levels in LCMV infected immunocompetent rats than in athymic rats or uninfected rats. D) Expression levels of CXCR4 in rats infected with LCMV, relative to uninfected rats. LCMV infection increased CXCR4 expression on PD 18 and PD 25, but only in the immunocompetent rats (Lewis and RNU/+), but not in the congenitally athymic rats (RNU/RNU). For A and C: * Significantly different from uninfected rats of the same genotype ($p<0.05$). For B and D: * Significantly different from RNU/RNU ($p<0.05$). n=3

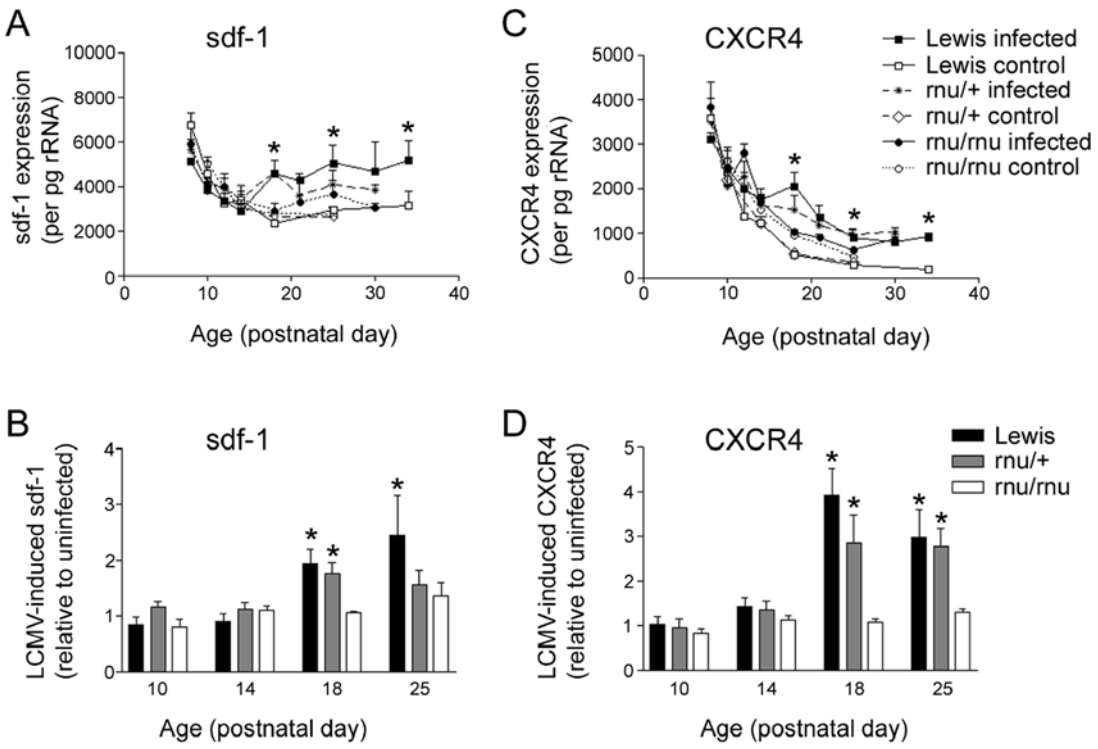
A
sdf-1
sdf-1 expression (per pg rRNA)
Age (postnatal day)
C
CXCR4
CXCR4 expression (per pg rRNA)
Age (postnatal day)
Lewis infected
Lewis control
rnu/+ infected
rnu/+ control
rnu/rnu infected
rnu/rnu control
B
sdf-1
LCMV-induced sdf-1 (relative to uninfected)
Age (postnatal day)
D
CXCR4
LCMV-induced CXCR4 (relative to uninfected)
Age (postnatal day)
Lewis
rnu/+
rnu/rnu

CHAPTER 4: LCMV INFECTION DISRUPTS BERGMANN GLIA AND DELAYS GRANULE CELL MATURATION, RESULTING IN A NEURONAL MIGRATION DISORDER

Introduction

One form of neuropathology in neonatal rats infected with LCMV that is of particular clinical relevance is the cerebellar neuronal migration disorder. LCMV-induced neuronal migration disturbances in rats is an important research focus because migration disorders are also seen in human congenital LCMV infection, as well as other congenital viral infections [14, 29, 191-192]. Consequences of neuronal migration include epilepsy, cerebral palsy, mental retardation, and other learning disorders.

In this study, our principal goals were to characterize the neuronal migration disorder in the cerebellum of rats neonatally infected with LCMV and to investigate its underlying mechanisms [36-37]. A second goal was to investigate the motor and behavioral abnormalities associated with LCMV induced cerebellar pathology.

Previously, we showed that LCMV infection in the neonatal rat leads to severe destructive lesions, primarily in the dorsal cerebellar lobules, while essentially sparing ventral lobules. However, the ventral lobules and the dorsal regions that escape destruction are not free of pathology, as they have a severe neuronal migration disorder. In the current studies, to determine what pathological process might lead to abnormal migration, we investigated the possibility that LCMV alters structural components necessary for granule cell migration and explored the notion that the virus disrupts the differentiation and proliferation of granule cells.

Particular structural components must be in place for cerebellar granule cell migration to occur properly. Under normal conditions, Bergmann glia provide a scaffold that guides granule cell migration. However, Bergmann glia are an early and prominent target of LCMV virus in the developing cerebellum. Shortly following inoculation with

LCMV, the cell bodies and processes of Bergmann glia contain large amounts of LCMV antigen, indicating viral infection of this cell population. Based on their infectability and their importance in governing granule cell migration, one possible mechanism underlying the neuronal migration disturbance is that LCMV corrupts Bergmann glia fibers.

Another structural component necessary for proper granule cell migration in the cerebellum is laminin, a glycoprotein component of the basal lamina, which lies adjacent to the meninges. In animals with laminin abnormalities, cerebellar granule cells exit the cell cycle prematurely, mature ectopically, establish abnormal neuronal connections in the outer molecular layer, and remain permanently ectopic [118-120]. Because LCMV infection leads to a robust inflammation of the meninges, the adjacent basal lamina and its laminin components are likely injured, as well. Thus, LCMV infection may disrupt the structure of the Bergmann glia, the laminin, or both to induce a neuronal migration disturbance in the cerebellum. Therefore, we will investigate the effects of LCMV infection on the structural integrity of Bergmann glia and laminin and will determine whether these structural alterations spatially correlate with the location of ectopic granule cells.

Abnormal neuronal migration may also be caused by alteration in the developmental timing of granule cell proliferation or maturation. For example, certain insults to the developing cerebellum, such as x-irradiation, abnormally prolong granule cell proliferation in the external granule cell layer, postpone their inward migration, and lead to permanent ectopias [121-124, 193]. We will investigate the possibility that LCMV-induced abnormalities in neuronal maturation lead to the migration disturbance by determining the maturational state of ectopically located neurons and by analyzing the expression for ATOH1, a granule cell specific transcription factor expressed during early proliferation of granule cells [194-195].

Recently, many similarities have been discovered between signaling molecules used by the immune system and signaling molecules used in normal patterning and

development of the brain [112, 125-126, 165, 168, 196]. Both systems use cytokines to traffic migrating cells [128, 196]. In the case of the immune system, cytokines are used to traffic immune cells to sites of infection and inflammation, while in the brain, cytokines are used to regulate neuronal migration during development and to traffic neuroprogenitors to sites of damage after stroke [128, 168]. Furthermore, some cytokines stimulate neuroproliferation and regulate astrocyte growth [193, 197-199]. Therefore, another possible explanation for the disturbed neuronal migration is that the inflammatory milieu alters the expression of genes involved in neuronal migration and neuronal proliferation.

To investigate this possibility, we will investigate the effect of LCMV on gene expression of CXCL12, CXCR4, and Sonic Hedge Hog (SHH). CXCL12 and CXCR4 are a chemokine/receptor pair involved in neuronal migration in the cerebellum and are upregulated in the inflammatory response [112, 126, 128, 166, 168]. SHH is a mitogen, produced by cerebellar Purkinje cells [200], that regulates granule cell proliferation [110, 200-201]. SHH is of particular interest in LCMV infection because it is regulated by IFN-γ [193, 199, 202], a cytokine whose expression is substantially upregulated by LCMV (chapter 2).

Among their many neurological deficits, children with congenital LCMV infection typically have movement abnormalities, including hypo- and hyperkinetic movements, gait disturbances and ataxia. These movement abnormalities likely reflect injury to forebrain and cerebellum, which are also vulnerable to LCMV-induced infection and injury in the rat. Despite the substantial brain pathology in rats following LCMV infection during development, the effect of this pathology on behavior has hardly been examined. A final goal of this study was to investigate the effect of LCMV infection in the neonatal rat on activity and coordination [203-204].

Materials and Methods

Animals

Pregnant Lewis rats were obtained from Harlan Sprague-Dawley (Indianapolis, IN). For more details, see materials and methods in chapter 1.

Virus

See materials and methods, chapter 1.

Infections

See materials and methods, chapter 1.

Perfusions, Histology, and Immunohistochemistry.

For evaluation of neuropathology, rats were sacrificed at a series of ages following infection. 3 - 4 Lewis rats were sacrificed at postnatal days (PD) 8, 10, 12, 14, 16, 18, 21, 25, 40, and 120. The rats were perfused via the left cardiac ventricle with 0.9% saline, followed by 4% paraformaldehyde in 0.1 M sodium phosphate buffer. The brains were removed and stored in 4% paraformaldehyde fixative.

For immunohistochemistry, the cerebella were sunk in 30% sucrose and then cut in 40um sections using a freezing microtome. For PCNA antibody, antigen retrieval was performed in a citrate buffer steam bath for 10 minutes. For all other antibodies, the sections were incubated with a goat serum blocking solution for 60 minutes. The sections were then incubated with the primary antibody overnight at 4°C in a humidified chamber. The following primary and secondary antibodies and dilutions were used: anti-LCMV (1:1000,), rabbit anti-GFAP GFAP 1:1000 (Sigma, Saint Louis Missouri), mouse-anti GFAP (1:1000, Sigma, Saint Louis, Missouri) monoclonal mouse anti-Neuron-specific beta-III tubulin antibody IgG2a (1:1000 R& D systems Minneapolis, Min), rabbit anti-human/mouse Caspase 3 active (1:1000R & D system, Minneapolis,

Min.) monoclonal mouse anti-calbindin D IgG1 (1:1000 Sigma, Saint Louis Missouri) mouse anti rat TAG1 IgM (1:10, DSHB, Iowa city Iowa) rabbit ant-BLBP (1:1000 Millipore), guinea pig anti-GLAST (1:1000, Millipore), rabbit anti-Laminin (1:1000, Sigma, Saint Louis Missouri) Mouse anti-NeuN IgG1 (1:500, Chemicon) mouse anti-PCNA IgG2a(1:500, Zymed, San Francisco, CA) rabbit anti-cxcr4 (1:500 Torrey Pines Biolabs, East Orange, NJ). All secondaries were alexa flour secondaries from Molecular Probes (Invitrogen) are were as follows; 488, 568 and 647 Goat anti-rabbit, 647 and 488 goat anti-mouse IgG1, 488 goat anti-mouse IgG2a, 567 goat anti-mouse IgM, 567 goat anti-guinea pig.

RT-PCR

mRNA and RT-PCR was conducted as described in chapter 1, but different primer and probe sets were used. TaqMan primer and probe sets for CXCR4, CXCL12, SHH and ATOH1 were purchased from Applied Biosystems Inc. (Foster City, CA).

Behavior

Lewis rats age 37-41 days were used for the following behavioral tasks. 8 sham injected controls and 9 LCMV infected rats were used.

Open Field

For the open field assay, rats were placed in a box measuring 24 inches x 24 inches x12 inches. They were placed in the box for two consecutive training days, followed by two days of recording where they were left for 30-45 minutes in the box and then returned to their cages. On the recording days, the animal's activity was recorded manually by two observers, one blinded to treatment group. Animal movements were recorded by tracing animal motion onto a paper grid identical to the grid in the box. Animal movements were traced for an entire minute, every five minutes for a 30 minute time span for a total of 6 recordings. Each animal was recorded on two separate

occasions. Animal's movements were averaged over the two separate recordings and totaled for a total number of line crosses over the 30 minute time span. Inter observer ratings were 98% [204].

Beam Walk

This test uses a series of different size square and round beams 100cm long that are placed roughly 30 cm above the level of the floor. The beam sizes were as follows; square beam was 1', 1 ¾', and ½' inch, the round beams were 1 ½', 1' and ¾'. The beginning side of the beam had no platform and was attached to a vertical beam ½' in diameter. The other end of the beam terminated in a platform with a 20 cm x 20 cm x 20 cm escape hut for the animals to walk into. A light was placed at the beginning end of the beam to motivate animals to walk towards the dark hut. Animals were trained to cross the beam on three consecutive days, and testing took place on the fourth day. Animals were trained by placing them at the start side of the beam. A plastic rod was used to tap the start end of the beam and make a noise to motivate the animals to cross to the escape hut. On each training day, animals were made to cross the largest beam three times and then each of the other sized beams one time for a total of 8 walks across a beam. Once animals had learned the task, or after a minimum of three training days, the test day took place in which animals were recorded using a digital video camera. Testing consisted of two trials on each beam. The video was then analyzed by a blinded researcher for total foot slips on each trial and time to cross the beam [203].

Results

Clusters of ectopic cells in the molecular layer are neurons

To determine if ectopic cells seen on H & E [36] are neurons, we used an antibody to NeuN, a marker for post mitotic neurons [205] . We first labeled LCMV injected and sham injected cerebella at PD 21, PD 25 and PD 40 which are time points

after inward granule cell migration is normally completed. Figure 19 shows anti-NeuN labeling in a PD21 LCMV (D) and sham injected (A) cerebellum and is representative of the labeling at PD21, 25 and 40. The arrow in Figure 19D points to a large cluster of neurons in the outer molecular layer located near the pial surface. The neurons in Figure 19D remained in the EGL after normal inward migration occurred, and their expression of NeuN signifies that they differentiated ectopically. Granule cells are also seen scattered throughout the molecular layer in LCMV cerebellum (arrowheads in Figure 19D), compared to the absence of neurons in the ML of the sham animal (Figure 19A). Therefore, ectopic cells were neurons and were only present in LCMV infected and not control animals.

In order to establish the time at which abnormal positioning of granule cells is first apparent, and to establish if this correlates with the timing of lymphocyte infiltration, we labeled neurons in infected and control cerebella with anti-NeuN and performed Nissl staining on adjacent sections, starting on PD8 and repeated the stain every two days after, until PD18, after which PD21, 25 and 40 were labeled. The time course of NeuN labeling reveled that granule cell position is similar between control and infected groups on PD8-PD14. At PD16, an increase in NeuN positive neurons in the molecular layer, exemplified by the PD18 cerebellum shown in Figure 19 (Figure 19D, Figure 21E, F), and a disorganization of NeuN positive cells at the IGL/ML becomes evident; similar to that shown by the smaller arrow in Figure 19D where NeuN positive cells from the IGL are located in between Purkinje cells in the Purkinje cell layer. Nissl staining of cerebella from PD8 onwards (not shown), and CD8+ immunohistochemistry [36] showed that lymphocyte infiltration is seen most strongly beginning PD14. Therefore, the appearance of NeuN pathology at PD16 occurs subsequent to lymphocyte infiltration, suggesting a role of the immune system in ectopic neuronal formation, the mechanism of which will be explored later. Ectopic NeuN labeled cells were present in the ML of all LCMV infected cerebella from PD16 onwards.

Bergmann Glia organization is abnormal but Laminin is intact in infected Lewis rats

To determine if Bergmann glia fibers are disrupted in LCMV infection, we used an antibody for Glial Fibrillary Acidic Protein (GFAP) [206], which labels Bergmann glia and astrocytes and we labeled cerebella from infected and sham injected control rats between PD8 and PD40. Normally, Bergmann glial cell bodies are neatly positioned in the Purkinje cell layer, clustered closely around Purkinje cell bodies (arrows in Figure 20A), and they send parallel processes up through the molecular layer (arrows in Figure 19B) that attach to the basal lamina. In LCMV infected animals, the glia become reactive and the processes retract some of their connections from the basal lamina (arrow in Figure 19E and also repeated later in Figure 25, arrow and arrowhead in Figure 25). Some Bergmann glial cell bodies move up into the molecular layer (arrowhead in Figure 19E),

To determine if ectopic neurons colocalize with regions where radial glia are retracted from the lamina, we co-labeled sections for GFAP and NeuN (Figure 19). Co-labeling revealed that clusters of ectopic neurons found near the pial surface were adjacent to gaps where radial glia fibers normally would be. This is demonstrated in Figure 19F, where only one or two intact parallel radial glial fibers can be seen near the pial cluster of ectopic neurons. Additionally, ectopic neurons found in the molecular layer correlated to regions of glial cell abnormalities in the ML. These abnormalities are shown by the arrows in Figure 19E, and their colocalization with ectopic neurons in the ML is evident in Figure 19F.

To visualize morphologic changes in the cell bodies and processes of Bergmann glia and astrocytes, we used an antibody for Brain Lipid Binding Protein (BLBP) [207], which is expressed specifically in radial glial fibers early in development, and later in development is expressed by all astrocytes and glia. Anti-BLBP labels cell bodies more clearly than anti-GFAP. BLBP labeling revealed reactive gliosis as well as the

movement of Bergmann glial cell bodies (arrows in Figure 20B and D) into the molecular layer. A change in Bergmann glia morphology was evident by PD18. Normally, Bergmann glia cell bodies are small with two primary processes emerging towards the pia membrane (arrows Figure 20 A and B). After LCMV infection, cell bodies enlarge and take on a golgi like morphology and their processes become ramified (Figure 20 D arrows). These are qualities of reactive gliosis. Cells positive for BLBP were also identified in the meninges of PD18 cerebellum (Figure 20D arrowhead), these cells are possibly reactive astrocytes which have moved into the pia.

To determine the time frame of reactive gliosis development and Bergmann glia cell body movement into the ML, astrocytes were labeled with GFAP and BLBP as early as PD8 onwards through PD40. Immunohistochemistry for GFAP and for BLBP revealed that the reactive gliosis began as early as PD8. Bergmann Glial cell bodies were still near the Purkinje cell layer at PD10 (Figure 20B), but were beginning to move into the molecular layer at this time point. By PD14, Bergmann glia and astrocyte cell bodies were seen throughout the ML.

Next, we investigated whether a destruction of the basal lamina occurs. This is important because the integrity of Bergmann glial parallel fibers is dependent, in part, on their end feet connection with the basal lamina [118-119]. The basal lamina juxtaposes the pial surface of the meninges, which are heavily infected with the virus and undergo T-cell mediated inflammation [36]. Damage to the lamina would disrupt Bergmann glia end feet connections and alter parallel fiber orientation. Despite inflammation of the meninges, labeling with anti-laminin I/II extracellular matrix protein in the basal lamina, revealed no physical disruptions in the basal lamina structure (arrow in Figure 19K, also shown in a separate triple label experiment later on in Figure 25F). There were some areas where the basal lamina was thinned in the infected cerebellum (Figure 19K arrow) but the structure was intact.

An alternative possibility was that the connection of Bergmann glial fibers with the laminin structure is disrupted after LCMV infection. Bergmann glia express two adhesion molecules, α-dystroglycan and integrin, necessary for end feet attachment to the lamina [118-119]. Knockout of either adhesion molecule leads to detachment of Bergmann end feet from the lamina and disorganization of radial glia fibers [118, 120]. To determine if LCMV virus might interfere with Bergmann glia attachment to the lamina through binding to alpha dystroglycan, we labeled sections with GFAP and anti-laminin (Figure 25). Co-labeling revealed that Bergmann glia parallel fibers were able to form connections with laminin despite infection with LCMV (arrow in Figure 25 F). Therefore, pathology in the Bergmann glia is not due to destruction of the basal lamina or their inability to form connections with the basal lamina.

Activated-caspase 3 expression is altered in infected animals

Another area of investigation that we incorporated into this series of experiments was immunohistochemistry looking at cell death in the cerebellum. We did this to determine if widespread neuronal apoptosis was occurring in migrating neurons (therefore contributing to hypoplasia) or if apoptosis in Bergmann glia fibers might be occurring and therefore interfere with granule cell migration. In earlier work, we found that TUNEL (terminal deoxynucleotidyl transferase dUTP nick end labeling) labeling in PD14 infected cerebella revealed widespread cell death in infected compared to sham injected controls. To determine if Bergmann glia or migrating neurons were undergoing apoptosis, we labeled the cerebella from PD18 animals with an antibody against activated caspase-3. We found that activated-caspase 3 labeled a specific cell population in the control animals as well as the infected animals (Figure 21A, Figure 22A). Infected animals, however, had many more activated-caspase 3 positive cells, suggesting that cell death may be contributing to an abnormal migration process.

An important factor to recognize when interpreting the results of the activated-caspase 3 immunohistochemistry is that Bergmann glia can express activated-caspase 3 in viable (non-dying) cells between PD8-PD21 in the rat cerebellum [208-211]. Therefore, when comparing our findings here, we looked for a difference between activated caspase-3 immunohistochemistry in the control compared to the infected cerebella. Of note was that, activated caspase-3 immunohistochemistry in infected animals was very different from that of controls (Figure 21B, Figure 22E). In infected cerebella, there was abundant activated caspase-3 labeling in the molecular layer (Figure 21B). Activated caspase-3 did not co-label with NeuN, but did co-label with GFAP (Figure 21 G and H, Figure 22 C and F). Therefore, activated caspase-3 labeling may suggest an increase in cell death of GFAP positive cells in the molecular layer of infected animals, or may be an indication that Bergmann glia have moved up into the molecular layer.

Because activated caspase-3 is normally expressed by Bergmann glia cell bodies during development, our next step was to determine if caspase-3 labeling was indicative of glia cell death or was simply serving as a marker for Bergmann glia. We used TUNEL labeling in adjacent sections to determine if TUNEL positive cells corresponded to activated-caspase 3 labeling. As a positive control, we labeled a PD14 infected cerebellum, which had previously been shown to have apoptotic TUNEL positive cells (Figure 22G). We found no TUNEL labeling in control animals (Figure 22I). However, infected animals had sparse TUNEL-positive cells in the EGL and IGL of the cerebellum (Figure 22J). The molecular layer was nearly devoid of TUNEL positive cells. This suggests that activated caspase-3 positive cells in the molecular layer of the infected cerebella are not TUNEL positive and therefore are not undergoing apoptosis, but instead, are likely displaced Bergmann glia cell bodies. Therefore, LCMV infection leads to a drastic disorganization of Bergmann glia localization in the cerebellum.

Prolonged presence of external granule layer (EGL) in LCMV-infected animals

Although Bergmann glial are abnormal in infected animals and likely contribute to the neuronal migration defect, another possible mechanism of ectopic neuron generation is alteration in the timing of granule cell proliferation and inward migration. In fact, studies in chemical and radiation insults to the EGL during the developmental period have shown that a regenerative process occurs after damage to EGL cells. This regeneration prolongs the period of granule cell proliferation, delays the exodus of granule cells from the EGL, and consequently leads to ectopic neurons [121-124]. To determine if this process underlies abnormal neuronal migration in LCMV, we first Nissl stained cerebellar sections at regular intervals from PD8 through PD25. Figure 23 reveals a thickened EGL in the infected animals in the dorsal and ventral lobules at PD18, 21 and 25. At PD18, the residual EGL is thin, but still present in sham injected control animals, while it is much thicker in infected cerebella. By PD 21, granule cell migration is normally complete, and there is no remaining EGL in control cerebella. In infected animals, however, a thin EGL persists in dorsal and ventral lobules. The EGL persists as long as PD25 in some lobules of the infected cerebellum. Thus, because of either prolonged proliferation or delayed migration, LCMV-infected granule cells remain in the EGL for an abnormally long period, and this persistence in the EGL likely contributes to the later neuronal ectopias.

Cells in EGL of infected animals are neurons delayed in differentiation

After establishing the prolonged presence of cells in the EGL of infected animals, our next goal was to determine the developmental state of these neurons. We hypothesized that granule cell differentiation is delayed in infected animals and that proliferation continues later in infected animals than in control animals. To test this

hypothesis, we labeled PD10 and PD18 infected and control cerebella with TUJ-1 and TAG-1. TUJ-1 is an antibody against beta-tubulin III, which is expressed early after neurons differentiate. TAG-1 is a marker for immature granule cell neurons expressed during axonogenesis, which occurs prior to inward migration [212].

TUJ-1 labeling of PD18 cerebella revealed that cells in the EGL of PD18 infected and control animals were neurons (Figure 25 I). At PD18, the thick layer of cells in the EGL of infected animals were lightly TUJ-1 positive (Figure 25 I), whereas the thin layer of EGL in the PD18 control were very strongly TUJ-1 positive (Figure 25 G). To determine if cells in the EGL of PD18 animals were at different differentiation states in the control vs. infected animals, we labeled with TAG-1. Figure 25 demonstrates that TAG-1 labeling at PD18 was absent in control animals (Figure 25 B), indicating that granule cell neurons have completed axonogenesis by PD18. However, infected animals had a thick layer of cells in the EGL that still labeled positive for TAG-1 (Figure 25 E). Thus, at PD18, the infected rats are delayed in their differentiation, in comparison to controls.

To determine if differentiation was delayed at earlier time points, we did the same set of labeling on PD10 cerebella. In Figure 24, TUJ-1 labeling at PD10 revealed that control animals have a thick layer of brightly labeled neurons (Figure 24 B), compared to infected, in which the EGL was primarily TUJ-1 negative (Figure 24 E). The brightness of TUJ-1 in the control, versus relative absence of TUJ-1 in the infected EGL, means that there is a thicker layer of differentiated neurons in the control at PD10 than in the infected. This suggests a relative immaturity of neurons in the EGL of infected animals, relative to controls. Figure 24 shows that TAG-1 labeled the entire thickness of the EGL of control animals at PD10 (Figure 24 H), signifying that nearly all granule cells at PD10 are undergoing axonogenesis in preparation for inward migration. In contrast, TAG-1 labeled only the inner one-half to two-thirds of the EGL of the infected animals (Figure 24 K), suggesting that the outer EGL remained immature in the infected animals.

Granule cell proliferation occurred later in infected animals

To determine if proliferation of cells in the EGL occurs later in LCMV infected animals, which would further support the hypothesis of a delayed maturation of granule cells in LCMV infection, we labeled for proliferating cell nuclear antigen (PCNA) in the cerebella of PD10, 18 and 21 animals. Anti-PCNA immunofluorescence indicated a thicker and prolonged presence of proliferating cells in the external granule layer in LCMV infected animals. At PD10, both control and infected animals had a thick layer of PCNA labeled cells, which were located in the outer one half to two-thirds of the EGL (Figure 26 A). Notably, the PCNA labeling was thicker in the infected PD10 cerebellum than in the control. At PD18, PCNA labeling was also thicker in the infected animals than in the controls (Figure 26 B). By PD21, PCNA labeling was absent in the control animals (Figure 26 C). In contrast, there was still a thin layer of PCNA positive cells in the EGL of infected animals. Taken together, PCNA immunofluorescence indicated that, early in the infection, proliferation of EGL cells is increased over control levels, and that such proliferation is prolonged in infected compared to control cerebella.

CXCL12 and CXCR4 are upregulated in infected animals, and CXCR4 expression is present in the EGL

One possible cause of abnormal neuronal development and migration in the cerebellum is that LCMV alters guidance and proliferation signals. One such signal and receptor pair, CXCL12 and CXCR4, is also a chemokine. During the immune response, CXCL12 is highly efficacious as a lymphocyte chemoattractant. However, it is expressed at a constitutive level in the brain in a manner that does not attract lymphocytes to the CNS [111, 113, 213.]. Its expression can be induced in astrocytes and endothelial cells by injury or infection with viruses [128, 187]. IL-β and TNF-α stimulate the upregulation of CXCL12 on astrocytes and endothelial cells [167, 187-188]. CXCL12 is also expressed by the meninges in normal non-inflammatory conditions, where it maintains

immature granule cells in the EGL during their proliferation and differentiation [111-113, 126, 166]. It also has neuroproliferative properties on granule cell neurons [165]. CXCR4 is the receptor for SDF-1, expressed by granule cell neurons [112, 126, 168].

To test whether CXCL12 expression or CXCR4 expression is altered following LCMV infection, we isolated RNA from the cerebella of infected animals and compared its expression levels to the expression in control animals. We also performed the experiment in a separate group of animals in which we isolated RNA from dorsal and ventral cerebella and analyzed the two regions separately. Because LCMV-induced pathology in the dorsal cerebellum is far more destructive, and cerebellar lamination is more disorganized than in the ventral cerebellum, we believed that the effect would be better seen by separating the two regions. We also included a suckle control group, in addition to the sham injected control, in order to control for potential non-specific effects induced by sham injection.

Our real-time PCR results for CXCL12 revealed a significant up-regulation of CXCL12 at PD10 in the dorsal cerebellum and at PD18, and PD25 in both the whole cerebellum and its separate ventral and dorsal regions (Figure 27 A and C). The real-time PCR for CXCR4 revealed a higher expression in the infected compared the control animals at PD 14, 18 and 25 (Figure 27 B and D).

To investigate the specific cells that account for the upregulated expression of CXCR4 and, more importantly, to determine whether CXCR4 expression is prolonged in the EGL of infected animals, we used an antibody to CXCR4 and labeled PD10 and PD18 cerebella. In control animals, CXCR4 labeled Purkinje cells and EGL cells at PD10 (Figure 24 A). In infected animals, there was a thicker layer of CXCR4 positive cells in the EGL and there was faint labeling of Purkinje cells (Figure 24 D). At PD18, CXCR4 expressing cells were evident in the EGL of infected animals (Figure 25 H), but virtually absent in the EGL of control animals (Figure 25 J), which was reflected in the mRNA expression of CXCR4 at PD18. Therefore, the increased expression of CXCR4

mRNA at PD18 was partially due to an increase of its expression in the EGL of infected animals compared to control.

An additional finding from the CXCR4 immunofluorescence was that CXCR4 labeling of Purkinje cell neurons differed in the control compared to the infected groups. At both PD10 and 18, CXCR4 clearly labeled Purkinje cells in control animals (Figure 24 A, Figure 25 H). However, CXCR4 did not label Purkinje cells as consistently in the infected animals. CXCR4 labeling of Purkinje dendrites was almost absent in the infected vs. the control animals (arrow/arrowhead in Figure 25 H and J). To determine if the decrease CXCR4 labeling of Purkinje cells was due to disruption of Purkinje cell integrity, or a decrease in arborization of Purkinje cells in infected animals, we labeled cerebella with anti-calbindin, expressed in Purkinje cell axons, dendrites, and cell bodies. In control animals, anti-calbindin labeled Purkinje cell bodies, dendrites and axons. In the infected animals, Purkinje cell bodies did not label as strongly and their dendritic projections, although present throughout the ML, were less organized and less consistently labeled (not shown). Therefore, because calbindin did label Purkinje cells and dendrites in the infected animals, the lack of CXCR4 labeling in infected cerebella represents a decrease in Purkinje cell neuron expression of CXCR4 and not the absence of the cell population in itself.

In summary, LCMV infection lead to an upregulation of the chemokine/receptor pair CXCL12/CXCR4, which are normally involved in regulating granule cell migration. Immunohistochemistry for CXCR4 localized its expression to granule cells in the external granule cell layer and demonstrated that LCMV infection lead to a thicker layer of CXCR4 expression in granule cells of the EGL in infected animals. The increased gene expression of the ligand, and receptor, as well as the localization of the receptor to the granule cells of the EGL supports a role for CXCL12/CXCR4 in inducing abnormal neuronal migration after LCMV infection.

SHH and ATOH1 expression

Once we determined that granule cell differentiation and proliferation was delayed in infected animals, our next step was to look at the expression of two genes that regulate granule cell proliferation. Sonic hedge hog (SHH) is one such mitogen, and was a likely candidate for altered expression because it is up regulated by IFN-γ , a cytokine produced in conditions of inflammation, such as viral infection [130, 193, 199]. ATOH1 was another candidate gene because of its specificity to the granule cell population [195]. ATOH1 is a transcription factor expressed specifically in immature granule cells precursors. Therefore, the results from a gene assay on the whole cerebellum for ATOH1 are representative of what is happening specifically in granule cells of the external granule cell layer. ATOH1 is also appropriate because it is a transcription factor for sonic hedgehog and increase proliferation of external granule cells [194]. Real-time PCR was conducted on both whole cerebella as well as dorsal and ventral cerebellum regions. The results are shown in Figure 28

LCMV infected resulted in significant differences in SHH expression. As shown in Figure 28, an effect was seen at PD12 and PD25, when there was an increase in SHH in infected, relative to control in both the whole cerebellum and in dorsal and ventral region samples. SHH was increased approximately 60% at PD12 in the infected animals over the control animals. A significant decrease in SHH was also seen at PD18 in the dorsal and ventral regions.

ATOH1 is developmentally regulated and normally decreases with age. Real-time PCR for ATOH in the cerebellum revealed the normal developmental down-regulation of this gene (Figure 28). When comparing the infected to control levels, an increase in ATOH1 mRNA was present in the infected cerebella at all time points except for PD14. When the dorsal cerebellum and ventral cerebellum samples were analyzed separately, ATOH1 expression in the infected vs. the control diverged. The dorsal cerebellum had higher ATOH1 expression in the infected compared to control animals at

PD 8, 10, 14, and 25, while the ventral cerebellum had higher expression at PD 18 and 25.

In summary, LCMV infection leads to an increase in both SHH expression and ATOH1 expression in the cerebellum. Because ATOH1 is a transcription factor for SHH and mediates proliferation of EGL neurons, LCMV induced increase in ATOH1 expression in the infected animals provides a potential mechanism underlying the increase in proliferation of granule cells in the EGL.

Coordination was severely disrupted in infected Lewis animals and performance correlated with cerebellar destruction

To determine the impact of LCMV induced cerebellar pathology on coordination and balance, we tested infected and control animals with a beam walk task. In this task, animals were trained to walk across square and round beams 100cm in length to a safety hut on a platform at the other end [203]. The square and round beams were of three progressively smaller diameters. Animals were assessed for their speed and number of foot slips crossing the beam. This task provides a good measurement for coordination and balance. All animals were tested between PD37-40, a time that followed the acute phase of infection (N=9 infected, N=8 controls).

The beam walk results revealed an impairment in the infected group, whose average time to cross was at least 5 times greater than the controls (Figure 29 B). This was true for every size square and round beam. Postmortem examination of the brains revealed severe cerebellum lesions in 7 of the 9 infected animals. The two animals without cerebella lesions performed better on the coordination tasks than the seven with cerebella lesions but were still worse than uninfected controls. Thus, animals infected with LCMV are adversely affected on measures of balance and coordination.

Open field activity demonstrates hyperactivity in infected animals

One observation we made during previous studies with LCMV infected animals was that infected animals were consistently more active in their home cages than control animals. To test the hypothesis that LCMV infected animals have higher activity levels, we used an open field paradigm [204]. Animals' activity was measured in an open field apparatus over 30 minutes. Animals were scored for the number of line crosses over a grid on the bottom the testing apparatus. Each animal was scored on two separate occasions. The results from the open field experiment showed a higher number of line crosses over the 30 min period in the infected animals, compared to control animals. Statistical analysis did not reach significance ($p<0.1$) because of the large variability in scores in the infected group.

Discussion

Our research, and research on other congenital brain infections, has shown that congenital brain infections lead to neuronal ectopias [214-217]. However, little is known regarding the mechanism of this infection-induced neuronal migration disturbance. The work presented here has confirmed that cell clusters in the molecular layer are indeed ectopic neurons, and has helped elucidate the mechanisms involved in the pathology. Additionally, the first behavioral studies on the effects of LCMV infection in the neonatal rat are presented here.

The three main components important for proper migration of neurons in the cerebellum are altered in LCMV infection. These are the scaffolding structure needed for migration, the time frame that migration normally occurs, and the quantity of proliferating cells [108-109, 115, 218]. A review of normal granule cell development in the cerebellum and migration tells us that granule cells proliferate in the outer 1/3rd of the external granule cell layer [219-220]. As granule cells move inwards and begin their

axonogenesis, they differentiate and express TAG-1[212, 219, 221]. They then move toward the inner 1/3 of the EGL, where they become more mature, express beta-tubulin III and faintly express NeuN [219]. Once they begin their inward migration across the ML and towards the IGL, they are NeuN positive [219]. Granule cell bodies adopt an elongated form and send out a leading process which juxtaposes with a Bergmann glia fiber, upon which they migrate downward towards the IGL [218].

For migration to occur normally, granule cells need to differentiate and migrate inwards at an appropriate time because proteins involved in the inward migration are developmentally regulated. They also need to maintain their proper location within the EGL during their developmental state. Proliferation, differentiation, and migration inwards are all tightly regulated by genes that change expression developmentally. For example, adhesion molecules are expressed by Bergmann glial cells to assist in granule cell migration [222]. In addition, secreted molecules and receptors regulate granule cell proliferation and location during development [103, 110, 165]. For example, sonic hedge hog is expressed developmentally by Purkinje cells and acts as a mitogen for granule cell proliferation [200]. One of the transcription factors through which SHH works is ATOH1, expressed specifically in granule cell precursors [194]. As granule cells mature and differentiate, they decrease expression of ATOH1 and become resistant to the effects of sonic hedge hog [103, 110, 195]. Another important molecule for normal migration is CXCL12 [112]. CXCL12 is secreted by the meninges and is chemoattractant for its receptor CXCR4, which is expressed on granule cells [112, 165, 168]. Both CXCL12 and CXCR4 are developmentally regulated.

Alterations in any of the above factors can disrupt neuronal migration. For example, knockout of largemyd, part of the alpha-dystoglycan adhesion molecule expressed by Bergmann glia fibers, leads to altered Bergmann glia morphology and neuronal migration disorders [183, 223]. Another example is that over expression of SHH leads to extended proliferation in the EGL and results in granule cell ectopias in the

ML [194, 199, 202]. A final example is that knockout of either CXCR4 or CXCL12 leads to premature inward migration of immature granule cells and results in clusters of ectopic granule cells in the ML and IGL of the cerebellum[126, 168].

In this study, we have examined Bergmann glia structure, granule cell differentiation state, and timing of granule cell proliferation. We determined that Bergmann glia are altered, and that differentiation and proliferation are delayed. The findings for each will be discussed below.

Bergmann glia morphology is severally disrupted and correlates to regions of neuronal ectopias

In this study, we discovered that Bergmann glia morphology is severely disrupted by LCMV infection. Bergmann glia normally have their cell bodies clustered around Purkinje cell bodies and normally extend parallel processes radially that connect with the basal lamina. In LCMV infection, Bergmann glia cell bodies were abnormally dispersed throughout the molecular layer. Their processes were no longer parallel and many had retracted from the basal lamina.

These findings are similar in other infections of the cerebellum, such as toxoplasmosis in the rat and cytolytic parvovirus infection of the hamster [214-215]. In toxoplasmosis infection of the cerebellum, despite the absence of toxoplasmosis pathogen, glia are reactive and Bergmann glia morphology is disrupted [215]. In parvovirus infection, despite the fact that Bergmann glial cells are not a target of the virus, glial cell bodies move into the ML and change their cell body appearance to Golgi-like cells [214]. They also temporarily retract some, but not all, of their processes from the glia limitans. Such features of Bergmann pathology in both toxoplasmosis and parvovirus infection were associated with ectopic granule cells.

The mechanism through which Bergmann glia become reactive and lose normal morphology in LCMV infection is unknown. Bergmann glia are infected by LCMV.

Therefore, one possibility is that the viral infection itself harms the cells and alters their morphology. Other examples where viral infection of Bergmann glia leads to similar pathology exist. For example, Fowl-gliosis inducing virus (FLV), an Avian Leukosis virus, infects mitotically active neurons and glia cells of the cerebellum [216]. FLV virus leads to disarray of Bergmann glial fibers and ectopic migration of granule cells neurons. However, Bergmann glia undergo similar morphologic changes in parvovirus and toxoplasmosis infection, neither of which directly infect Bergmann glial cells. Such findings suggest that Bergmann glia can become reactive in the absence of direct infection.

An alternative possibility is that inflammation in the cerebellum may be harming Bergmann glia and therefore altering their morphology. Inflammatory cytokines and chemokines are harmful to cells and are expressed by infiltrating immune cells [134-135]. LCMV infection leads to a robust infiltration of T-cells and therefore, these may cause glia to become reactive and change their morphology. One argument against T-cells inducing the Bergmann glia changes is that in parvovirus infection, Bergmann glia become reactive in the absence of T-cells, and adopt an immune-like function, taking on the cellular function of clearing dead debris from the surrounding area [214]. Therefore, it is possible that altered Bergmann glia morphology in LCMV infection is a result of Bergmann glia changing function to becoming immune-like cells in the response to the virus, as well as a result of damaging chemokine and cytokine effects on the Bergmann glia integrity.

In addition, non-infectious insults to the cerebellum can likewise induce Bergmann glia abnormalities and ectopic granule neuron formation [122, 224]. This tells us that, in the absence of infection, but presence of insult to nearby cells, Bergmann glia become activated and their morphology is disrupted, leading to neuronal ectopias. Therefore, although Bergmann glia are infected by LCMV virus, it is likely that this is not the primary cause of their altered morphology. Alternatively, Bergmann glia

pathology in LCMV infection is most likely a result of the destruction induced by the immune system on other infected cells, which creates a caustic environment for all cells through the release of cytokines and chemokines.

Delayed neuronal differentiation and prolonged proliferation likely contributes to ectopic granule cell formation

In this study, we found that granule cell differentiation was delayed and that proliferation was prolonged in the LCMV infected animals. Normally, granule cells are finished proliferating, have reached a differentiated state, and are nearly done migrating by PD18 [104, 109]. In LCMV infected cerebella, a thick proliferative layer remains in the EGL and strongly expresses TAG-1. In addition, PD10 cerebella of infected animals show a thicker layer of proliferative cells and a smaller proportion of cells in the EGL expressing markers of differentiated neurons like TUJ-1 and TAG-1. A thicker layer of TUJ-1 and TAG-1 negative cells which are PCNA positive are present at PD10, and a prolonged TAG-1 and PCNA is present at PD18. These findings strongly suggest that the infected EGL is developmentally less mature than the control. Because inward migration of granule cells depends upon the expression of tightly regulated developmental cues [218], prolonged proliferation and differentiation in LCMV infection may create problems for internal migration.

One way that increased proliferation and delayed maturation can cause ectopias is that, an increased quantity of granule cells are attempting inward migration at a given time, which may place a higher burden on glial cells. This would be especially problematic in the face of diminished Bergmann glia integrity. Granule cells tend to migrate in a chainlike fashion along a Bergmann glia fiber. Too many granule cells on a single fiber could create a type of a “traffic jam”. This would be further worsened by a

break in a Bergmann fiber, leading to a backup in migrating cells and subsequent ectopias.

Altered gene expression of CXCL12/CXCR4 and of SHH and ATOH1 likely underlies the prolonged EGL proliferation seen after infection with LCMV.

CXCR4 and CXCL12 ATOH1 and SHH

LCMV infection alters the expression of genes involved in granule cell development and migration. First, we found up-regulation of CXCL12 and its ligand CXCR4 in both the ventral and dorsal regions of the cerebellum. CXCL12 and CXCR4 normally maintain granule cells in the EGL while they proliferate and mature [165, 168]. Our results show that an LCMV infection during the neonatal period can up-regulate CXCL12 and CXCR4 expression in the cerebellum. Furthermore, immunohistochemical staining confirmed that one location of CXCR4 expression was in the EGL. Because CXCL12 and CXCR4 are normally involved in migration and development, changes in their expression would likely alter migration of granule cells. In LCMV infection, granule cell expression of CXCR4 in the EGL continues past the normal time point, perhaps prolonging the presence of the EGL. It is possible that an increase in CXCL12 expression enhances the chemoattractant effect on the granule cells which express the receptor, and therefore contributes to the mechanism of prolonged granule cell presence in the external layer. Furthermore, CXCL12 works with SHH to increase proliferation of granule cells up to 50% [165] and therefore may be playing a role in the increased proliferation of granule cells in LCMV infection.

Sonic hedge hog and ATOH1 are also important for normal cerebellar development. Sonic hedge hog is a mitogen expressed by Purkinje cells [200]. Sonic hedgehog binds to its receptor, smoothened, on granule cell precursors and leads to increased proliferation. As granule cells mature, they become more resistant to sonic

hedgehog signaling through their expression of phospho-CREB [103, 201]. Studies have linked IFN-γ expression to an up-regulation of sonic hedge hog signaling and a consequent increase in granule cell proliferation, leading to increased cellularity of the molecular layer and prolonged presence of the EGL [193, 199]. In fact, constitutive expression of IFN-γ leads to increased granule cell proliferation in medulloblastoma, and in vitro studies in cultured granule cells confirm that there is direct binding of the IFN-y signal transducer, STAT1, to the SHH promoter [193, 199, 202]. IFN-γ also increases granule cell proliferation, which can be blocked by inhibition of SHH signaling, therefore, demonstrating that IFN-γ has its proliferative effects through SHH [193]. This is relevant for LCMV infection, because we know from real-time data that IFN-γ is upregulated after infection and we have shown here that SHH is increased 60% at PD12 in infected cerebella.

Because of the increased CXCL12 and SHH expression in this model, together with the known neuroproliferative role of these molecules, our data supports a role for LCMV infection in inducing neuroproliferation through the increase in SHH and CXCL12 expression.

In these experiments, we also determined that ATOH1 expression was increased in LCMV infection. ATOH1, also known as MATH1 in the mouse and HATH1 in the human, is a transcription factor expressed specifically in granule cell neurons and is important for inducing neuroproliferation by SHH [194-195]. In fact, knockout of ATOH1 inhibits SHH neuroproliferative effects on granule cells and decreases granule cell proliferation [194].

The increased expression of ATOH1 reported here could be interpreted in two ways. One interpretation is that it represents an increase in the actual neuroprogenitor cell population at the time point sampled. This is a very plausible explanation because, based on immunofluorescence, we know there is an increase in EGL proliferation in LCMV infected animals. Another possibility is that ATOH1 expression is increased, and

because ATOH1 has proliferation properties, it has a direct effect on proliferation. LCMV is known to interfere with gene expression, demonstrates specifically by interfering with transcription initiation of growth hormone level in the infected mouse brain [225]. Possibly, LCMV infection up-regulates ATOH1 by interfering with gene transcription, and thereby impacts granule cell proliferation. Whether or not this up-regulation is secondary to the virus itself, or a consequence of the immune response to viral infection, will be an area of future investigation.

Behavior – how does this relate to human disease?

LCMV infection affects coordination

We showed here that LCMV infection has a detrimental effect on balance and coordination in rats. The cerebellum plays a central role in balance and coordination. Animals infected with LCMV develop severe destructive lesion in their cerebellar vermis and hemispheres. Therefore, it is expected that their balance and coordination would be compromised. Some humans with congenital LCMV infection have isolated cerebellar hypoplasia as their sole neuroimaging abnormality. These children often have ataxia and gait disturbance as their principal neurologic deficits. Thus, the impaired balance and coordination observed in rats with LCMV infection mimics the behavioral deficits observed in children with isolated cerebellar hypoplasia who were prenatally infected with the same virus.

LCMV infection increases open field activity

In this study, we found that LCMV infected animals had increased activity in the open field apparatus. Increased open field activity in rats mimics attention deficit hyperactivity disorder (ADHD) in children [226-229]. Cerebellar hypoplasia has been associated with learning disorders such as dyslexia and ADHD [229-230] . More specifically, ADHD in humans has been associated with decreased volume in the

cerebellar vermal regions, based on brain imaging studies [230-231]. In the rat, vermal lesions resulted in an increase in activity levels measured by open field [227]. As demonstrated in this study, rats infected with LCMV have substantial cerebellar lesions and hypoplasia. Thus, the hyperactivity observed in the infected rats may be due to the cerebellar pathology. Whether the hyperactivity in the rats is due to pathology in the cerebellum or elsewhere, it closely mimics the abnormal behavior of many children with congenital LCMV infection, who, providing they are not rendered hypoactive by severe spasticity, are often hyperactive with a poor attention span (Bonthius et al., 2007).

Figure 19 Labeling of Neurons, Bergmann glia and laminin on PD21 in LCMV infected and control cerebella: All pictures were taken from the same lobule (lobe 9). NeuN labeling in the infected (D) reveals the presence of ectopic neurons in the outer layer of the ML (arrow) and within the ML itself (arrowhead). A loss in IGL organization around the PCL is also seen in infected animals (smaller arrow) where IGL granule neurons move up in between Purkinje cells in the PCL. NeuN labeling in the control animal (A) reveals the absence of neurons in the ML and a delineated boundary between IGL and ML. GFAP labeling (B, E) reveals the normal parallel orientation of Bergmann radial glia fibers in the control (B) compared to a disorganization of the fibers in the infected (E). GFAP labeling in the infected also revealed the presence of reactive astrocytes in the molecular layer (arrowheads) and areas where Bergmann glia fibers were absent or where gaps in fibers formed near the pial surface (arrows). The composite of GFAP and NeuN labeling shows that gaps in Bergmann glia overlay with areas where ectopic granule cells are seen (arrows in F). Panels G-L are the region labeled with anti-laminin, G and J show dapi labeling of cell bodies, H and K show laminin labeling for the control and infected animal. Laminin is present and intact in the infected animal, but there are regions of invaginations and thinning in the laminin (arrow, K). The composites in I and L show that the laminin in the control (I) is on the outer region of all cell bodies, where as the laminin in L is below an inflamed meninges (arrowhead) and invaginations go into the EGL (arrowhead). n=4 for NeuN and GFAP, n=3 for laminin

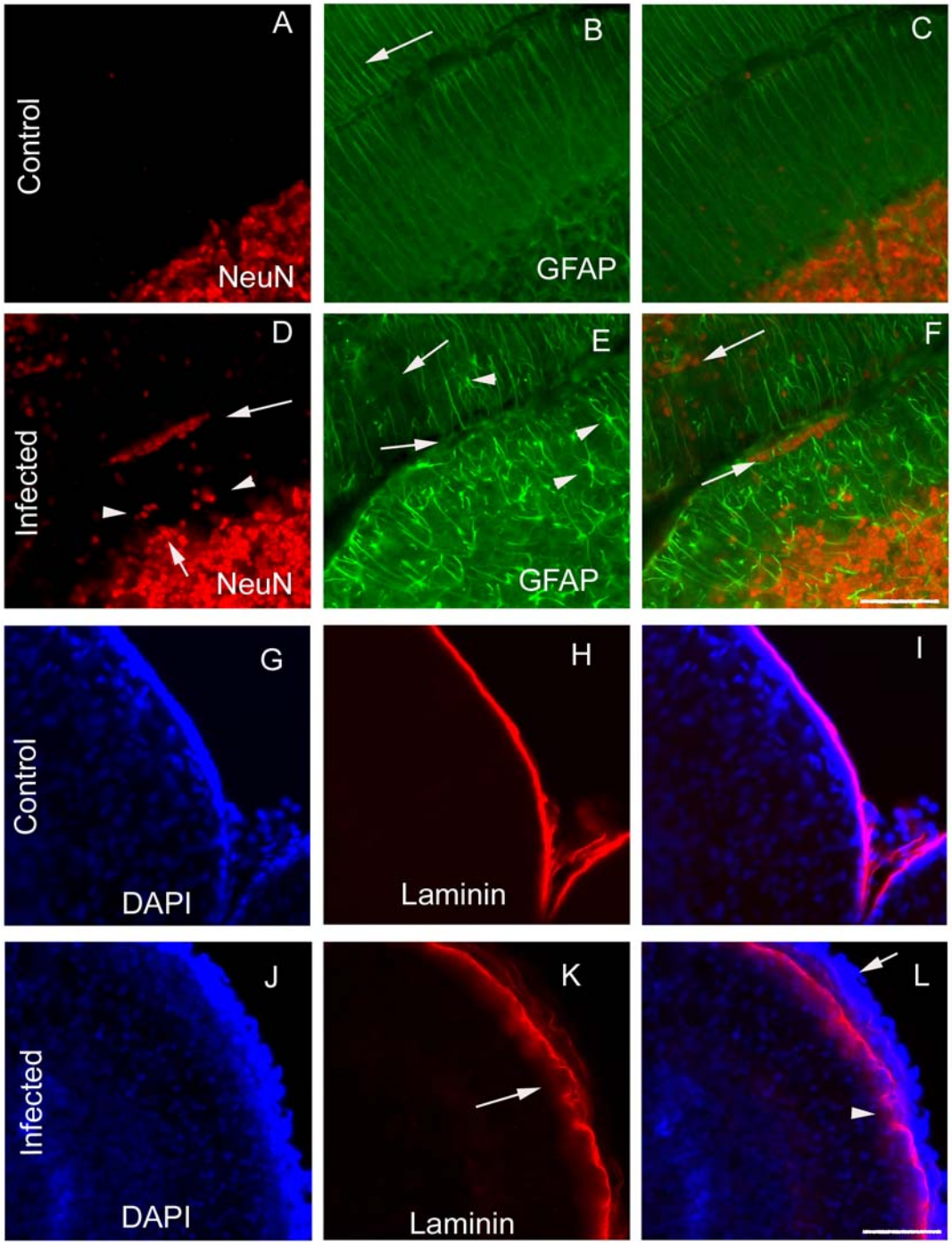
A
Control
NeuN
B
GFAP
C
D
Infected
NeuN
E
GFAP
F
G
Control
DAPI
H
Laminin
I
J
Infected
DAPI
K
Laminin
L

Figure 20 Labeling with BLBP: BLBP is a glia and astrocyte marker which labels cell bodies more specifically than GFAP, this revealed normal organization of radial glia fibers at PD10 (A) and PD18 (C) in control animals. In contrast, BLBP labeling in infected animals revealed reactive gliosis, seen by much brighter and thicker staining glia fibers at both PD10 and PD18. At PD10, Bergmann glia cell bodies were near their normal location in the Purkinje cell layer, although a few had begun to move up into the ML. By postnatal day 18 (D), many astrocyte and glia cell bodies were located within the molecular layer (arrows) and had taken on a golgi like appearance with reactive ramified processes. BLBP positive cells were also seen in the inflamed meninges (arrowhead in D). n=2

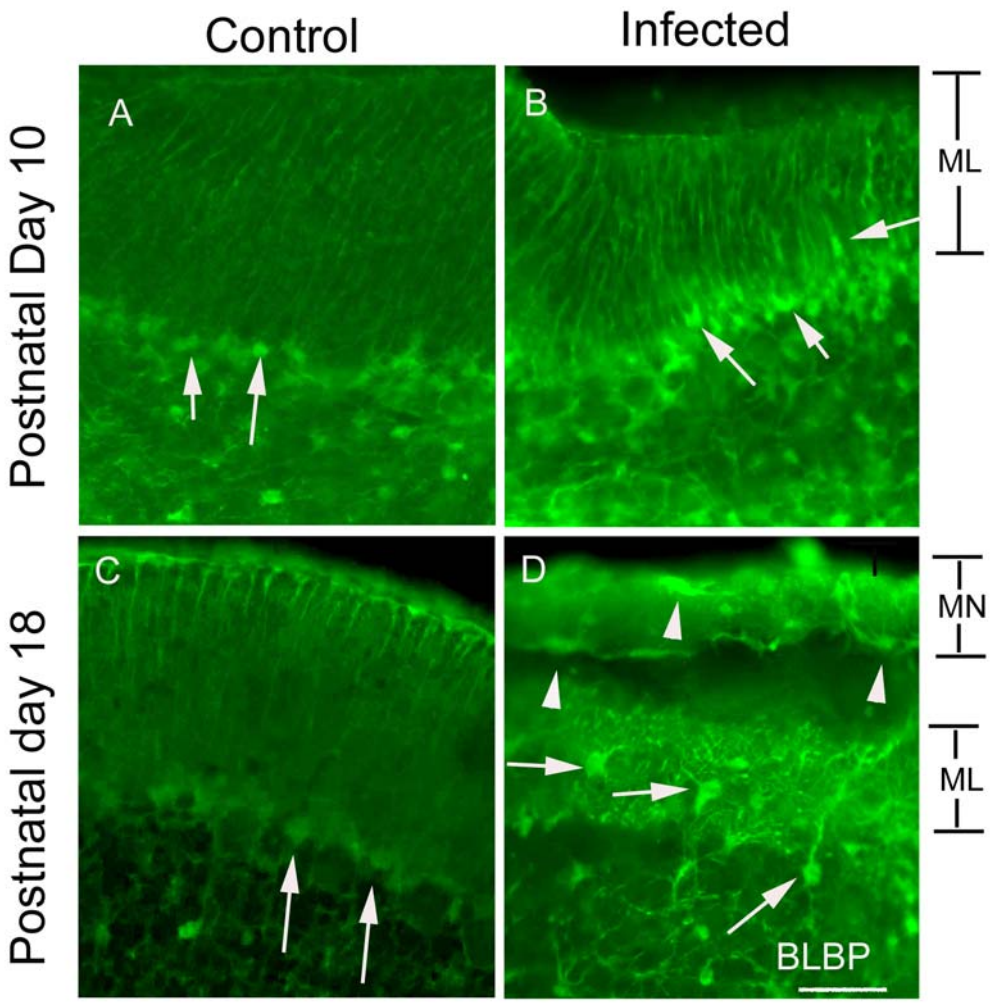
Control
Infected
Postnatal Day 10
Postnatal day 18
A
B
C
D
ML
MN
ML
BLBP

Figure 21 Labeling with activated-caspase 3, NeuN, and GLAST in PD18 infected and control cerebella: Sections were triple labeled for NeuN, GLAST and activated caspase 3 and representative pictures from ventral lobe 8 are shown here. The top panel shows activated-caspase 3 labeling in green in the control (A) and infected (B) animals. In the control, all activated-caspase 3 positive cells (arrows) are arranged around Purkinje cell bodies (arrowheads). The areas of activated caspase labeled cells in the control correspond to Bergmann glia cells bodies which are clearly seen in panel E and I where gray depicts labeling for GLAST (a glia specific glutamate transporter) (arrows in E and I). Activated-caspase 3 in the infected animal labeled many cells in the ML of the cerebellum; these cells did not correspond to NeuN labeling (D and E). Some activated-caspase 3 labeled cells in the infected were located around the Purkinje cells and corresponded to GLAST positive cell bodies (arrows) around Purkinje cells (arrowheads) (F and J) suggesting a glia cell origin. n=3

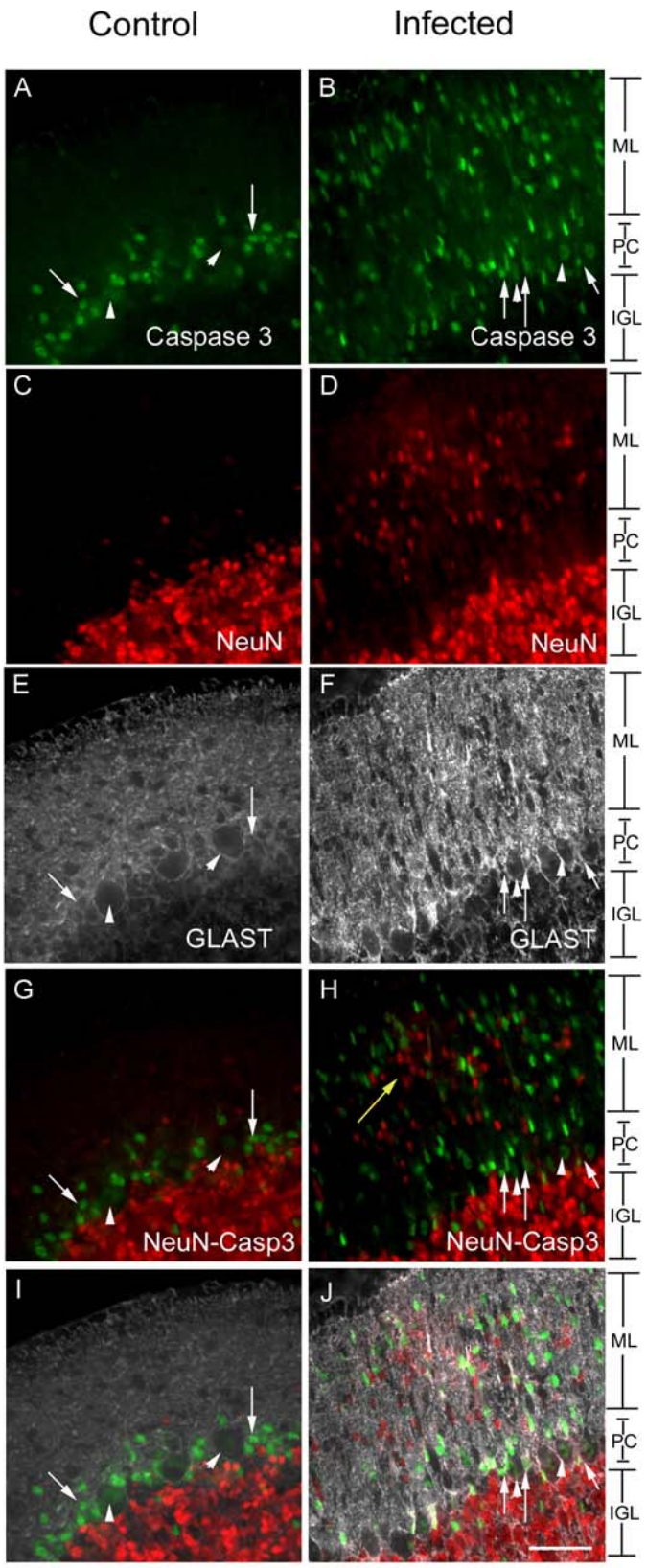
Control
Infected
A
B
Caspase 3
Caspase 3
C
D
NeuN
NeuN
E
F
GLAST
GLAST
G
H
NeuN-Casp3
NeuN-Casp3
I
J
ML
PC
IGL

Figure 22 Double labeling with GFAP and activated-caspase 3, and TUNEL labeling on adjacent sections: This showed that activated-caspase 3 positive cells co-localized with GFAP and were not TUNEL positive. In the control animals (A, B, C, and H), activated caspase 3 labeled cells in the Purkinje cell layer (arrows A). These cells corresponded to cell bodies of glia by GFAP labeling (arrows in B) and in the composite of GFAP and activated-caspase 3 there was a clear co-labeling of GFAP and activated-caspase 3. TUNEL staining in an adjacent section (H) revealed no TUNEL positive cells, providing evidence that activated-caspase 3 positive cells in the control were not undergoing apoptosis. In infected animals, activated-caspase 3 (D) co-localized to cells that were GFAP positive (E). TUNEL staining in an adjacent section revealed very few TUNEL positive cells (arrows in I) providing evidence that activated-caspase 3 was not indicative of cell death, and was expressed in glia. A PD14 infected animal (G) was labeled for TUNEL as a positive control because it had been shows previously to have a high number of TUNEL positive cells after LCMV infection. n=2 for GFAP and activated-caspase 3 labeling, n=1 for TUNEL

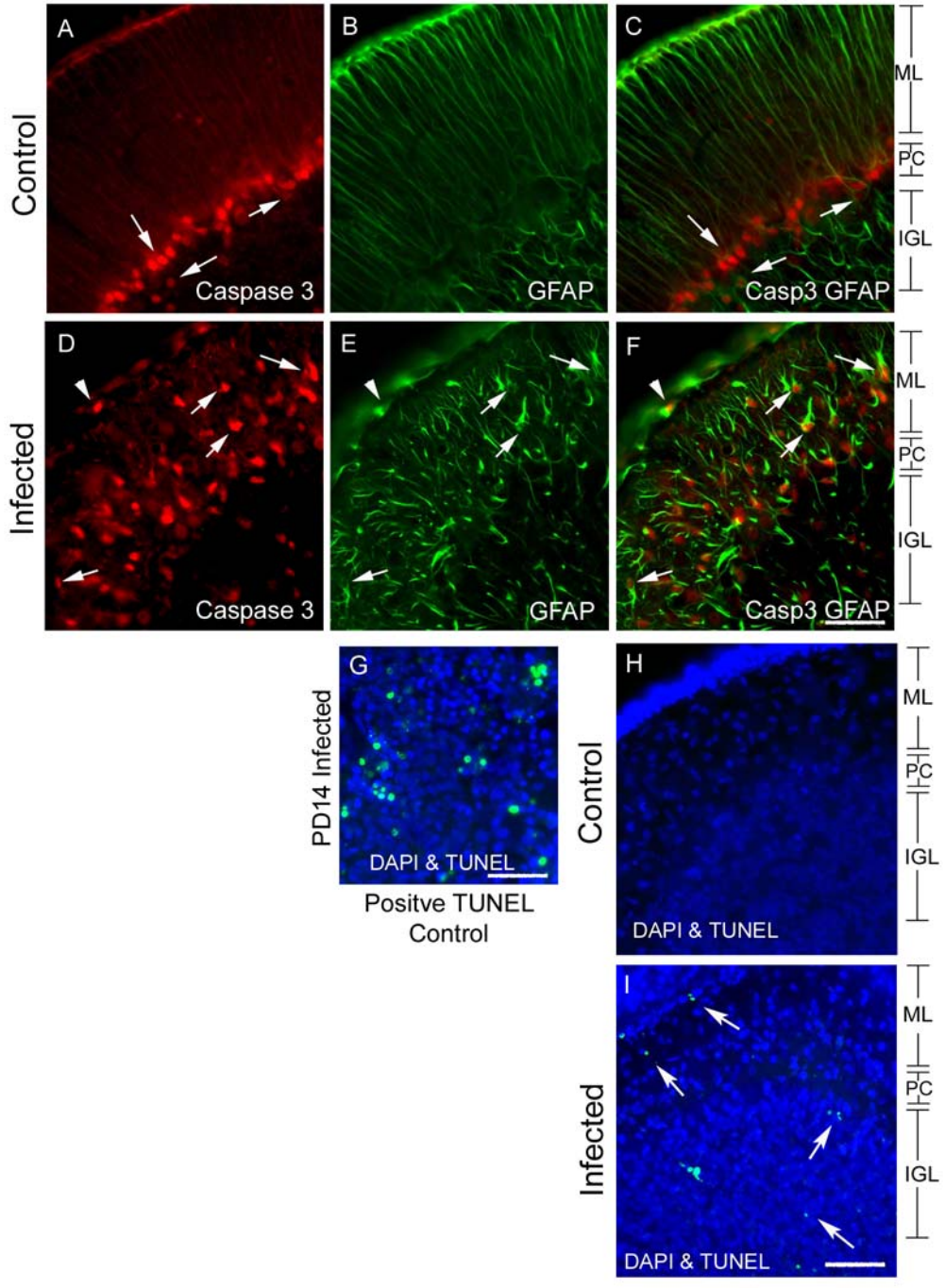
A
B
C
Control
Caspase 3
GFAP
Casp3 GFAP
ML
PC
IGL
D
E
F
Infected
Caspase 3
GFAP
Casp3 GFAP
ML
PC
IGL
G
PD14 Infected
DAPI & TUNEL
Positve TUNEL
Control
H
Control
DAPI & TUNEL
ML
PC
IGL
I
Infected
DAPI & TUNEL
ML
PC
IGL

Figure 23 Nissl stain of PD18, 21, and 25 cerebellum sections: The top two rows show a Nissl stain of whole sections of the cerebellum in infected and uninfected animals at postnatal days 18, 21 and 25. A drastic hypoplasia is evident in the infected cerebella at all time points, and a destructive process is also seen. In addition, an extended presence of the external granule cell layer (EGL) is seen in infected animals. In the uninfected animal, this is thin at PD18 and gone by PD 21 as the granule cells mature and migrate inwards. In the infected cerebella, a clear presence of the EGL is seen even at PD25. The bottom 4 rows are 10x magnifications of ventral and dorsal lobules in the corresponding brain sections. Magnification bar in the top panel is 1mm and in the bottom panel is .5mm. n=3

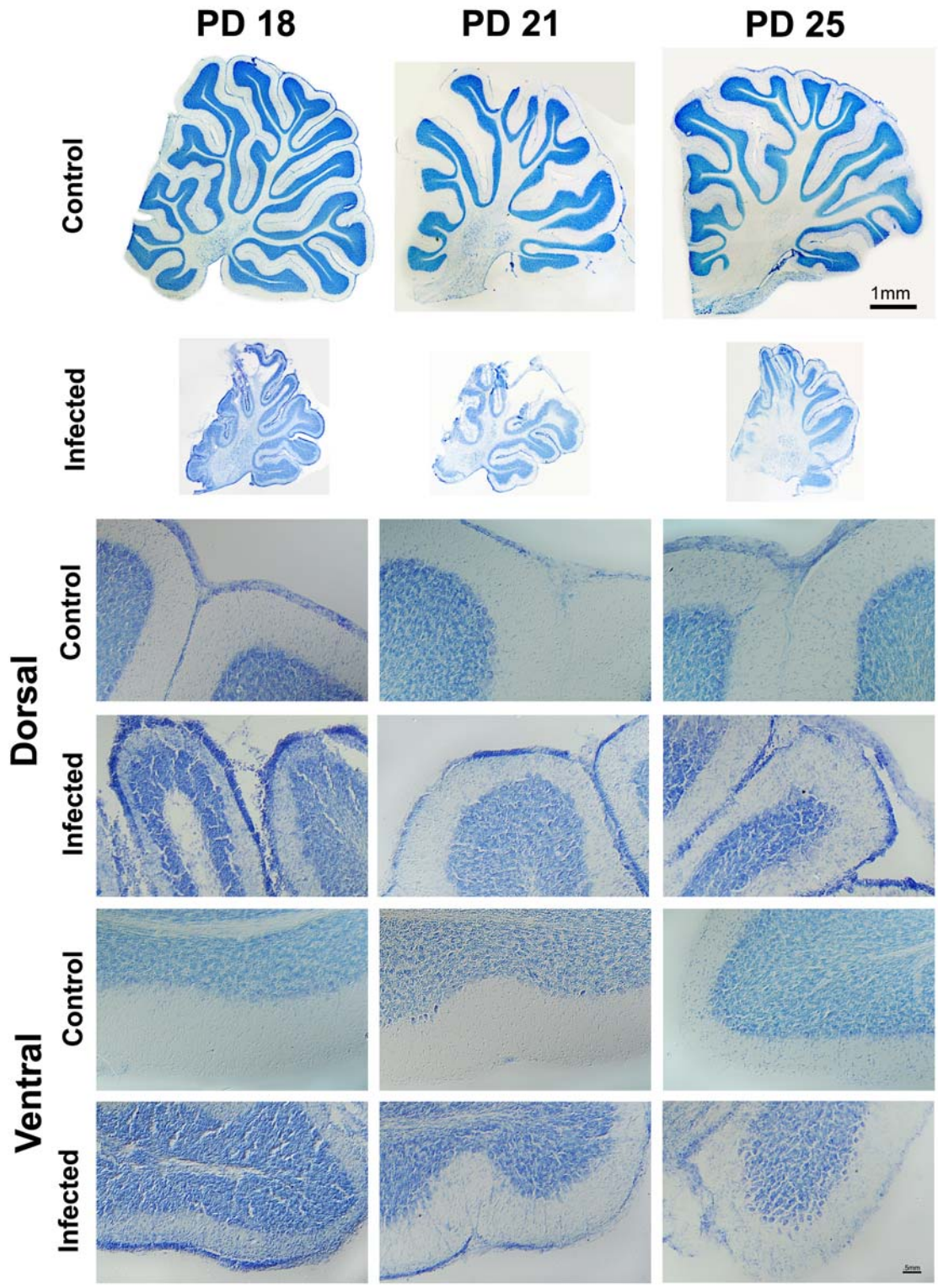
PD 18
PD 21
PD 25
Control
Infected
1mm
Dorsal
Control
Infected
Ventral
Control
Infected
5mm

Figure 24 TUJ1, TAG1, and CXCR4 labeling in the cerebellum of infected and control animals at PD10: CXCR4 labeled the EGL of both control (A) and infected (B) animal, and the thickness of the EGL was greater in the infected compared to control animals (brackets in A, D). CXCR4 also strongly labeled Purkinje cells (arrow in A) and processes (arrowhead in A) in the control, but only weakly labeled Purkinje cells (arrow in D) in the infected animal (arrows in A and B). TUJ1 labeled nearly the entire thickness of the control cerebellum's EGL (arrow in B). TUJ1 only labeled a very thin inner part of the EGL in the infected animal (arrow). A composite of CXCR4 for the control (C) and the infected (F) reveals that in the control, CXCR4 and TUJ1 labeling colocalizes to and is very uniform in thickness. In the infected cerebellum, the entire EGL is CXCR4 positive but only the inner layer is expressing the differentiated neuronal marker TUJ1. Labeling for TAG1, revealed the entire EGL of the control animal was TAG1 positive, (H, I) whereas only the inner half of the EGL was TAG1 positive in the infected animal (K, L). This suggests that the outer EGL in the infected animal is in a premitotic, undifferentiated state, compared to the control where the entire EGL at PD10, expresses markers specific to postmitotic neurons. n=3 for TAG1 and CXCR4 labeling, n=2 for TUJ1

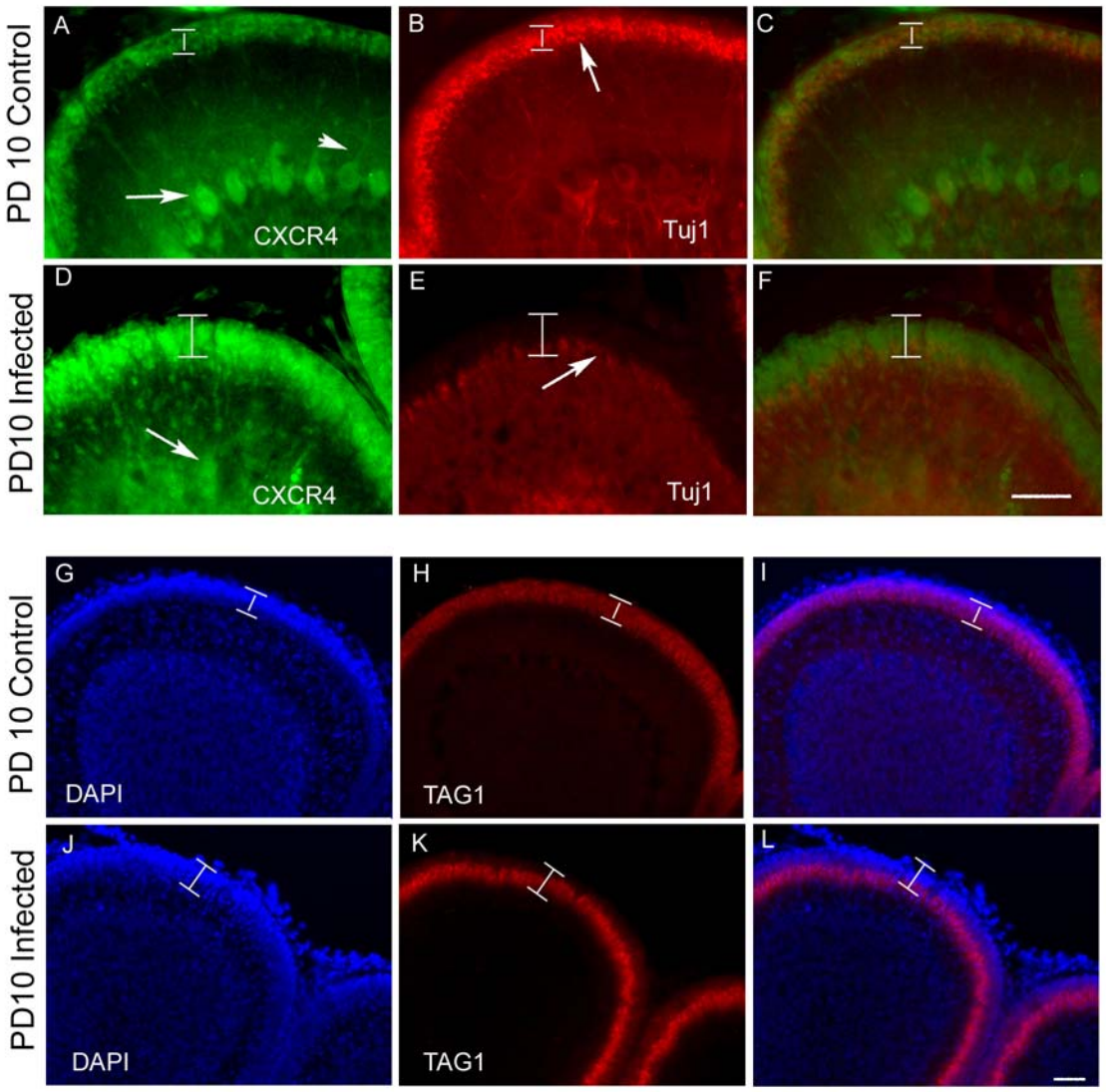
PD 10 Control
PD10 Infected
A
B
C
D
E
F
CXCR4
Tuj1
CXCR4
Tuj1
G
H
I
J
K
L
DAPI
TAG1
DAPI
TAG1

Figure 25 TAG, GFAP, laminin triple labeling and TUJ in an adjacent section, and CXCR4 in another adjacent section for PD18 infected and control cerebella: The most important aspect of this Figure is the TAG1 labeling (B, E) which reveals TAG1 expression only in the EGL of the infected cerebellum (E). Triple labeling (F) with GFAP, TAG, and Laminin show that the TAG1 positive cells are in their normal orientation, beneath the laminin, in the ML of the cerebellum. Laminin and GFAP labeling also reveals that in the control, Bergmann glia fibers make a regular pattern of parallel connections with the laminin (arrow, G), whereas in the infected, Bergmann glia connections (arrow F) with the Lamina are father spaced apart, leaving gaps without Bergmann fibers reaching the Lamina (arrowhead F). TUJ1 labeling of the control (G) and infected (I) reveals that a thickened EGL in the infected animal is present and is TUJ1 positive, which is evidence that these cell are neurons beginning to differentiate. CXCR4 labeling (H and J) is different in the control (H) and infected (I). CXCR4 clearly label Purkinje cell bodies (arrows) and processes (arrowhead) in the control animal but no CXCR4 is seen in the EGL at this time point. In contrast, CXCR4 only labels very few Purkinje cell bodies (arrow) in the infected animal and CXCR4 labeling is still present in the EGL (arrowheads). n=3 for TAG, n=2 for TAG, GFAP, laminin triple label, n=2 for TUJ1, n=3 for CXCR4

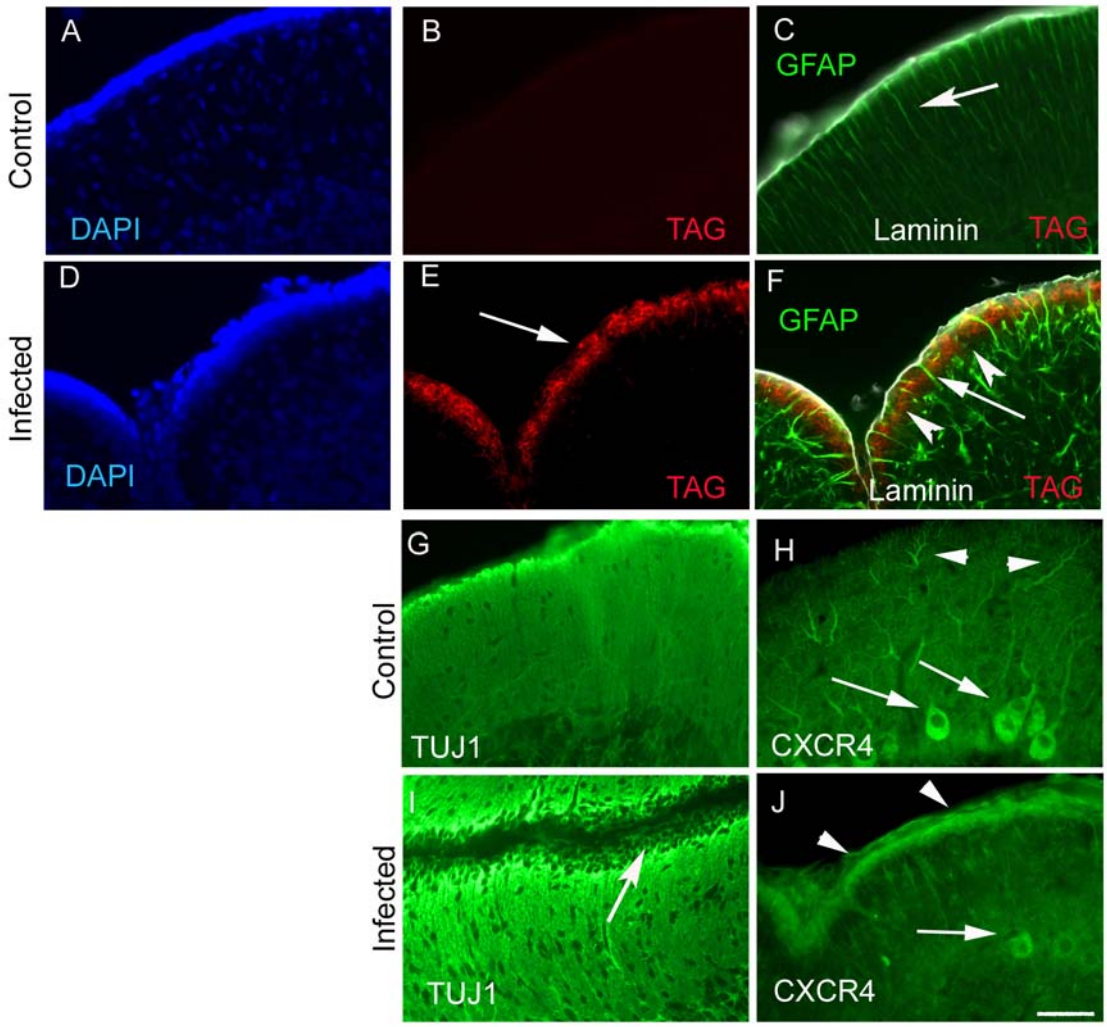
Control
Infected
A
DAPI
B
TAG
C
GFAP
Laminin
TAG
D
DAPI
E
TAG
F
GFAP
Laminin
TAG
Control
G
TUJ1
H
CXCR4
Infected
I
TUJ1
J
CXCR4

Figure 26 PCNA labeling for proliferating cells: An antibody against proliferating cell nuclear antigen (PCNA) was used to label for proliferating cells in the cerebella of PD10 (A), PD18 (B), and PD21 (C) control and infected animals. Control cerebella are shown on the left column, dapi is in the top column and PCNA in the bottom column. PCNA labeling at all time points revealed a thicker layer of proliferating cells in the infected, compared to control EGL and at PD21 there was no PCNA labeling in the control cerebellum whereas there was in the infected, indicating an increased quantity of proliferation at PD10-PD21 in addition to a prolongation of proliferation in infected animals at PD21. n=3

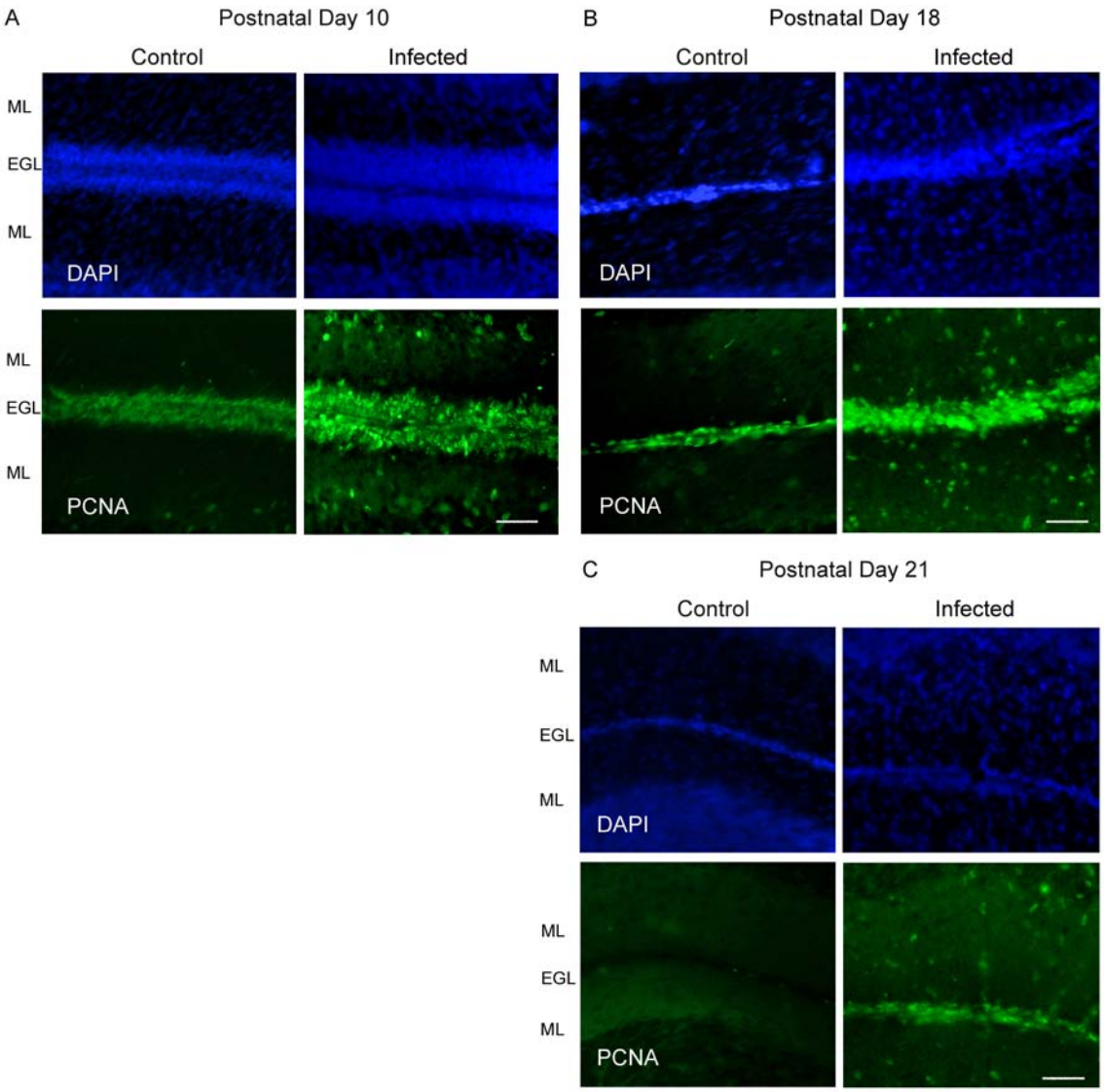

Figure 27 CXCR4 and CXCL12 expression in the whole cerebellum and dorsal and ventral cerebellum: A. Whole cerebellum expression of CCL12 revealed a significant decrease at PD10 in the infected cerebella (P<.04) and a significant increase at P18 and PD25 (P<.03, P<.05) in infected cerebella. B. CXCR4 expression was increased in the infected whole cerebellum at PD18 and 25 (P<.006, P<.023). C. CXCL12 expression was increased in the dorsal and ventral cerebella infected with LCMV. This increase occurred at PD10, PD18 and 25 (P<.0001, P<.002, P<.05, LSD post hoc). D. CXCR4 expression was higher in the infected dorsal and ventral cerebellum compared to the control cerebellum at PD14, PD18, and PD25. (P<.04, P<.002, P<.003, LSD post hoc). n=3 or more

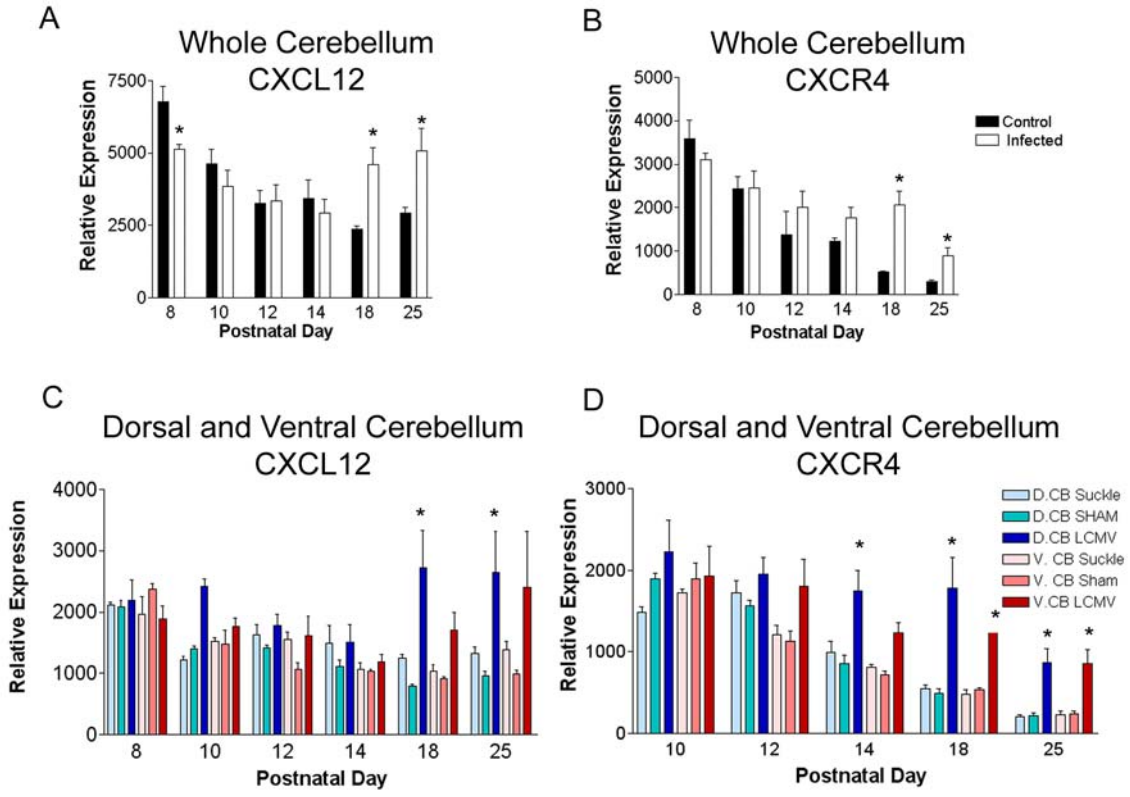

Figure 28 SHH and ATOH1 expression in the whole cerebellum and dorsal and ventral cerebellum: A and C, SHH expression is increased in the infected whole cerebellum at PD12 and PD25 but did not reach significance using the Bonferroni post hoc test but did reach significance with the LSD post hoc ($P<.05$). A significant decrease in SHH expression was seen at PD18 in the infected dorsal cerebellum compared to the control cerebellum ($P<.01$). B and D, ATOH1 expression in the whole cerebellum was significantly higher in the infected compared to control animals at PD18 and PD25 ($P<.01$, $P<.05$). There was also a trend towards increased expression at PD8 and PD10 that did not reach significance. ATOH1expression was different in the dorsal versus the ventral cerebella. At PD8, the infected ventral cerebellum had significantly less ATOH1 expression than sham injected control ($P<002$), while the dorsal cerebellum expression was 3 times higher in the infected than the control but did not reach significance. At PD10, ATOH1 expression in the infected dorsal cerebellum was nearly 3 times higher than in the dorsal control ($P<.025$). ATOH1 expression was also higher in both dorsal and ventral infected cerebella compared to control and PD14 and 25 but did not reach significance. n=3 or more

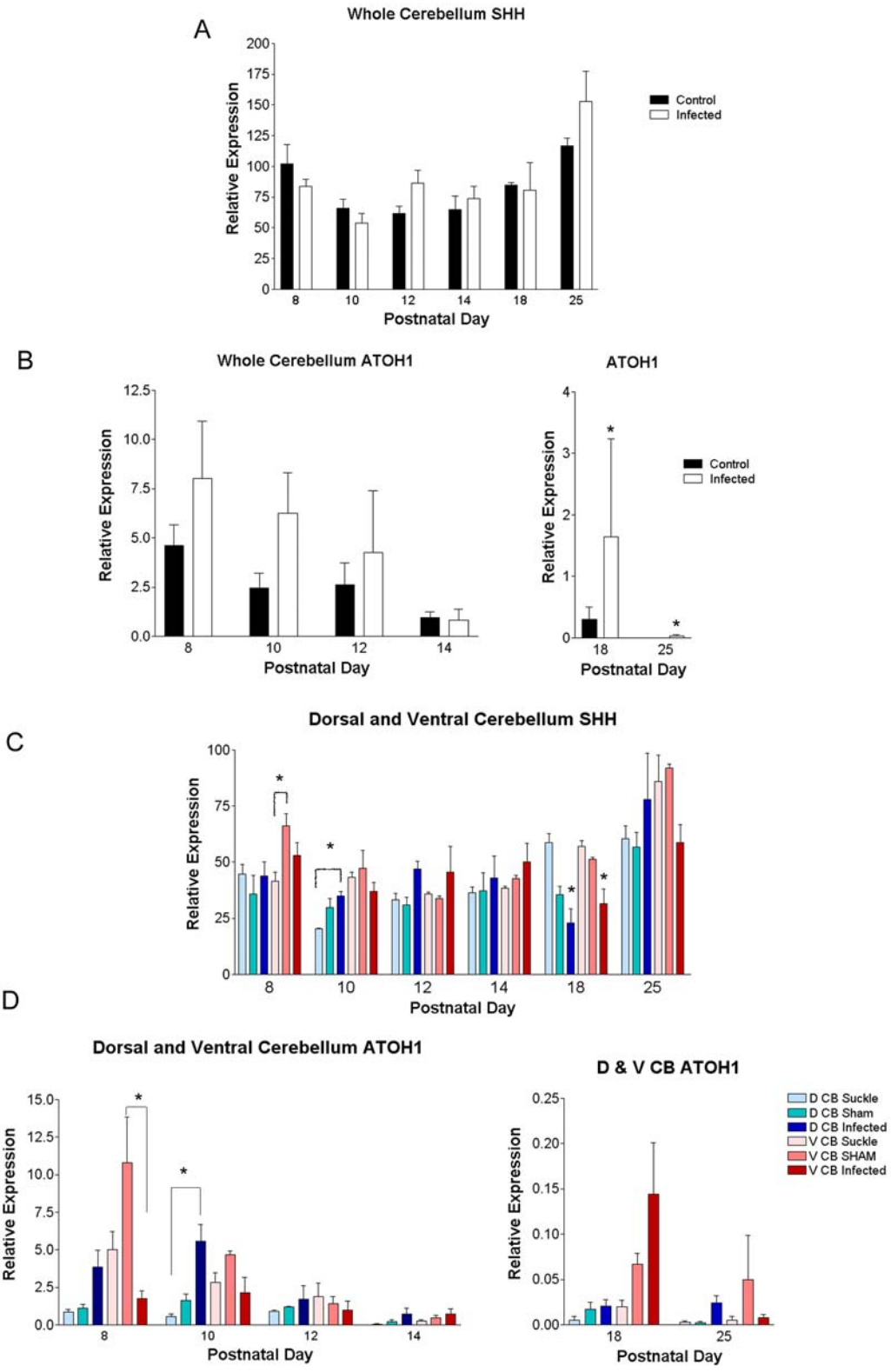
A
Whole Cerebellum SHH
Relative Expression
Postnatal Day
Control
Infected
B
Whole Cerebellum ATOH1
ATOH1
Relative Expression
Postnatal Day
Control
Infected
C
Dorsal and Ventral Cerebellum SHH
Relative Expression
Postnatal Day
D
Dorsal and Ventral Cerebellum ATOH1
D & V CB ATOH1
Relative Expression
Postnatal Day
D CB Suckle
D CB Sham
D CB Infected
V CB Suckle
V CB SHAM
V CB Infected

Figure 29 Open field activity and balance measure for Lewis animals infected with LCMV: A. This graph shows the total number of times animals crossed a grid in the open field apparatus measured over a 30 minute time period. LCMV infected rats where more than 2 times more active than non-infected. This did not reach significance (P<.1). B. This is a graph of time in seconds, to cross rod and square beams of various diameters. LCMV infected animals were significantly impaired compared to control animals on all beams (P<.0001). n= 8 control, n=9 infected

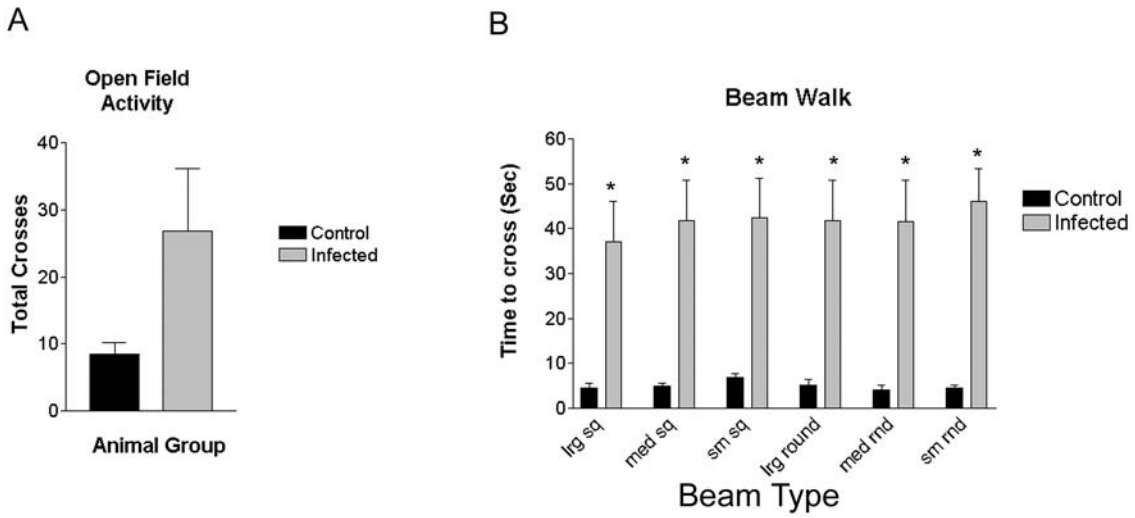

CHAPTER 5: T-CELLS BOTH PROTECT AND A DAMAGE THE BRAINS OF NEONATAL RATS INFECTED WITH LCMV

Introduction

Previous studies have correlated the presence of CD8 T-cells and, to a lesser extent CD4 T-cells, to regions of brain destruction in neonatal rats infected with LCMV [36-37]. Chapter 3 presents a study in which cerebella from T-cell competent Lewis and RNU/+ animals were compared to the cerebella from T-cell deficient RNU/RNU animals. The results demonstrated that, in the absence of T-cells, cerebellar hypoplasia develops, but destructive lesions do not. However, in the presence of T-cells, not only do destructive lesions occur, but abnormal neuronal migration occurs as well. Furthermore, abnormal neuronal migration does not occur in the absence of T-cells. These findings demonstrate that the disruption of neuronal migration in LCMV infection is immune-mediated. However, the mechanism by which the immune system leads to ectopic cells is unknown. Uncovering this mechanism is one of aims of this chapter.

Previous studies have also shown that LCMV infection induces a substantial loss of granule cells from the dentate gyrus. However, unlike the cerebellum, the dentate gyrus does not undergo a massive lymphocytic infiltration during LCMV infection, despite a heavy viral burden. Furthermore, unlike the cerebellum, the dentate gyrus cell loss is delayed in its onset and does not occur until after the peaks of infection and inflammation have passed. These observations have led some to conclude that the cell loss from the dentate gyrus is not immune-mediated. However, direct experiments to determine the role of the immune system in LCMV-induced dentate gyrus pathology have not been conducted. A second aim of this chapter is to investigate this issue.

In order to better characterize the role of the immune system in LCMV-induced pathology, I have developed an adoptive transfer model of the disease in which T-cells are experimentally reconstituted in RNU/RNU rats that congenitally lacked them [232].

Our goal was to use this model to help elucidate the role of T-cells in the loss of dentate granule cells and the mechanism of immune-mediated neuronal migration disturbances in the cerebellum. Both pathologies have important implications for human disease. The loss of cells in the dentate gyrus has implications for epilepsy, learning, and memory disorders [233-234]. Abnormal neuronal migration is observed in many congenital infections, including LCMV, and contributes strongly to the motor dysfunction, learning disabilities, and epilepsy that commonly accompany congenital infections.

Furthermore, by using a T-cell deficient vs. T-cell competent model we can explore whether signaling molecules, such as SHH and the transcription factor ATOH1, are altered in the presence and absence of the immune system. In chapter 3, we reported the elevation of inflammatory cytokines, including IFN-γ and TNF-α, in the RNU/+ and RNU/RNU brains. IFN-γ is a regulator of sonic hedgehog (SHH), a mitogen for granule cell precursors [193, 199]. Therefore, one possible cause of increased proliferation in the EGL is that IFN-γ increases SHH and thereby increases granule cell proliferation in LCMV infection. In these experiments, we examine whether SHH is upregulated in a T-cell dependent manner. Likewise, we have found previously that Bergmann glia morphology is corrupted in LCMV infection. Comparison of immune-competent and immune-deficient rats will elucidate the importance of the immune system in the disruption of Bergmann glia.

Materials and Methods

Animals

RNU/+ rats on a hooded background were obtained from the National Cancer Institute (NCI-Frederick (Frederick, MD). The RNU/+ rats were bred with RNU/RNU males. Thus, the litters of the RNU/+ dams were approximately 50% RNU/+ and 50% RNU/RNU. For more details, see materials and methods in chapter 1.

LCMV Virus and Infections

As described in previous chapters, rats received intracranial inoculations of Armstrong-4 LCMV (0 or 1000 pfu) on postnatal day 4.

Splenocyte Isolation

Splenocytes were isolated from animals for two purposes: first, for the adoptive transfer experiments, and second, for flow cytometry quantification of cell type. For adoptive transfer experiments, splenocytes were isolated from the spleens of adult animals primed with LCMV virus 8-12 days previously. Flow cytometry of these isolated splenocytes was performed on two separate occasions.

Splenocytes were also isolated from pups at PD14 and PD18 from RNU/+ infected, RNU/RNU infected and RNU/RNU infected + adoptive transfer groups. This was done to compare the lymphocyte population in each group and to determine the success of the adoptive transfer. See chapter 1 for details regarding the methodology of splenocyte isolation.

Adoptive transfer

Heterozygote (RNU/+) animals were injected IP with 1x10^5 PFU of LCMV for generation of donor splenocytes. Splenocytes were harvested 8-12 days after injection of virus following the splenocyte isolated procedure described above. 12 x 10^6 splenocytes, at a concentration of 30 x 10^6/ml, were then injected IP into PD5 RNU/RNU pups, which had been infected intracranially on PD4 with LCMV. Splenocytes were injected through a 27-guage needle in a volume of 0.4 ml. Flow cytometry on lymphocytes isolated from spleen and brain was conducted at PD14 and PD 18 to confirm successful delivery of T-cells for at least two separate experimental adoptive transfers. For control purposes, splenocytes were also delivered to LCMV naive PD5 RNU/RNU pups.

Brain Lymphocyte Isolation

Lymphocytes were isolated from the brains of infected RNU/+, infected RNU/RNU, and infected RNU/RNU + adoptive transfer (AD.T) animals at PD 14 (n=2 per group) and PD18 (n=2 per group), following the lymphocyte isolation method in chapter 1. Cell proportions were analyzed using flow cytometry, as described in chapter 1.

Flow cytometry

Analysis of cell populations with flow cytometry was carried out as described in Chapter 1.

Perfusions, Histology, and Immunohistochemistry.

For evaluation of neuropathology, rats were sacrificed at a series of ages following infection. The following five genotype/treatment groups were included: RNU/+ sham injected control, RNU/+ LCMV infected, RNU/RNU sham injected control, RNU/RNU LCMV infected, RNU/RNU LCMV infected + AD.T. Three to 6 animals were included in each genotype/treatment group at PD 14, 18, 25, 40 and 120. The rats were anesthetized with pentobarbital and perfused via the left cardiac ventricle with 0.9% saline, followed by 4% paraformaldehyde in 0.1 M sodium phosphate buffer. The brains were removed and stored in 4% paraformaldehyde fixative.

For histological analysis, the cerebellar vermis was removed, dehydrated through a graded series of alcohol, embedded in paraffin, and cut on a rotary microtome in the sagittal plane into 5 μm-thick sections. The sections were mounted on slides and stained with hematoxylin and eosin (H&E) for assessment of neuropathology.

For immunohistochemistry, the cerebella were sunk in 30% sucrose and cut in 40um-thick sections using a freezing microtome.

Immunohistochemistry protocol

Endogenous peroxidases were blocked by incubation with 3% hydrogen peroxide for 30 minutes. Antigen retrieval was performed for the PCNA antibody only, and was done using a citrate buffer steam bath for 20 minutes. For PCNA antigen immunostaining, the sections were incubated with a horse serum blocking solution for 60 minutes. The sections were then incubated with anti-PCNA antibody (mouse anti-PCNA IgG2a1:500, Zymed, San Francisco, CA) overnight at 4°C. Detection was performed using a biotinylated horse anti-mouse (Vector Laboratories, Burlingame, CA). The reaction was completed with the ABC Elite (Vector Laboratories, Burlingame, CA) and diaminobenzidine (DAB) substrate.

For immunofluorescence, the following primary and secondary antibodies were used: rabbit anti-GFAP (1:1000; Sigma, St. Louis, Missouri), mouse-anti GFAP (1:1000; Sigma, St. Louis, Missouri) monoclonal mouse anti-Neuron-specific beta-III tubulin antibody IgG2a (1:1000; R& D Systems, Minneapolis, MN), rabbit anti-human/mouse Caspase 3 active (1:1000; R & D Systems, Minneapolis, MN.) mouse anti rat TAG1 IgM (1:10; DSHB, Iowa City, IA) Mouse anti-NeuN IgG1 (1:500; Chemicon). Alexa fluor goat conjugated antibodies were used at a dilution of 1:500 for each experiment and are listed in chapter 3.

RT-PCR

mRNA isolation and RT-PCR were conducted as described in chapter 1, but with different primer and probe sets. TaqMan primer and probe sets for CXCR4, CXCL12, SHH and ATOH1 were purchased from Applied Biosystems Inc. (Foster City, CA).

Behavior

All behavior experiments were conducted on animals between PD37 and PD42. All groups were tested on an open field task and beam walk task, as described in the methods of chapter 3. The following groups were tested: RNU/+ control (n=8), RNU/+

infected (n=10), RNU/RNU control (n=7), RNU/RNU infected (n=7), RNU/RNU infected + AD.T. (n=10).

Results

Adoptive transfer of splenocytes returned T-cell-mediated pathology to RNU/RNU infected rats

To elucidate the role of T-cells in LCMV-induced pathology, we established an adoptive transfer model. Donor immunocompetent adult animals were primed with LCMV; splenocytes were isolated 8-10 days later and transferred into congenitally athymic rat pups that had been infected with LCMV 24 hours previously. Flow cytometry revealed the percentages of CD4 and CD8 cells in the isolated splenocytes used for adoptive transfer experiments. The flow cytometry analysis from 2 donor spleens showed that 13-15% of the harvested cells were CD3+CD8+ positive, while 18-26 % were CD3+CD4+ positive To confirm the success of the adoptive transfer in returning T-cells to RNU/RNU neonatal pups, flow cytometry was conducted on lymphocytes isolated from the infected brain and spleen of RNU/+, RNU/RNU, and RNU/RNU AD.T rats at PD14 (n=2) and PD18 (n=2). Flow cytometry revealed the presence of CD3+CD8+ and CD3+CD4+ T-cells in the spleen and brain of the RNU/RNU AD.T animals (Figure 30 C), and confirmed their absence in the spleen and brain of their RNU/RNU infected counterparts (Figure 30 B). The proportions of CD3+CD8+ and CD8+CD4+ cells were similar in RNU/RNU AD.T and RNU/+ animals (Figure 30 A and C).

Further evidence of successful adoptive transfer was seen in the disease phenotype. In chapter 3, we found that LCMV infection leads to spasticity, hind limb hypotonia, and ataxia in T-cell competent animals, while the infection induces only jitteriness in the athymic (RNU/RNU) rats. We confirmed those findings in this study. Furthermore, adoptive transfer of splenocytes to RNU/RNU LCMV-infected animals

induced spasticity, hindlimb hypotonia, and ataxia in the RNU/RNU animals that would otherwise have had jitteriness alone. Thus, the adoptive transfer of splenocytes restored the principal disease symptoms.

To control for potential non-specific pathology induced by the delivery of splenocytes, adoptive transfer was also performed in sham-injected control (uninfected) RNU/RNU animals (n=6). These animals did not develop any evidence of CNS disease, and their brains were normal on gross examination. Therefore, the phenotype and disease that developed after adoptive transfer of splenocytes was specific to viral presence and not due to non-specific T-cell priming against the CNS.

Gross and microscopic examination of the brains provided further evidence that the adoptive transfer successfully returned classic LCMV pathology to the RNU/RNU rats. Figure 31 shows the cerebellar histology for RNU control, RNU/RNU infected and RNU/RNU infected + AD.T. As observed previously, LCMV infection in the RNU/RNU animal induced no destructive lesions, but did cause a notable hypoplasia, compared to the uninfected control (Figure 31, D&E). In contrast, LCMV infection in the adoptively transferred RNU/RNU rat led to massive tissue destruction, especially in the dorsal lobules (Figure 31, F). This pathology following adoptive transfer perfectly recapitulates the pathologic changes observed in animals with intact immune systems.

To quantify the degree of cerebellar tissue reduction among groups, we calculated the cerebellum-to-hemisphere brain weight ratio. These results are graphed in Figure 31G and show that LCMV led to reductions in cerebellar weight in all infected animals. However, the cerebellum-to-hemisphere weight ratio was much more severely reduced in the athymic rats that received the adoptive transfer than in those that did not. This profound loss of brain mass reflects the combination of hypoplasia and tissue destruction.

Role of T-cells in viral clearance and cerebellum pathology

In chapter 3, we reported that nude animals had higher viral titers in their cerebella at PD 40 than did their RNU/+ littermates. These elevated viral titers in the nude animals reflected impaired viral clearance. To confirm that the difference in viral clearance between RNU/+ and RNU/RNU cerebella was due to the lack of lymphocytes in the RNU/RNU rats and not to some other factor, we examined the presence and distribution of viral antigen in the cerebellum of the RNU/+, RNU-/- and RNU/RNU AD.T animals.

Immunohistochemistry for LCMV in PD40 and PD120 cerebella revealed the presence of virus in RNU/+, RNU/RNU and RNU/RNU + AD.T at both time points. However, the quantity and location of the virus depended on the immune status of the animal. Figure 32 shows sections from PD40 animals. In these samples, it is evident that virus is still present in the cerebella of all animals. However, there was much denser staining for viral antigen in the RNU/RNU cerebellum than in the animals with T-cells. The cell types infected at PD40 were also different in the T-cell deficient versus T-cell competent rats. In particular, astrocytes remained infected at PD40 in the RNU/RNU animals (black arrowhead Figure 32 F) whereas astrocytes were free of virus in all animals with T-cells. Furthermore, the adoptive transfer of splenocytes cleared the virus from Purkinje cells in the RNU/RNU infected animals, while the virus persisted in Purkinje cells in the animals that did not receive the adoptive transfer (black arrows in Figure 32 A, C, D, &F).

At PD120, RNU/+ and RNU/RNU + AD.T had viral protein present only in neuron cell bodies, including granule cells in the IGL (white arrowheads Figure 33 A, B, D, E) and Purkinje cell bodies in the RNU/+ animals (black arrow in Figure 33 A) but not the RNU/RNU AD.T cerebellum. There was no virus in the white matter of either T-cell competent animal (Figure 33 D, E). In contrast, the molecular layer of RNU/RNU infected cerebella had LCMV antigen in Bergmann glia (black arrowhead Figure 33 C),

as well as Purkinje cell bodies and dendrites (black arrow Figure 33 F, G). Widespread LCMV antigen persisted in astrocytes within the medullary white matter regions of the cerebellum of the T-cell deficient rats (arrowhead Figure 33 F). In stark contrast, astrocytes were free of LCMV antigen in both the RNU/+ rats and in the RNU/RNU rats that had received the adoptive transfer of splenocytes (Figure 33 D&E). Thus, T-cells are required for the clearance of viral antigen from Bergmann glia, Purkinje cells, and astrocytes.

Virus mediated pathology vs. immune mediated pathology of the hippocampus

One mystery in LCMV infection is the pathology induced in the hippocampus, where LCMV specifically and heavily infects dentate granule cells. However, unlike the cerebellum, the dentate gyrus does not undergo an acute destructive process. Instead, a normal complement of granule cells is typically generated, but undergoes a delayed-onset cell loss several months post-infection [36-37]. The mechanism underlying this cell loss has been unknown. In particular, whether the cell loss is virus-mediated, immune-mediated, both, or neither has been unclear.

To explore the role of T-cells in the hippocampal pathology we compared T-cell competent (RNU/+ and RNU/RNU + AD.T) and T-cell deficient RNU/RNU animals at PD40 and PD120. These time points were chosen because PD40 was previously shown to be the approximate time that hippocampal pathology begins, while PD 120 is a time at which hippocampal cell loss is well underway [36].

At PD40, differences in pathology were already evident between animals deficient in lymphocytes versus those with lymphocytes (Figure 34). In particular, rats deficient in lymphocytes had a clear reduction in the width of the dentate gyrus following LCMV infection, reflecting cell loss from the dentate gyrus (Figure 34 C). In contrast, rats that received the adoptive transfer of lymphocytes had no reduction in dentate gyrus

width or any other evident pathology (Figure 34 B). Likewise, the immune-competent RNU/+ animals had no evident hippocampal pathology (the RNU/+ animals were identical to the RNU/RNU adoptive transfer animals and are not shown). Thus, the initial dropout of dentate gyrus granule cells occurred only in animals lacking T-lymphocytes and did not occur in animals possessing them, suggesting that T-lymphocytes protect the hippocampus against LCMV-induced cellular losses, at least at the early time points.

Figure 35 shows that the location of viral antigen within the hippocampus on PD40 likewise differed strongly between animals with and without T-lymphocytes. In particular, in the RNU/RNU animals, substantial amounts of viral labeling was present within granule cells of the dentate gyrus and throughout the hippocampus and perihippocampal regions (Figure 35 B and C). In stark contrast, no viral antigen was present in neurons or astrocytes of the RNU/+ or RNU/RNU +AD.T animals (Figure 35 A). Thus, the presence of T-lymphocytes was necessary for the clearance of virus from hippocampal astrocytes and granule neurons.

At PD120, hippocampal pathology continued to depend on the immune status of the animal. At this time point, both the RNU/+ and the RNU/RNU + AD.T. displayed a thinning of the dentate gyrus in LCMV infected animals (Figure 34, arrow E). Thus, in the hippocampus of immune-competent animals, LCMV-induced pathology was now evident that had not been present earlier. However, pathology in the athymic animals was even more severe. In the infected RNU/RNU rats, the dentate gyrus was obliterated, as virtually no dentate granule cells existed anymore (Figure 34 F).

At PD120, the distribution of viral antigen continued to differ substantially between T-cell deficient and T-cell competent animals. In particular, astrocytes remained diffusely infected throughout the hippocampal formation of RNU/RNU animals (Figure 34 E and F), while viral antigen remained absent from animals with T-lymphocytes (Figure 34 D). These results demonstrate that, in the absence of T-cells, astrocytes in the forebrain remain infected with LCMV and there is a complete loss of dentate gyrus cells.

When lymphocytes are present, either from native sources or from adoptive transfer, astrocytes are cleared of viral antigen, and the dentate gyrus is partially rescued. Thus, lymphocytes exert at least a partial or temporary protective effect against LCMV-induced neuronal loss from the dentate gyrus.

Migration pathology in the cerebellum

In chapter 3, we demonstrated that ectopic clusters of granule cells were found only in T-cell competent animals. In chapter 4 we showed that LCMV infection severely alters the structure of Bergmann glia and leads to granule cell ectopias within the molecular layer. We further found that EGL granule cells in the infected animals remained in a proliferative state for longer and were delayed in their differentiation. To determine which of these mechanisms were immune-mediated versus viral-mediated, we compared these effects in congenitally athymic rats (RNU/RNU), their immunocompetent littermates (RNU/+), and athymic rats that received splenocytes via adoptive transfer (RNU/RNU + AD.T). We used immunohistochemistry to examine Bergmann glia fibers, NeuN labeling, and specific labeling of the differentiation state and proliferation state of neurons in the EGL.

Anti-NeuN and anti-GFAP by genotype

Immunohistochemistry for NeuN, a marker for post-mitotic neurons [205], showed that clusters of ectopic neurons near the surface of the cerebellum (residual EGL) were present only in T-cell competent (RNU/+ and RNU/RNU + AD.T) animals. This is exemplified in Figure 36, where an island of ectopic cells is seen in the outer ML of the RNU/RNU + AD.T cerebellum (Figure 36 arrow F and I). (Note that RNU/+ LCMV and RNU/RNU AD.T LCMV animals were identical in pathology and therefore only RNU/RNU AD.T are shown in the Figures). No difference in NeuN labeling was seen between RNU/RNU infected (Figure 36D) and RNU/RNU sham injected control rats (Figure 36 E). GFAP labeling in the ventral lobules showed reactive gliosis in both T-

cell deficient (arrow Figure 36 B) and T-cell competent animals (arrow Figure 36C). Bergmann glia in the T-cell competent animals had retracted some processes from the basal lamina, leaving gaps without parallel fibers (arrowheads Figure 36 C); whereas there were no gaps in Bergmann glia parallel processes in the RNU/RNU infected animals. Gaps in Bergmann glia of the RNU/RNU AD.T rats corresponded with the location of ectopic neurons (Figure 36 I). Therefore, although reactive gliosis occurred in all infected animals, radial glial fiber retraction from the basal lamina occurred only in T-cell competent animals.

Differentiation and proliferation of granule cells in the EGL

In chapter 4, we discovered that in the Lewis infected animals, neurons were in a more immature state, continuing their expression of TAG-1 and PCNA later in infected animals, compare to sham injected controls. We sought to determine if this delayed expression occurs in RNU/RNU animals and what role T-cells play in the pathology. TAG-1 is expressed by granule cells when they undergo axonogenesis, shortly prior to internal migration [212, 221]. TUJ-1 is neuron-specific class III beta-tubulin and labels differentiated neurons and their processes. To determine if TAG-1 expression is different in the infected versus control animals of the RNU genotype and if the expression is different in T-cell competent verses control, we co-labeled for TAG-1 and TUJ-1 in the cerebella of each genotype (Figure 37). We also labeled cerebella for PCNA to determine if there was a difference in proliferation of granule cells (Figure 38).

Figure 37 shows that TAG-1 is no longer expressed by PD18 in control animals (Figure 37 D). In contrast, TAG-1 expression is still present in the infected RNU/RNU (Figure 37 E) and infected RNU/RNU AD.T rats (Figure 37 F). There is a very thin layer of TAG-1 expression in the RNU/RNU infected animal and a thick layer of TAG-1 labeling in both T-cell competent animals (RNU/+ not shown but was identical to RNU/RNU AD.T). This suggests that the immune system is necessary for the prolonged

and thicker layer of TAG-1 expression in the EGL. However, the thin layer of TAG-1 expression in the RNU/RNU animals is evidence that a T-cell independent mechanism also contributes to delayed expression of TAG-1.

TUJ-1 labeling, shows a very thin layer of neurons in the EGL of control RNU/RNU rats (Figure 37 B) compared to a much thicker layer in the infected RNU/RNU AD.T rats (Figure 37 C). The composite of TAG-1 and TUJ-1 demonstrates that TUJ-1 expression is localized to the inner one-third of the EGL in the RNU/RNU AD.T animals, while TAG-1 is in the outer two-thirds (Figure 37 I). This means that two-thirds of the RNU/RNU AD.T EGL is in a differentiation state, not yet expressing the early neuronal marker TUJ1, and is still immature. In comparison, TUJ-1 labeling co-localized with the entire TAG-1 label in the infected RNU/RNU animals (Figure 37 H). The co-localization of TAG-1 and TUJ-1 to these neurons signifies that these TAG-1 positive neurons are at the end of their differentiation and are more mature than the TAG-1 positive but TUJ-1 negative neurons in the RNU/RNU AD.T animals.

As shown in Figure 38, PCNA labeling revealed a thicker layer of proliferating cells in the EGL of infected T-cell competent versus infected T-cell deficient animals. In control (A) and T-cell deficient LCMV infected animals (B) there was only one thin layer of PCNA positive cells in the EGL at PD18. In contrast, T-cell competent animals (C, E) had a thick layer of PCNA positive cells in the EGL. This indicates that, in the presence of an intact immune system, external granule cells undergo a prolonged proliferation in LCMV infection. LCMV does not have this effect in T-cell deficient animals.

SHH and ATOH1

We used real-time PCR to quantify SHH and ATOH1 expression from whole cerebella of LCMV and sham injected RNU/+ and RNU/RNU animals (Figure 39). Results of the gene expression assay revealed a 48% upregulation of SHH in the infected cerebella of both RNU/+ and RNU/RNU animals (Figure 39 A). Likewise, ATOH1

expression was elevated by LCMV infection in both genotypes. Upregulation was up to 5 fold above control values in the RNU/+ and 12 fold above control in RNU/RNU animals (Figure 39 B).

Behavior

Another area of interest is how LCMV infection affects behavior and coordination in the animals and what component of behavior is viral vs. immune mediated. For the open field paradigm, we found that LCMV infection in the congenitally athymic animals had no effect on behavior. The number of line crosses over a 30min period was unchanged by LCMV infection in the RNU/RNU rats (Figure 40 B). In contrast, infection of the RNU/+ and RNU/RNU AD.T animals substantially increased open field activity. The RNU/+ group was 2 fold more active than the sham injected control while the RNU/RNU AD.T was 3 fold more active than the sham injected control and 2.3 fold more active than the LCMV injected RNU/RNU group. These data indicate that LCMV infection induces hyperactivity and this altered behavior depends on the presence of T-cells.

To determine the role of the virus versus the immune response in coordination, we used a beam walk apparatus. Figure 40A shows the measure for time to cross the beam in all animal groups, for each rod of varying widths. T-cell competent rats took significantly more time to cross the medium and small rods than T-cell deficient and non-infected control groups. Animals that received splenocytes by adoptive transfer were especially impaired. In fact, RNU/RNU+ AD.T was impaired compared to all other groups on all beams except for the largest square beam. Postmortem analysis of the brains found that large destructive cerebellar lesions were obvious in 7 of the 10 RNU/RNU animals receiving the AD.T, but in only 3 of the 10 RNU/+ animals. No destructive cerebellar lesions were evident in the infected RNU/RNU rats. Therefore, the

more severe impairment in balance and open field activity correlated, on a group basis, with the incidence of destructive cerebellar lesions.

Discussion

In this series of experiments, we established a neonatal AD.T model of congenital LCMV infection, and with it, we discovered three main findings. First, we demonstrated that lymphocytes are necessary for protection of the dentate gyrus, while they cause destruction in the cerebellum. Second, we found that both the virus and the immune system contribute to the neuronal migration disturbance, through a combination of altering Bergmann glial fibers, increasing the thickness of the EGL, and changing the expression of genes that govern granule cell maturation and migration. Finally, we determined that lymphocytes are necessary for the impaired coordination and hyperactivity seen in LCMV infection of the neonatal rat.

In the absence of T-cells, the hippocampal dentate gyrus rapidly atrophies, and astrocytes in the forebrain are persistently infected.

In our initial description of the Lewis rat model of congenital LCMV, we discovered that neurons of the hippocampal dentate gyrus and surrounding astrocytes were infected with virus [36]. By PD49, astrocytes had cleared LCMV, but the virus persisted in the dentate gyrus neurons. No structural pathology of the dentate was evident at that time point. By PD120, the dentate of the Lewis LCMV infected rat was significantly thinner than the control. Because the acute immune response occurs within the first three weeks of LCMV infection, while the hippocampus pathology does not arise until the fourth month, we hypothesized that the thinning of the dentate gyrus was T-cell independent.

Three different hypotheses exist regarding the mechanism of dentate gyrus loss in LCMV infection. One is that LCMV infection leads to excitotoxicity in the dentate gyrus

and, as a result, a slow loss of neurons occurs over time [233-234]. The second theory is that LCMV infection in the dentate gyrus depletes the neuroprogenitor population [235]. The dentate gyrus has a progenitor population which proliferates throughout life [236-237]. Sharma et. al. used BRDU incorporation and showed that LCMV depleted this neuroprogenitor population [235]. They suggested that dentate gyrus cells were no longer being produced and that this led to thinning of the dentate gyrus by 4 months of age. The third theory is that, after LCMV infection, astrocytes chronically express neurotoxic cytokines, such as IL-1β and TNF-α in the hippocampus which results in a gradual death of dentate granule cells [75, 238]. In support of this theory, Orr and co-workers used an adenoviral vector to suppress IL-1β expression in the hippocampus and showed a partial protection of the dentate gyrus granule cells [238].

Our adoptive transfer model provided us with an excellent tool to help determine whether or not one of the previously described theories could account for the dentate gyrus loss. Our initial characterization suggested that the dentate gyrus cell loss was not immune mediated, and therefore we expected the dentate gyrus to have similar or worse pathology in the RNU/RNU animals compared to RNU/+ and RNU/RNU+AD.T. We found that the RNU/RNU infected animal had a complete loss of their dentate gyrus, which was partially prevented by the AD.T of splenocytes. We also found that there was a greater viral burden in neurons and astrocytes of the LCMV infected RNU/RNU rat. In fact, astrocytes throughout the forebrain and hippocampus remained chronically infected as far as four months after infection.

The complete disappearance of the dentate gyrus in the RNU/RNU infected rat brings into doubt the theory that dentate gyrus pathology is secondary to a loss of neuroprogenitors. The dentate gyrus has a pool of neuroprogenitor cells that divide throughout life leading to a thickening of the dentate with age. However, the dentate gyrus is already partially formed by PD4, when animals were injected with LCMV virus [237]. Dentate cells that are already present at this point do not depend on the

neuroprogenitor population to maintain them. Hence, if death of neuroprogenitors causes the hippocampus thinning in LCMV infection then the dentate cells born before infection at PD4 should still be present in the RNU/RNU animals. However, by PD120 the RNU/RNU+ hippocampus is devoid of dentate granule cells.

The theory that excitotoxicity harms dentate granule cells is neither supported nor rejected by our findings. One can speculate that, because granule cell neurons are infected more heavily in RNU/RNU animals than in RNU/+ animals, the damaging effect of the virus itself on the cells could lead to a deregulation of the hippocampal circuit. This deregulation in GABAergic neurotransmission could lead to excitotoxicity of granule cell neurons and further disinhibition of hippocampal GABAergic cells, which could culminate in excitotoxicity [233].

Because astrocytes are persistently infected in the RNU/RNU animals, which also have the most severe pathology, our findings do support the theory that neurotoxic immune mediators produced by astrocytes have detrimental effects on dentate granule cell survival. The chronic presence of virus likely affects the immune response of infected astrocytes, inducing the release of cytokines. Therefore, our finding correlate with Orr et. al.'s suggestion that IL-1β underlies dentate granule cell death in LCMV [238].

The role of T-cells in cerebellar pathology

T-cells are necessary for destruction in the cerebellum

Previously we showed that LCMV infection led to destruction of the cerebellum and that areas of destruction correlate with areas where T-cell infiltration was greatest [36]. This was followed by the observation in chapter 3 that, in the absence of T-cells, no cerebellar destruction occurred in infected animals. In contrast, porencephalic cysts were present in RNU/+ animals. In this chapter, we have taken it one step further and demonstrated that destruction of the cerebellum occurs in RNU/RNU infected animals

after delivery of splenocytes. Taken together, these studies show that lymphocytes are necessary for cerebellar destruction in LCMV infected animals.

T-cells are necessary for viral clearance from glia and
partial clearance from neurons in the cerebellum

In chapter 3, we found that viral targets were identical in RNU/+ versus RNU/RNU animals. We also found that peak viral titers were identical in animals, regardless of the presence or absence of lymphocytes, but that viral titers fell more slowly in rats that lack T-cells. Here, we investigated the targets of virus at later time points to determine if chronic viral presence differed, depending on immune status. We found that astrocytes were persistently infected in the RNU/RNU animals, as were Purkinje cells. The fact that delivery of T-cells resulted in viral clearance from astrocytes of the RNU/RNU animals means that chronic infection of astrocytes and Purkinje cells is a function of T-cell absence and not of genotype differences.

Another important observation made in the RNU/RNU animal was that Bergmann glia and their processes remained very heavily infected, while these same cells were cleared of virus in animals with T-cells. However, in spite of infection, their cell bodies could clearly be seen in the normal histological location and their processes remained in a parallel orientation. This is significant because it suggests that persistent viral infection of Bergmann glia does not alter their orientation. This suggests that viral infection of Bergmann glia alone does not underlie the migration pathology. This will be discussed further below.

Formation of ectopic neuron clusters is T-cell dependent,
resulting from abnormal Bergmann glia fibers

Our initial characterization of the cerebellum in infected Lewis, RNU/+ and RNU/RNU animals revealed the presence of ectopic clusters of cells in the ML ([36] and chapter 5). In this present study, we confirmed that these clusters were neurons (and not

lymphocytes) and found that they were present only in T-cell competent animals. In chapter 5, we showed that Bergmann glia were altered and that granule cell differentiation was delayed, while proliferation was prolonged in LCMV infection of the Lewis genotype.

A comparison of T-cell competent LCMV infected RNU/+ and RNU/RNU AD.T animals to RNU/RNU T-cell deficient rats has provided further mechanistic details regarding the pathogenesis of the ectopic cell formations. The two primary findings here were, first that Bergmann glia fibers are pathologic in T-cell competent animals. Specifically, Bergmann glial processes retracted from the basal lamina, leaving gaps in the molecular layer where no radial glial fibers were present. These gaps corresponded to areas with ectopic cells. Another feature in T-cell competent animals was delayed differentiation of neurons in the EGL, seen by a prominent expression of TAG-1 in T-cell competent cerebella at PD18, compared to a very mild expression in the RNU/RNU infected animal and no expression in the controls. The layer of proliferative cells in the EGL was also thicker in infected T-cell competent animals compared T-cell deficient infected and compared to sham injected control animals.

Gene expression analysis of SHH showed that it was increased in LCMV infection, thus providing a mechanism for increased granule cell proliferation. SHH is a mitogen for granule cell precursors [110, 200]. Furthermore, ATOH1 expression was also increased in infected cerebellum, compared to controls. Because ATOH1 is a granule cell specific gene, changes in expression in whole cerebellum mRNA reflect gene expression exclusively for that specific cell population [195]. Increased ATOH1 expression in the infected animals means that an increase in granule cell precursor number or an increase of this transcription factor within the granule cells themselves occurs after LCMV infection. The fact that both ATOH1 and SHH expression were increased in LCMV infected animals, independent of T-cell status, suggests that SHH and ATOH1 expression are altered by the virus infection itself. However, as presented in

chapter 2, RNU/RNU animals do mount an initial T-cell independent cytokine/chemokine response. Because SHH is regulated by mediators of inflammation, such as IFN-γ [193, 199, 202], this innate immune response in RNU/RNU infected animals may participate in the regulation of SHH and/or ATOH1, and thus may be responsible for their increased expression and subsequent increase in neuronal proliferation.

An increase in ATOH1 expressing cells, seen in both RNU/+ and RNU/RNU infected animals, should correlate with an increase in immature granule cells in the cerebellum after infection of both genotypes. We did see some evidence of this through TAG-1 labeling. TAG-1 labeling was still present in RNU/RNU infected compared to control cerebella, providing evidence for a delayed differentiation of granule cells, even in the RNU/RNU infected, T-cell deficient, animals. However, we did not see a thicker layer of PCNA labeling or a thicker EGL on Nissl stain in the infected RNU/RNU animals. Taken together, although granule cell maturation may be delayed in all infected animals, Bergmann glia fiber disruption occurs only in the presence of T-cells, thus resulting in a T-cell mediated impairment of migration and a T-cell dependent thickening of the EGL.

LCMV-induced behavioral changes are T-cell dependent

The biology and pathogenesis of LCMV in congenital infection is very interesting on the histological level, but ultimately, the clinical importance is revealed by how it affects behavior. In our first characterization of behavior, in chapter 4, we looked only at T-cell competent Lewis animals and discovered a mild hyperactivity and a severe coordination deficit. Here, we used animals of different immune status and discovered that hyperactivity and impaired coordination occurred only in T-cell competent animals. Therefore, the presence of T-cells is necessary for the development of hyperactivity and coordination impairments after infection with LCMV.

Figure 30 Flow cytometry for CD8+, CD4+, CD161+ (NK) and CD45ra cells (B-cells). The different colors represent different cell populations selected in the encircled region in each square. The purple is CD8+CD3+, the orange is CD4+CD3+, the dark blue is CD161+CD3- and the green are cells that were not found in either of the two CD8+CD3+ or CD4+CD8+. Flow cytometry revealed the absence of CD8+ and CD4+ cells in the RNU/RNU rat brain (B), compared to the presence of CD8+ and CD4+ cells in the RNU/+ animal (A). Adoptive transfer reconstituted the immune system and returned CD8+ and CD4+ cells to the RNU/RNU brain (C). CD161+CD3- cells were present in all genotypes. n=3

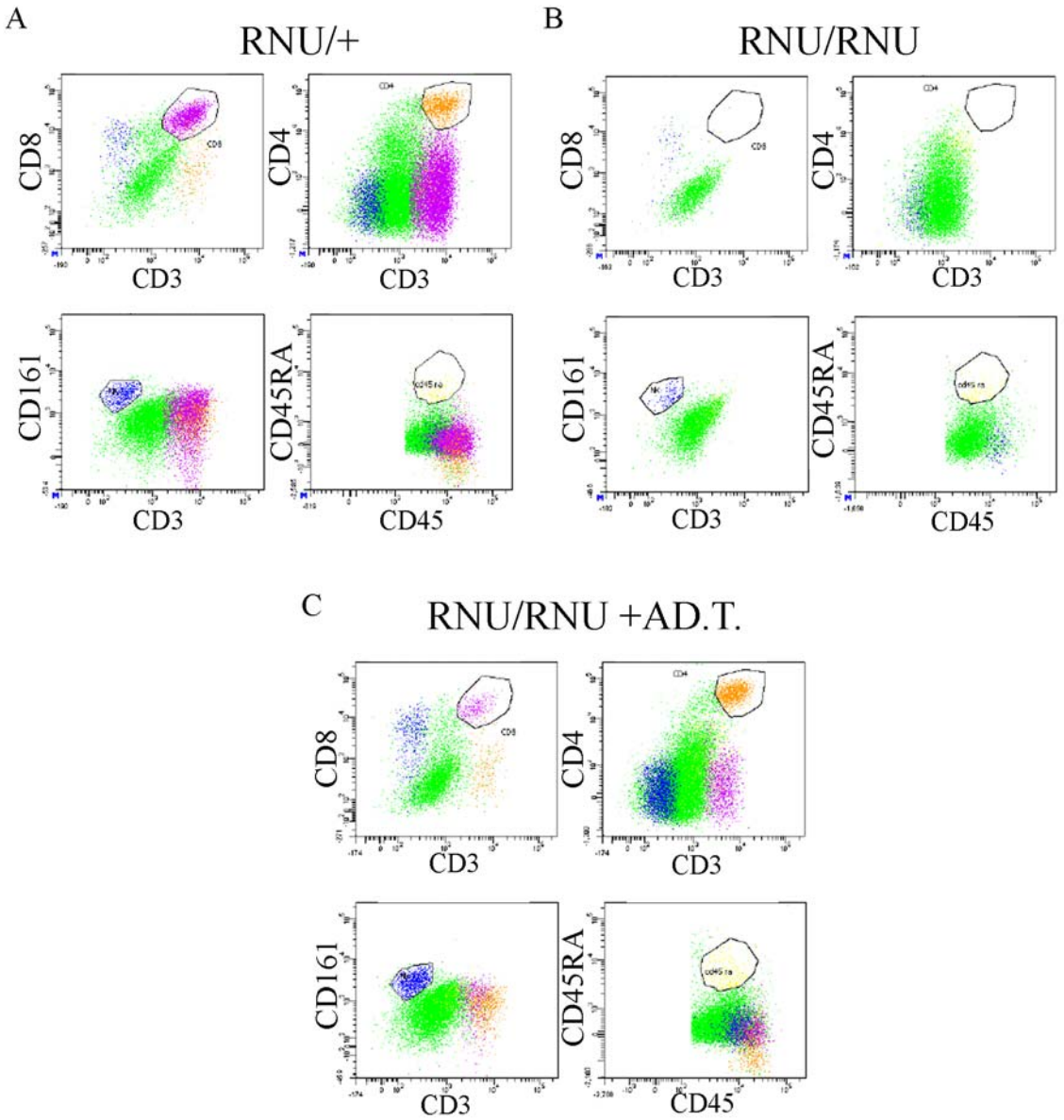

Figure 31 Cerebellar hypoplasia in LCMV infected RNU/RNU animals with and without T-cells: The top panel shows gross pathology for RNU/RNU control (a) RNU/RNU LCMV (b) and RNU/RNU AD.T (c). The middle panel shows cross sections at the microscope level for the above genotypes. The bottom row is a graph of cerebellum to hemisphere weight ratio. A significant hypoplasia by gross pathology, microscopic pathology and a 58% reduction in cerebellum/hemisphere ratio for RNU/RNU + AD.T and 34% reduction for RNU/RNU weight is evident in both infected RNU/RNU animals ($P<.001$, $P<.001$) (N=6 controls, N=6 LCMV, N=8 LCMV +AD.T). This hypoplasia reached a significance of $P<.001$ for brain weights for RNU/RNU animals with and without T-cells. The RNU/RNU + AD.T also has porencephalic destructive lesions arrow (c) and arrow (f). The RNU/RNU LCMV + AD.T is representative of the pathology seen in the RNU/+ animals. (G) shows that RNU/+ animal infected with LCMV a 42% decrees in cerebellum/hemisphere weight $P<.0001$ (g) (n=9 control, n=10 LCMV). Magnification bar is 1mm. n=6 RNU/RNU control, n=7 RNU/RNU infected, n=8 RNU/RNU AD.T., n=8 RNU/+ control, n=8 RNU+ infected,

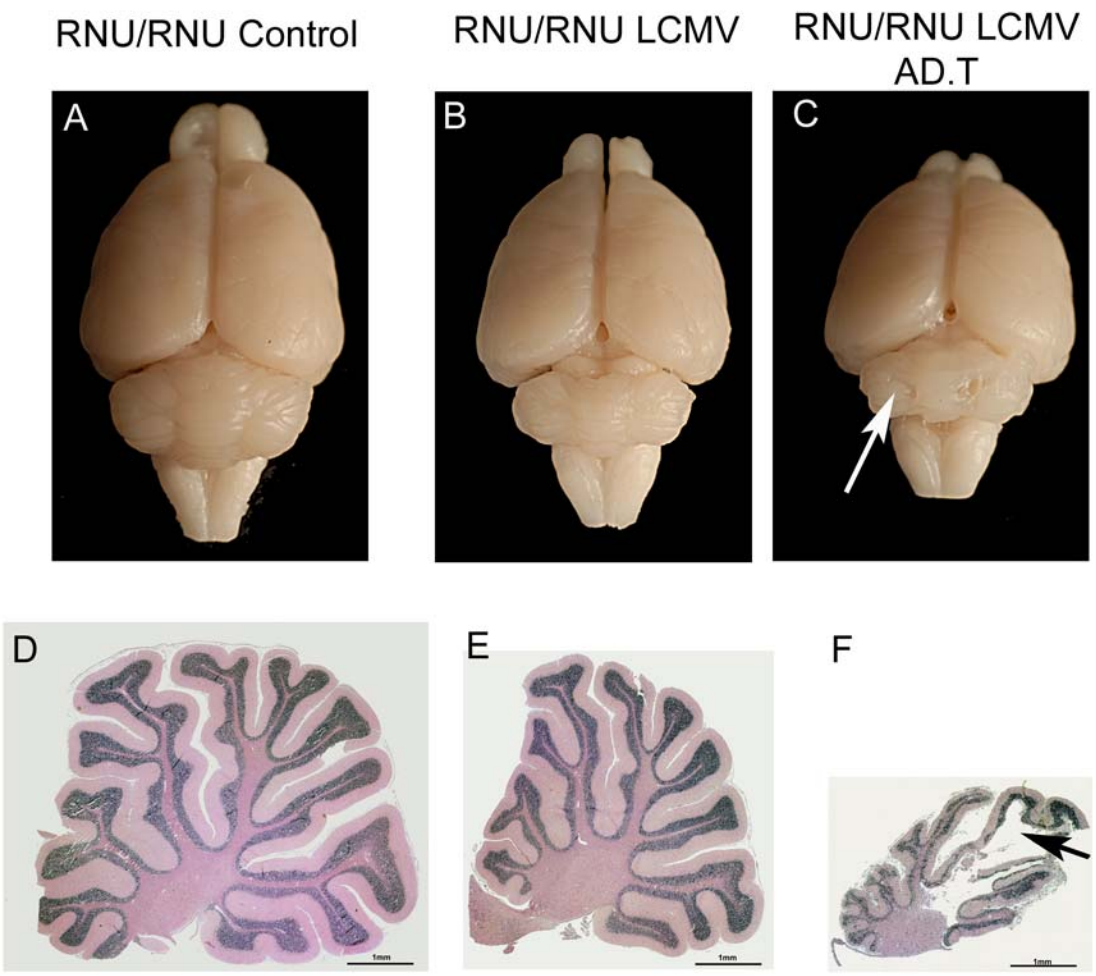
RNU/RNU Control
RNU/RNU LCMV
RNU/RNU LCMV AD.T
A
B
C
D
E
F
G
Cerebellum/Hemisphere Ratio
Cerebellum weight (mg) / hemisphere weight (mg)
0.3
0.2
0.1
0.0
*
*
*
*
RNU/+ Control
RNU/+ LCMV
RNU/RNU Control
RNU/RNU LCMV
RNU/RNU LCMV AD.T
Animal Group

Figure 32 LCMV antigen in PD40 Cerebellum: In this Figure, LCMV virus was identified using an antibody against LCMV. This Figure shows that LCMV virus is cleared from astrocytes in RNU/+ and RNU/RNU animals receiving AD.T compared to RNU/RNU T-cell deficient animals. The top row of the Figures is taken from the molecular layer of dorsal lobe 5 and the bottom row is taken in the inner lobule white matter of dorsal lobe 5. The most salient feature is the absence of LCMV presence in the inner white matter (black arrowhead D,E) of the T-cell competent animals compared to a persistent infection of astrocytes in the inner white matter of RNU/RNU infected cerebella (black arrowhead F). Other observations are that the AD.T animal has far fewer antigen positive cells than the RNU/RNU infected animal. Cell types infected in T-cell competent vs. deficient animals also differ. The RNU/RNU infected animal has a heavy viral burden in astrocyte-like cells in the molecular layer (white arrowhead C), compared to only a few LCMV positive cells in the ML of T-cell competent cerebella (white arrowhead A, B). Purkinje cells (black arrows) and IGL cells (white arrows) are also uniformly infected in the RNU/RNU infected animals (C, F) compared to a more sparse labeling of Purkinje cells the RNU/+ (black arrow A and D) and absolutely no Purkinje cell labeling in the AD.T animal (B, E). Magnification bar is 100um. n=2

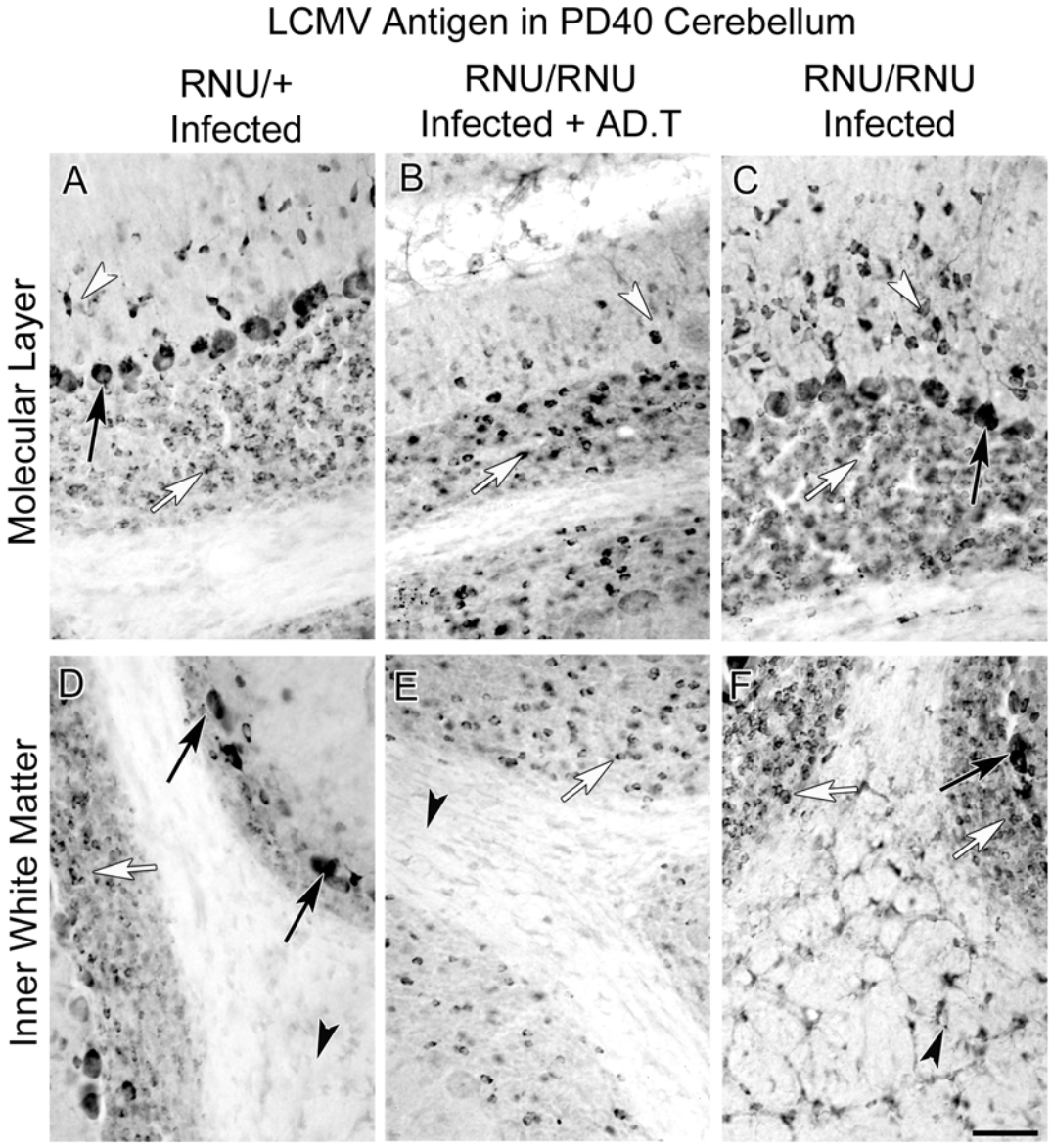
LCMV Antigen in PD40 Cerebellum
RNU/+
Infected
RNU/RNU
Infected + AD.T
RNU/RNU
Infected
Molecular Layer
Inner White Matter
A
B
C
D
E
F

Figure 33 LCMV antigen in the cerebellum at PD120: Genotype is arranged in columns and each row is a different region of the cerebellum. The first column shows RNU/+ LCMV infected cerebella, the second shows RNU/RNU LCMV and the third shows RNU/RNU LCMV + AD.T. In both RNU/+ and RNU/RNU AD.T animals, LCMV is present in some, but not all granule cells (white arrowheads). Sparse Purkinje cells remained infected in the RNU/+ animals (black arrow), no antigen is seen in Purkinje cells of the RNU/RNU with AD.T cerebellum. In contrast, RNU/RNU LCMV infected animals deficient in T-cells have very dark labeling for viral antigen in Purkinje cells (black arrows) and Purkinje cell processes. Purkinje cell processes are infected only in T-cell deficient animals. Bergmann glia (black arrowhead C) and astrocytes in the inner white matter (black arrowhead F) remain infected only in T-cell deficient RNU/RNU animals. In contrast, there are no infected astrocytes in the white matter (black arrowhead D, E) of the T-cell competent RNU/+ and RNU/RNU AD.T rat cerebella. Magnification bar is 100um. n=2

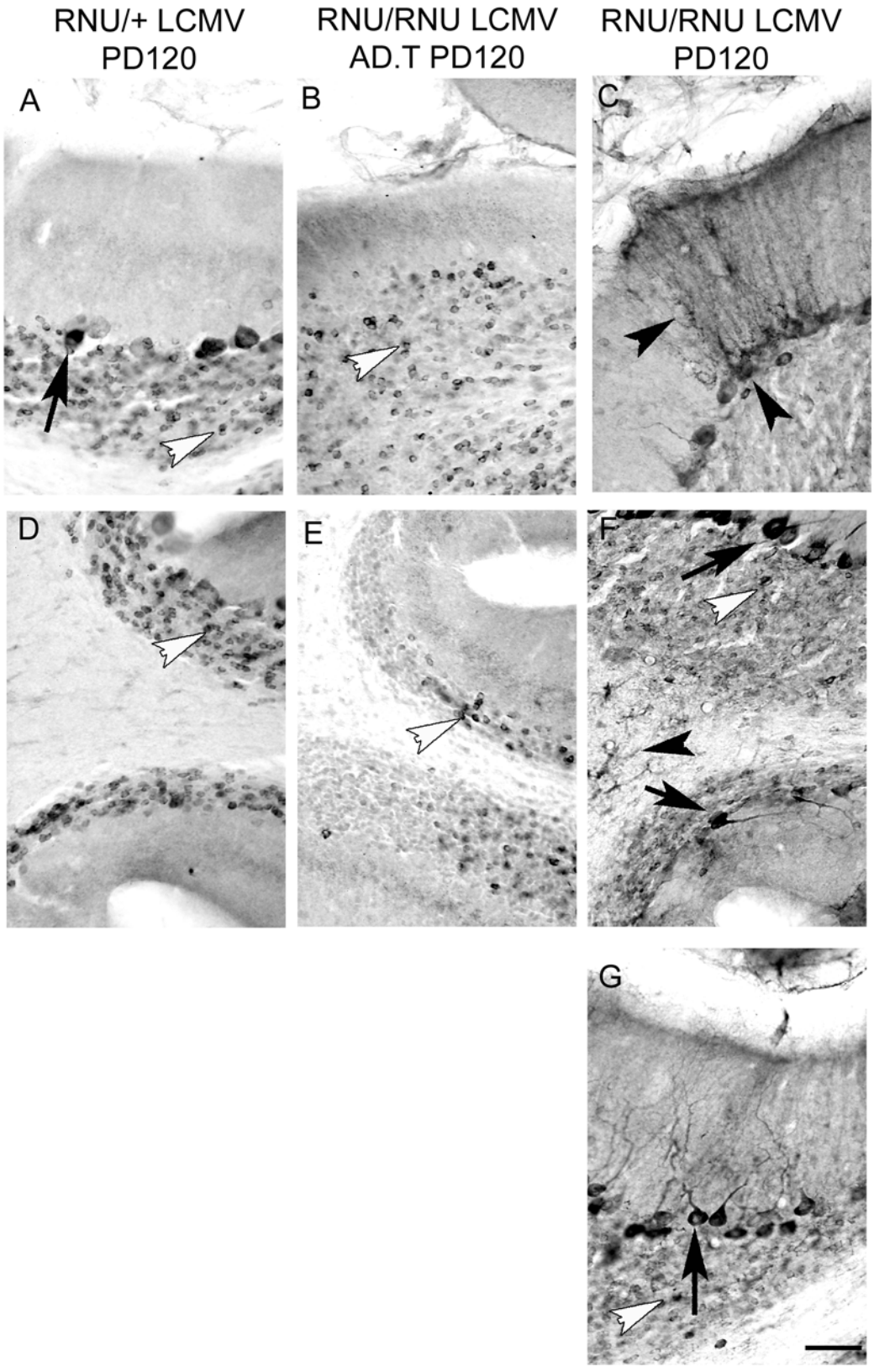
RNU/+ LCMV
PD120
RNU/RNU LCMV
AD.T PD120
RNU/RNU LCMV
PD120
A
B
C
D
E
F
G

Figure 34 Pathology in the hippocampus of T-cell competent and T-cell deficient animals at PD40 and PD120: The top two rows of this Figure are a low magnification and high magnification of PD40 RNU/RNU animals. Figure A shows the hippocampus of a control animal, B is the hippocampus of an RNU/RNU LCMV animal receiving the adoptive transfer, and C is the RNU/RNU LCMV, T-cell deficient animal. The hippocampus dentate gyrus (arrow) is very similar in thickness for both the RNU/RNU control (A) and RNU/RNU LCMV AD.T animal (B), but is noticeably reduced in thickness in the RNU/RNU LCMV T-cell deficient animal. Figure D-F are the same treatment groups but at PD120. The dentate gyrus is thinner in the RNU/RNU LCMV AD.T animals (arrow, E) than the control animal (arrow, D). A striking disappearance of the dentate granule cells occurs in the RNU/RNU LCMV T-cell deficient animal (arrow, F) Magnification bar for A-C and C-E is 500um, and 50um for the higher magnification pictures. n=2

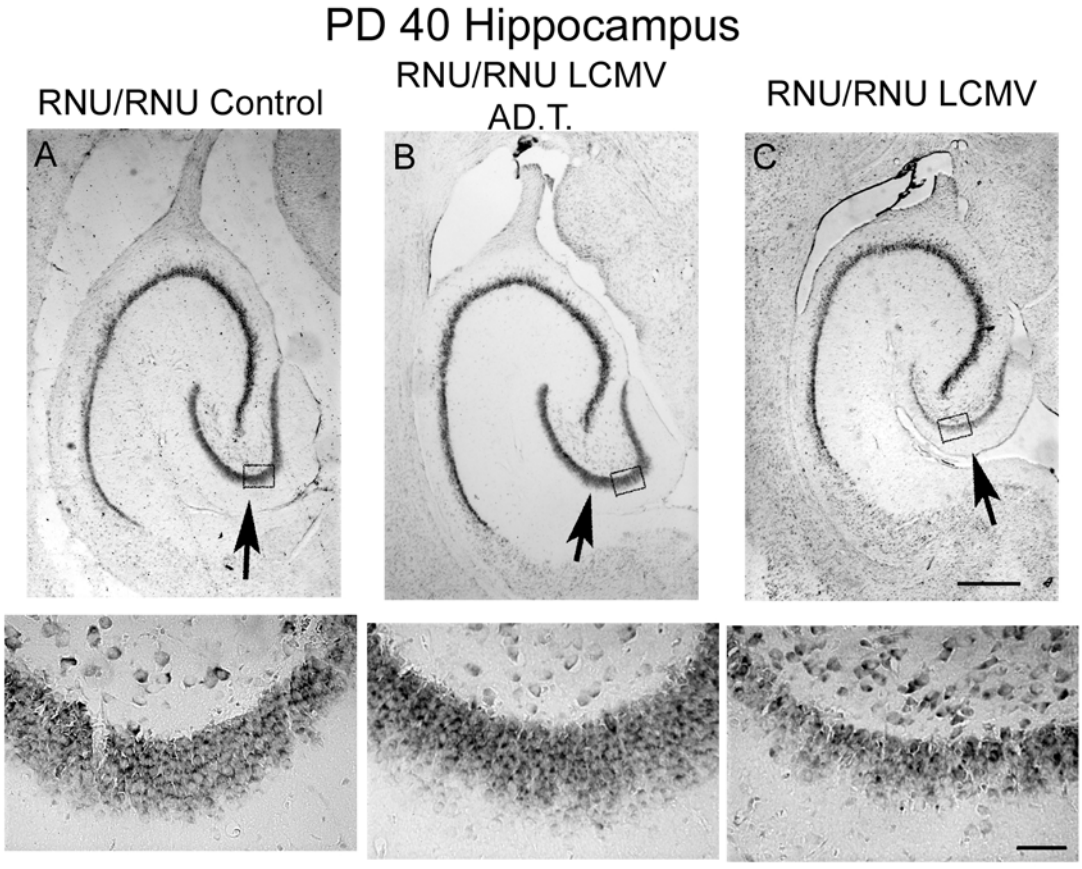
PD 40 Hippocampus
RNU/RNU Control
RNU/RNU LCMV AD.T.
RNU/RNU LCMV
A
B
C
PD 120 Hippocampus
RNU/RNU Control
RNU/RNU LCMV AD.T.
RNU/RNU LCMV
D
E
F

Figure 35 Labeling of the infected forebrain from T-cell deficient and T-cell competent animals reveals that T-cells are necessary for the clearance of astrocytes and neurons. The first column shows the anti-LCMV labeling in RNU/RNU LCMV animals who received the adoptive transfer, the second column is the hippocampus from a T-cell deficient RNU/RNU rat. The third column is a higher magnification of the second column. Virus was present only in the hippocampus region of the T-cell deficient animal. At PD40, virus was located in the dentate granule neurons (arrow C) and astrocytes (arrowhead, B). At PD120 no virus was found in the T-cell competent RNU/RNU AD.T animal (D), compared to widespread viral infection of astrocytes in the RNU/RNU rat. Viral antigen is particularly concentrated in the region surrounding the dentate gyrus (Arrow E). Higher magnification of regions in E show that labeled cells have the morphology of astrocytes (arrows F). Magnification bar for C and F is 50um. Magnification bar for A, B, D, E is 500um. n=2

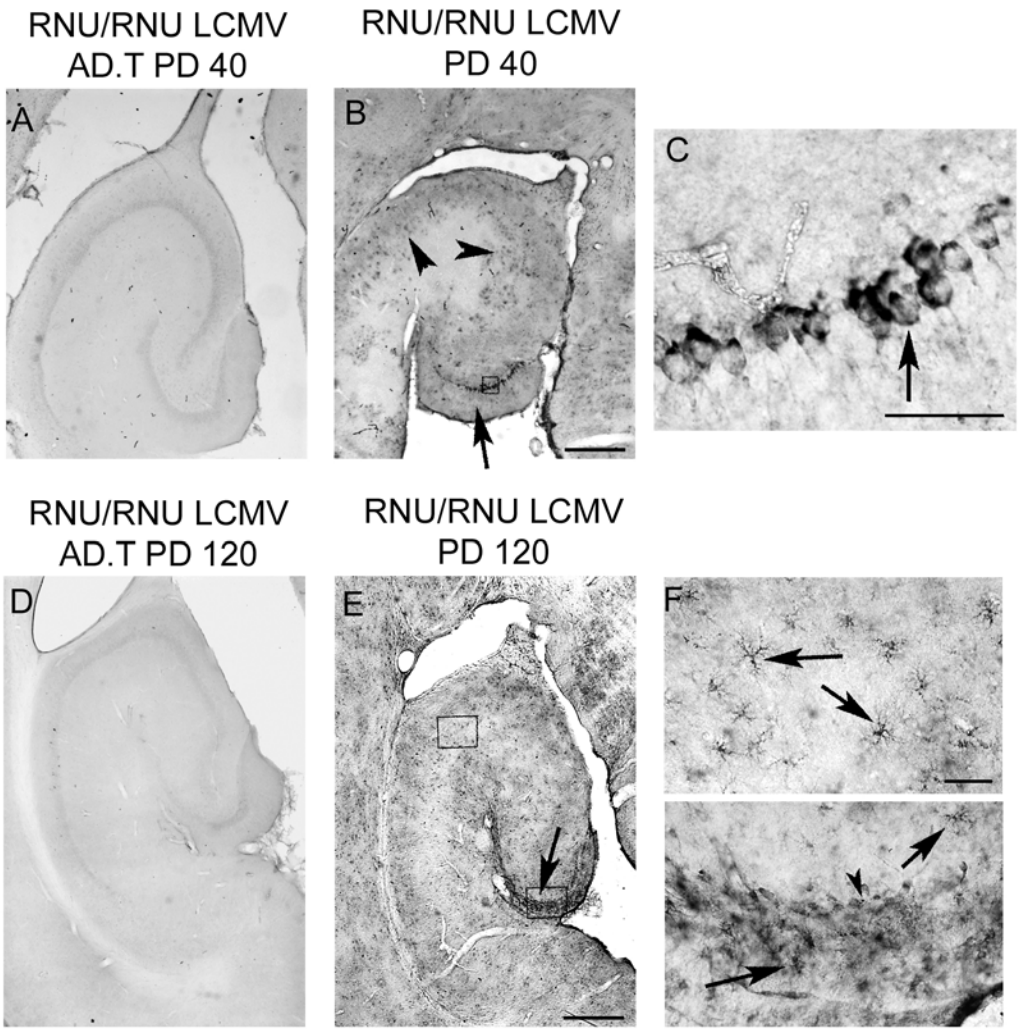
RNU/RNU LCMV
AD.T PD 40
RNU/RNU LCMV
PD 40
A
B
C
RNU/RNU LCMV
AD.T PD 120
RNU/RNU LCMV
PD 120
D
E
F

Figure 36 GFAP and NeuN labeling in the cerebellum of T-cell competent and T-cell deficient animals: NeuN labeling, in red, shows the presence of ectopic neurons in T-cell competent animals (arrows F) and not in the RNU/RNU control (arrows pointing at EGL D) or the RNU/RNU T-cell deficient animal (arrows pointing at EGL E). These ectopic neurons correspond to regions where Bergmann glia parallel fibers are disrupted (arrowhead in C). GFAP labeling reveals the presence of reactive gliosis and astrocyte cell bodies in the molecular layer of both LCMV infected animals (arrows in B and C). There are no astrocyte cell bodies in the ML of the control cerebellum (A). Despite the presence of reactive astrocytes in RNU/RNU LCMV animals, Bergmann glia parallel fibers maintain a regular pattern of parallel orientation (arrowhead B), and no large gaps in parallel fiber structure are seen, in contrast to those seen in the T-cell competent animal (arrowhead C). Magnification bar is 100um. n=3 or more

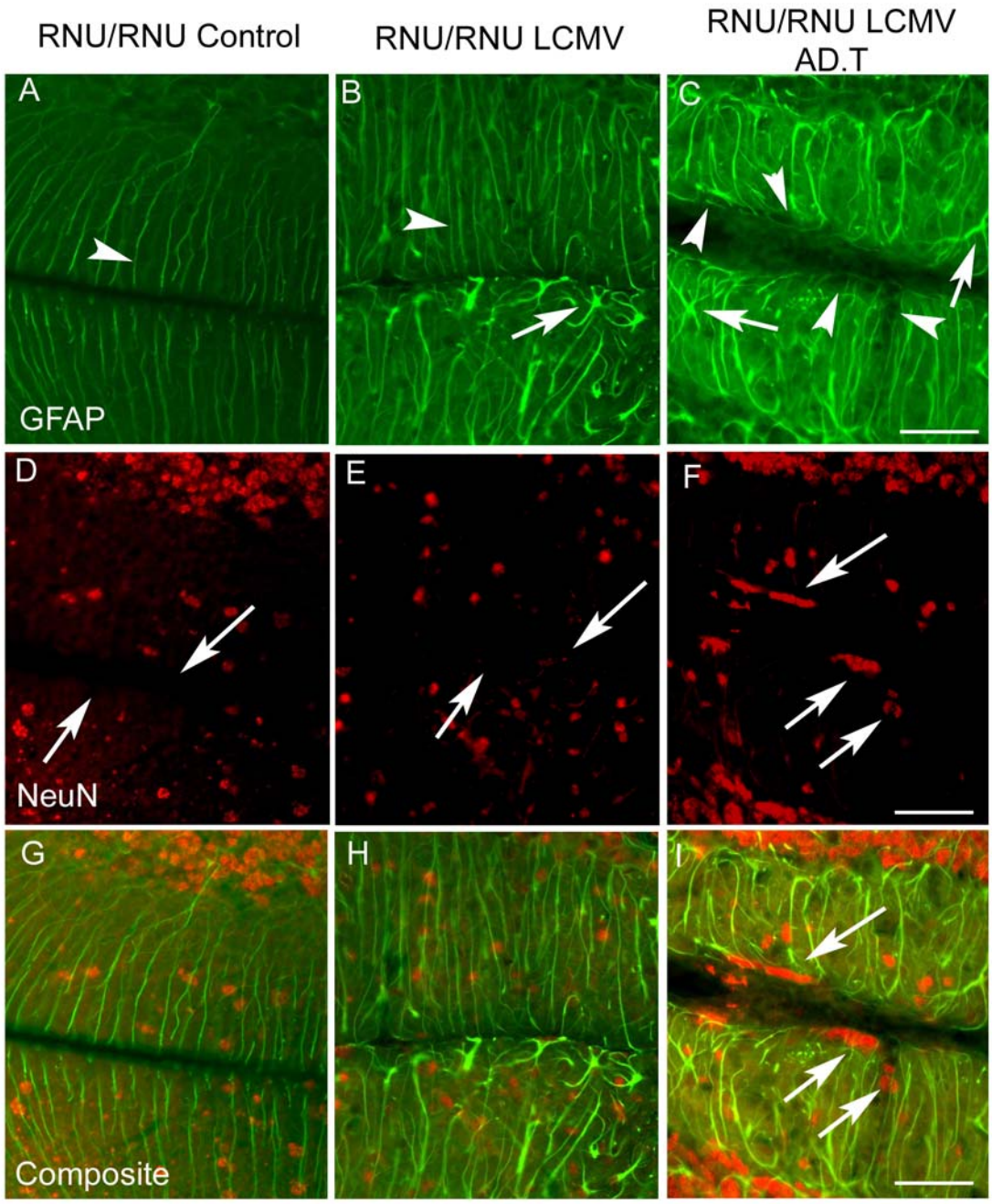
RNU/RNU Control
RNU/RNU LCMV
RNU/RNU LCMV AD.T
A
B
C
GFAP
D
E
F
NeuN
G
H
I
Composite

Figure 37 TAG1 and TUJ1 labeling in the cerebellum of PD18 T-cell competent and T-cell deficient RNU/RNU animals: The first column is RNU/RNU non-infected sham injected control cerebellum, the second column is RNU/RNU LCMV, and the third column is RNU/RNU LCMV with AD.T. TUJ1 labeling, shown in the top row, is different in each treatment group. A bright layer of TUJ1 labeled cells is present in all genotypes representing the condensed cell bodies of the granule cells in the EGL (arrows). A much thickening layer of TUJ1 labeled cells is present in the RNU/RNU LCMV AD.T animal (arrow C) Purkinje cell bodies and dendrites are clearly labeled with TUJ1 in the control (arrowhead A) and dimly labeled in RNU/RNU LCMV with and without ADT (arrowhead B and C). The second row shows TAG1 labeling, red, in the three treatment groups. There are no TAG1 positive cells in the control, only a thin layer of TAG1 positive cells in RNU/RNU LCMV animals (arrows in E) and a thick layer of TAG1 positive cells in the RNU/RNU AD.T EGL (arrows F). A composite of TAG1 and TUJ1 shows that TUJ1 positive cells are in the inner EGL (lower arrow I) while TAG1 expression is in the inner and outer layer (upper arrow I). TAG1 is a marker expressed earlier in granule cell maturation, and TUJ1 is expressed in all differentiated neurons. The thicker TAG1 and TUJ1 labeling in the AD.T animal is evidence for an increase in EGL thickness and a delayed maturation of neurons in the presence of T-cells. Magnification bar is 100um. n=2

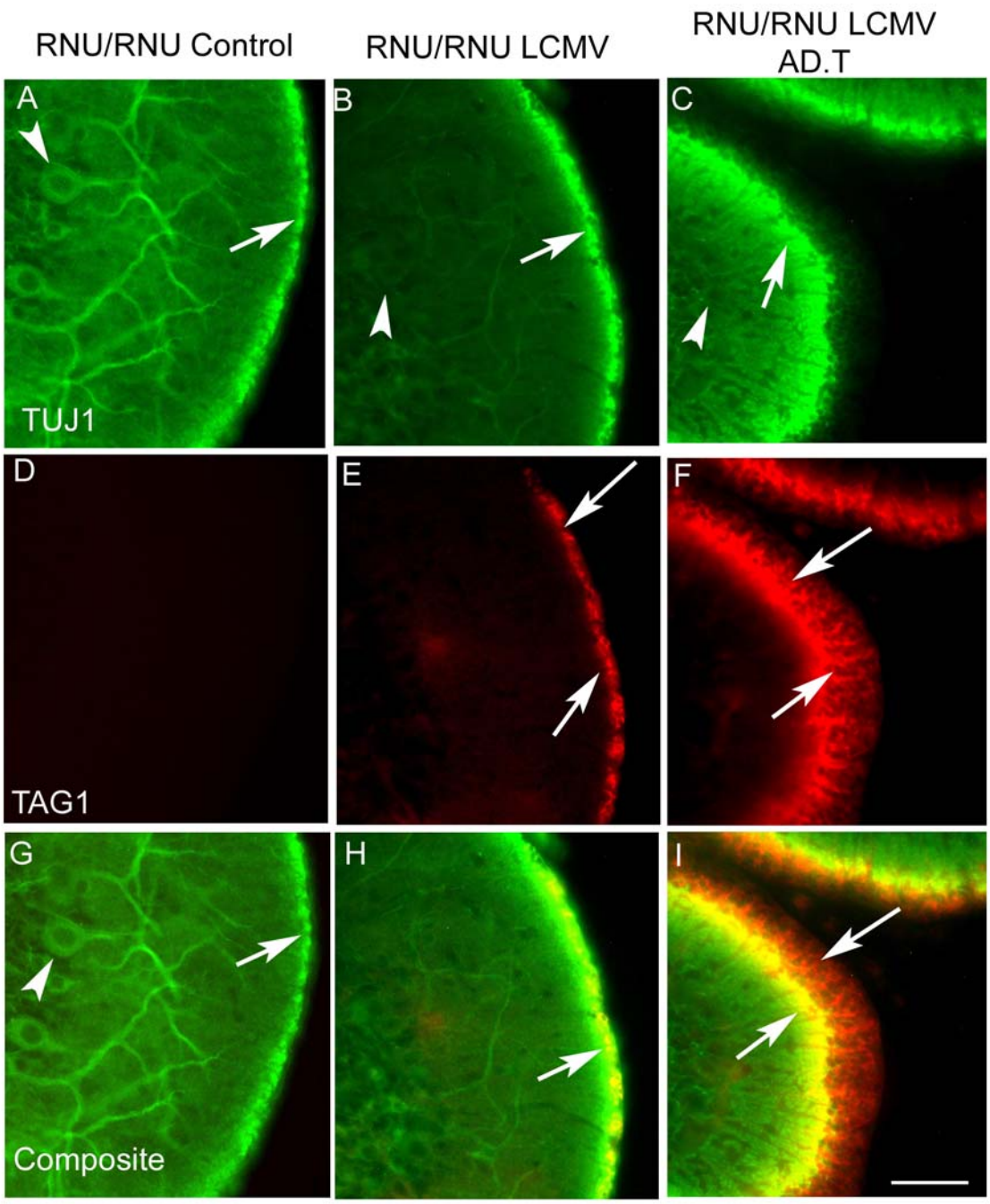
RNU/RNU Control
RNU/RNU LCMV
RNU/RNU LCMV AD.T
A
B
C
TUJ1
D
E
F
TAG1
G
H
I
Composite

Figure 38 PCNA labeling of proliferating cells in T-cell competent and deficient cerebella: In this Figure, proliferating cells were identified in the cerebella of PD18 control RNU/+ and RNU/RNU compared to T-cell competent and T-cell deficient RNU/+ and RNU/RNU rats by using an antibody for proliferating cell nuclear antigen (PCNA). The top row compares control and T-cell deficient and T-cell competent RNU/RNU rats and the bottom row compares RNU/+ control to RNU/+ LCMV cerebellum. PCNA labeling revealed a thicker layer of proliferating cells in the T-cell competent LCMV infected animals (C, E) compared to both the LCMV infected T-cell deficient RNU/RNU animal (B) and control rats from both genotypes (A, D). Magnification bar is 50um. n=3

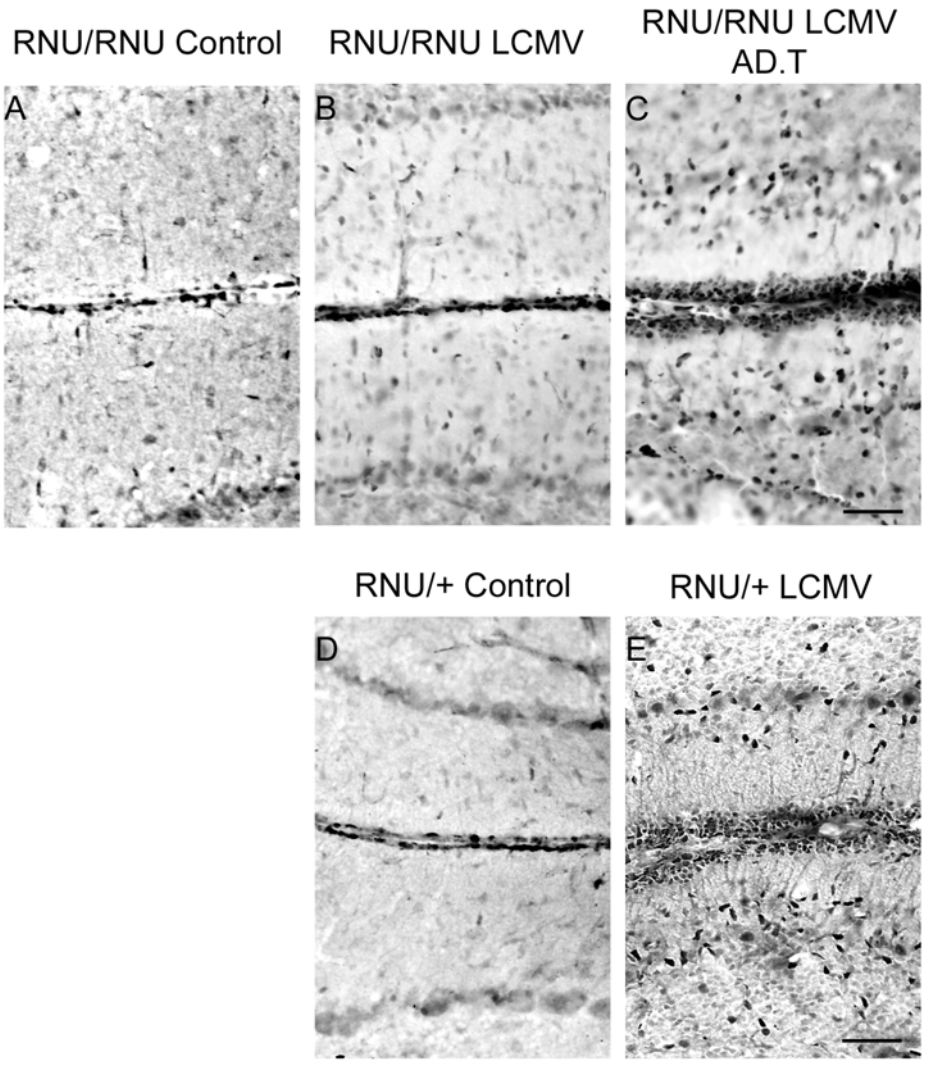

Figure 39 SHH and ATOH1 expression in the cerebella of infected and control RNU/+ and RNU/RNU animals: 1a. SHH expression, at PD14 RNU/RNU infected and RNU/+ infected Shh expression was 48% and 45% higher than control ($P<.04$, $P<.005$). There were no significant changes at the other time points. 1b. ATOH1 expression. At PD14 Atoh1 expression is 12 times higher in RNU/+ and 5 times higher in RNU/RNU infected over control ($P<.009$, $P<.05$). ATOH1 expression was also elevated at PD 18 and PD25 but did not reach significance. n=3 or more

A

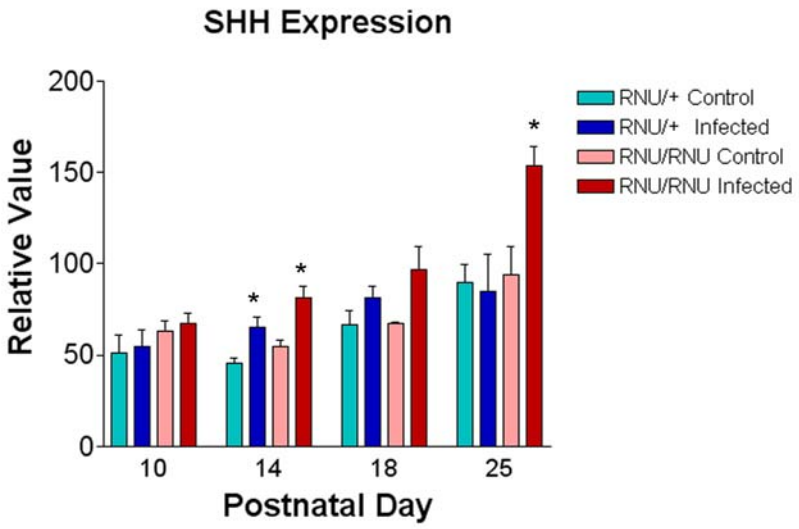
SHH Expression
Relative Value
200
150
100
50
0
10
14
18
25
Postnatal Day
RNU/+ Control
RNU/+ Infected
RNU/RNU Control
RNU/RNU Infected
*
*
*

B

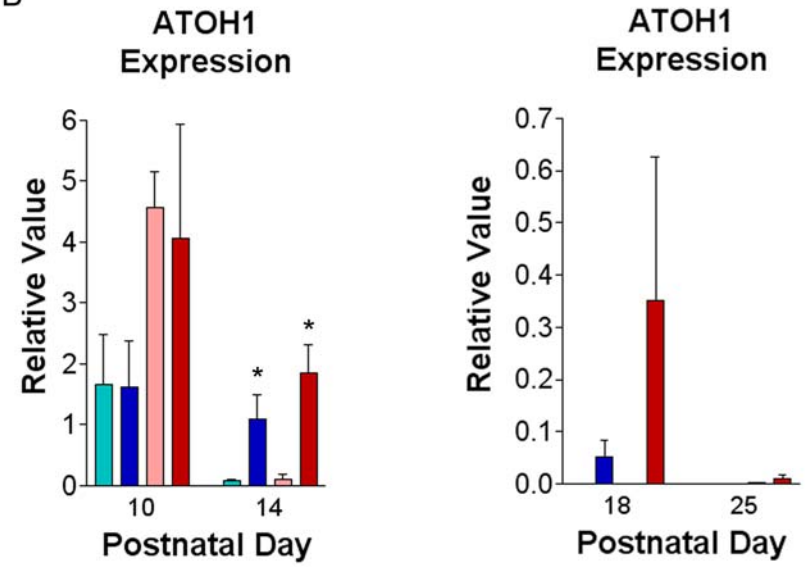
ATOH1
Expression
Relative Value
6
5
4
3
2
1
0
10
14
Postnatal Day
*
*
ATOH1
Expression
Relative Value
0.7
0.6
0.5
0.4
0.3
0.2
0.1
0.0
18
25
Postnatal Day

Figure 40 Measures of Balance and activity in T-cell competent and T-cell deficient animals: a. This graph shows the time it took animals to cross square or rod beams of various sizes. The infected animals with intact immune systems were impaired on this task. There were no significant differences for the largest sq beam. RNU/RNU+ AD.T was significantly impaired compared to control med sq, sm sq, lrg rod, med rod and sm rod (respective to all rod $P<.0001$). It was also significantly impaired compared to RNU/RNU LCMV group ($P<.012$ for med square and $P<.0001$ for the other beams) (RNU/+ control N=8, RNU/+ LCMV N=10, RNU/RNU control N=7, RNU/RNU LCMV N=7, RNU/RNU AD.T N=10). The RNU/+ animal group was impaired on the med rod and sm rod but this did not reach significance with the Bonferroni post hoc for multiple comparisons, it was significant using the LSD post hoc ($P<.04$). b. This graph shows the total crosses made over a grid on the open field apparatus. Crosses over the 30min period were totaled and graphed by genotype and treatment. LCMV infected rats with T-cells had significantly higher line crosses when compared to control and LCMV infected animas without T-cells. The following P values were, RNU/+ LCMV vs. RNU/+ control ($P<.006$), RNU/+ vs. RNU/RNU LCMV ($P<.005$), RNU/RNU AD.T vs. RNU/RNU control and vs. RNU/RNU LCMV ($P<.0001$). There was no significant difference between RNU/RNU LCMV infected and control group ($P=1$). n= 7 or more for each group

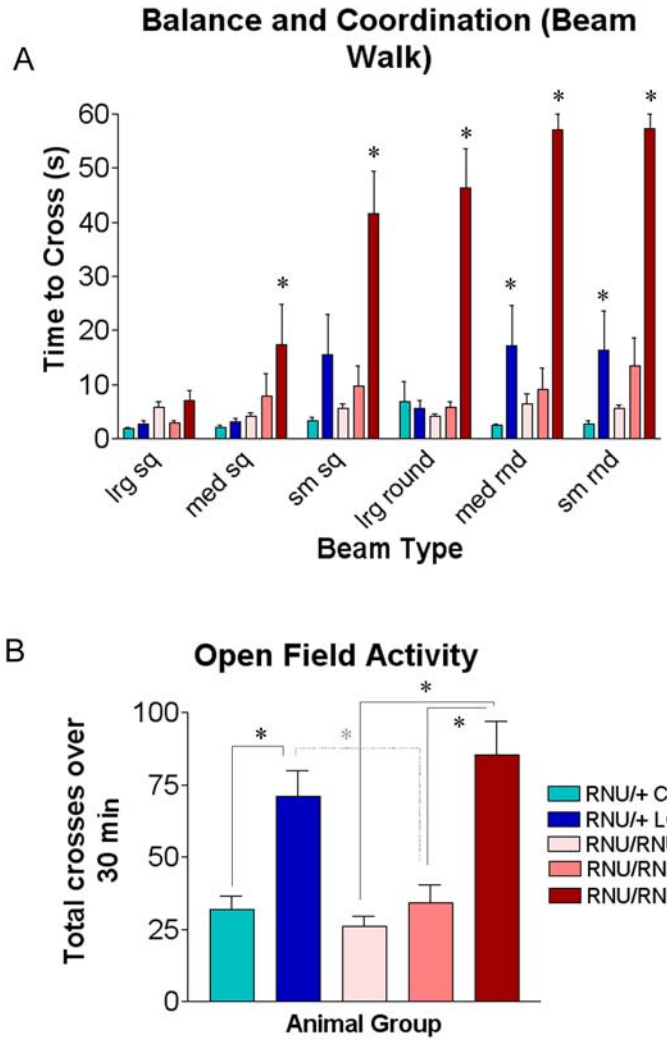
A
Balance and Coordination (Beam Walk)
Time to Cross (s)
60
50
40
30
20
10
0
lrg sq
med sq
sm sq
lrg round
med rnd
sm rnd
Beam Type
B
Open Field Activity
Total crosses over 30 min
100
75
50
25
0
Animal Group
RNU/+ Control
RNU/+ LCMV
RNU/RNU Control
RNU/RNU LCMV
RNU/RNU LCMV AD.T

CHAPTER 6: DISCUSSION

General Discussion

Prior to the work presented in these chapters, the following major questions existed in the field of congenital LCMV research. First, why does a different immune response and destructive pathology occur in some brain regions compared to others? Second, what aspects of LCMV pathology are T-cell dependent vs. T-cell independent? And finally, by what mechanism does LCMV infection lead to altered neuronal migration in the cerebellum?

In our research, we have discovered that the immune response is very important in inducing LCMV pathology. The immune response mediates different pathological consequences in different brain regions, including causing cerebellum destruction and neuronal migration abnormalities. The role of the immune system in pathology is an important research question because it is clinically relevant and may be a target for future pharmaceutical intervention. Furthermore, the role that the immune response plays in inducing brain disease after LCMV infection is an important research area because it is applicable to a broad range of pathogens and inflammatory insults. Activation of the immune system during pregnancy has been associated with many developmental disorders such as low IQ, autism, and schizophrenia [239-244]. As mentioned in the intro, Erickson et. al. recently reported that a cohort of military age men born in the year following a large flu epidemic had lower IQ ratings than men born the year before or the year after [239].

Additional evidence suggesting a central role of the immune system in inducing developmental brain disorders can be seen by looking at the cerebellar pathology that results in animals neonatally infected with a range of pathogens. Cerebellar pathology has been described in many different neonatal/congenital infections including Tamiami virus, Borna virus and toxoplasmosis in the mouse, parvovirus infection in the hamster

and cat, Fowl glioma inducing virus in the chicken, feline panleukopenia virus in kittens, Akabane Bunyviridae virus in calves, bovine virus diarrhea virus (BVDV) in pigs, hog cholera virus in hogs, and the virus that causes shaking mink syndrome in mink [214-217, 245-248]. Not all of these viruses target the same neuronal population in the brain. Some are cytolytic, like parvovirus [214], while others, such as Borna virus and Tamiami virus are non-cytolytic [217, 249]. Toxoplasmosis gondii is very different because it is a protozoa and because cerebellar migration abnormalities in the rat cerebellum occur even in the absence of its physical presence in the cerebellum [215].

Further evidence that the immune system can damage the cerebellum, even in the absence of a pathogen, comes from graft-verses-host disease in the rat [250]. This was discovered by transplanting a cell-graft to pregnant rats which led to a systemic immune response. Analysis of the rat pups found a cerebellar hypoplasia that was not caused by nutritional deprivation but by the cell-graft treatment itself. The link between viral- or parasite- induced cerebellar pathology across species and the cerebellar pathology seen in the case of graft-versus-host disease, is the immune response. Therefore, activation of the immune response during development may have an underestimated impact on brain development and pathology.

The main findings from this work provide important evidence for the role of the immune system in both protection against damage in the hippocampus, while destruction and interference with migration in the cerebellum. These will be discussed below.

A Differential Immune Response Occurs by Brain Region and is Partially Astrocyte Derived

The first key question we addressed was, why do brain regions with equally high viral titters, have different strength of immune response and different brain pathology? To address this question, first, we explored whether there was a higher cytokine and chemokine response in some brain regions compared to others. We found that the

cerebellum and olfactory bulbs, which are regions that undergo destruction, have higher expression of all cytokines and chemokines when compared to the septum and the hippocampus. To determine if a difference in astrocyte response underlies the difference in subsequent lymphocyte recruitment, we used astrocyte cultures and found that cerebellum astrocytes mount a stronger cytokine and chemokine response after infection compared to hippocampus astrocytes. To compare the cytokines expressed in-vitro to the T-cell independent expression of cytokines in vitro, we compared cytokine expression in the T-cell impaired RNU/RNU animal to T-cell competent animals. The high expression of TNF-α, CCL2, CCL5, and CXCL10 in both cerebellum astrocyte cultures and in T-cell deficient RNU/RNU animals is evidence that these cytokines have a non-T cell source in-vivo and that astrocytes are a likely source of cytokine and chemokine expression after LCMV infection. These particular cytokines were expressed early and in a T-cell independent manner and therefore may be important for lymphocyte recruitment. The stronger expression seen in the cerebellum, compared to the hippocampus and septum supports a role of regional differences of cytokine and chemokine expression in subsequent differences in lymphocyte recruitment by brain region.

During this part of our study, we also quantified lymphocyte infiltration and proportions of lymphocyte subtypes in different brain regions. We found that lymphocytes were recruited up to 50 fold higher in the cerebellum than in the other brain regions. The proportion of each lymphocyte population was similar in each brain region. At PD 18, which is the time point when cerebellar lesions begin to appear, natural killer lymphocytes were significantly higher in quantity in the dorsal cerebellum compared to all other regions. This is of particular interest because natural killer cells have cytotoxic properties, and are especially important in the clearance of noncytolytic virus [69]. The higher presence of NK cells at PD18 correlates with a time point when cerebellar damage is first observed. Determining if natural killer cells are necessary for the development of

cerebellar lesion in the rat model of congenital LCMV is one potential area of future study.

One alternative explanation for a higher lymphocyte infiltration in the cerebellum, compared to the other brain regions, is that the blood brain barrier is weaker in the cerebellum compared to other regions. Brain infections by different viruses including LCMV lead to breakdown in vessel integrity and weaken the BBB [251]. Break down of the blood brain barrier can facilitate lymphocyte infiltration into the brain [76, 251]. Whether this occurs uniformly throughout the brain, or differs regionally has not been studied for LCMV infection. Studies in other virus infections have found regional differences in BBB integrity correlating with brain pathology [252]. Cytokines influence BBB integrity. Here, we determined that a regional difference in cytokine and chemokine expression occur after LCMV infection. Therefore, cytokine induced weakness of the BBB is a possible mechanism leading to more BBB disruption and higher subsequent lymphocyte infiltration in the cerebellum compared to the hippocampus.

What Aspects of LCMV Damage are T-cell Dependent?

The next major question in congenital LCMV was what pathology is secondary to the damaging affects of T-cells? More specifically, what role do T-cells play in the cerebellum hypoplasia, cerebellum destruction, and hippocampus loss of dentate gyrus cells? To answer this question, we started by comparing T-cell competent RNU/+ rats to their athymic littermates which were deficient of thymus derived T-cell. During the process of studying differences between these genotypes, we developed an adoptive transfer model, allowing us to return T-cells to athymic RNU/RNU rats.

From this study, we discovered three major findings. First, T-cells play a protective role against LCMV induced injury in the hippocampus but a damaging role in the cerebellum. Second, infected brain cells, including astrocytes and neurons, are unable

to clear LCMV virus in the absence of T-cells. And third, in the absence of T-cells, LCMV infection causes cerebellar hypoplasia.

To expand on this, we found that, in the absence of T-cells, granule cells of the hippocampal dentate gyrus were completely lost. When T-cells were delivered to athymic RNU/RNU animals early in the infection, only a moderate dentate gyrus thinning resulted. Therefore, T-cells play a protective role. Possible mechanisms of dentate granule cell loss were discussed in chapter 5. One likely candidate is that chronically infected astrocytes secrete harmful cytokines which are neurotoxic. In the absence of T-cells, astrocytes in the hippocampus are chronically infected. We showed in chapter 1 that cultured cerebellum astrocytes express high levels of TNF-α and moderate levels of IL-1β after infection with LCMV, both of which have neurotoxic properties [131-132, 253]. Orr and colleagues reported that astrocytes near the hippocampus dentate gyrus in LCMV infected Lewis rats immunohistochemically label for anti-IL-1β [238]. Furthermore, they found that inhibition of IL-1β expression, through an adenoviral delivery of IL-1ra, rescued the dentate gyrus loss. Therefore, dentate granule cells loss is subsequent to an increase in cytokine expression. In the case of RNU/RNU rats, astrocytes are persistently infected with LCMV. Thus, cytokine expression in RNU/RNU animals is likely prolonged, therefore resulting in higher exposure of dentate neurons to the neurotoxic cytokines, thus accounting for the gradual and complete disappearance of dentate granule cell neurons.

In contrast to a protective role in the hippocampus, T-cells lead to a destruction of the cerebellum. Destructive pathology in the cerebellum was only seen in animals with T-cells. Furthermore, viral clearance in the cerebellum was only seen in animals with T-cells. Hence, in the process of clearing viral antigen from the cerebellum, T-cells induced considerable damage. In contrast, T-cell deficient rats sustained high titers in the cerebellum, and did not undergo damage, but did have hypoplasia.

The mechanism underlying cerebellum hypoplasia is unknown. The mechanism is T-cell independent but could be viral induced or caused by T-cell independent immune mechanisms such as cytokine/chemokine secretion. LCMV virus heavily infects immature granule cell neurons [36]. One possibility is that the LCM virus might hijack cellular machinery needed for normal proliferation, thereby decreasing generation of granule cells and resulting in hypoplasia. Alternatively, LCMV infection might be slowing down granule cell maturation. Instead of having a normal number of granule cells maturing and migrating inwards, LCMV infection might cause immature granule cells to remain in an immature premitotic phase, resulting in decreased numbers of granule cells reaching maturation and thus decreased granule cells migrating inwards. This would lead to a cerebellar hypoplasia. Our molecular data for ATOH11, a transcription factor expressed only in granule cell precursor cells, showed an increased expression in all LCMV infected animals, suggesting that there is larger pool of immature granule cells after LCMV infection, therefore supporting a role of LCMV in inhibiting granule cell maturation. A third possibility is that LCMV infection leads to death of EGL and IGL neurons through expression of damaging cytokines. Support for this hypothesis is that RNU/RNU rats express very high levels of TNF-α at PD8. TNF-α can be cytotoxic and result in neuron cell death [134, 253]. Cerebellum hypoplasia is seen starting very early in LCMV infection, being evident as early as PD14. TNF-α expression at PD8 could damage cerebellum granule neurons, leading to hypoplasia.

Migration is Altered in a T-cell Dependent Manner Through Two Mechanisms: Damaged Bergmann Fibers, and Increased Granule Cell Proliferation

The last question we addressed was what mechanism underlies the abnormal migration of granule cell neurons after neonatal infection with LCMV? When we started researching the mechanisms of the migration disorder, we were studying LCMV in the

Lewis rat only and had not yet discovered that migration was only altered in a T-cell dependent manner. This provided us first with a description of the migration abnormality in a T-cell competent animal, and gave us a few mechanisms to explore in terms of their T-cell dependent or independent derivation. In the process of our study in RNU/RNU rats, we discovered that migration was altered only in T-cell competent animals. Therefore, after characterizing the neuronal migration disorder in the Lewis, we used the T-cell deficient animals and the adoptive transfer method to determine the mechanism of T-cell induced abnormal migration after LCMV infection.

is a schematic illustration describing the pathology leading to abnormal migration in LCMV infection.

A shows the normal organization of Bergmann glia. Bergmann glia send out fibers in a parallel organization that are perpendicular to the molecular layer. These fibers connect with the basal lamina and provide a path upon which granule cells migrate to reach the IGL. In LCMV infected, but T-cell deficient animals, shown in Figure 41 B, Bergmann glia become reactive, displaying some thickening of their processes. Furthermore, Bergmann glia cell bodies and astrocytes move into the molecular layer but Bergmann glia radial processes remain largely intact and although there is a delay in external granule cell maturation (mitotic cells in the EGL Figure 41 B) granule cells are still able to migrate inwards along the intact Bergmann glia fibers. In the LCMV infected and T-cell competent animals, shown in Figure 41 C, two major features emerge. First, Bergmann glia fibers are drastically disrupted. Gaps in radial glia fibers occur, leaving regions of the ML and EGL without radial glia fibers. In the absence of radial glia fibers, migrating granule cells have no scaffold to follow on their inward journey to the IGL. A second feature is an increase proliferation of the granule cells in the EGL (shown by mitotic cells in the EGL). As a result, a drastic increase in the number of granule cells needing to migrate inwards occurs. When an increase in the number of migrating granule

cells is combined with a lack of fibers upon which to migrate, the formation of ectopic neurons in the ML and near the basal lamina occurs.

Future Direction

In this work, I have presented significant results towards understanding the role of the immune system in inducing brain pathology and the mechanism of LCMV induced neuronal migration disorder in the cerebellum. However, congenital LCMV infection is in early stages of research elucidating the mechanism of brain pathology as well as potential areas of therapeutic intervention. Fortunately, the neonatal rat model is an excellent tool to study congenital LCMV. Unlike many other models of developmental disease, the neonatal rat model recapitulates all of the human brain pathology and therefore serves as an excellent research tool for studying the pathogenesis of the disease. The one limitation of the neonatal rat model is that, as of now, there are very few transgenic rats available. Hopefully, transgenic rats will become more widely available in the next decade, allowing for a broader range of experimental studies into the pathogenesis of LCMV in the developing nervous system.

The following future directions are of priority in congenital LCMV infection. First, I showed compelling evidence that a difference in regional astrocyte response exists after LCMV infection. Discovering the possible mechanism accounting for the stronger immune response in astrocytes of the cerebellum versus astrocytes of the hippocampus is one area of future research. In addition, determining if there is a difference in the microglia population between the cerebellum and hippocampus is another future area for this research. Second, I showed that LCMV induces cerebellar hypoplasia in the absence of T-cells. Research into the mechanism of LCMV induced cerebellar hypoplasia is one area that has been untouched and will be a focus of future research. Finally, I showed that T-cells are necessary for cerebellar destruction, while in contrast, they protect the hippocampus from delayed dentate granule cell loss. Determining which T-cell

populations, CD8 versus CD4, are important for the cerebellum and hippocampus pathology is another important area of future research.

Regional astrocyte and microglia differences in cytokine production

One important finding from this research is that after infection with LCMV, cultured astrocytes from the cerebellum mount a stronger immune response than cultured astrocytes from the hippocampus. An area of future research is to determine what mechanism underlies the difference in immune response between astrocytes from the cerebellum versus astrocytes from the hippocampus. One hypothesis is that astrocytes differ morphologically and physiologically between brain regions. We have observational support for a morphologic difference. On observation, astrocyte cultures from the cerebellum appear morphologically different from hippocampus astrocyte cultures. Astrocytes from the hippocampus are more satellite in appearance compared to a cobblestone appearance of cultured cerebellum astrocytes. In addition, when these astrocytes are split and counted on a hemocytometer, cerebellum astrocytes are approximately ½ the diameter of hippocampus astrocytes. Although this has not been formally quantified, these differences have been seen in repeated cultures. We hypothesize that these morphological differences in astrocytes between brain regions may represent a difference in astrocyte subtypes present in the cultures. More specifically, we hypothesize that there is a larger portion of radial glia fibers in cerebellum astrocyte cultures.

Bergmann glial fibers, the radial glial population in the cerebellum, are numerous in the cerebellum and remain a constant population throughout life. In contrast, radial glial fibers in other areas of the brain are only present during active neuronal migration. Various studies of infection in the cerebellum have reported that Bergmann glia become reactive and adopt immune like functions [214-215]. If Bergmann glia comprise a

significant portion of astrocytes in the astrocyte cultures from the cerebellum, this could account for a source of cytokine and chemokine production in culture.

To investigate the differences in morphology of hippocampus and cerebellum cultures, a future goal is to describe the difference in morphology of hippocampus astrocytes versus cerebellum astrocytes. This should be followed by immunohistochemistry for Bergmann glia, using a Bergmann glia specific marker to determine if Bergmann glia cells account for a significant population within the astrocyte culture.

Microglia

Another area of important research is to determine the role microglia play in the cytokine/chemokine response after LCMV infection. One hypothesis is that microglia populations differ by brain region and therefore contribute to the differential immune response in the cerebellum versus the hippocampus. Two future experiments may be done to explore this hypothesis. First, one experiment should use immunohistochemistry to characterize the microglia populations in vivo. Careful note of the type of microglia, i.e. ramified versus amoeboid, should be documented.

To enhance this study, mixed astrocyte/microglia cultures should be made from the hippocampus and the cerebellum and analyzed for cytokine/chemokine expression. To do this, the same astrocyte isolation protocol presented in Chapter 1 can be used, with two main differences; the media needs to contain 15% bovine serum instead of 10% because microglia thrive in a higher serum environment, and no shaking of cultures should be performed in order to preserve the microglia component of the culture. Using immunohistochemistry, microglia should be counted in each culture to determine if there is a difference in the proportion of microglia in the hippocampus and cerebellum cultures. Then, the procedure for cytokine/chemokine quantification using RT-PCR (see Chapter 1) can be done to compare gene levels in cultures that have microglia versus cultures in

which microglia have been removed. I expect that astrocyte/microglia mixed cultures will mount a stronger cytokine response than cultures without microglia. I also expect that the cytokine expression for both the astrocyte/microglia mixed cultures and astrocyte cultures will be higher for the cerebellum than for the hippocampus.

Hypoplasia

One novel and important finding from this research was that cerebellar hypoplasia is induced even in the absence of T-cells. Up until now, we have not explored the mechanism underlying this hypoplasia. One hypothesis is that LCMV virus leads to a death of neuroprogenitors in the EGL and as a consequence, fewer EGL cells are generated resulting in hypoplasia. I will propose two experiments to explore this hypothesis. RNU/RNU animals should be used for both experiments because these animals are T-cell deficient and provide a way to study the T-cell independent hypoplastic process.

First, RNU/RNU animals should be infected with LCMV virus and sacrificed at various time points. Brains should be collected, sectioned, and a Nissl or H& E stain should be done to examine cytoarchitecture. The thickness of the EGL can then be quantified. I expect that there will be regions in some lobules where the EGL thickness is diminished, representing a decrease in granule cell precursors. Furthermore, we should explore the possibility that neuroprogenitors are dying, resulting in a slow granule cell loss. To do this, TUNEL labeling will be done in cerebella from PD14 RNU/RNU LCMV infected and control animals. The number of TUNEL-positive cells will be quantified for three sections per brain and at least three animals per group. We expect that there will be at least a two fold increase in TUNEL-positive cells in the cerebellum of RNU/RNU animals. Double labeling for neuronal markers such as TAG-1 and NeuN will be done to confirm neuronal origin of TUNEL-positive cells.

Specific T-cell population and pathology

In this thesis, I have introduced an adoptive transfer model which allowed me to determine the importance of T-cells in the cerebellum and hippocampus pathology. This is a great tool because it can be used to explore the role of specific lymphocyte populations in disease pathology. One future goal is to separate CD8 T-cells and CD4 T-cells to determine what respective role each population plays in congenital LCMV. To do this experiment, I propose to isolate splenocytes from primed adult RNU/+ animals and then use a complement lysis method to deplete either the CD4 or CD8 population. This is a good approach because it is efficient and cost effective. To do this, an antibody against the cell population to be depleted, either CD8 or CD4, is added to the isolated splenocytes. Complement is then added and complement lysis performed. Once this procedure has been done, flow cytometry will be used to determine the efficacy of complement lysis. The procedure can be repeated if a purer population is desired. Splenocytes depleted of CD4 and splenocytes depleted of CD8 will then be adoptively transferred to infected RNU/RNU pups and an examination of pathology and behavior will be done (repeated from Chapter 6). I expect that in the absence of CD8 T-cells, no cerebellar destruction will occur. In addition, in the absence of CD4 T-cells, cerebellar destruction will be minimal. CD8 cells likely play a damaging role in the cerebellum. However, their cytotoxic property and activation is often dependent on the presence of CD4 T-cells. Therefore, I suspect that both populations are necessary for the destructive pathology to occur.

After doing the above experiment, we can explore the role of specific CD4 T-cell populations, such as CD4 T-helper cells versus CD4 T-regulatory cells (T-reg), in LCMV infection. This experiment will be very useful in studying the hippocampus pathology as well as the cerebellum pathology. T-reg cells play an important role in attenuating the immune response and protecting from immune-mediated damage [254]. One hypothesis is that a larger T-reg population might be recruited to the hippocampus and might account

for protection of the hippocampus compared to destruction of the cerebellum. To do this experiment, a Miltenyi magnetic kit can be used to deplete or select for T-reg cells. A splenocyte population consisting of only T-reg cells or depleted of T-reg cells can then be transferred to RNU/RNU pups via adoptive transfer. If T-reg cells are playing an important role in protecting against cytotoxic-mediated damage, we expect that after depletion of T-reg cells, the dentate granule loss in the hippocampus and the cerebellum destruction will be more severe.

Summary

Congenital virus infection is a source of considerable neurological disease in children and very little is known about the pathogenesis. We have described new findings regarding the mechanism of brain-induced injury in congenital LCMV. Specifically, we have shown that the immune response plays a very important role in pathology, leading to a destruction of the cerebellum while at the same time protecting the hippocampus against significant cell loss. Further examination into specific cell populations involved in the immune response and therapeutic interventions to protect the developing fetus should be high priority for future research in congenital LCMV.

Figure 41 Schematic of granule cell migration disorder.

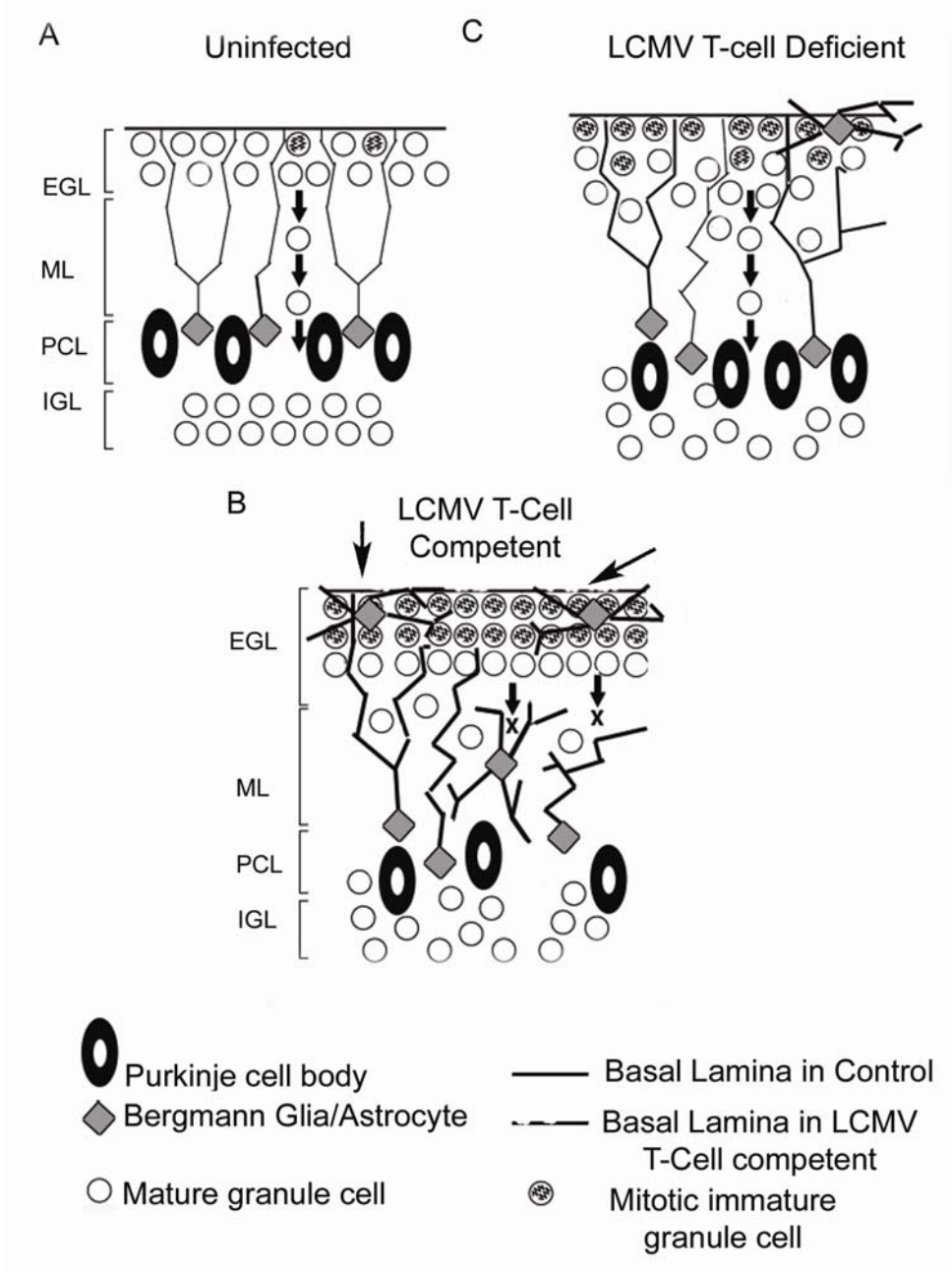

REFERENCES

1. Wright, R., et al., *Congenital lymphocytic choriomeningitis virus syndrome: a disease that mimics congenital toxoplasmosis or Cytomegalovirus infection.* Pediatrics, 1997. **100**(1): p. E9.

2. Bale, J.F., Jr. and J.R. Murph, *Congenital infections and the nervous system.* Pediatr Clin North Am, 1992. **39**(4): p. 669-90.

3. Bonthius, D.J., *Lymphocytic choriomeningitis virus: a prenatal and postnatal threat.* Adv Pediatr, 2009. **56**: p. 75-86.

4. Buchmeier, M.J., et al., *The virology and immunobiology of lymphocytic choriomeningitis virus infection.* Adv.Immunol., 1980. **30**: p. 275-331.

5. Bonthius, D.J., Klein de Licona H, Bonthius NE, Karacay B, *The arenaviruses.* In Friedman N, Rust R, editors. Neurological complications of pediatric infectious disease. New York: Humana Press., 2007.

6. Rowe, W.P., et al., *Arenoviruses: proposed name for a newly defined virus group.* J.Virol., 1970. **5**(5): p. 651-652.

7. Lehmann-Grube, F., et al., *Mechanism of recovery from acute virus infection. I. Role of T lymphocytes in the clearance of lymphocytic choriomeningitis virus from spleens of mice.* J.Immunol., 1985. **134**(1): p. 608-615.

8. Buchmeier, M.J., Zajac AJ., *Lymphocytic choriomeningitis virus.* In: Ahmed R, Chen I, editors. Persistant Viral Infections. New York: Wiley;, 1999: p. 575-605.

9. Klein de Licona, H., Rabe G., Bonthius NE, Bonthius DJ, *Congenital lymphocytic choriomeningitis virus infection. .* In: Gilman S, editor. MedLink- Neurobase edition 4. San Diego; Arbor Publishing Coorportaion. , 2008.

10. Barton, L.L., et al., *Congenital lymphocytic choriomeningitis virus infection.* Arch.Pediatr.Adolesc.Med., 1996. **150**(4): p. 440.

11. Barton, L.L. and M.B. Mets, *Congenital lymphocytic choriomeningitis virus infection: decade of rediscovery.* Clin.Infect.Dis., 2001. **33**(3): p. 370-374.

12. Asnis, D.S., et al., *Lymphocytic choriomeningitis virus meningitis, New York, NY, USA, 2009.* Emerg Infect Dis. **16**(2): p. 328-30.

13. Biggar, R.J., T.J. Schmidt, and J.P. Woodall, *Lymphocytic choriomeningitis in laboratory personnel exposed to hamsters inadvertently infected with LCM virus.* J.Am.Vet.Med.Assoc., 1977. **171**(9): p. 829-832.

14. Bonthius, D.J. and S. Perlman, *Congenital viral infections of the brain: lessons learned from lymphocytic choriomeningitis virus in the neonatal rat.* PLoS.Pathog., 2007. **3**(11): p. e149.

15. *Lymphocytic choriomeningitis virus infection in organ transplant recipients--Massachusetts, Rhode Island, 2005.* MMWR Morb Mortal Wkly Rep, 2005. **54**(21): p. 537-9.

16. *Brief report: Lymphocytic choriomeningitis virus transmitted through solid organ transplantation--Massachusetts, 2008.* MMWR Morb Mortal Wkly Rep, 2008. **57**(29): p. 799-801.

17. Fischer, S.A., et al., *Transmission of lymphocytic choriomeningitis virus by organ transplantation.* N Engl J Med, 2006. **354**(21): p. 2235-49.

18. Geisbert, T.W. and P.B. Jahrling, *Exotic emerging viral diseases: progress and challenges.* Nat Med, 2004. **10**(12 Suppl): p. S110-21.

19. McCormick, J.B. and S.P. Fisher-Hoch, *Lassa fever.* Curr Top Microbiol Immunol, 2002. **262**: p. 75-109.

20. Armstrong C, L.R., *Experimental lymphocytic choriomeningitis of monkeys and mice produced by a virus encountered in studies of the 1933 St. Louis encephalitis epidemic.* Public Health Res, 1933. **49**: p. 1019-1022.

21. Meyer, H.M., Jr., et al., *Central nervous system syndromes of "vital" etiology. A study of 713 cases.* Am J Med, 1960. **29**: p. 334-47.

22. Childs, J.E., et al., *Lymphocytic choriomeningitis virus infection and house mouse (Mus musculus) distribution in urban Baltimore.* Am.J.Trop.Med.Hyg., 1992. **47**(1): p. 27-34.

23. Emonet, S., et al., *Mouse-to-human transmission of variant lymphocytic choriomeningitis virus.* Emerg Infect Dis, 2007. **13**(3): p. 472-5.

24. Stephensen, C.B., et al., *Prevalence of serum antibodies against lymphocytic choriomeningitis virus in selected populations from two U.S. cities.* J.Med.Virol., 1992. **38**(1): p. 27-31.

25. Dykewicz, C.A., et al., *Lymphocytic choriomeningitis outbreak associated with nude mice in a research institute.* JAMA, 1992. **267**(10): p. 1349-53.

26. Komrower, G.M., B.L. Williams, and P.B. Stones, *Lymphocytic choriomeningitis in the newborn; probable transplacental infection.* Lancet, 1955. **268**(6866): p. 697-8.

27. Ackermann, R., et al., *[Prenatal infection with the virus of lymphocytic choriomeningitis: report of two cases (author's transl)].* Dtsch.Med.Wochenschr., 1974. **99**(13): p. 629-632.

28. Mets, M.B., et al., *Lymphocytic choriomeningitis virus: an underdiagnosed cause of congenital chorioretinitis.* Am.J.Ophthalmol., 2000. **130**(2): p. 209-215.

29. Bonthius, D.J., et al., *Congenital lymphocytic choriomeningitis virus infection: spectrum of disease.* Ann.Neurol., 2007. **62**(4): p. 347-355.

30. Barton, L.L., et al., *Congenital lymphocytic choriomeningitis virus infection in twins.* Pediatr.Infect.Dis.J., 1993. **12**(11): p. 942-946.

31. Larsen, P.D., et al., *Hydrocephalus complicating lymphocytic choriomeningitis virus infection.* Pediatr.Infect.Dis.J., 1993. **12**(6): p. 528-531.

32. Jamieson, D.J., R.N. Theiler, and S.A. Rasmussen, *Emerging infections and pregnancy.* Emerg Infect Dis, 2006. **12**(11): p. 1638-43.

33. Enders, G., et al., *Congenital lymphocytic choriomeningitis virus infection: an underdiagnosed disease.* Pediatr Infect Dis J, 1999. **18**(7): p. 652-5.

34. Jahrling, P.B. and C.J. Peters, *Lymphocytic choriomeningitis virus. A neglected pathogen of man.* Arch Pathol Lab Med, 1992. **116**(5): p. 486-8.

35. Schulte, D.J., et al., *Congenital lymphocytic choriomeningitis virus: an underdiagnosed cause of neonatal hydrocephalus.* Pediatr Infect Dis J, 2006. **25**(6): p. 560-2.

36. Bonthius, D.J., et al., *Critical role for glial cells in the propagation and spread of lymphocytic choriomeningitis virus in the developing rat brain.* J.Virol., 2002. **76**(13): p. 6618-6635.

37. Bonthius, D.J., et al., *Lymphocytic choriomeningitis virus infection of the developing brain: critical role of host age.* Ann.Neurol., 2007. **62**(4): p. 356-374.

38. Gilden, D.H., et al., *Immunopathogenesis of acute central nervous system disease produced by lymphocytic choriomeningitis virus. I. Cyclophosphamide-mediated induction by the virus-carrier state in adult mice.* J.Exp.Med., 1972. **135**(4): p. 860-873.

39. Doherty, P.C. and R.M. Zinernagel, *Capacity of sensitized thymus-derived lymphocytes to induce fatal lymphocytic choriomeningitis is restricted by the H-2 gene complex.* J.Immunol., 1975. **114**(1 Pt 1): p. 30-33.

40. Oldstone, M.B., *A suspenseful game of 'hide and seek' between virus and host.* Nat Immunol, 2007. **8**(4): p. 325-7.

41. Zinkernagel, R.M. and P.C. Doherty, *Immunological surveillance against altered self components by sensitised T lymphocytes in lymphocytic choriomeningitis.* Nature, 1974. **251**(5475): p. 547-548.

42. Zinkernagel, R.M. and P.C. Doherty, *Restriction of in vitro T cell-mediated cytotoxicity in lymphocytic choriomeningitis within a syngeneic or semiallogeneic system.* Nature, 1974. **248**(450): p. 701-702.

43. Doherty, P.C. and R.M. Zinkernagel, *A biological role for the major histocompatibility antigens.* Lancet, 1975. **1**(7922): p. 1406-9.

44. Zinkernagel, R.M. and P.C. Doherty, *MHC-restricted cytotoxic T cells: studies on the biological role of polymorphic major transplantation antigens determining T-cell restriction-specificity, function, and responsiveness.* Adv Immunol, 1979. **27**: p. 51-177.

45. Dobbing, J. and J. Sands, *Comparative aspects of the brain growth spurt.* Early Hum Dev, 1979. **3**(1): p. 79-83.

46. Altman, J., *Autoradiographic and histological studies of postnatal neurogenesis. 3. Dating the time of production and onset of differentiation of cerebellar microneurons in rats.* J Comp Neurol, 1969. **136**(3): p. 269-93.

47. Monjan, A.A., et al., *Pathogenesis of cerebellar hypoplasia produced by lymphocytic choriomeningitis virus infection of neonatal rats. 1. Evolution of disease following infection at 4 days of age.* J.Neuropathol.Exp.Neurol., 1973. **32**(1): p. 110-124.

48. Monjan, A.A., G.A. Cole, and N. Nathanson, *Pathogenesis of cerebellar hypoplasia produced by lymphocytic choriomeningitis virus infection of neonatal rats: protective effect of immunosuppression with anti-lymphoid serum.* Infect.Immun., 1974. **10**(3): p. 499-502.

49. Monjan, A.A., et al., *Cerebellar hypoplasia in neonatal rats caused by lymphocytic choriomeningitis virus.* Science, 1971. **171**(967): p. 194-196.

50. Monjan, A.A., A.M. Silverstein, and G.A. Cole, *Lymphocytic choriomeningitis virus-induced retinopathy in newborn rats.* Invest Ophthalmol., 1972. **11**(10): p. 850-856.

51. Hinds, J.W. and N.A. McNelly, *Aging of the rat olfactory bulb: growth and atrophy of constituent layers and changes in size and number of mitral cells.* J Comp Neurol, 1977. **72**(3): p. 345-67.

52. Hinds, J.W., *Autoradiographic study of histogenesis in the mouse olfactory bulb. I. Time of origin of neurons and neuroglia.* J Comp Neurol, 1968. **134**(3): p. 287-304.

53. Hinds, J.W., *Autoradiographic study of histogenesis in the mouse olfactory bulb. II. Cell proliferation and migration.* J Comp Neurol, 1968. **134**(3): p. 305-22.

54. Altman, J. and G.D. Das, *Autoradiographic and histological evidence of postnatal hippocampal neurogenesis in rats.* J Comp Neurol, 1965. **124**(3): p. 319-35.

55. Altman J, B.S., *Birthdates of the prenatally generated neurons of the cerebellar system: an analysis with thymidine autoradiography.* In: Development of the cerebellar system. New York: CRC Press. , 1997: p. 99-107.

56. Lois, C. and A. Alvarez-Buylla, *Proliferating subventricular zone cells in the adult mammalian forebrain can differentiate into neurons and glia.* Proc Natl Acad Sci U S A, 1993. **90**(5): p. 2074-7.

57. Bonthius, D.J., Taggard D, Mahoney J, Assouline J *The topography of lymphocytic choriomeningitis virus (LCMV) and of its putative receptor in the developing rat brain. .* J Neurovirology, 2000. **6**: p. 437.

58. Dorries, R., *The role of T-cell-mediated mechanisms in virus infections of the nervous system.* Curr Top Microbiol Immunol, 2001. **253**: p. 219-45.

59. Guidotti, L.G. and F.V. Chisari, *Noncytolytic control of viral infections by the innate and adaptive immune response.* Annu Rev Immunol, 2001. **19**: p. 65-91.

60. Cserr, H.F. and P.M. Knopf, *Cervical lymphatics, the blood-brain barrier and the immunoreactivity of the brain: a new view.* Immunol Today, 1992. **13**(12): p. 507-12.

61. Gehrmann, J., *Microglia: a sensor to threats in the nervous system?* Res Virol, 1996. **147**(2-3): p. 79-88.

62. Gehrmann, J., Y. Matsumoto, and G.W. Kreutzberg, *Microglia: intrinsic immuneffector cell of the brain.* Brain Res Brain Res Rev, 1995. **20**(3): p. 269-87.

63. Rock, R.B., et al., *Role of microglia in central nervous system infections.* Clin Microbiol Rev, 2004. **17**(4): p. 942-64, table of contents.

64. Wang, X. and Y. Suzuki, *Microglia produce IFN-gamma independently from T cells during acute toxoplasmosis in the brain.* J Interferon Cytokine Res, 2007. **27**(7): p. 599-605.

65. Xu, J. and E.A. Ling, *Upregulation and induction of major histocompatibility complex class I and II antigens on microglial cells in early postnatal rat brain following intraperitoneal injections of recombinant interferon-gamma.* Neuroscience, 1994. **60**(4): p. 959-67.

66. Sethna, M.P. and L.A. Lampson, *Immune modulation within the brain: recruitment of inflammatory cells and increased major histocompatibility antigen expression following intracerebral injection of interferon-gamma.* J Neuroimmunol, 1991. **34**(2-3): p. 121-32.

67. Boelen, E., et al., *Inflammatory responses following Chlamydia pneumoniae infection of glial cells.* Eur J Neurosci, 2007. **25**(3): p. 753-60.

68. Frei, K., et al., *On the cellular source and function of interleukin 6 produced in the central nervous system in viral diseases.* Eur.J.Immunol., 1989. **19**(4): p. 689-694.

69. Guidotti, L.G. and F.V. Chisari, *Noncytolytic control of viral infections by the innate and adaptive immune response.* Annual Review of Immunology, 2001. **19**: p. 65-91.

70. Li, L., et al., *The function of microglia, either neuroprotection or neurotoxicity, is determined by the equilibrium among factors released from activated microglia in vitro.* Brain Res, 2007. **1159**: p. 8-17.

71. Mizuno, T., et al., *Interferon-gamma directly induces neurotoxicity through a neuron specific, calcium-permeable complex of IFN-gamma receptor and AMPA GluR1 receptor.* FASEB J, 2008. **22**(6): p. 1797-806.

72. Strijbos, P.J. and N.J. Rothwell, *Interleukin-1 beta attenuates excitatory amino acid-induced neurodegeneration in vitro: involvement of nerve growth factor.* J Neurosci, 1995. **15**(5 Pt 1): p. 3468-74.

73. Zou, J.Y. and F.T. Crews, *TNF alpha potentiates glutamate neurotoxicity by inhibiting glutamate uptake in organotypic brain slice cultures: neuroprotection by NF kappa B inhibition.* Brain Res, 2005. **1034**(1-2): p. 11-24.

74. Saukkonen, K., et al., *The role of cytokines in the generation of inflammation and tissue damage in experimental gram-positive meningitis.* J Exp Med, 1990. **171**(2): p. 439-48.

75. Bogdan, I., et al., *Tumor necrosis factor-alpha contributes to apoptosis in hippocampal neurons during experimental group B streptococcal meningitis.* J Infect Dis, 1997. **176**(3): p. 693-7.

76. Doherty, P.C., et al., *Dissection of an inflammatory process induced by CD8+ T cells.* Immunol Today, 1990. **11**(2): p. 55-9.

77. Brankin, B., et al., *Adhesion molecule expression and lymphocyte adhesion to cerebral endothelium: effects of measles virus and herpes simplex 1 virus.* J Neuroimmunol, 1995. **56**(1): p. 1-8.

78. Nottet, H.S. and H.E. Gendelman, *Unraveling the neuroimmune mechanisms for the HIV-1-associated cognitive/motor complex.* Immunol Today, 1995. **16**(9): p. 441-8.

79. Wekerle, H., et al., *Interaction of T lymphocytes with cerebral endothelial cells in vitro.* Brain Pathol, 1991. **1**(2): p. 107-14.

80. Christian, A.Y., et al., *Host immune response to vesicular stomatitis virus infection of the central nervous system in C57BL/6 mice.* Viral Immunol, 1996. **9**(3): p. 195-205.

81. Kang, S.S. and D.B. McGavern, *Inflammation on the mind: visualizing immunity in the central nervous system.* Curr Top Microbiol Immunol, 2009. **334**: p. 227-63.

82. Cserr, H.F., C.J. Harling-Berg, and P.M. Knopf, *Drainage of brain extracellular fluid into blood and deep cervical lymph and its immunological significance.* Brain Pathol, 1992. **2**(4): p. 269-76.

83. Kang, S.S. and D.B. McGavern, *Lymphocytic choriomeningitis infection of the central nervous system.* Front Biosci, 2008. **13**: p. 4529-43.

84. Joly, E., L. Mucke, and M.B. Oldstone, *Viral persistence in neurons explained by lack of major histocompatibility class I expression.* Science, 1991. **253**(5025): p. 1283-1285.

85. Mucke, L. and M.B. Oldstone, *The expression of major histocompatibility complex (MHC) class I antigens in the brain differs markedly in acute and persistent infections with lymphocytic choriomeningitis virus (LCMV).* J.Neuroimmunol., 1992. **36**(2-3): p. 193-198.

86. Hoftberger, R., et al., *Expression of major histocompatibility complex class I molecules on the different cell types in multiple sclerosis lesions.* Brain Pathol, 2004. **14**(1): p. 43-50.

87. Vass, K. and H. Lassmann, *Intrathecal application of interferon gamma. Progressive appearance of MHC antigens within the rat nervous system.* Am J Pathol, 1990. **137**(4): p. 789-800.

88. Wong, G.H., et al., *Inducible expression of H-2 and Ia antigens on brain cells.* Nature, 1984. **310**(5979): p. 688-91.

89. Doherty, P.C., J.E. Allan, and R. Ceredig, *Contributions of host and donor T cells to the inflammatory process in murine lymphocytic choriomeningitis.* Cell Immunol., 1988. **116**(2): p. 475-481.

90. Baenziger, J., et al., *Induction or prevention of immunopathological disease by cloned cytotoxic T cell lines specific for lymphocytic choriomeningitis virus.* Eur.J.Immunol., 1986. **16**(4): p. 387-393.

91. Cole, G.A., N. Nathanson, and R.A. Prendergast, *Requirement for theta-bearing cells in lymphocytic choriomeningitis virus-induced central nervous system disease.* Nature, 1972. **238**(5363): p. 335-7.

92. Gilden, D.H., G.A. Cole, and N. Nathanson, *Immunopathogenesis of acute central nervous system disease produced by lymphocytic choriomeningitis virus. II. Adoptive immunization of virus carriers.* J.Exp.Med., 1972. **135**(4): p. 874-889.

93. Allan, J.E. and P.C. Doherty, *Natural killer cells contribute to inflammation but do not appear to be essential for the induction of clinical lymphocytic choriomeningitis.* Scand.J.Immunol., 1986. **24**(2): p. 153-162.

94. Homann, D., et al., *Evidence for an underlying CD4 helper and CD8 T-cell defect in B-cell- deficient mice: failure to clear persistent virus infection after adoptive immunotherapy with virus-specific memory cells from muMT/muMT mice.* J.Virol., 1998. **72**(11): p. 9208-9216.

95. Cerny, A., et al., *Immunity to lymphocytic choriomeningitis virus in B cell-depleted mice: evidence for B cell and antibody-independent protection by memory T cells.* Eur.J.Immunol., 1986. **16**(8): p. 913-917.

96. Doherty, P.C., S. Hou, and P.J. Southern, *Lymphocytic choriomeningitis virus induces a chronic wasting disease in mice lacking class I major histocompatibility complex glycoproteins.* J.Neuroimmunol., 1993. **46**(1-2): p. 11-17.

97. Asensio, V.C. and I.L. Campbell, *Chemokine gene expression in the brains of mice with lymphocytic choriomeningitis.* J.Virol., 1997. **71**(10): p. 7832-7840.

98. Asensio, V.C., C. Kincaid, and I.L. Campbell, *Chemokines and the inflammatory response to viral infection in the central nervous system with a focus on lymphocytic choriomeningitis virus.* J.Neurovirol., 1999. **5**(1): p. 65-75.

99. Nansen, A., et al., *CCR2+ and CCR5+ CD8+ T cells increase during viral infection and migrate to sites of infection.* Eur.J.Immunol., 2000. **30**(7): p. 1797-1806.

100. Campbell, I.L., et al., *Cerebral expression of multiple cytokine genes in mice with lymphocytic choriomeningitis.* J Immunol, 1994. **152**(2): p. 716-23.

101. Christensen, J.E., et al., *Fulminant lymphocytic choriomeningitis virus-induced inflammation of the CNS involves a cytokine-chemokine-cytokine-chemokine cascade.* J Immunol, 2009. **182**(2): p. 1079-87.

102. Pearce, B.D., et al., *Lymphocytic responses and the gradual hippocampal neuron loss following infection with lymphocytic choriomeningitis virus (LCMV).* J Neuroimmunol, 1999. **101**(2): p. 137-47.

103. Vaillant, C. and D. Monard, *SHH pathway and cerebellar development.* Cerebellum, 2009. **8**(3): p. 291-301.

104. Altman, J., *Postnatal development of the cerebellar cortex in the rat. I. The external germinal layer and the transitional molecular layer.* J Comp Neurol, 1972. **145**(3): p. 353-97.

105. Fujita, S., *Quantitative analysis of cell proliferation and differentiation in the cortex of the postnatal mouse cerebellum.* J Cell Biol, 1967. **32**(2): p. 277-87.

106. Fujita, S., M. Shimada, and T. Nakamura, *H3-thymidine autoradiographic studies on the cell proliferation and differentiation in the external and the internal granular layers of the mouse cerebellum.* J Comp Neurol, 1966. **128**(2): p. 191-208.

107. Miale, I.L. and R.L. Sidman, *An autoradiographic analysis of histogenesis in the mouse cerebellum.* Exp Neurol, 1961. **4**: p. 277-96.

108. Trenkner, E., D. Smith, and N. Segil, *Is cerebellar granule cell migration regulated by an internal clock?* J Neurosci, 1984. **4**(11): p. 2850-5.

109. Yacubova, E. and H. Komuro, *Intrinsic program for migration of cerebellar granule cells in vitro.* J Neurosci, 2002. **22**(14): p. 5966-81.

110. Dahmane, N. and A. Ruiz i Altaba, *Sonic hedgehog regulates the growth and patterning of the cerebellum.* Development, 1999. **126**(14): p. 3089-100.

111. Reiss, K., et al., *Stromal cell-derived factor 1 is secreted by meningeal cells and acts as chemotactic factor on neuronal stem cells of the cerebellar external granular layer.* Neuroscience, 2002. **115**(1): p. 295-305.

112. Vilz, T.O., et al., *The SDF-1/CXCR4 pathway and the development of the cerebellar system.* European Journal of Neuroscience, 2005. **22**(8): p. 1831-1839.

113. Zhu, Y., et al., *Role of the chemokine SDF-1 as the meningeal attractant for embryonic cerebellar neurons.* Nature Neuroscience, 2002. **5**(8): p. 719-720.

114. Komuro, H. and P. Rakic, *Distinct modes of neuronal migration in different domains of developing cerebellar cortex.* J Neurosci, 1998. **18**(4): p. 1478-90.

115. Rakic, P., *Neuron-glia relationship during granule cell migration in developing cerebellar cortex. A Golgi and electronmicroscopic study in Macacus Rhesus.* J Comp Neurol, 1971. **141**(3): p. 283-312.

116. Gregory, W.A., et al., *Cytology and neuron-glial apposition of migrating cerebellar granule cells in vitro.* J Neurosci, 1988. **8**(5): p. 1728-38.

117. Komuro, H. and P. Rakic, *Dynamics of granule cell migration: a confocal microscopic study in acute cerebellar slice preparations.* J Neurosci, 1995. **15**(2): p. 1110-20.

118. Moore, S.A., et al., *Deletion of brain dystroglycan recapitulates aspects of congenital muscular dystrophy.* Nature, 2002. **418**(6896): p. 422-5.

119. Belvindrah, R., et al., *Integrin-linked kinase regulates Bergmann glial differentiation during cerebellar development.* Mol Cell Neurosci, 2006. **33**(2): p. 109-25.

120. Li, X., et al., *Differentiation and developmental origin of cerebellar granule neuron ectopia in protein O-mannose UDP-N-acetylglucosaminyl transferase 1 knockout mice.* Neuroscience, 2008. **152**(2): p. 391-406.

121. Altman, J., W.J. Anderson, and K. Wright, *Reconstitution of the external granular layer of the cerebellar cortex in infant rats after low-level x-irradiation.* Anat Rec, 1969. **163**(3): p. 453-71.

122. Altman, J., W.J. Anderson, and K.A. Wright, *Early effects of x-irradiation of the cerebellum in infant rats: decimation and reconstitution of the external granular layer.* Exp Neurol, 1969. **24**(2): p. 196-216.

123. Altman, J., *Experimental reorganization of the cerebellar cortex. 3. Regeneration of the external germinal layer and granule cell ectopia.* J Comp Neurol, 1973. **149**(2): p. 153-80.

124. Pisu, M.B., et al., *Proliferation and migration of granule cells in the developing rat cerebellum: cisplatin effects.* Anat Rec A Discov Mol Cell Evol Biol, 2005. **287**(2): p. 1226-35.

125. Tran, P.B., et al., *Chemokine receptor expression by neural progenitor cells in neurogenic regions of mouse brain.* Journal of Comparative Neurology, 2007. **500**(6): p. 1007-1033.

126. Ma, Q., et al., *Impaired B-lymphopoiesis, myelopoiesis, and derailed cerebellar neuron migration in CXCR4- and SDF-1-deficient mice.* Proceedings of the National Academy of Sciences of the United States of America, 1998. **95**(16): p. 9448-9453.

127. Stumm, R.K., S. Schulz, and V. Hoellt, *The chemokine receptor CXCR4 directs cellular migration in the embryonic and lesioned adult brain.* Journal of Neurochemistry, 2005. **94**: p. 138-138.

128. Imitola, J., et al., *Directed migration of neural stem cells to sites of CNS injury by the stromal cell-derived factor 1alpha/CXC chemokine receptor 4 pathway.* Proc Natl Acad Sci U S A, 2004. **101**(52): p. 18117-22.

129. Das, S. and A. Basu, *Inflammation: a new candidate in modulating adult neurogenesis.* J Neurosci Res, 2008. **86**(6): p. 1199-208.

130. Campbell, I.L., *Cytokines in viral diseases.* Curr Opin Immunol, 1991. **3**(4): p. 486-91.

131. Relton, J.K. and N.J. Rothwell, *Interleukin-1 receptor antagonist inhibits ischaemic and excitotoxic neuronal damage in the rat.* Brain Res Bull, 1992. **29**(2): p. 243-6.

132. Quagliarello, V.J., et al., *Recombinant human interleukin-1 induces meningitis and blood-brain barrier injury in the rat. Characterization and comparison with tumor necrosis factor.* J Clin Invest, 1991. **87**(4): p. 1360-6.

133. Wright, J.L. and R.E. Merchant, *Histopathological effects of intracerebral injections of human recombinant tumor necrosis factor-alpha in the rat.* Acta Neuropathol, 1992. **85**(1): p. 93-100.

134. Chao, C.C., et al., *Interleukin-1 and tumor necrosis factor-alpha synergistically mediate neurotoxicity: involvement of nitric oxide and of N-methyl-D-aspartate receptors.* Brain Behav Immun, 1995. **9**(4): p. 355-65.

135. Hu, S., P.K. Peterson, and C.C. Chao, *Cytokine-mediated neuronal apoptosis.* Neurochem Int, 1997. **30**(4-5): p. 427-31.

136. Li, H., et al., *Different neurotropic pathogens elicit neurotoxic CCR9- or neurosupportive CXCR3-expressing microglia.* J Immunol, 2006. **177**(6): p. 3644-3656.

137. Cheeran, M.C., et al., *Cytomegalovirus induces cytokine and chemokine production differentially in microglia and astrocytes: antiviral implications.* J Neurovirol, 2001. **7**(2): p. 135-47.

138. Bordey, A. and H. Sontheimer, *Ion channel expression by astrocytes in situ: comparison of different CNS regions.* Glia, 2000. **30**(1): p. 27-38.

139. Lehre, K.P., et al., *Differential expression of two glial glutamate transporters in the rat brain: quantitative and immunocytochemical observations.* J Neurosci, 1995. **15**(3 Pt 1): p. 1835-53.

140. Han, B.C., et al., *Regional difference of glutamate-induced swelling in cultured rat brain astrocytes.* Life Sci, 2004. **76**(5): p. 573-83.

141. Lubrich, B., et al., *Differential expression, activity and regulation of the sodium/myo-inositol cotransporter in astrocyte cultures from different regions of the rat brain.* Neuropharmacology, 2000. **39**(4): p. 680-90.

142. Belmadani, A., et al., *Selective toxicity of ochratoxin A in primary cultures from different brain regions.* Arch Toxicol, 1999. **73**(2): p. 108-14.

143. Tong, N., et al., *Neuronal fractalkine expression in HIV-1 encephalitis: roles for macrophage recruitment and neuroprotection in the central nervous system.* J Immunol, 2000. **164**(3): p. 1333-1339.

144. Cardona, A.E., et al., *Control of microglial neurotoxicity by the fractalkine receptor.* Nat.Neurosci., 2006. **9**(7): p. 917-924.

145. Glezer, I., A.R. Simard, and S. Rivest, *Neuroprotective role of the innate immune system by microglia.* Neuroscience, 2007. **147**(4): p. 867-83.

146. Festing, M.F., et al., *An athymic nude mutation in the rat.* Nature, 1978. **274**(5669): p. 365-6.

147. Schuurman, H.J., *The nude rat.* Hum Exp Toxicol, 1995. **14**(1): p. 122-5.

148. Streit, W.J. and G.W. Kreutzberg, *Lectin binding by resting and reactive microglia.* J Neurocytol, 1987. **16**(2): p. 249-60.

149. Pozo, D., et al., *CD161 (human NKR-P1A) signaling in NK cells involves the activation of acid sphingomyelinase.* J Immunol, 2006. **176**(4): p. 2397-406.

150. Sunderland, C.A., W.R. McMaster, and A.F. Williams, *Purification with monoclonal antibody of a predominant leukocyte-common antigen and glycoprotein from rat thymocytes.* Eur J Immunol, 1979. **9**(2): p. 155-9.

151. Woollett, G.R., et al., *Molecular and antigenic heterogeneity of the rat leukocyte-common antigen from thymocytes and T and B lymphocytes.* Eur J Immunol, 1985. **15**(2): p. 168-73.

152. Sergent-Tanguy, S., et al., *Cell surface antigens on rat neural progenitors and characterization of the CD3 (+)/CD3 (-) cell populations.* Differentiation, 2006. **74**(9-10): p. 530-41.

153. Ljungdahl, A., et al., *Interferon-gamma-like immunoreactivity in certain neurons of the central and peripheral nervous system.* J Neurosci Res, 1989. **24**(3): p. 451-6.

154. Schmidt, B., et al., *Rat astrocytes express interferon-gamma immunoreactivity in normal optic nerve and after nerve transection.* Brain Res, 1990. **515**(1-2): p. 347-50.

155. Tedeschi, B., J.N. Barrett, and R.W. Keane, *Astrocytes produce interferon that enhances the expression of H-2 antigens on a subpopulation of brain cells.* J Cell Biol, 1986. **102**(6): p. 2244-53.

156. Zujovic, V., et al., *Fractalkine modulates TNF-alpha secretion and neurotoxicity induced by microglial activation.* Glia, 2000. **29**(4): p. 305-15.

157. Harrison, J.K., et al., *Role for neuronally derived fractalkine in mediating interactions between neurons and CX3CR1-expressing microglia.* Proc Natl Acad Sci U S A, 1998. **95**(18): p. 10896-901.

158. del Cerro, M., N. Nathanson, and A.A. Monjan, *Pathogenesis of cerebellar hypoplasia produced by lymphocytic choriomeningitis virus infection of neonatal rats. II. An ultrastructural study of the immune-mediated pathology.* Lab Invest, 1975. **33**(6): p. 608-617.

159. Welsh, R.M., P.W. Lampert, and M.B. Oldstone, *Prevention of virus-induced cerebellar diseases by defective- interfering lymphocytic choriomeningitis virus.* J.Infect.Dis., 1977. **136**(3): p. 391-399.

160. Zhao, X., et al., *TNF-alpha stimulates caspase-3 activation and apoptotic cell death in primary septo-hippocampal cultures.* J Neurosci Res, 2001. **64**(2): p. 121-31.

161. Bonthius, D.J., et al., *Lymphocytic choriomeningitis virus infection of the developing brain: critical role of host age.* Ann Neurol, 2007. **62**(4): p. 356-74.

162. Altman J, a.S.A.B., *The generation, movements, and settling of cerebellar granule cells and the formation of the parallel fibers.* . In: Development of the cerebellar system. New York: CRC Press, Boca Raton., 1997: p. 334-361.

163. Belmadani, A., et al., *The chemokine stromal cell-derived factor-1 regulates the migration of sensory neuron progenitors.* J Neurosci, 2005. **25**(16): p. 3995-4003.

164. Zhu, Y., et al., *Role of the chemokine SDF-1 as the meningeal attractant for embryonic cerebellar neurons.* Nat Neurosci, 2002. **5**(8): p. 719-20.

165. Klein, R.S., et al., *SDF-1 alpha induces chemotaxis and enhances Sonic hedgehog-induced proliferation of cerebellar granule cells.* Development, 2001. **128**(11): p. 1971-1981.

166. McGrath, K.E., et al., *Embryonic expression and function of the chemokine SDF-1 and its receptor, CXCR4.* Dev Biol, 1999. **213**(2): p. 442-56.

167. Calderon, T.M., et al., *A role for CXCL12 (SDF-1alpha) in the pathogenesis of multiple sclerosis: regulation of CXCL12 expression in astrocytes by soluble myelin basic protein.* J Neuroimmunol, 2006. **177**(1-2): p. 27-39.

168. Zou, Y.R., et al., *Function of the chemokine receptor CXCR4 in haematopoiesis and in cerebellar development.* Nature, 1998. **393**(6685): p. 595-599.

169. Zou, Y.R., et al., *Function of the chemokine receptor CXCR4 in haematopoiesis and in cerebellar development.* Nature, 1998. **393**(6685): p. 595-9.

170. Ma Q, J.D., Borghesani PR, Segal RA, Nagasawa T, Kishimoto T, Bronson RT, Springer TA, *Impaired B-lymphopoiesis, myelopoiesis, and derailed cerebellar neuron migration in CXCR4-and SDF-deficient mice.* Proc Natl Acad Sci U S A., 1998. **95**: p. 9448-9453.

171. Bonthius, D.J., L. Barton, H. Klein de Licona, N.E. Bonthius and B. Karacay, ed. *The arenaviruses*. The Neurological Manifestations of Pediatric Infectious Diseases and Immunodeficiency Syndromes, ed. L.L.B.a. N.R.Friedman. 2008, Humana Press: New York. 135-150.

172. Carson, M.J. and J.G. Sutcliffe, *Balancing function vs. self defense: the CNS as an active regulator of immune responses.* J Neurosci Res, 1999. **55**(1): p. 1-8.

173. Simpson, J.L., J.R. Niebyl, and S.G. Gabbe. , ed. *Normal and Problem Pregnancies*. 5th ed. Obstetrics, ed. C. Livingstone. 2007, Elsevier: philadelphia.

174. Buckley, R.H., ed. *Lymphopoiesis in the fetus*. 17th ed. Nelson Textbook of Pediatrics, ed. M.K.a.H.B. Jensen. 2004, Saunders: Philadelphia, PA.

175. Wilson, C.B., *The ontogeny of T lymphocyte maturation and function.* J Pediatr, 1991. **118**(3): p. S4-9.

176. Greenhow, T.L. and P.S. Weintrub, *Your diagnosis, please. Neonate with hydrocephalus.* Pediatr Infect Dis J, 2003. **22**(12): p. 1099, 1111-2.

177. Suzuki, Y., et al., *Microglia and macrophages as innate producers of interferon-gamma in the brain following infection with Toxoplasma gondii.* Int J Parasitol, 2005. **35**(1): p. 83-90.

178. Lieberman, A.P., et al., *Production of tumor necrosis factor and other cytokines by astrocytes stimulated with lipopolysaccharide or a neurotropic virus.* Proc Natl Acad Sci U S A, 1989. **86**(16): p. 6348-52.

179. Bonthius, D.J., et al., *Congenital lymphocytic choriomeningitis virus infection: spectrum of disease.* Ann Neurol, 2007. **62**(4): p. 347-55.

180. Rakic, P., *Principles of neural cell migration.* Experientia, 1990. **46**(9): p. 882-91.

181. Bonthius, D.J., et al., *Critical role for glial cells in the propagation and spread of lymphocytic choriomeningitis virus in the developing rat brain.* J Virol, 2002. **76**(13): p. 6618-35.

182. Weller, M., et al., *Jagged1 ablation results in cerebellar granule cell migration defects and depletion of Bergmann glia.* Dev Neurosci, 2006. **28**(1-2): p. 70-80.

183. Qu, Q. and F.I. Smith, *Neuronal migration defects in cerebellum of the Largemyd mouse are associated with disruptions in Bergmann glia organization and delayed migration of granule neurons.* Cerebellum, 2005. **4**(4): p. 261-70.

184. Yue, Q., et al., *PTEN deletion in Bergmann glia leads to premature differentiation and affects laminar organization.* Development, 2005. **132**(14): p. 3281-91.

185. Bonthius, D.J., et al., *Purkinje cell deficits in nonhuman primates following weekly exposure to ethanol during gestation.* Teratology, 1996. **53**(4): p. 230-236.

186. Stumm R, H.V., *CXC chemokine receptor 4 regulates neuronal migration and axonal pathfinding in the developing nervous system: implications for neuronal regeneration in the adult brain.* J Mol Endocrin, 2007. **38**: p. 377-382.

187. Peng, H., et al., *HIV-1-infected and/or immune activated macrophages regulate astrocyte SDF-1 production through IL-1beta.* Glia, 2006. **54**(6): p. 619-29.

188. Croitoru-Lamoury, J., et al., *Expression of chemokines and their receptors in human and simian astrocytes: evidence for a central role of TNF alpha and IFN gamma in CXCR4 and CCR5 modulation.* Glia, 2003. **41**(4): p. 354-70.

189. Schuurman, H.-J., *The nude rat.* Human & Experimental Toxicology, 1995. **14**: p. 122-125.

190. Volpe, J.J., *Cerebellum of the premature infant: rapidly developing, vulnerable, clinically important.* J Child Neurol, 2009. **24**(9): p. 1085-104.

191. Joseph, L.D., Pushpalatha, and S. Kuruvilla, *Cytomegalovirus infection with lissencephaly.* Indian J Pathol Microbiol, 2008. **51**(3): p. 402-4.

192. Hayward, J.C., et al., *Lissencephaly-pachygyria associated with congenital cytomegalovirus infection.* J Child Neurol, 1991. **6**(2): p. 109-14.

193. Sun, L., Z. Tian, and J. Wang, *A direct cross-talk between interferon-gamma and sonic hedgehog signaling that leads to the proliferation of neuronal precursor cells.* Brain Behav Immun, 2009.

194. Flora, A., et al., *Deletion of Atoh1 disrupts Sonic Hedgehog signaling in the developing cerebellum and prevents medulloblastoma.* Science, 2009. **326**(5958): p. 1424-7.

195. Ben-Arie, N., et al., *Math1 is essential for genesis of cerebellar granule neurons.* Nature, 1997. **390**(6656): p. 169-72.

196. Deverman, B.E. and P.H. Patterson, *Cytokines and CNS development.* Neuron, 2009. **64**(1): p. 61-78.

197. Bakhiet, M., et al., *RANTES promotes growth and survival of human first-trimester forebrain astrocytes.* Nat Cell Biol, 2001. **3**(2): p. 150-7.

198. Klein, R.S., et al., *SDF-1 alpha induces chemotaxis and enhances Sonic hedgehog-induced proliferation of cerebellar granule cells.* Development, 2001. **128**(11): p. 1971-81.

199. Wang, J., et al., *Inducible production of interferon-gamma in the developing brain causes cerebellar dysplasia with activation of the Sonic hedgehog pathway.* Molecular and Cellular Neuroscience, 2004. **27**(4): p. 489-496.

200. Wallace, V.A., *Purkinje-cell-derived Sonic hedgehog regulates granule neuron precursor cell proliferation in the developing mouse cerebellum.* Curr Biol, 1999. **9**(8): p. 445-8.

201. Wechsler-Reya, R.J. and M.P. Scott, *Control of neuronal precursor proliferation in the cerebellum by Sonic Hedgehog.* Neuron, 1999. **22**(1): p. 103-14.

202. Wang, J., et al., *Dysregulated Sonic hedgehog signaling and medulloblastoma consequent to IFN-alpha-stimulated STAT2-independent production of IFN-gamma in the brain.* J Clin Invest, 2003. **112**(4): p. 535-43.

203. Carter, R.J., J. Morton, and S.B. Dunnett, *Motor coordination and balance in rodents.* Curr Protoc Neurosci, 2001. **Chapter 8**: p. Unit 8 12.

204. Pierce, R.C. and P.W. Kalivas, *Locomotor behavior.* Curr Protoc Neurosci, 2007. **Chapter 8**: p. Unit 8 1.

205. Weyer, A. and K. Schilling, *Developmental and cell type-specific expression of the neuronal marker NeuN in the murine cerebellum.* J Neurosci Res, 2003. **73**(3): p. 400-9.

206. McLendon, R.E. and D.D. Bigner, *Immunohistochemistry of the glial fibrillary acidic protein: basic and applied considerations.* Brain Pathol, 1994. **4**(3): p. 221-8.

207. Feng, L., M.E. Hatten, and N. Heintz, *Brain lipid-binding protein (BLBP): a novel signaling system in the developing mammalian CNS.* Neuron, 1994. **12**(4): p. 895-908.

208. Finckbone, V., et al., *Regional differences in the temporal expression of non-apoptotic caspase-3-positive bergmann glial cells in the developing rat cerebellum.* Front Neuroanat, 2009. **3**: p. 3.

209. Oomman, S., et al., *Bergmann glia utilize active caspase-3 for differentiation.* Brain Res, 2006. **1078**(1): p. 19-34.

210. Oomman, S., et al., *Non-lethal active caspase-3 expression in Bergmann glia of postnatal rat cerebellum.* Brain Res Dev Brain Res, 2005. **160**(2): p. 130-45.

211. Oomman, S., et al., *Active caspase-3 expression during postnatal development of rat cerebellum is not systematically or consistently associated with apoptosis.* J Comp Neurol, 2004. **476**(2): p. 154-73.

212. Stottmann, R.W. and R.J. Rivas, *Distribution of TAG-1 and synaptophysin in the developing cerebellar cortex: Relationship to Purkinje cell dendritic development.* Journal of Comparative Neurology, 1998. **395**(1): p. 121-135.

213. Bleul, C.C., et al., *A highly efficacious lymphocyte chemoattractant, stromal cell-derived factor 1 (SDF-1).* J Exp Med, 1996. **184**(3): p. 1101-9.

214. Oster-Granite, M.L. and R.M. Herndon, *The pathogenesis of parvovirus-induced cerebellar hypoplasia in the Syrian hamster, Mesocricetus auratus. Fluorescent antibody, foliation, cytoarchitectonic, Golgi and electron microscopic studies.* J Comp Neurol, 1976. **169**(4): p. 481-521.

215. Stahl, W., M. Sekiguchi, and Y. Kaneda, *Cerebellar anomalies in congenital murine toxoplasmosis.* Parasitology Research, 2002. **88**(6): p. 507-512.

216. Toyoda, T., et al., *Cerebellar hypoplasia associated with an avian leukosis virus inducing fowl glioma.* Vet Pathol, 2006. **43**(3): p. 294-301.

217. Gilden, D.H., H.M. Friedman, and N. Nathanson, *Tamiami virus induced cerebellar heterotopia.* J Neuropathol Exp Neurol, 1974. **33**(1): p. 29-41.

218. Komuro, H. and E. Yacubova, *Recent advances in cerebellar granule cell migration.* Cell Mol Life Sci, 2003. **60**(6): p. 1084-98.

219. Ishizaki, Y., *Control of proliferation and differentiation of neural precursor cells: focusing on the developing cerebellum.* J Pharmacol Sci, 2006. **101**(3): p. 183-8.

220. Hervas, J.P., et al., *Proliferative activity in the cerebellar external granular layer evaluated by bromodeoxyuridine labeling.* Biotech Histochem, 2002. **77**(1): p. 27-35.

221. Furley, A.J., et al., *The axonal glycoprotein TAG-1 is an immunoglobulin superfamily member with neurite outgrowth-promoting activity.* Cell, 1990. **61**(1): p. 157-70.

222. Berciano, M.T., B. Conde, and M. Lafarga, *INTERACTIONS BETWEEN ASTROGLIA AND ECTOPIC GRANULE CELLS IN THE CEREBELLAR CORTEX OF NORMAL ADULT-RATS - A MORPHOLOGICAL AND CYTOCHEMICAL STUDY.* Experimental Brain Research, 1990. **80**(2): p. 397-408.

223. Smith, F.I. and Q. Qu, *Defects in radial neuronal migration in the cerebellum of the largemyd mouse are associated with disruptions in Bergmann glia organization and delayed migration of granule neurons.* Glycobiology, 2005. **15**(11): p. 1223-1223.

224. Yamanaka, H. and K. Obata, *Displaced granule cells in the molecular layer of the cerebellar cortex in mice treated with methylazoxymethanol.* Neurosci Lett, 2004. **358**(2): p. 132-6.

225. Klavinskis, L.S. and M.B. Oldstone, *Lymphocytic choriomeningitis virus selectively alters differentiated but not housekeeping functions: block in expression of growth hormone gene is at the level of transcriptional initiation.* Virology, 1989. **168**(2): p. 232-5.

226. Berntson, G.G. and K.M. Schumacher, *Effects of cerebellar lesions on activity, social interactions, and other motivated behaviors in the rat.* J Comp Physiol Psychol, 1980. **94**(4): p. 706-17.

227. Supple, W.F., Jr., R.N. Leaton, and M.S. Fanselow, *Effects of cerebellar vermal lesions on species-specific fear responses, neophobia, and taste-aversion learning in rats.* Physiol Behav, 1987. **39**(5): p. 579-86.

228. Steinlin, M., *Cerebellar disorders in childhood: cognitive problems.* Cerebellum, 2008. **7**(4): p. 607-10.

229. Soliva, J.C., et al., *Cerebellar neurometabolite abnormalities in pediatric attention/deficit hyperactivity disorder: a proton MR spectroscopic study.* Neurosci Lett, 2010. **470**(1): p. 60-4.

230. Valera, E.M., et al., *Meta-analysis of structural imaging findings in attention-deficit/hyperactivity disorder.* Biol Psychiatry, 2007. **61**(12): p. 1361-9.

231. Rapoport, J.L., et al., *Imaging normal and abnormal brain development: new perspectives for child psychiatry.* Aust N Z J Psychiatry, 2001. **35**(3): p. 272-81.

232. Bell, E.B., et al., *The stable and permanent expansion of functional T lymphocytes in athymic nude rats after a single injection of mature T cells.* J Immunol, 1987. **139**(5): p. 1379-84.

233. Pearce, B.D., et al., *Viral infection of developing GABAergic neurons in a model of hippocampal disinhibition.* Neuroreport, 2000. **11**(11): p. 2433-2438.

234. Pearce, B.D., et al., *Persistent dentate granule cell hyperexcitability after neonatal infection with lymphocytic choriomeningitis virus.* J.Neurosci., 1996. **16**(1): p. 220-228.

235. Sharma, A., et al., *Neonatal viral infection decreases neuronal progenitors and impairs adult neurogenesis in the hippocampus.* Neurobiol Dis, 2002. **11**(2): p. 246-56.

236. Bayer, S.A., J.W. Yackel, and P.S. Puri, *Neurons in the rat dentate gyrus granular layer substantially increase during juvenile and adult life.* Science, 1982. **216**(4548): p. 890-2.

237. Schlessinger, A.R., W.M. Cowan, and D.I. Gottlieb, *An autoradiographic study of the time of origin and the pattern of granule cell migration in the dentate gyrus of the rat.* J Comp Neurol, 1975. **159**(2): p. 149-75.

238. Orr, A.G., et al., *Interleukin-1 Mediates Long-Term Hippocampal Dentate Granule Cell Loss Following Postnatal Viral Infection.* J Mol Neurosci, 2009.

239. Eriksen, W., J.M. Sundet, and K. Tambs, *Register data suggest lower intelligence in men born the year after flu pandemic.* Ann Neurol, 2009. **66**(3): p. 284-9.

240. Tardieu, M. and Y. Mikaeloff, *Environmental factors, brain development, and intelligence in adulthood.* Ann Neurol, 2009. **66**(3): p. 266-7.

241. van den Pol, A.N., *Viral infection leading to brain dysfunction: more prevalent than appreciated?* Neuron, 2009. **64**(1): p. 17-20.

242. Torrey, E.F. and M.R. Peterson, *Slow and latent viruses in schizophrenia.* Lancet, 1973. **2**(7819): p. 22-4.

243. Kirch, D.G., *Infection and autoimmunity as etiologic factors in schizophrenia: a review and reappraisal.* Schizophr Bull, 1993. **19**(2): p. 355-70.

244. Bilbo, S.D. and J.M. Schwarz, *Early-life programming of later-life brain and behavior: a critical role for the immune system.* Front Behav Neurosci, 2009. **3**: p. 14.

245. Kilham, L. and G. Margolis, *Cerebellar Ataxia in Hamsters Inoculated with Rat Virus.* Science, 1964. **143**: p. 1047-8.

246. Miyazato, S., et al., *Encephalitis of cattle caused by Iriki isolate, a new strain belonging to Akabane virus.* Nippon Juigaku Zasshi, 1989. **51**(1): p. 128-36.

247. Hewicker-Trautwein, M. and G. Trautwein, *Porencephaly, hydranencephaly and leukoencephalopathy in ovine fetuses following transplacental infection with bovine virus diarrhoea virus: distribution of viral antigen and characterization of cellular response.* Acta Neuropathol, 1994. **87**(4): p. 385-97.

248. Gavier-Widen, D., et al., *Investigations into shaking mink syndrome: an encephalomyelitis of unknown cause in farmed mink (Mustela vison) kits in Scandinavia.* J Vet Diagn Invest, 2004. **16**(4): p. 305-12.

249. Pletnikov, M.V., et al., *Neonatal Borna disease virus infection (BDV)-induced damage to the cerebellum is associated with sensorimotor deficits in developing Lewis rats.* Brain Res Dev Brain Res, 2001. **126**(1): p. 1-12.

250. Griffin, W.S., et al., *Graft-versus-host disease impairs cerebellar growth.* Nature, 1978. **275**(5678): p. 315-7.

251. Andersen, I.H., O. Marker, and A.R. Thomsen, *Breakdown of blood-brain barrier function in the murine lymphocytic choriomeningitis virus infection mediated by virus-specific CD8+ T cells.* J.Neuroimmunol., 1991. **31**(2): p. 155-163.

252. Phares, T.W., et al., *Regional differences in blood-brain barrier permeability changes and inflammation in the apathogenic clearance of virus from the central nervous system.* Journal of Immunology, 2006. **176**(12): p. 7666-7675.

253. Beg, A.A. and D. Baltimore, *An essential role for NF-kappaB in preventing TNF-alpha-induced cell death.* Science, 1996. **274**(5288): p. 782-784.

254. Majlessi, L., R. Lo-Man, and C. Leclerc, *Regulatory B and T cells in infections.* Microbes Infect, 2008. **10**(9): p. 1030-5.